

# **Defining the cellular heterogeneity of healthy human skin using single cell technologies**

James Carlton Fletcher

Doctor of Philosophy

June 2020

Institute of Cellular Medicine, William Leech Building, Framlington  
Place, Newcastle Upon Tyne, NE2 4HH

Registration Date: 1<sup>st</sup> March 2016

Research Programme: 8440F PhD ICM (FT)

Supervisors: Professor Muzlifah Haniffa, Professor Nick Reynolds



# **i. Table of Contents**

i. Table of Contents.....	3
ii. List of Figures and Tables .....	7
iii. Declaration.....	12
iv. Abbreviations.....	13
v. Abstract.....	16
vi. Acknowledgements.....	17
Chapter 1. Literature Review .....	19
1.1    Introduction.....	21
1.2    Cellular Anatomy of the Epidermis .....	22
1.2.1    Functionality of Keratinocytes.....	22
1.2.2    Epidermal water barrier properties .....	22
1.2.3    Immunomodulation in keratinocytes .....	23
1.2.4    Epidermal Layers and Keratinisation.....	25
1.2.5    The Basement Membrane .....	25
1.2.6    Stratum Basale .....	25
1.2.7    Stratum Spinosum.....	26
1.2.8    Stratum Granulosum .....	26
1.2.9    Stratum Lucidum .....	27
1.2.10    Stratum Corneum.....	27
1.2.11    Hair Follicles.....	27
1.2.12    Melanocytes .....	28
1.2.13    Merkel Cells.....	29
1.3    Epidermal Immune Cells .....	29
1.3.1    Langerhans Cells.....	29
1.3.2    Inflammatory Dendritic Epidermal Cells.....	31
1.3.3    Epidermal T cells .....	32
1.4    Cellular Anatomy of the Dermis.....	33
1.4.1    Fibroblasts.....	33
1.4.2    Vascular endothelium .....	35
1.4.3    Pericytes.....	37
1.4.4    Lymphatic endothelium .....	38
1.4.5    Schwann cells.....	39

1.5	Dermal antigen presenting cells.....	40
1.5.1	Dendritic Cells .....	40
1.5.2	Dermal DCs .....	41
1.5.3	cDC1s.....	41
1.5.4	cDC2s.....	42
1.5.5	pDCs .....	42
1.5.6	Macrophages .....	43
1.5.7	Monocytes.....	43
1.5.8	Monocyte-derived DCs.....	44
1.5.9	Monocyte-derived macrophages.....	44
1.6	Dermal lymphoid cells.....	45
1.6.1	Microenvironmental differences between Dermal and Epidermal T cells ...	45
1.6.2	Innate lymphoid cells.....	45
1.6.3	Mast cells .....	46
1.7	High Dimensional Single Cell Analysis Technologies.....	48
1.7.1	CyTOF .....	48
1.7.2	Single Cell RNA Sequencing.....	49
1.7.3	Analysis of single cell RNA sequencing data.....	51
1.7.4	Interpretation of single cell RNA sequencing data .....	52
1.8	Single cell sequencing protocols.....	53
1.8.1	Plate based sequencing .....	53
1.8.2	Droplet based sequencing .....	54
1.9	Project Aims.....	56
Chapter 2. Methods.....		58
2.1	Materials .....	60
2.1.1	Buffers.....	60
2.2	Generation of single cell suspensions from skin.....	63
2.2.1	Preparation of whole skin digest.....	63
2.2.2	Optimisation of collagenase digestion of whole skin .....	63
2.2.3	Dermal and epidermal peeling .....	64
2.2.4	Comparison of collagenase digestion between whole skin and peeled dermis and epidermis.....	64
2.2.5	Freezing cells for short term storage.....	64
2.3	Flow cytometry .....	65
2.3.1	Flow cytometry analysis of cell suspensions .....	65
2.3.2	FACS isolation of skin cells .....	65

2.4	Mass cytometry (CyTOF).....	66
2.4.1	Mass cytometry analysis of cell suspensions.....	66
2.4.2	Metal tagged antibody conjugation.....	66
2.4.3	Antibody testing on beads.....	67
2.4.4	Antibody testing on cells .....	68
2.4.5	Antibody titration.....	68
2.5	Immunohistochemistry (IHC).....	68
2.5.1	Whole mount immunofluorescence staining of dermis and epidermis.....	68
2.5.2	Immunohistochemistry on skin sections.....	70
2.5.3	H&E staining .....	70
2.5.4	Antibody staining.....	70
2.6	Single cell RNA sequencing .....	71
2.7	Data analysis .....	71
2.7.1	Statistics and graphs.....	72
2.7.2	Flow Analysis .....	72
2.7.3	Mass cytometry clustering analysis .....	72
2.7.4	Microscopy imaging and analysis.....	72
2.7.5	Figure preparation.....	72
2.8	Single cell RNA sequencing data analysis.....	72
2.8.1	Alignment and quality control of scRNA-seq data.....	72
2.8.2	Doublet detection and exclusion.....	73
2.8.3	Data normalization and feature selection.....	73
2.8.4	Data embedding, visualization and clustering .....	73
2.8.5	Calculation of differential gene expression .....	73
2.8.6	Trajectory analysis .....	74
2.8.7	CellPhoneDB .....	74
Chapter 3. Optimising the .....		75
sampling of skin cell heterogeneity .....		75
3.1	Chapter 3 Introduction .....	77
3.2	Results.....	79
3.2.1	Optimisation of tissue dissociation .....	79
3.2.2	Overnight collagenase dissociation increases immune cell liberation with little effect on viability .....	81
3.2.3	Separation of dermis and epidermis leads to increased cell liberation by type IV collagenase .....	83
3.2.4	FACS improves sampling of rare skin cell types.....	88

3.2.5	Dissociation of human skin leads to loss of follicular structures.....	92
3.2.6	Distorted distribution of basal and suprabasal keratinocytes.....	95
3.3	Discussion.....	98
Chapter 4.	Single cell analysis of the cellular composition of human skin.....	101
4.1	Chapter 4 Introduction.....	103
4.2	Results.....	103
4.2.1	Droplet based single cell sequencing of healthy human skin.....	103
4.2.2	Skin APCs are highly heterogeneous.....	112
4.2.3	DCs with dermal signatures isolated from the epidermis.....	112
4.2.4	Langerhans cells can display low HLA-DR protein expression.....	112
4.2.5	Innate and adaptive lymphoid cell heterogeneity.....	115
4.2.6	Tissue microenvironmental differences affect lymphocyte transcription....	118
4.2.7	Epidermal mast cells are present at low numbers in healthy skin.....	121
4.2.8	Mass cytometric proteomic profiling of human skin.....	121
4.2.9	Skin cells display mismatches in RNA and protein expression.....	131
4.3	Discussion.....	132
Chapter 5.	Stromal cell heterogeneity.....	136
within human skin.....		136
5.1	Chapter 5 Introduction.....	138
5.2	Results.....	138
5.2.1	Cellular heterogeneity of the stromal cells within skin.....	138
5.2.2	Fibroblasts in human skin vary in immunomodulatory gene expression ....	143
5.2.3	Melanocyte and schwann cell transcriptome profiles.....	143
5.2.4	Heterogeneity of pericytes and lymphatic endothelial cells.....	145
5.2.5	Three distinct clusters of vascular endothelial cells.....	145
5.2.6	Specialised leukocyte trafficking structures are present in healthy skin ....	150
5.2.7	Keratinocyte heterogeneity follows keratinisation.....	156
5.2.8	Distinct differentiation pathway of lamellar body-producing KCs.....	160
5.2.9	CD83+ Inflammatory keratinocytes reside in healthy skin.....	160
5.2.10	CD83+ keratinocytes may interact with epidermal T cells.....	168
5.3	Discussion.....	171
Chapter 6.	Summarising Discussion.....	177
6.1	Chapter 6 Introduction.....	179
6.2	The novelty of findings from skin single cell analysis.....	179

6.2.1	Relevance of optimisation to future skin studies .....	179
6.2.2	Capture of rare cell types for comprehensive sequencing .....	180
6.2.3	Proteomic profiling of human skin by CyTOF .....	182
6.2.4	Focussed analysis of cellular heterogeneity in scRNA-seq data .....	183
6.2.5	Dermal nonimmune and vascular heterogeneity.....	183
6.2.6	Keratinocyte heterogeneity and immunomodulation.....	184
6.3	Single cell sequencing publications .....	185
6.4	The power of investigative scRNA-seq .....	186
6.5	Further work.....	187
6.6	Concluding remarks .....	191
7	Appendix tables .....	192
8	References .....	211
9	Publications and Presentations .....	240
9.1	Publications.....	240
9.2	Presentations .....	243

## ii. List of Figures and Tables

### Chapter 2

**Page 61:** Table 1 – List of antibodies used.

### Chapter 3

**Page 80:** Figure 1 – Optimisation of collagenase digestion duration.

**Page 82:** Figure 2 – Gating strategy for the optimisation of collagenase digestion duration.

**Page 84:** Figure 3 – Comparison of collagenase digestion duration of whole skin.

**Page 84:** Figure 4 – Comparison of collagenase digestion duration of dermis.

**Page 84:** Figure 5 – Comparison of collagenase digestion duration of epidermis.

**Page 86:** Figure 6 – Gating strategy for the optimisation of whole skin collagenase digestion.

**Page 86:** Figure 7 – Gating strategy for the optimisation of dermis collagenase digestion.

**Page 86:** Figure 8 – Gating strategy for the optimisation of epidermis collagenase digestion.

**Page 89:** Figure 9 – Gating strategy for the sampling of dermal skin cell types for scRNA-seq.

**Page 90:** Figure 10 – Gating strategy for the sampling of epidermal skin cell types for scRNA-seq.

**Page 91:** Table 2 – Sampling difference of skin cells with and without sorting.

**Page 93:** Figure 11 – Hair follicles are lost during tissue processing.

**Page 94:** Figure 12 – Hair follicle bulbs are found deep within the reticular dermis.

**Page 96:** Figure 13 – Follicular keratinocytes are present in surgically removed skin.

**Page 96:** Figure 14 – Follicular keratinocytes are not present in 200µm depth skin.

**Page 96:** Figure 15 – Follicular keratinocytes are not present in peeled epidermis.

**Page 96:** Figure 16 – Follicular keratinocytes are not present in peeled dermis.

**Page 97:** Figure 17 – The stratum corneum alone remains after overnight epidermal collagenase digestion.

#### **Chapter 4**

**Page 105:** Figure 18 – Experimental overview of 10X sequencing of healthy adult human skin.

**Page 107:** Figure 19 – Broad cellular heterogeneity of healthy adult skin.

**Page 107:** Figure 20 – UMAP visualization of scRNA-seq analysis of healthy adult skin cells annotated by sample.

**Page 108:** Figure 21 – UMAP visualisation of scRNA-seq analysis of healthy adult skin cells annotated by 10x lane.

**Page 108:** Figure 22 – UMAP visualisation of scRNA-seq analysis of healthy adult skin cells annotated by tissue.

**Page 109:** Table 3 – Cell numbers per sample of detailed annotations of adult skin scRNA-seq data.

**Page 110:** Figure 23 – QC Violin plots of UMIs and genes found per cell in each 10x lane.

**Page 110:** Figure 24 – Top differentially expressed genes between the cell types in healthy adult skin.

**Page 113:** Figure 25 – Heterogeneity of APC populations in healthy human skin.

**Page 113:** Figure 26 – UMAP visualisation of scRNA-seq analysis of skin APC populations annotated by tissue.



**Page 114:** Figure 27 – UMAP visualisation of scRNA-seq analysis of skin APC populations annotated by 10x lane.

**Page 116:** Figure 28 – Lymphoid cell heterogeneity in healthy human skin.

**Page 116:** Figure 29 – UMAP visualisation of scRNA-seq analysis of skin lymphoid cell populations annotated by tissue.

**Page 117:** Figure 30 – Gamma delta TCR expression in healthy skin.

**Page 117:** Figure 31 – Functional gene variance in skin innate lymphoid cells.

**Page 119:** Figure 32 – Tissue microenvironment-specific gene expression in skin T cells.

**Page 120:** Figure 33 – Tissue microenvironment-specific gene expression in skin NK cells.

**Page 122:** Figure 34 – Tissue microenvironment-specific gene expression in skin mast cells.

**Page 124:** Figure 35 – Protein expression heterogeneity of epidermal cells in healthy skin.

**Page 125:** Figure 36 – Protein expression heterogeneity of dermal cells in healthy skin.

**Page 126:** Figure 37 – Manual gating versus clustering of epidermal CyTOF data.

**Page 127:** Figure 38 – Manual gating versus clustering of dermal CyTOF data.

**Page 128:** Figure 39 – Gating strategy for CyTOF analysis of healthy adult epidermis cells.

**Page 129:** Figure 40 – Gating strategy for CyTOF analysis of healthy adult dermis cells.

## **Chapter 5**

**Page 140:** Figure 41 – Heterogeneity of nonimmune cell populations in healthy human skin.

**Page 141:** Figure 42 – UMAP visualisation of scRNA-seq analysis of nonimmune cells annotated by sample.

**Page 142:** Figure 43 – UMAP visualisation of scRNA-seq analysis of nonimmune cells annotated by 10x lane.

**Page 144:** Figure 44 – Top differentially expressed genes between the nonimmune cells in healthy skin.

**Page 147:** Figure 45 – The potential morphology of VE1 and VE2 cells within a single dermal papilla.

**Page 148:** Figure 46 – Expression of endothelial adhesion markers is higher in ACKR1+ cells.

**Page 149:** Figure 47 – Vascular endothelial cell adhesion marker heterogeneity.

**Page 151:** Figure 48 – Whole mount imaging of SNCG expression on dermal vasculature.

**Page 152:** Figure 49 – Potential interactions between the vasculature and dermal leukocytes.

**Page 153:** Figure 50 – Heterogeneity in immunomodulatory gene expression between vascular endothelial cell clusters.

**Page 155:** Figure 51 – VE3 cells express lower levels of cell-cell adhesion proteins.

**Page 157:** Figure 52 – Force-directed graph visualization of scRNA-seq analysis of keratinocytes.

**Page 158:** Figure 53 – Force-directed graph visualization of scRNA-seq analysis of keratinocytes annotated by sample.

**Page 159:** Figure 54 – Keratinocyte subset markers in healthy adult skin.

**Page 161:** Figure 55 – Trajectory visualization of adult skin keratinocytes.

**Page 162:** Figure 56 – Expression of lamellar body-related genes in specific keratinocyte clusters.

**Page 163:** Figure 57 – CD83+ KCs express higher levels of immunomodulatory genes.

**Page 165:** Figure 58 – Whole mount imaging of CD83 expression on keratinocytes.

**Page 166:** Figure 59 – In situ visualization of CD83+ keratinocytes in healthy adult skin.

**Page 167:** Figure 60 – Percentage of CD83+ keratinocytes found in healthy adult epidermis.

**Page 169:** Figure 61 – Potential interactions between CD83+ keratinocytes and epidermal T cells.

**Page 170:** Figure 62 – CD83+ keratinocytes express higher levels of T cell interacting genes.

**Page 170:** Figure 63 – Diagram representing the receptor-ligand interactions between CD83 KCs and T cells that are unique to the epidermis.

### **Appendix tables**

**Page 192:** Appendix Table 1 – Detailed nonimmune cluster differentially expressed genes.

**Page 201:** Appendix Table 2 – Detailed keratinocyte cluster differentially expressed genes.

**Page 205:** Appendix Table 3 – Gene symbols listed with standardised nomenclature.

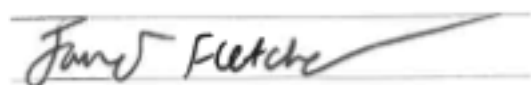
### iii. Declaration

The contents and construction of this thesis are my own work, with the following exceptions:

Computational analysis of single cell RNA sequencing data was done by Dr Peter Vegh. This data was interpreted and annotated primarily by myself, with the exception of the APC data (**Chapter 4, Figure 25**) which was annotated by Dr Gary Reynolds. Single cell RNA sequencing plots were generated by Dr Peter Vegh and Dr Gary Reynolds in R and Scanpy, and figures were generated by myself in Adobe Illustrator. Individual contributions to figure generation are also mentioned in each figure legend where applicable.

Immunohistochemistry experiments were carried out by myself as well as the Newcastle Molecular Pathology Node staff. Molecular Pathology Node staff embedded all FFPE blocks and cut all slides used from fixed material prepared by myself. Slides from different donors were stained for H&E, shown in **Figures 11, 12** and **17**, by either myself or Molecular Pathology Node staff. Two colour staining shown in **Figure 59** was carried out by Molecular Pathology Node staff. Where otherwise not mentioned, staining was carried out by myself. All immunohistochemistry imaging and figure generation was carried out by myself. Whole mount immunofluorescence staining experiments, shown in **Figures 48** and **58**, were designed by myself and samples from different donors were stained by myself or David Dixon.

Flow and mass cytometry experiments were designed and carried out by myself, and the cell sorter and mass cytometer were operated by Newcastle Flow Cytometry Core Facility staff. Library preparation of single cell RNA sequencing data was carried out by Emily Stephenson, and libraries were sent to the Wellcome Sanger Institute for sequencing.



James Fletcher

## **iv. Abbreviations**

A disintegrin and metalloproteinase (ADAM)

Antigen presenting cell (APC)

Approximate graph abstraction (AGA)

C-c motif chemokine ligand (CCL)

C-c motif chemokine receptor (CCR)

Central nervous system (CNS)

Colony stimulating factor 1 receptor (CSF1R)

Conventional DC (cDC)

Cutaneous lymphoid antigen (CLA)

Cytometry by time of flight (CyTOF)

Cytotoxic T cell (Tc)

Dendritic cell (DC)

Dermo-epidermal junction (DEJ)

E-selectin (SELE)

Extracellular matrix (ECM)

Fibroblast (Fb)

Flow Cytometry Core Facility (FCCF)

Fluorescence activated cell sorting (FACS)

Foetal calf serum (FCS)

Force atlas (FA)

Force-directed graph (FDG)

Formalin-fixed paraffin embedded (FFPE)

Forward scatter (FSC)

G-protein coupled receptor 5 (LGR5)

Gamma synuclein (SNGG)

Helper T cell (Th)

High endothelial venule (HEV)

IL1 receptor like 1 (IL1RL1)

Interfollicular epidermis (IFE)

Interferon (IFN)

Immunofluorescence (IF)  
Immunohistochemistry (IHC)  
Inducible nitrogen oxide synthase (iNOS)  
Inflammatory dendritic epidermal cell (IDEC)  
Innate lymphoid cell (ILC)  
Interleukin (IL)  
Intracellular adhesion molecule 1 (ICAM1)  
Keratinocyte (KC)  
Killer cell immunoglobulin-like receptor (KIR)  
Langerhans cells (LCs)  
Lymphatic endothelium (LE)  
Lymphoid tissue (LT)  
Major histocompatibility complex (MHC)  
Matrix metalloproteinase (MMP)  
Monocyte-derived DC (moDC)  
Myelin basic protein (MBP)  
Myelin protein zero (MPZ)  
Natural killer (NK)  
Natural killer T (NKT)  
Non-lymphoid tissue (NLT)  
P-selectin (SELP)  
Partition-based approximate graph abstraction (PAGA)  
Pathogen-associated molecular pattern (PAMP)  
Pattern recognition receptor (PRR)  
Peripheral blood mononuclear cells (PBMCs)  
Phosphate buffered saline (PBS)  
Plasmacytoid DC (pDC)  
Platelet-derived growth factor subunit B (PDGF-B)  
Podoplanin (PDPN)  
Principal component analysis (PCA)  
Principal components (PC)  
Quality control (QC)

Quantitative PCR (qPCR)  
Regulatory T cell (Treg)  
Roswell Park Memorial Institute media (RPMI)  
Side scatter (SSC)  
Single cell RNA sequencing (scRNA-seq)  
Smart-seq2 (SS2)  
Stearoyl-CoA desaturase-1 (SCD1)  
T cell receptor (TCR)  
t-stochastic neighbour embedding (tSNE)  
TNF- and iNOS-producing DC (TIP-DC)  
Toll-like receptor (TLR)  
Transepidermal water loss (TEWL)  
Transforming growth factor beta (TGF $\beta$ )  
Tris buffered saline (TBS)  
Tumour necrosis factor (TNF)  
Tyrosinase (TYR)  
Tyrosinase related protein 1 (TYRP1)  
Tyrosinase related protein 2 (TYRP2)  
Uniform Manifold Approximation and Projection (UMAP)  
Unique molecular identifier (UMI)  
Vascular adhesion molecule 1 (VCAM1)  
Vascular endothelial growth factor (VEGF)  
Vascular endothelium (VE)

## **v. Abstract**

Skin is a complex organ comprising many synergising cell types. It serves a vital role in the immune system as the first line of defence against pathogens. In homeostatic conditions, skin must be primed to respond to an overwhelming diversity of pathogens from the environment while simultaneously avoiding excessive immune responses and autoimmunity. Understanding of the intercellular heterogeneity that is required for this balance during steady state is crucial to understanding how these cells act during dysregulation, and could aid in the understanding of diseases such as eczema and psoriasis.

Healthy adult skin, obtained from reconstructive surgery, was enzymatically dissociated and profiled using single cell RNA sequencing and mass cytometry, and further validated using flow cytometry and immunohistochemistry. By sequencing 82,490 single cells from healthy adult human skin of three donors, it was possible to profile the different transcriptomic states of keratinocytes, melanocytes, vascular and lymphatic endothelium, pericytes, fibroblasts, schwann cells, lymphoid cells and antigen presenting cells. 1,959,717 single cells from four donors were analysed using a 37-marker mass cytometry panel, allowing for a comparison between the proteomes and transcriptomes of skin cells.

Interrogation of the stromal cells at high resolution revealed previously unreported heterogeneity, including the presence of specialised vascular endothelial structures in healthy skin, which appear to mirror the high endothelial venules found in lymphoid tissues. These structures may be critical to leukocyte infiltration during homeostasis and inflammatory conditions.

This study provides a powerful resource, as a repository of healthy skin single cell heterogeneity, for future research into deviations from health, including inflammation, infection and disease.



## **vi. Acknowledgements**

I would like to thank my supervisors Professor Muzlifah Haniffa and Professor Nick Reynolds, particularly Professor Haniffa for providing me with the opportunity to undertake this work and supervising me throughout this experience. I would also like to thank the staff and students of the II Theme and Academic Haematology for the ever friendly and helpful environment in the labs and the offices, in particular the members of the Haniffa Lab. Additionally I would like to thank the staff of FCCF, Pathology Node and Bioimaging for their assistance in designing experiments, as well as Xiao Wang and Catharien Hilkens for their advice during annual assessments.

Particular thanks go to the patients who kindly donated samples, and the surgeons and nurses who collected these, without which this work would not have been possible.

Thanks Mum, Dad and Zoe for all of your support, for putting up with years of complaining, and all the lifts home at 2am after fun-filled evenings of experiments. Thank you Boy, for your confidence in my ability, and your years of complaining for me to finish this. Thank you Eoin, for making me believe I could succeed at Postgraduate study. Thank you Dave, for meaning I wasn't the only one who lost my sanity. And most of all thank you Rachel, how much your support through this process meant can't be put into words.



**1**

## **Chapter 1. Literature Review**



## 1.1 Introduction

Skin encompasses many subsets of heterogeneous stromal cells, antigen presenting cells and lymphoid cells. These cells perform a wide variety of functions in both steady state and inflammation. Purification and analysis of skin cells in the context of diseases and treatment targets has historically relied on knowledge of marker expression derived from bulk cell analysis and mouse models (Rinkevich et al., 2015; Liu et al., 2009). These approaches derive two major drawbacks to be addressed. i) Bulk analysis of cells can mask heterogeneity by losing rare, yet potentially functionally important, expression to averaging. Separation of cell signatures with such methods also relies heavily on *a priori* knowledge, which introduces bias into the analysis. ii) Murine models of the various components of skin have been extensively compared to human populations (Reynolds & Haniffa, 2015; Zomer & Trentin, 2018; Hagai et al., 2018), providing valuable information from readily manipulatable organisms. However, murine cells and *in vitro* cultured human skin cells have many transcriptional differences with *in vivo* human cell populations (Harman et al., 2013; Reynolds & Haniffa, 2015). Human skin is an accessible model organ to interrogate tissue cell populations with high dimensional single cell analysis, and by using these techniques, this thesis aims to categorise the cell types present in healthy adult human skin and improve the understanding of the cellular heterogeneity present therein.

This literature review will attempt to collate the findings within the literature of known heterogeneity within the cell populations of skin in both the epidermis and dermis, with the aim of identifying the areas of interest and gaps in the literature with which a comprehensive single cell study of skin could add insight in a significant way. This review will also aim to help annotate the data generated in this study, and ground the findings therein.

It will also cover the use of single cell technologies, namely mass cytometry and single cell RNA sequencing (scRNA-seq), and discuss the merits and issues to consider with using such technologies and interpreting the data they can produce. Finally, this review

will cover the use of scRNA-seq to interrogate skin in the literature, the reported findings and the strengths and weaknesses of these studies.

## **1.2 Cellular Anatomy of the Epidermis**

The epidermis is the apical layer of skin, covering almost the entire human body as the interface to the environment. It comprises primarily layers of keratinocytes which differentiate from nuclear cells at the basal layer to anuclear keratinized structures at the apex. The basal layer also contains melanocytes, which primarily produce melanin to protect against UV damage, and Merkel cells which receive touch signals in touch-sensitive skin as well. Throughout the epidermis Langerhans cells (LCs) and T cells shape the epidermal immune system, maintaining tolerance while sensing for pathogenic disturbance.

### **1.2.1 Functionality of Keratinocytes**

Keratinocytes are the primary cell type of the epidermis, making up over 95% of its cells (Wikramanayake et al., 2014). They provide the mechanical and water barrier functions of the epidermis, and also provide vital support to the epidermal immunological barrier.

Keratinocytes produce keratins, fibrous proteins with high physical toughness which support the cells' cytoskeletons and give the epidermis its strength and flexibility (Fuchs, 1995). Throughout differentiation, production changes to different sets of keratins. For example, in the basal layer keratinocytes produce keratins 5 and 14, and keratins 1 and 10 are solely expressed by suprabasal keratinocytes (Alam et al., 2011). At the apex of the epidermis, terminally differentiated keratinocytes (corneocytes) lack nuclei, organelles and cytoplasm and contain high amounts of suprabasal keratins as well as additional structural proteins including involucrin and filaggrin, which further support the physical barrier of the epidermis (Steinert & Marekov, 1995).

### **1.2.2 Epidermal water barrier properties**

The epidermis, when intact, is also a near-impermeable barrier to water, and keratinocytes facilitate this vital function required to avoid organisms drying out. This is

maintained by the presence of insoluble keratin proteins, and the production of lamellar bodies – secretory organelles containing water-repellent lipids and lipid-associated proteins (Feingold, 2012). Keratinocytes secrete lamellar bodies into the extracellular matrix (ECM) to form a continuous barrier of water-repellent molecules across the epidermis. Lamellar body expression is increased in the upper layers of the epidermis, and both secretion and production are increased as part of the wound healing process (Menon et al., 1994).

The contents of lamellar bodies include a variety of hydrophobic lipids. They also contain supporting proteins such as the lipid transport channel ABCA12, and the vesicle transport protein CLIP1 (Raymond et al., 2008). Lamellar body dysregulation is associated with specific ichthyoses (a group of skin diseases resulting in severely dry skin), due to the effects they have on the water retaining properties of the epidermis. Akiyama *et al.* link multiple loss of function mutations in *ABCA12* with harlequin ichthyosis (Akiyama et al., 2005). Mutations in *SPINK5* can also cause unregulated lamellar body secretion, leading to symptoms of ichthyosis (Bitoun et al., 2002). Raymond *et al.* show that human keratinocytes are differentially lamellar body enriched or lacking, and further investigation into the heterogeneity between the two fractions may aid in the understanding of the formation and possible treatment of ichthyoses (Raymond et al., 2008).

Lamellar body secretion is also upregulated in response to injury, in order to restore the damaged water barrier at a site of injury. This is regulated by a gradient of extracellular calcium ions, from low in the basal layer to high in the stratum corneum, which keeps homeostatic lamellar body release under control (Menon et al., 1994). This gradient is disrupted by physical injuries, which increase transepidermal water loss (TEWL) until the resulting lamellar body secretions can restore the water barrier (Menon et al., 1994). TEWL occurs at a low rate in homeostatic conditions as the epidermal water barrier is not entirely impermeable, and increases in this rate can be used to measure the extent of certain skin diseases.

### **1.2.3 Immunomodulation in keratinocytes**

The immunological barrier of the epidermis is a result of keratin-dense corneocytes providing a physical barrier to pathogenic invasion, homeostatic immune surveillance by LCs and T cells, and immunological support directly from keratinocytes (Grice & Segre, 2011; Schön, 2019). Keratinocytes can secrete chemokines including C-c motif chemokine ligand (CCL)27, which attracts memory T cells by C-c motif chemokine receptor (CCR)10 expression, allowing for the guidance of the skin immune system (Homey et al., 2002). Keratinocytes can even present antigen via major histocompatibility complex (MHC) class II expression during inflammation to aid in T cell priming (Kim et al., 2009). In the absence of inflammation, T cell homeostatic responses to the skin microbiome are assisted by steady state MHC class II expression in keratinocytes, which can induce Th1 activation through presentation of commensal antigens (Tamoutounour et al., 2019).

Psoriatic keratinocytes express high levels of CCL20, perpetuating the local inflammation by leukocyte chemotaxis (Harper et al., 2009). Harper *et al.* show that Th17 cytokine secretion can induce CCL20 production, but further than this the origin of inflammatory psoriatic keratinocytes has not been fully explored (Harper et al., 2009). As well as sending signals to leukocytes, keratinocytes also receive signals from the immune system. IL20 secreted from infiltrating monocytes in psoriatic skin stimulates proliferation in IL20R-expressing keratinocytes, contributing to the thickened epidermis: a key feature of psoriasis (Sa et al., 2007; Myles et al., 2013).

Keratinocytes also directly produce anti-microbial molecules during inflammation including human beta-defensin 2, an anti-microbial protein against gram negative bacteria, which is secreted from keratinocyte lamellar bodies (Oren et al., 2003). The cathelicidin LL-37 is also produced by keratinocytes in psoriatic skin, as well as in response to injury (Frohm et al., 1997; Dorschner et al., 2001). LL-37 is capable of killing both gram negative and gram positive bacteria (Dorschner et al., 2001).

A better understanding of whether specific keratinocyte subsets are responsible for these immunomodulatory functions, and how this may link to the development of inflammatory skin diseases such as psoriasis, could aid in treatment development.



#### **1.2.4 Epidermal Layers and Keratinisation**

The epidermis is arranged into multiple layers of keratinocytes with different specialised functions. Keratinocyte morphology, structure, gene expression and, as a result of all these, function, changes dramatically throughout the ~60 day span of differentiation from basal keratinocyte to terminally differentiated corneocyte (Halprin, 1972).

Basal keratinocytes enter the suprabasal layer and differentiate in a process called keratinisation, whereby their protein expression changes as they physically move to the more superficial layers. They exchange expression of basal keratins (e.g. keratins 5 and 14) for suprabasal keratins (e.g. keratins 1 and 10), and eventually de-nucleate as part of terminal differentiation into corneocytes, expressing high levels of terminal markers such as involucrin and filaggrin, which aid in the physical barrier of the epidermis (Jones et al., 2007; Alam et al., 2011). These corneocytes eventually shed from the skin (Jones et al., 2007).

#### **1.2.5 The Basement Membrane**

The epidermis is anchored to the dermis by an acellular basement membrane, also known as the dermo-epidermal junction (DEJ). This structure is a common dividing protein fibre layer found in many tissues, and consists largely of collagen IV fibres (Behrens et al., 2012). The dermal ECM is attached to the basement membrane by collagen VII, and basal keratinocytes are attached by integrin alpha 6/beta 4 complexes (Behrens et al., 2012).

#### **1.2.6 Stratum Basale**

The deepest layer of the epidermis is called the Stratum Basale, or basal layer, and is a monolayer of basal keratinocytes which also contains melanocytes and Merkel cells. It is connected to the basal lamina of the basement membrane (Goleva et al., 2019). Basal keratinocytes are sometimes considered to be stem cells, as they divide and migrate to replace the upper layers of keratinocytes (Blanpain & Fuchs, 2006). There are varying theories as to the distribution of dividing keratinocytes in the epidermis. Two schools of thought are either that specialised stem cells found in the interfollicular epidermis basal

layer and in hair follicles divide laterally to replenish the non-dividing cells as they leave the basal layer during keratinisation; or that any basal keratinocyte can become mitotic, and that the stochastic destination of daughter cells in either the basal or suprabasal layers maintains cell numbers in both layers (Jones et al., 2007; Lechler & Fuchs, 2005).

Previously an intermediate cell type was theorised called the transit amplifying cell (Potten, 1981). Experiments in mouse show the arrangement of mouse keratinocytes in discrete hexagonal columns called epidermal proliferative units (Mackenzie, 1970). One stem cell per column divides to produce multiple transit amplifying cells, with limited mitotic capability, which in turn divide to maintain the epidermis (Jones et al., 2007).

Keratinocyte division mechanics are mostly studied in mouse and such studies are difficult to undertake in human, requiring lineage tracing and live imaging experiments, which are further confounded by the slow turnover of keratinocytes *in vivo* (Ghazizadeh & Taichman, 2001; Halprin, 1972). Skin organoid cultures are being developed rapidly in recent years, which may be one possible model with which to interrogate human keratinocyte mitosis, although this is still one step away from *in vivo* work (Lee et al., 2020).

### **1.2.7 Stratum Spinosum**

The stratum spinosum, or suprabasal layer, is directly above the basal layer and consists of suprabasal keratinocytes. The suprabasal layer is multiple cells thick, and this thickness varies widely with body site (Chopra et al., 2015). LCs are also found in the suprabasal layer (Jaitley & Saraswathi, 2012).

### **1.2.8 Stratum Granulosum**

The stratum granulosum, or granular layer, is above the suprabasal layer. It varies between 3-5 cells thick depending on the body site, and consists of granular keratinocytes which are flatter, have thicker membranes and are beginning to undergo keratinization by producing lamellar bodies and keratohyalin, which is a granular formation of keratins and other proteins (Westerhof & Dingemans, 1986; Hollander et al., 2015).

### **1.2.9 Stratum Lucidum**

The stratum lucidum is a thin layer of translucent keratinocytes which is only present in thick skin such as palms and soles (Sharma & Yousef, 2017). Keratinocytes in this layer are filled with eleidin – a clear, lipid-rich protein that contributes to the skin water barrier (Sharma & Yousef, 2017).

### **1.2.10 Stratum Corneum**

The stratum corneum is the most superficial layer of the epidermis. Here, keratinocytes have undergone keratinisation (also called cornification) and have lost most of their organelles, including nuclei, becoming corneocytes (Eckhart et al., 2013). These keratin rich corneocytes provide a mechanical and pathogenic barrier to the outside environment. The number of layers varies widely depending on body site (Maiti et al., 2020). These cells are eventually shed from skin in the process of desquamation (Eckhart et al., 2013).

### **1.2.11 Hair Follicles**

Hair-bearing skin contains many hair follicles, which are keratinocyte structures that are continuous with the basal epidermis. They span deep into the reticular dermis, and are associated with multiple types of glands.

Hair follicles have a bulb at their deepest point, which is directly supplied with venous and arteriolar capillaries, and contains a niche of leucine-rich repeat-containing G-protein coupled receptor 5 (LGR5)+ stem cells (Jaks et al., 2008). The hair follicle shaft leads to the skin surface and is connected to arrector pili muscle structures, which can contract to raise hairs. Arrector pili muscle cells express common muscle markers including alpha smooth muscle actin (Morioka et al., 2011).

Sebaceous glands also connect to the hair follicle shaft, and are made up of vesicle-filled cells which produce high amounts of lipids to release as sebum (Lovász et al., 2017). Sebaceous gland cells express sebum-producing enzymes including Stearoyl-CoA desaturase-1 (SCD1) (Joost et al., 2016). Sebum release is holocrine, requiring cell

membrane rupture to release the molecules into the hair follicle shaft, and as such mitotic sebaceous gland cells turn over regularly in the base of the gland to replace these lost cells (Horsley et al., 2006). Kobayashi *et al.* recently demonstrated that innate lymphoid cells (ILCs) are required to regulate the division of these sebaceous gland stem cells via tumour necrosis factor (TNF) signalling (Kobayashi et al., 2019). Interactions such as this support the need to investigate skin stromal cells together with leukocytes when interrogating homeostasis.

Using scRNA-seq on mouse skin, Joost *et al.* revealed transcriptomic heterogeneity between keratinocytes in different spatial locations of the hair follicle, including those in the inner and outer cell layers of the bulb and those higher up in the hair follicle shaft (Joost et al., 2016). The existence of different spatial niches in hair follicles was previously reported, but confirmation by scRNA-seq can be useful by providing the entire transcriptomic differences that coincide with the otherwise limited protein expression diversity that was known (Schepeler et al., 2014).

### **1.2.12 Melanocytes**

Melanocytes are found in the basal layer of the epidermis and produce the pigment melanin to protect against UV exposure. Melanocytes are rarer than keratinocytes, found at a 1:10 ratio in the basal layer (Cichorek et al., 2013). They produce melanin through a process called melanogenesis in organelles called melanosomes, and can use their dendritic morphology to transfer these organelles to neighbouring keratinocytes (Singh et al., 2017). Melanogenesis is a pathway involving the enzymes tyrosinase (TYR) and tyrosinase related proteins 1 and 2 (TYRP1/2), which convert the amino acid tyrosine into eumelanin or pheomelanin (Cichorek et al., 2013).

Melanocytes differentiate from pluripotent embryonic neural crest cells via an intermediate melanoblast stage (Adameyko et al., 2009). Pluripotent embryonic neural crest cells can also differentiate into Schwann cells (Adameyko et al., 2009). In adult skin melanocytes can be replaced by self-renewing hair follicle precursors (Nishimura et al., 2002).

### **1.2.13 Merkel Cells**

Skin is innervated with sympathetic, parasympathetic and sensory neurons. These neurons are found in the dermis. Merkel cells in the basal layer of the epidermis are soft touch receptors, innervated by dermal sensory neurons which reach the basement membrane. They are found primarily in touch sensitive thick skin (Morrison et al., 2009).

Murine studies have shown that Merkel cells use Piezo2, an ion channel activated by mechanical force, to initiate an action potential (Woo et al., 2015). Atoh1 expression is also important for Merkel cell function, as skin from mouse knockouts for Atoh1 lack Merkel cells, and does not respond to soft touch with sensory neuron firing patterns (Maricich et al., 2009).

Merkel cells are not well studied with single cell techniques, partly due to their scarcity and the difficulty of isolating them from human skin. They are primarily studied using either murine Merkel cells, which are more frequent than human Merkel cells – particularly in whisker follicles; or Merkel cell carcinoma samples, which may not reflect healthy skin Merkel cell phenotypes and will include bulk analysis contamination from other epidermal cell types (Wright et al., 2017; Knepper et al., 2019). Because much of what is understood about Merkel cells arises from cancerous tissue, there is room in the literature to hone in on the expression profiles and functionality of these cells in healthy skin.

## **1.3 Epidermal Immune Cells**

The epidermis is one of the largest organs by surface area and the first point of contact for the vast majority of foreign bodies, antigens both harmful and inert, and pathogens. As such it is a specialised site of immunological defence, requiring a diverse array of immune cells capable of maintaining the homeostatic balance of inflammation and tolerance.

### **1.3.1 Langerhans Cells**

LCs are found in the epidermis, in which they are the primary antigen presenting cell (APC) subset. They process epidermal antigens and migrate to skin draining lymph nodes in order to activate specific T cell responses (Furio et al., 2010). LCs have dendrites which increase their surface area for antigen capture and presentation. They can be characterised by their expression of CD1a, CD1c, langerin and Birbeck granules (Valladeau et al., 2000). Due to their similar ontogeny to macrophages, LCs are often described as a subset of macrophages (Guilliams et al., 2014). They have also been grouped together with dermal conventional dendritic cells (cDCs) due to sharing many common gene signatures, although they remain to be transcriptomically distinct (Carpentier et al., 2016).

As with dendritic cells, LCs are professional antigen presenting cells and express high levels of MHC class II (Bertram et al., 2019). They are capable of CCR7 mediated migration, and express cDC gene signatures such as the transcription factor *Zbtb46* (Deckers et al., 2018). However, they also display macrophage qualities such as FLT3 independent development, self renewal and a developmental dependence on tissue microenvironment signals (Deckers et al., 2018).

LCs are commonly distinguished from other skin cells by the expression of langerin (CD207) – a C-type lectin involved in antigen presentation (Valladeau et al., 2000; Hunger et al., 2004). Langerin is expressed on the cell surface membrane and collects in LC-specific organelles called Birbeck granules after interacting with antigens. High expression of CD1 family proteins, particularly CD1a and CD1c, also allows LCs to effectively present lipid antigens to T cells in skin draining lymph nodes. In common with all APCs, LCs express high levels of MHC class II. They also express high levels of FcεR1, a receptor for the heavy chain of IgE, which mediates inflammatory allergy responses in mast cells (Shin & Greer, 2015). In LCs, this process results in the secretion of both inflammatory cytokines such as TNFα and interleukin (IL)6 as well as anti-inflammatory cytokines such as IL10, suggesting that FcεR1 expression on LCs contributes towards the maintenance of homeostatic inflammatory balance (Shin & Greer, 2015). Further experiments have shown that FcεR1 may also improve antigen presentation efficiency of IgE-bound antigens (Shin & Greer, 2015). Often, however, studies into LCs analyse all

CD1a or langerin expressing skin cells (Patterson et al., 2002; Greter et al., 2012), which may misrepresent the true extent of epidermal cell heterogeneity (Bertram et al., 2019).

Yolk sac-derived LC precursors seed the epidermis during embryonic haematopoiesis (Gomez Perdiguero et al., 2015). In addition, in late embryogenesis foetal liver haematopoiesis produces monocytes which can migrate to skin and also differentiate into LCs (Hoeffel et al., 2012). LCs of both origins are capable of self-renewal throughout adulthood, which has been shown in mouse (Hoeffel et al., 2012; Merad et al., 2002). After LC migration in response to inflammation, skin LCs can be replaced by monocyte-derived LCs from circulating monocytes and inflammation-induced LC proliferation (Collin et al., 2006; Deckers et al., 2018; Chorro et al., 2009).

Langerhans cells, as tissue resident APCs, differ from circulating dendritic cells (DCs) in part due to their microenvironment. It could be speculated that, as the most common cell type in the epidermis, keratinocytes provide the signals and interactions that shape LC phenotype. For example LC expression of EpCAM, a homotypic adhesion molecule, allows LCs to bind to other epidermal cells, in particular keratinocytes (Deckers et al., 2018). Furthermore, keratinocytes secrete IL34 which binds to colony stimulating factor 1 receptor (CSF1R) on LCs, contributing to their differentiation and self-renewal (Wang et al., 2012). Keratinocytes can also secrete CCL20, a chemokine that can attract monocyte derived LCs to reseed the epidermis after inflammation (Harper et al., 2009).

LCs are capable of migration across the basement membrane to the dermis, and subsequently to the lymphatics (Ohl et al., 2004). Upregulation of CCR7 in response to infection facilitates lymphatic homing by lymphatic endothelial-mediated CCL21 chemoattraction (Ohl et al., 2004; Ouweland et al., 2010). Ohl *et al.* have shown with CCR7 knockout mice that CCR7 is not required for basement membrane trafficking (Ohl et al., 2004). Yoshino *et al.* have shown that this trafficking occurs in steady state as well as inflammation, suggesting that LCs may continuously survey healthy skin for antigens (Yoshino et al., 2003).

### **1.3.2 Inflammatory Dendritic Epidermal Cells**

Non-LC dendritic cells are also found in human epidermis during inflammation.

Inflammatory dendritic epidermal cells (IDECs) were first characterised in eczema and psoriasis skin as CD1a<sup>low</sup> FcεR1<sup>high</sup> (and later shown to be CD207<sup>-</sup> (Yoshida et al., 2014)) DCs lacking other LC characteristics like Birbeck granules (Wollenberg et al., 1996).

IDECs are DCs which infiltrate skin during local inflammation (Yoshida et al., 2014). IDEC origins are particularly challenging to confirm in human without the use of lineage tracing or live imaging techniques that can be used in mouse models, but model cells with an IDEC phenotype have been generated from human monocyte-derived DCs by treatment with reducing agents (Dijkstra et al., 2008; Novak et al., 2002).

IDECs are primarily found in the basal layer of the epidermis, having migrated from dermal vasculature, whereas LCs are mostly suprabasal, being positioned for early sensing of antigens breaching the skin surface (Otsuka et al., 2018). This difference in antigen sensing is further supported by Yoshida *et al.*'s finding that, unlike LCs, IDEC dendrites do not penetrate the tight junctions to the stratum corneum (Yoshida et al., 2014). IDECs have high levels of mannose receptor expression and endosomes, both of which are associated with high antigen uptake and presentation in macrophages (Wollenberg et al., 2002). IDECs also display a proinflammatory cytokine profile, with *in vivo* culture models having been shown to secrete Th1-inducing IL12 and IL18 cytokines (Novak, Valenta, et al., 2004).

### 1.3.3 Epidermal T cells

T cells are a vital part of skins immunological defence, with resident memory T cells constantly surveilling for their cognate pathogenic antigens. While the majority of blood T cells are circulating naïve T cells, in skin most are resident memory T cells which persist outside of infection without circulating (Clark et al., 2006). T cell skin homing occurs in T cells which were activated in skin draining lymph nodes and is facilitated by expression of cutaneous lymphoid antigen (CLA), which aids vascular extravasation by adhesion to endothelial selectins, and the chemokine receptor CCR4, as well as CCR10 on a subset of skin homing T cells (Matsuo, Nagakubo, et al., 2018, p.4; Soler et al., 2003, p.4). Naïve CD45RA<sup>+</sup> T cells can also be found in skin at low levels (Cose et al., 2006).



T cells are further divided into CD8+ cytotoxic (Tc), CD4+ helper (Th) and FOXP3+ regulatory (Treg) T cells, all of which are found within healthy skin (Sabat et al., 2019). Most T cells in skin express the alpha and beta T cell receptor (TCR) chains, and as such are called  $\alpha\beta$  T cells. A rare  $\gamma\delta$  T cell subset also exists in skin. In mouse these epidermal  $\gamma\delta$  T cells are named dendritic epidermal T cells, and display unique functional roles in wound healing (MacLeod et al., 2013).

The lymphocyte compartment of skin is partially shaped by the skin microbiome. Homeostatic immune responses occur in steady state as epidermal T cells must recognise and respond to the skin microbiota without mounting inappropriate or excessive inflammatory responses (Tamoutounour et al., 2019). The skin lymphocyte compartment relies on this homeostatic interplay for its development, and it has been shown in mice that an absence of skin microbiota results in heavily altered T cell phenotypes (Naik et al., 2012). Commensal bacteria are also involved in the localisation of skin T cells. High numbers of Treg cells become localised to hair follicles where more microbes are found (Sanchez Rodriguez et al., 2014; Belkaid & Harrison, 2017). Little research has been done on the differences between dermal and epidermal T cells in regards to epidermal access to the skin microbiome, and this could potentially be an interesting avenue to investigate through single cell research.

## **1.4 Cellular Anatomy of the Dermis**

The dermis is the deeper layer of skin, below the superficial epidermis. It is much less cellularly dense than the epidermis, comprising primarily extracellular matrix and the fibroblasts producing and maintaining it. It is split into two distinct regions: the apical papillary dermis, which follows the peaks and troughs of the epidermal papillae, and the reticular dermis, approximately 100 $\mu$ m below the DEJ (Philippeos et al., 2018). The dermis is supplied by blood and lymphatic vessels, and is innervated at touch-sensitive skin sites. This direct blood supply also provides the dermis with leukocyte access, including dendritic cell and monocyte influx during inflammatory conditions.

### **1.4.1 Fibroblasts**

Fibroblasts produce and maintain the collagenous extracellular matrix that makes up the structure of the dermis. As well as homeostatic ECM maintenance, this involves wound healing and scarring during skin perturbation (Rinkevich et al., 2015). Fibroblasts also have a variety of other homeostatic and inflammatory functions including cytokine and chemokine secretion in response to inflammation, and homeostatic tissue signal production.

The dermal extracellular matrix consists primarily of collagens and elastins. Dermal fibroblasts produce a wide array of collagen subtypes including types I, III, IV, V, VI and VII, each with different physical properties which give the strength required for the ECM (Tracy et al., 2016). Elastin produced by fibroblasts is formed into the elastic fibres that provide elasticity to skin (Rnjak-Kovacina & Weiss, 2013). Fibroblasts also continue to maintain the ECM through the production of ECM-specific proteases including matrix metalloproteinases (MMPs) and A disintegrin and metalloproteinases (ADAMs), individual members of which degrade different ECM proteins (Bonnans et al., 2014).

During wound healing and infection, dermal fibroblasts aid in immune and inflammatory responses. Production of proinflammatory cytokines including TNF $\alpha$  and IL6, and chemokines including CCL1, help to directly address infection, modulate the immune response and recruit APCs to sites of potential infection (Fahey et al., 1995; Yaszay et al., 2001; Bautista-Hernández et al., 2017).

Fibroblast heterogeneity is reported on multiple levels. Spatial heterogeneity exists between fibroblasts found in the papillary and reticular dermis. Driskell *et al.* report functional heterogeneity during wound healing: wounded mouse skin required CD26+ papillary fibroblasts for hair follicle repair, and Dlk1+Sca1- reticular fibroblasts for dermal ECM repair (Driskell et al., 2013). Phillippeos *et al.* later sorted for these two mouse fibroblast subsets and, using microarray analysis, reported gene ontology terms of ECM organization and Wnt signalling for reticular and papillary fibroblasts respectively (Phillippeos et al., 2018). Functional heterogeneity is also reported within these spatial groups as well. Tabib *et al.* actually report that, by single cell RNA sequencing analysis, human fibroblasts do not appear to group at all by papillary vs

reticular and instead cells from both compartments were mainly separated by transcript expression of homeostatic vs fibrotic ECM production genes (Tabib et al., 2018a). This could perhaps suggest that these spatial differences are exacerbated by other microenvironmental signals during wounding.

#### **1.4.2 Vascular endothelium**

The epidermis is avascular and exchanges nutrients via diffusion from the dermis to the basal layers. The increasingly superficial layers of epidermis are composed of decreasingly viable cells through keratinisation, matching nutrient supply with demand. The dermis, however, is heavily vascularised.

Arterioles run through the dermis ~1mm deep and parallel to the surface (Braverman, 2000). These supply vascular capillaries, a single vessel of which loops and branches out into each of the dermal papilla before joining the collecting venule. Dermal capillaries consist of a monolayer of vascular endothelial cells surrounded by a basement membrane, with interspersed pericytes attached to the apical surface.

The primary function of dermal endothelium is to facilitate water and nutrient exchange with the cells in skin. This is facilitated by the expression of various aquaporins and ion transport channels on the surface of endothelial cells (Verkman, 2002). Dermal capillaries are also surrounded in a basement membrane made primarily of collagen IV produced by the endothelial cells it surrounds. This is anchored to the endothelial cells by integrins such as the integrin alpha 6/beta4 complex, and keeps the capillaries in place by attaching to collagen VII in the ECM (Watanabe et al., 2018; Tani et al., 1996).

Extravasation is a vital function for the resolution of infection via inflammation, as well as for immune system homeostasis in skin. The passage of leukocytes into skin is mediated by vascular endothelial cells and their protein expression profiles. This is a four-step process: chemoattraction, rolling adhesion, hard adhesion and transmigration. Chemoattraction is the process of attracting cells down a chemical gradient. Endothelial cells secrete chemokines, particularly in inflammatory conditions, such as CCL2 and IL8, to attract leukocytes expressing CCR2 and CXCR1 respectively (Goebeler et al., 1997).

Rolling adhesion is mediated by weakly binding adhesion molecules such as E-selectin (SELE) and P-selectin (SELP), which slow the leukocytes to be trafficked (McEver & Zhu, 2010). This aids more strongly binding adhesion molecules, such as intracellular adhesion molecule 1 (ICAM1) and vascular adhesion molecule 1 (VCAM1), to initiate hard adhesion, arresting cell movement and attaching it to the endothelium (Cook-Mills et al., 2011). Finally, transmigration occurs, allowing a cell to pass through either the cytoplasm of an endothelial cell or to pass between endothelial cells (Feng et al., 1998). This is mediated by endothelial cell expression of proteins such as CD31, CD99 and F11R, and blocking these proteins can prevent transmigration *in vivo* (Schenkel et al., 2002; Qing et al., 2001; Woodfin et al., 2011).

Increases in leukocyte trafficking are required during times of immune challenge and inflammation, and are a result of upregulation of the proteins that facilitate extravasation. The mechanisms behind this rely on cell to cell communication occurring within the dermis or through the blood. TNF $\alpha$  reception by vascular endothelial cells induces highly increased expression of adhesion molecules VCAM1, ICAM1, and SELE as well as cytokines including IL8 and monocyte-attracting CCL2 (Xia et al., 1998; Yang et al., 2009; Makó et al., 2010).

Demyanets *et al.* show that IL33 mediates a similar effect via interaction with IL1 receptor like 1 (IL1RL1/ST2) rather than the IL1 receptor, increasing surface expression of VCAM1, ICAM1 and SELE as well as secretion of CCL2, IL6 and IL8 (Demyanets Svitlana et al., 2011), and Puhlmann *et al.* report that the same proteins can be upregulated on endothelial cells by IL1 $\beta$  (Puhlmann et al., 2005), although O'Carroll *et al.* report that the relative upregulation of each protein varies between each stimulus in brain microvasculature (O'Carroll et al., 2015), which likely holds true for dermis as well.

These cytokines can come systemically from the blood, or from other cell types within skin during local inflammation. UVB induced inflammation causes production of TNF $\alpha$  by keratinocytes and fibroblasts (although fibroblasts first require IL1 $\alpha$  co-stimulation), as well as pro-inflammatory inducible nitrogen oxide synthase (iNOS) production in endothelial cells, which is further increased by the detection of TNF $\alpha$  (Clingen et al.,

2001; Fujisawa et al., 1997; Suschek et al., 2004). An increase in TNF $\alpha$  production from keratinocytes has also been observed in lesional psoriatic skin (Johansen et al., 2006). Inflammatory skin diseases such as psoriasis and eczema can be powerful models for the effects of general skin inflammation, which can only otherwise be directly modelled in animal models.

Leukocyte trafficking primarily occurs in the venular ends of capillaries. It is unknown exactly how this specificity is regulated, but there is experimental evidence towards two mechanisms. The first is the reduced hydrodynamic forces from blood flow, which may control protein expression on endothelium via shear stress (Cicha et al., 2009; Young et al., 2009). The second is heterogeneity in gene expression. While there is no morphological division or clearly demarcated midpoint, gene expression differences between the arterial and venular ends of these capillaries have been reported in studies in mice – *ACKR1*, a surface protein that prolongs chemokine secretion, is specific to venular capillaries (Thiriot et al., 2017). There is notable disagreement on this topic, however, as experimental evidence both for (Young et al., 2009) and against (Ley K & Gaehtgens P, 1991) shear-stress induced extravasation control has been published, and hard evidence of transcriptional heterogeneity is recent and limited in scope (Thiriot et al., 2017). Investigating this phenomenon at single cell level could add insight into the vasculature field in general.

### **1.4.3 Pericytes**

Specialised smooth muscle cells called pericytes wrap around and attach to dermal vascular capillaries. Pericytes are found between the vascular basement membrane and the endothelial cells, and are anchored to the endothelial cells by adhesion plaques containing N-cadherin (Bergers & Song, 2005). They interact with vascular endothelial cells via direct cell-cell gap junction contact, which has been shown to be necessary for Transforming growth factor beta (TGF $\beta$ )-induced pericyte differentiation and Platelet-derived growth factor subunit B (PDGF-B)-induced pericyte recruitment, to give two examples (Zonneville et al., 2018; Hellstrom et al., 1999).

The main function of pericytes is that of small vessel vascular smooth muscle cells: to modulate blood flow through capillaries by contracting and relaxing to cause vasoconstriction and vasodilation in capillaries. They have also been proposed to guide angiogenesis via chemotactic vascular endothelial growth factor (VEGF) expression and inhibit angiogenesis via CXCR3 secretion, and even to promote efficient wound healing in skin specifically (Bodnar et al., 2016, 2013). They can also act pro-inflammatorily during infection with chemokine production promoting leukocyte skin infiltration, and antigen presentation capabilities to activate T cells (Venetz et al., 2010; Pober et al., 2017).

Pericytes express smooth muscle markers necessary for contraction such as alpha smooth muscle actin, but can be distinguished from skeletal muscle particularly by expression of RGS5, a G-protein signalling regulator expressed specifically in pericytes (Mitchell et al., 2008).

#### **1.4.4 Lymphatic endothelium**

As well as blood capillaries, the dermis is also supplied by a network of lymphatics. These vessels, made of a monolayer of lymphatic endothelial cells, facilitate tissue immune surveillance via the collection of leukocytes from skin to lymph nodes, assisting in antigen presentation. Lymphatic vessels also contribute to a vital portion of interstitial fluid recirculation and the absorption of specific fats and salts from tissue (Escobedo & Oliver, 2017).

Lymphatic capillary vessels are much larger than vascular capillaries (~100µm compared to ~10µm diameter (Wang et al., 2014)). They are subcategorised based on their location and the direction of lymph flow. Afferent lymphatics bring lymph to lymph nodes, and these are found throughout the dermis. Efferent lymphatics take lymph away from lymph nodes (Sawa et al., 2007). These are less common and directly connect lymph nodes or bring circulated nutrients to the vasculature. As efferent lymphatic vessels branch off of lymph nodes, they aren't found in the dermis (Sawa et al., 2007). In the dermis, lymphatic vessels are one-way. Smaller initial lymphatic vessels extend from close to the DEJ to around 500µm deep, draining interstitial fluid and immune cells

(Wang et al., 2014). These converge at larger collecting lymphatics at around 500µm deep, which carry lymph back to the lymph nodes. The larger collecting vessels contain valves to prevent backflow because of the low pressure gradient of the lymphatics, which is mostly circulated by skeletal muscle movement (Wang et al., 2014). Protein expression heterogeneity has been observed between these two types of vessel, which ties into their differing functions. Wang *et al.* found higher levels of CCL21 expression in initial lymphatics, matching their need to attract and collect activated immune cells, as well as increased expression of podoplanin (PDPN) in the collecting vessels (although the exact function of PDPN in lymphatics is not known) and the presence of valves distinguishing the intersect between the two vessel types (Wang et al., 2014; Astarita et al., 2012).

Migration of leukocytes to lymph nodes is facilitated by the secretion of the chemokine CCL21 from lymphatic endothelial cells, which attracts activated DCs and T cells upon their upregulation of the cognate receptor CCR7 (Vaatmeri et al., 2017). Lymphatic nutrient recirculation is aided by expression of various proteins. For example LYVE1, a common cell surface marker of lymphatic endothelial cells, can internalise the dermal ECM component hyaluronan (Lawrance et al., 2016). The interplay between these two seemingly distinct functionalities of lymphatic vessels has yet to be fully explored, a point that is reiterated by Chakraborty *et al.*'s review questioning the link in terms of metabolic syndrome (Chakraborty et al., 2010), and it would be interesting to explore the possibility functional heterogeneity of lymphatic endothelial cells at a single cell level.

#### **1.4.5 Schwann cells**

The dermis is innervated for autonomic control of blood flow, hair follicle movement and gland secretion among other functions, as well as for touch sensation from epidermal merkel cells. The axons of these nerves span throughout the dermis, and the cell bodies reside in the spinal cord. While some mRNA is transported down axons, this does mean that the majority of neural mRNA isn't found in the dermis, which could lead to difficulties in detecting dermal neuron transcripts (Sahoo et al., 2018).

Schwann cells in close contact to these axons are found throughout the dermis and provide supporting functions to dermal neurons. Schwann cells are functionally divided into myelinating and non-myelinating. Myelinating schwann cells tightly surround axons and improve action potential speeds by providing insulation, and inducing saltatory conduction between the myelin gaps (Salzer, 2015). They express the protein constituents of the myelin sheath, including myelin protein zero (MPZ) and myelin basic protein (MBP) (Le et al., 2005). Nonmyelinating schwann cells provide other homeostatic functions to the nerve axons, including axonal maintenance, regeneration and remodelling (Griffin & Thompson, 2008). They express markers not found on myelinating schwann cells including the nerve growth factor receptor p75NTR as well as the adhesion marker NCAM (Gonçalves et al., 2019; Kim et al., 2019).

## **1.5 Dermal antigen presenting cells**

Monocytes, macrophages and dendritic cells are leukocytes which professionally present antigen to T cells in order to initiate immune responses, as well as contributing to immune regulation and general homeostasis via other functions such as phagocytosis and cytokine secretion (Haniffa et al., 2015). APCs are the first responders of the innate immune system, and as the large surface area of skin is constantly exposed to foreign antigens, dermal APCs are particularly important.

APCs are highly heterogeneous across and within tissues, and characterising and labelling particular subsets across studies can be problematic. Subset definition is often classified by surface marker expression, function or ontogeny. APC origin and differentiation has been well mapped in mice, but the picture in humans is still incomplete due to the lesser availability of human samples, heterogeneity within human subsets compounding the ability to accurately resolve progenitors and the complexity of embryonic haematopoiesis and tissue microenvironment contribution making it difficult to track cells from their precursors to their fully differentiated states.

### **1.5.1 Dendritic Cells**



DCs are key initiators of the immune response, linking innate to adaptive immunity by processing antigen in non-lymphoid tissue (NLT) and migrating to lymphoid tissue (LT) to present it to naïve T cells. Their morphology is typically specialised in the form of long reaching dendrites which significantly increase the surface area of the cell, providing increased opportunity for antigen uptake and presentation to take place (Mellman & Steinman, 2001). Peripheral blood DCs are commonly divided into cDCs, which display dendritic morphology and can be further divided into CD141<sup>+</sup> cDC1 DCs and CD1c<sup>+</sup> cDC2 DCs, and plasmacytoid DCs (pDCs), which have a plasma cell-like morphology (Rhodes et al., 2019). In skin, phenotypically similar subsets have been identified (Haniffa et al., 2012). A recent single cell study of human blood by Villani *et al.* has further classified these known DC subsets into six transcriptomically distinct subsets, creating an opportunity to delineate the microenvironmentally-generated differences between skin and blood DCs at a single cell level (Villani et al., 2017).

### **1.5.2 Dermal DCs**

In the skin, DCs are found closer to the surface than macrophages and T cells (Wang et al., 2014). This facilitates their role as immune sentinels, allowing them to sense antigen quickly when pathogens invade the physiological barrier of the skin. Dermal CD141<sup>+</sup> DCs and CD1c<sup>+</sup> DCs are found in the skin, matching the blood cDC1 and cDC2 populations respectively (Haniffa et al., 2012).

### **1.5.3 cDC1s**

In the blood, cDC1 DCs can be identified by the expression of markers that are mostly unique to them, such as CD141, CLEC9A, XCR1 and CADM1 (Carpentier et al., 2016). They are alternately named throughout the literature by marker expression, for example as CD141<sup>+</sup> DCs, or XCR1<sup>+</sup> DCs in mouse (Balan & Dalod, 2016; Breton et al., 2016). They are the least common of the DC subsets within the blood (Balan & Dalod, 2016). cDC1s possess strong cross presentation capabilities, allowing them to present exogenous antigen to CD8<sup>+</sup> T cells on MHC I molecules. cDC1 DCs have been shown to induce both Th1 and Th2 T cell responses depending on the stimulus (Segura et al., 2012).

In the skin, cDC1s migrate to skin draining lymph nodes in order to both present and cross present endogenous and exogenous antigen respectively (Haniffa et al., 2012). They express similar markers to blood cDC1s (Haniffa et al., 2012).

#### **1.5.4 cDC2s**

cDC2 DCs express CD1c, CD11b and CD11c (Plantinga et al., 2013). They are present in much higher numbers than cDC1s and are much more diverse in regards to function and gene expression. It is thought that this is due to either heterogeneity within the subset or the effects of micro-environmental factors and transient changes such as inflammation (Haniffa et al., 2015). It is likely that both factors have an impact on the diversity of cDC2s. They express many pattern recognition receptors (PRRs). This allows for detection of a wide range of pathogens. They also express the anti-fungal proteins CLEC6A and CLEC7A, and can polarise Th1, 2 and 17 responses depending on the stimulus (Lundberg et al., 2013). In skin, cDC2 can upregulate expression of langerin, which could possibly confound the use of langerin as a marker for LCs in whole skin (Bigley et al., 2015).

#### **1.5.5 pDCs**

pDCs share similar morphology to plasma cells. They are commonly identified by expression of CD123, CD303 and CD304 (Boiocchi et al., 2013), although Villani et al show that isolating peripheral blood mononuclear cells (PBMCs) using these markers also captures an AXL+ SIGLEC6+ classical DC subset (Villani et al., 2017). They are specialised towards anti-viral activity. pDCs detect foreign nucleic acids via toll-like receptors (TLRs) 7 and 9, and produce type 1 interferons (IFNs) in response to inhibit viral replication (Kadowaki et al., 2001). Like cDC1s, pDCs can polarise T cells towards either Th1 or Th2 responses (Haniffa et al., 2015).

pDCs are developmentally dependent on the transcription factor E2-2, which upregulates pDC-specific gene expression and simultaneously downregulates genes specific to cDC DCs such as CD11c (Cisse et al., 2008). The requirement of E2-2 for pDC development has been experimentally supported by the loss of pDCs in E2-2 knockout mice (Hansen et al., 2015). pDCs are reportedly absent from the skin in steady state, but

can infiltrate tissue from the blood during inflammation, and are found in inflammatory eczema skin (Novak, Allam, et al., 2004).

### **1.5.6 Macrophages**

Macrophages are noncirculating tissue-specific APCs. Macrophages have high phagocytic activity for defence against pathogens as well as fulfilling a wide range of tissue specific homeostatic requirements. This includes wound healing and extracellular matrix remodelling in the dermis (Okabe & Medzhitov, 2016), regulation of haematopoiesis in the bone marrow (Heideveld & van den Akker, 2017) and synaptic pruning in the central nervous system (CNS) (Hong et al., 2016). Tissue specific macrophages display heterogeneity in the signals required for their differentiation. For example, TGF $\beta$  secreted in the CNS is required, alongside other signals, for microglial differentiation (Butovsky et al., 2014). The transcription factor PPAR- $\gamma$  has been shown to be required for alveolar macrophage development in mice as well (Schneider et al., 2014).

Skin resident macrophages are highly autofluorescent due to the presence of melanin granules within their cytoplasm (Haniffa et al., 2009). They can be identified by expression of CD14, CD11b and FXIIIa (Haniffa et al., 2015). As APCs, macrophages also present antigen to activate T cells, but to a lesser degree than DCs (Tamoutounour et al., 2013).

Tissue resident macrophages were previously thought to arise primarily from circulating monocytes migrating into tissue and differentiating into macrophages (Ginhoux & Guilliams, 2016). It has more recently been made apparent that while this does occur, the relative contribution of monocyte-derived macrophages to tissue resident macrophages is tissue specific, and in most tissues they are not the main contributors of tissue resident macrophages, which have been shown to self-renew from embryonic seeded cells (Hashimoto et al., 2013; Ginhoux & Guilliams, 2016).

### **1.5.7 Monocytes**

Human monocytes are commonly divided into CD14<sup>+</sup> CD16<sup>-</sup>, CD14<sup>-</sup> CD16<sup>+</sup> and CD14<sup>+</sup> CD16<sup>+</sup> subsets (Ziegler-Heitbrock et al., 2010). Identification of further heterogeneity has

since been reported, tangentially to the CD14/CD16 split (Wong et al., 2012), yet human monocytes are still often simplified into these three subsets today (Ong et al., 2019). This surface marker strategy has also been shown, using scRNA-seq on PBMCs, to fail to fully distinguish the transcriptomic states of blood monocytes (Villani et al., 2017). This is one strong example of the need for unbiased high resolution techniques to confidently delineate cellular heterogeneity.

Monocytes are not terminally differentiated, and have the capacity to differentiate into various monocyte-derived cells, including DCs and macrophages (Sprangers et al., 2016). Undifferentiated monocytes are not thought to be found in steady state human skin, but have the potential to migrate into the skin and differentiate into monocyte-derived cells during inflammation *in vivo* (Sprangers et al., 2016).

#### **1.5.8 Monocyte-derived DCs**

Monocyte-derived DCs are found in mouse skin expressing cDC2 transcripts (Tamoutounour et al., 2013). They have not been isolated from human skin and instead are widely studied as *in vitro* derived cells by culturing monocytes with IL4 and GM-CSF (Saalbach et al., 2015; Williams et al., 2017), but they are thought to be CD14<sup>+</sup> CD1c<sup>+</sup>, a cell compartment which has not yet been fully categorised in human skin (Durand & Segura, 2015). It is also possible that they are transient with inflammation, and that circulating monocytes infiltrate the skin to add to the DC pool as a response to inflammation.

#### **1.5.9 Monocyte-derived macrophages**

Skin resident monocyte-derived macrophages are CD14<sup>+</sup>, and unlike embryonic HSC derived macrophages are negative for autofluorescence (McGovern et al., 2014). These cells aren't found in patients suffering from an IRF8 mutation which results in a total lack of monocytes, supporting their lineage as monocyte-derived cells (Hambleton et al., 2011; McGovern et al., 2014). Monocyte-derived macrophages were previously attributed to being dermal DCs due to expression of DC markers including CD141, which is no longer thought to be the case (McGovern et al., 2014).

Inflammation causes the transient development of various subsets of APCs with different phenotypes to steady state subsets (Chu et al., 2011). These cells have been difficult to study due to their transient nature. Studies into inflammatory events in humans are particularly challenging as the exact points of immune system challenge and resolution cannot be easily tracked. Parallels can be drawn from studying inflammatory skin conditions and the differences in the immune compartment to healthy skin. TNF- and iNOS-producing DCs (TIP-DCs) are present in psoriatic skin, where they agitate symptoms by secreting pro-inflammatory TNF and iNOS (Chu et al., 2011).

## **1.6 Dermal lymphoid cells**

### **1.6.1 Microenvironmental differences between Dermal and Epidermal T cells**

T cells in skin are found in both the epidermis and dermis, and few specific differences between these populations have been highlighted in the literature. Dermal T cells largely match the previous description of epidermal T cells, however the dermis contains many more T cells than the epidermis due to the presence of dermal vascular and lymphatic capillaries (Gebhardt et al., 2011). Wang *et al.* showed using whole mount immunofluorescence microscopy that while T cells were found throughout the papillary dermis, they were much more common 40-60µm below the DEJ, deeper on average than dermal DCs (Wang et al., 2014). Deeper into the reticular dermis, T cells were almost entirely perivascular, being found close to blood vessels (Wang et al., 2014). Epidermal T cells are found close to the basement membrane (Clark et al., 2006). CD103-resident memory T cells are more common in the dermis as opposed to CD103+ T cells residing in the epidermis, a phenotype which is upregulated by keratinocyte co-culture, and results in increased secretion of cytokines including INF $\gamma$  and TNF $\alpha$  (Watanabe et al., 2015).

### **1.6.2 Innate lymphoid cells**

Multiple subsets of innate lymphoid cells reside in the dermis, primarily natural killer (NK) cells and ILC1/2/3, which mirror the adaptive functions of Tc and Th cells respectively. Skin NK cells recognise virally infected cells through the expression of receptors including killer cell immunoglobulin-like receptors (KIRs), primarily detecting

the loss of MHC class I expression in infected cells (Campbell & Purdy, 2011). They respond to these cells through the secretion of granzymes and perforin, which lyse the target cells (Pardo et al., 2002). Natural killer T (NKT) cells have also been reported in skin, which express TCR on their surface, unlike other NK cells (Balato et al., 2009). NKTs recognise CD1 presentation of lipid antigens, and reportedly infiltrate psoriasis and eczema affected skin (Gober et al., 2008).

ILC1/2/3 are analogous to innate Th cells in that they modulate inflammation through cytokine secretion. Three ILC subsets (ILC1, ILC2 and ILC3) are reported in various connective and mucosal tissues (Kim, 2015). ILC1s produce IFN-gamma in response to IL12 and IL15, and can display cytotoxic properties similarly to CD8 T cells and NK cells (Fuchs et al., 2013). ILC2s express IL1RL1, allowing recognition of IL33, and secrete proinflammatory cytokines including IL5 and IL13 (Kim et al., 2013). ILC3 are mainly found within mucosal tissue, and secrete IL22 to induce antimicrobial protein expression in nonimmune cells (Cella et al., 2009; Fuchs et al., 2013).

### **1.6.3 Mast cells**

Mast cells are tissue resident leukocytes which are found in low numbers in close proximity to dermal blood vessels (Janssens et al., 2005). Mast cells contribute to both innate and adaptive immune responses in skin. Adaptive responses occur via IgE antigen recognition, mediated by FcεRI expressed on the surface of mast cells (Douaiher et al., 2014). Antigen recognition causes degranulation, whereby mast cells release high quantities of inflammatory granules. These contain proteases which break down the ECM and DEJ (Kaminska et al., 1999). Histamine release from these granules increases vascular permeability, which combined with chemokine and cytokine secretion, as well as mast cell spatial proximity to the vasculature, promotes leukocyte migration into the dermis (Gurish et al., 1991; Ashina et al., 2015). Inappropriate mast cell degranulation in response to inert antigens is a critical mechanism behind allergic responses as well as some autoimmune diseases (Douaiher et al., 2014).

Mast cells can also mediate inflammation innately by responding to pathogen-associated molecular patterns (PAMPs) binding to TLRs (Matsushima et al., 2004). This

causes secretion of inflammatory mediators including TNF $\alpha$  and IL13, without resulting in degranulation (Matsushima et al., 2004). Stratification between innate and adaptive mast cells has not been reported, and it is not specifically known whether the same mast cell can respond with equal vim to IgE crosslinking as to PAMP recognition. Protein expression heterogeneity has been reported in dermal mast cells – for example, CD25- mast cells appear to have increased migration capacity (Deho' et al., 2014). Mucosal mast cells differentiate from the same circulating precursor as skin mast cells, but tissue-specific differences in protease contents have been shown (Gurish & Austen, 2012). Despite these findings, as of yet there is no widely accepted categorisation of dermal mast cell subsets.

Mast cells can infiltrate into the epidermis during skin inflammation, and this occurs in inflammatory skin diseases including eczema (Sehra et al., 2016). Sehra *et al.* showed that mast cell-deficient mice produced less keratinocyte terminal differentiation proteins, such as filaggrin and involucrin, and therefore had reduced barrier function (Sehra et al., 2016). This suggests that epidermal mast cells in eczema may be part of a protective response rather than a cause of the inflammation. The relationship between dermal and epidermal mast cells in inflammatory skin conditions has not been fully explored, and a better understanding of whether all skin mast cells, or only a subset, are capable of supporting keratinocyte terminal differentiation, could be relevant for the treatment of such skin conditions.

There are a wide array of cell types, subtypes and cell states reported in skin, and although a lot of heterogeneity is reported in marker expression and function of these cells, there have been relatively few definitive studies correlating these findings and unambiguously categorising all of the cell types in skin. High dimensional single cell analytical techniques are one approach with which this could be achieved.

## **1.7 High Dimensional Single Cell Analysis Technologies**

Techniques for high dimensional analysis of single cells have been advancing rapidly in recent years. There are multiple techniques with different advantages, disadvantages and data outputs that can be best used in a complementary fashion, and this thesis will be focussing on the use of cytometry by time of flight (CyTOF) and scRNA-seq to distinguish heterogeneity at the single cell level of proteomic and transcriptomic expression respectively.

### **1.7.1 CyTOF**

Mass cytometry, or CyTOF, is a technique derived from flow cytometry which allows for the simultaneous detection of more markers. In theory this could go up to 100 markers, but in practice due to the constraints of available metal tags the upper limit is around 40 (Tanner et al., 2013; Giesen et al., 2014; Yao et al., 2014). This can be further increased by running concurrent barcoded samples with overlapping panels. The basics of the technique involve staining fixed and permeabilized cells with antibodies bound to metal isotopes of specific unique molecular masses, then vaporising individual cells and passing the surviving metal contents through a mass spectrometer (Tanner et al., 2013). This detects the molecular mass of the metals present in each cell, which determines the equivalent markers that were present on, or within, the cell.

CyTOF drastically lowers the issue of spectral overlap that occurs in flow cytometry as, unlike the broad absorption and emission spectra in flow cytometry, the readouts are well defined mass integers. However, this comes with separate compensation issues. 'Spill over' can occur due to the sensitivity of the machine within a mass difference of +/- 1. This is also compounded by isotopic impurities in the metals used. Metal oxidation



can also result in mass values of +16 (Tanner et al., 2013). Unlike flow cytometry compensation, these spill overs are difficult to remove computationally, however the percentages of isotopic impurities and oxidation are universal physical properties of these elements, so accounting for them with clever panel design is possible (Tanner et al., 2013). Ensuring that, when relative expression is known, abundantly expressed markers are not placed in adjacent mass channels to rarely expressed markers will reduce the impact of mass channel spill over (Tanner et al., 2013). The lack of light scattering properties by CyTOF removes some valuable data provided by flow cytometry. Cell size and the presence of doublets are much harder to verify as a result.

CytoF is also much slower than flow cytometry, and as the cells are vaporised they cannot be sorted for downstream functional studies. The size of the metals conjugated to antibodies also reduces the number of antibodies that can physically bind to each cell, reducing the separation between cells with low and high marker expression. These issues potentially limit the data output of CyTOF.

Alcántara-Hernández *et al.* used mass cytometry to profile the DC compartment from skin, blood, spleen and tonsil (Alcántara-Hernández et al., 2017). They identified that pDC-like AXL+ DCs aren't found in healthy human skin (Alcántara-Hernández et al., 2017). This finding is noteworthy as these cells were only recently identified as distinct from pDCs (Villani et al., 2017), and pDCs are also reportedly absent in healthy skin. Investigating the presence or absence of skin AXL+ DCs in a disease setting where pDCs are found in skin, such as psoriasis (Nestle et al., 2005), could shed further light on the cells' possible functionality. The authors also identify a mismatch in published mRNA expression of CLEC9A in skin cDC1 with a lack of protein expression in these cells (Alcántara-Hernández et al., 2017). This finding highlights that direct cross-technology study of protein and mRNA expression could provide a lot of power to future research of all skin cell subsets.

### **1.7.2 Single Cell RNA Sequencing**

scRNA-seq allows for the interrogation of cell populations in a less biased fashion than other cell analysis techniques by relying on all or most of a cell's transcribed mRNA,

which better reflects the functional capabilities of a cell than selected surface protein markers. Analysing RNA content per single cell also overcomes the limitations of bulk analysis, whereby populations with specific properties are indistinguishable from the tissue as a whole, and these properties are either drowned out or incorrectly attributed to a more common cell type.

scRNA-seq experiments involve three steps: single cell separation, sequencing, and analysis. The development of improved techniques usually focusses on the single cell separation stage, where time, cost and cell recovery are important variables, although the use of different primers and enzymes also has knock-on effects on the cDNA quality at sequencing. Over recent years many bespoke and commercial scRNA-seq technologies have emerged with the aims of reducing cost and increasing throughput (Tang et al., 2009; Picelli et al., 2014; Hughes et al., 2019).

The experimental steps leading up to single cell separation can have large effects on the quality of the final data. While cell suspensions such as PBMCs need minimal preparation, tissues like skin need to be first dissociated to a single cell suspension. Enzymatic treatments including trypsin and collagenase are common, and often require 37°C incubation which can impact cell phenotype and transcriptome (O’Flanagan et al., 2019; Botting et al., 2017). After dissociation, removal of low quality cells (dead or dying cells and doublets) greatly improves data quality, as computational removal of these cells is more difficult, and this also increases the cost efficiency of sequencing. These steps are often done using fluorescence activated cell sorting (FACS) or magnetic bead separation steps, and an important consideration when removing cells is balancing the introduction of biases into the data via pre-selection with ensuring data quality is high.

The single cell separation step involves segregating each cell before lysis, and barcoding each mRNA molecule so that it can be computationally attributed to its cell of origin. There are many methods available to date, but most fall under plate-based or droplet based separation. Plate based approaches use methods such as FACS, or even manual pipetting under a microscope, to place one cell into each well of a plate. Droplet based

approaches make use of microfluidics and concentration calculations to estimate the capture of one cell per stream droplet, similarly to flow cytometry.

Reverse transcription, library preparation, PCR amplification and sequencing are required in the same manner as bulk RNA sequencing. Pooling of single cell material can occur before or after library preparation, depending on when barcoding occurs in the specific protocol used. After sequencing, the raw data is stored as fastq files, which have to be aligned to a reference genome.

### **1.7.3 Analysis of single cell RNA sequencing data**

The resulting data is represented as a count table of single cells against genes, with each cell of the table containing the unique molecular identifier (UMI) count of one gene in one cell. With scRNA-seq experiments typically analysing thousands to hundreds of thousands of cells, and thousands of genes per cell, this results in enormous datasets, which are impossible to visualise, and are computationally demanding to analyse without first simplifying the data. Much of scRNA-seq data analysis can be described as the simplification and visualisation of high dimensional data into fewer dimensions.

The data must be normalised so that highly expressed genes do not drown out uncommon genes in downstream analysis. Low quality data must be filtered out, which usually involves the removal of cells with low gene counts, which are likely to be low quality; cells with high mitochondrial gene expression, which are often dying cells releasing their mitochondrial contents into the cytoplasm; and genes found in very few cells, which may be erroneously mapped (Luecken & Theis, 2019).

After normalisation and quality control (QC), principal component analysis (PCA) is computed. This generates new dimensions (principal components (PCs)) by summarising the most variable aspects in the data. In this way the first PC will be a numerical product of the genes responsible for the most variance in the scRNA-seq dataset, the second PC will account for the next set of high variance genes and so on. PCA results in a dataset with tens of dimensions (one per PC) from a dataset with thousands of dimensions (one per gene). Finally, to identify populations of transcriptomically similar cells in an

unbiased way, the data is clustered. Cells with similar PCA data are grouped together into discrete clusters, which can be compared and contrasted to annotate the cell types they represent by looking at the genes which are differentially expressed between each cluster (Luecken & Theis, 2019). Each of these steps can be performed using a variety of methods with different pros and cons, and in recent years, new computational packages for scRNA-seq analysis are frequently developed.

#### **1.7.4 Interpretation of single cell RNA sequencing data**

After scRNA-seq raw data is analysed, the result is a set of clusters, each labelled with an integer. To impose biological meaning on these clusters, gene expression must be interpreted. As the data contains expression values for thousands of genes in each cell in each cluster, annotation is often done by interpreting the most differentially expressed genes between clusters, which represent the transcripts that identify cells in one cluster as functionally different to cells in other clusters. Differential gene expression is also often simplified down to the average expression level in a cluster, and the percentage of cells within a cluster expressing the gene.

The results of differential gene expression analysis depend on context. The differential expression of each cluster is determined by the cells in the other clusters it is compared with. Iterative rounds of annotation and re-clustering can be useful as, in a diverse set of cells, distinct cell types such as immune cells and stromal cells will be readily segregated. However, minute differences between similar immune cells will be masked by the much greater variance in the dataset, such as immune versus nonimmune. Re-clustering and re-analysing only immune cells in this case could reveal further heterogeneity.

There is also merit to analysing the highest expressed genes in each cluster independently of the rest of the data. This will be much more consistent, as it does not depend on context, although biologically meaningful data may be masked by high ubiquitous expression, for example of housekeeping genes (Miao et al., 2020).

Applying biological interpretation to the data can be done manually, by comparing gene expression to published literature of each gene. This is very time consuming, but

integrating published information about a gene within and without the context of the analysed tissue can result in very focussed findings. This is however prone to introducing bias in two major ways, either from the available published data or from the interpreting scientist. Introducing bias from *a priori* knowledge is against the core principles of most scRNA-seq experiments, but is necessary to some extent, as the gene expression data is meaningless without the functional implications of expressing these genes. Because such manual comparisons are difficult to quantify, the individual interpreting the data may also be inadvertently swayed towards, or even actively seek out, papers that agree with their theories.

Automated approaches to annotation are also readily available, such as using gene ontology tools to analyse the common functionalities of all genes in a differentially expressed gene set. These methods reduce interpretation bias, but ultimately the *a priori* knowledge bias still exists, in the form of the particular database of assigned gene ontologies used, rather than in the meaning assigned through manual analysis of papers. There is a need to use known information about gene markers to annotate single cell data, which inevitably introduces biases. This should be considered and balanced in a way that doesn't rule out novel findings, nor force them.

## **1.8 Single cell sequencing protocols**

### **1.8.1 Plate based sequencing**

Smart-seq2 (SS2) is a plate based single cell separation protocol for the generation of high quality, low throughput single cell RNA sequencing data. It involves separation of single cells into each well of a 96-well plate using FACS, and manual library preparation of each cell. It results in full length RNA sequencing via template switching during reverse transcription, reducing the 3' bias introduced by oligo(dT) priming (Picelli et al., 2014). This protocol improves on the original SmartSeq protocol published by the same group in 2012 with various alterations to cell lysis and reverse transcription that improve final cDNA yield. (Ramsköld et al., 2012)

As with all sequencing techniques, SS2 introduces biases into the results. Primarily, amplification is based on the presence of polyadenylation, and so RNA without PolyA tails will not be included in the analysis, in practice meaning only mRNA will be sequenced (Picelli et al., 2014). The main downside to SS2 is the throughput. The maximum number of cells which can be sequenced at once (per sequencer) is eight lanes of multiplexed 96-well plates, giving data for less than a thousand cells (Picelli et al., 2014). Collection and preparation of eight 96 well plates is also an arduous procedure. Data analysis is also difficult, as technical and biological noise is high for single cells and must be accounted for (Picelli et al., 2013).

Apostolidis *et al.* used a modified SS2 protocol to sequence 88 skin cells from one healthy donor and 96 cells from one systemic sclerosis patient (Apostolidis et al., 2018). Analysing the differentially expressed genes between endothelial cells in the two donors, they found two disease-specific markers, *HSPG2* and *APLNR*, that they validate by immunohistochemistry (IHC) and 8 patients by quantitative PCR (qPCR) (Apostolidis et al., 2018). This is a strong use of single cell sequencing to delineate population specific expression differences that would be obscured in bulk sequencing data. The single donor for both normal and disease state makes it difficult to make any statistical conclusions from this single cell data set, although the two genes the paper presents as novel systemic sclerosis markers were tested more rigorously by IHC and qPCR in multiple patients. A similar approach would be required to support other findings in the rest of the single cell skin dataset.

Philippeos *et al.* sorted CD90+/- CD45- CD31- CDH1- cells from human dermis of a single donor, aiming to enrich for fibroblasts, and subsequently sequenced 184 of these cells using SmartSeq2 (Philippeos et al., 2018). Analysis of this data revealed three fibroblast clusters, with differential gene expression characterising *DCN* and *LUM* as pan-fibroblast markers and identifying markers which separate the three clusters. They used these markers to generate a staining panel which confirmed the lack of spatial distinction between these fibroblast identities (Philippeos et al., 2018).

## **1.8.2 Droplet based sequencing**

Droplet based single cell separation is an automated process using calibrated microfluidics to separate cells into oil droplets (Macosko et al., 2015). This procedure generally trades precision for speed and lower cost. 10x Sequencing is one such protocol for the generation of lower quality, higher throughput scRNA-seq data when compared with plate based approaches such as SS2 (Coombe et al., 2016). The protocol differs in the single cell separation step, which uses a microfluidics machine called the Chromium Controller to rapidly create an emulsion of single cells contained within oil droplets which contain the reagents require for downstream sequencing, such as lysis buffer, as well as uniquely barcoded RNA capture beads. These barcode each RNA strand so that it can be traced back to its original cell post sequencing. This method can separate thousands of cells within a period of about six minutes, without the need for time consuming cell sorting and manual pipetting steps (Coombe et al., 2016). Thousands of cells can be sequenced on each of up to eight lanes simultaneously, allowing for the collection of a large amount of single cell data. However, the read coverage is much lower than SS2 as the entire cDNA fragments within each bead are not read (Goodwin et al., 2016). This results in either a 3' or 5' bias in the data depending on the primer sequences on the RNA capture beads.

Tabib *et al.* used 10x sequencing to profile 8,522 skin cells from six donors (Tabib et al., 2018a). The authors controlled for body site by collecting only mid-forearm skin, but mixed male and female donors. Skin samples were digested using the Miltenyi Biotec Whole Skin Dissociation Kit, and the cell suspension was run through the 10x protocol without dead cell or doublet removal. After clustering analysis, the authors list the cell types found before analysing the fibroblast data alone in further detail. They present their findings as two major subgroups of fibroblasts in human skin, with further heterogeneity within those groups (Tabib et al., 2018a). They also present the lack of correlation between murine and human fibroblast heterogeneity based on murine lineage markers. They confirmed the presence of morphologically distinct fibroblasts expressing either *SFRP2* and *DPP4* or *FMO* and *LSP1* (Tabib et al., 2018a). The authors claim that sequencing 2,742 cells is a high enough number that rare cells are unlikely to have been missed, which is potentially a contentious point. High numbers of rare

populations are required to give the statistical power to resolve the population as a distinct cluster (Luecken & Theis, 2019).

Cheng *et al.* profiled a total of 92,889 single cells from 12 donors: 3 different healthy donors from each of foreskin, scalp and trunk, and 3 inflamed trunk samples (Cheng *et al.*, 2018). The high sample numbers and comparison of healthy skin with inflammatory diseases resulted in the finding of some disease specific gene expression patterns (Cheng *et al.*, 2018). However, the authors had the tissue at 4°C for two days prior to digestion and sequencing. While the low temperature may help to offset this, the long duration *ex vivo* may have caused many transcriptional changes due to stress responses. The lack of reception of normal homeostatic signals from the blood may have also altered tissue gene expression within this time period.

## 1.9 Project Aims

The aim of this project is to use single cell RNA sequencing and mass cytometry to delineate the heterogeneity present in the *a priori* defined cell types of human skin within the literature. By comparing the transcriptomes of all immune and nonimmune cells within skin, the aim is to find the transcripts that best separate human skin cell populations. Mass cytometry will be employed in parallel to compare high dimension protein expression and outline the differences in protein and RNA expression in these cells. This exploratory data generation should generate hypotheses to test further through the possible discovery of previously unreported cell types, as well as by finding potential functions that cells may be performing based on transcript expression. IHC and flow cytometry will be used to validate the protein expression of such interesting findings within the scRNA-seq dataset. To summarise briefly, the aims of this thesis are as follows:

- To investigate skin tissue dissociation for comprehensive capture, high cell recovery and low cell death
- To categorise the cellular heterogeneity in human skin using scRNA-seq
- To compare transcript expression to protein expression using CyTOF
- To validate the findings from scRNA-seq using IHC and flow cytometry





## Chapter 2. Methods



The first mention of a reagent is followed by its supplier and product number in brackets. Each subsequent mention, where this information is not shown, refers to the same product.

## 2.1 Materials

Antibodies used for flow cytometry, CyTOF, IHC and immunofluorescence (IF) are listed in **Table 1** along with their clones and suppliers. Cell washes were performed at 500g for 5 minutes unless otherwise stated. Incubations were performed at 37°C, 5% CO<sub>2</sub> unless otherwise stated. Where not specified, percentage concentrations are v/v.

### 2.1.1 Buffers

- RF-10 media consists of Roswell Park Memorial Institute media (RPMI)(Sigma, R0883) supplemented with 10% foetal calf serum (FCS)(Life technologies, 10270106), 100U/ml Penicillin (Sigma, P0781), 100µg/ml Streptomycin (Sigma, P0781) and 1% L-Glutamine (Sigma, G7513).
- Flow buffer consists of Dulbecco's phosphate buffered saline (PBS)(Sigma, D8537) supplemented with 2% FCS and 2mM EDTA (Sigma, E7889).
- Sort buffer consists of PBS supplemented with 0.5% FCS and 2mM EDTA. Freezing media consists of 10% DMSO (OriGen Biomedical, CP-50) and 90% FCS.
- Wash buffer for CyTOF consists of PBS supplemented with 2% FCS.
- Citrate buffer consists of 0.21% (w/v) citric acid (Sigma, 606081) and 14mM NaOH (Sigma, 221465) made in up water and prior to each experiment was set to pH 6 using a pH meter, 1M HCl (Sigma, 258148) and 1M NaOH.
- Tris buffered saline (TBS) buffer consists of 0.0605% (w/v) Tris HCL (Sigma, T3253), 0.8% (w/v) NaCl and 38mM HCl made in up water and prior to each experiment was set to pH 7.6 using a pH meter, 1M HCl and 1M NaOH.

**Table 1**

<b>Flow Cytometry</b>			
<b><u>Antigen</u></b>	<b><u>Fluorochrome</u></b>	<b><u>Clone</u></b>	<b><u>Manufacturer</u></b>
CD56	FITC	NCAM16.2	BD
CD141	PerCP/Cy5.5	M80	Biolegend
CD31	APC	WM59	Biolegend
CD1a	AF700	HI149	Biolegend
CD11c	APC/Cy7	Bu15	Biolegend
EpCAM	VioBlue	HEA125	Miltenyi
CD3	Bv605	SK7	Biolegend
CD4	Bv711	RPA-T4	Biolegend
HLA-DR	Bv785	L243	Biolegend
CD207	PE	10E2	Biolegend
CD14	PE/Dazzle	HCD14	Biolegend
CD49f	PE/Cy7	GoH3	eBioscience
CD45	BuV395	HI30	BD
CD3	FITC	SK7	BD
CD19	FITC	4G7	BD
CD20	FITC	L27	BD
CCR7	BV605	3D12	BD
CD1c	PE/Cy7	L161	Biolegend
CD34	APC/Cy7	581	Biolegend
CD73	FITC	AD2	BD
ACKR1	PE	NaM185-2C3	BD
SELP	Bv421	AK4	BD
SELE	Bv605	68-5H11	BD
ICAM1	Bv711	HA58	BD

<b>Mass Cytometry (*Custom conjugated using Fluidigm metal kit)</b>			
<b><u>Antigen</u></b>	<b><u>Metal tag</u></b>	<b><u>Clone</u></b>	<b><u>Manufacturer</u></b>
CD45	89Y	HI30	Fluidigm
CD103	*141Pr	Ber-Act8	Biolegend
FoxP3	*142Nd	259D/C7	Biolegend
CD127 (IL-7Ra)	143Nd	A019D5	Fluidigm
CD69	144Nd	FN50	Fluidigm
CD31	145Nd	WM59	Fluidigm
CD203c	*146Nd	NP4D6	Biolegend
CD11c	147Sm	Bu15	Fluidigm
CD34	148Nd	581	Fluidigm
CD25 (IL-2R)	149Sm	2A3	Fluidigm
Siglec 8	*150Nd	7C9	Biolegend

CD14	151Eu	M5E2	Fluidigm
GATA3	*152Sm	TWAI	Biologend
CD62L (L-selectin)	153Eu	DREG-56	Fluidigm
CD3	154Sm	UCHT1	Fluidigm
CD45RA	155Gd	HI100	Fluidigm
CD117 (ckit)	*156Gd	104D2	Biologend
CD123 (IL-3R)	*158Gd	6H6	Biologend
CD161	159Tb	HP-3G10	Fluidigm
Tbet	160Gd	4B10	Fluidigm
CD370 (CLEC9A)	161Dy	8F9	Fluidigm
CD8a	162Dy	RPA-T8	Fluidigm
CD294 (CRTH2)	163Dy	BM16	Fluidigm
CD49F/alpha 1	164Dy	G0H3	Fluidigm
CD163	165Ho	GHI/61	Fluidigm
CD5	*166Er	UCHT2	Biologend
CD197 (CCR7)	167Er	G043H7	Fluidigm
CD73	168Er	AD2	Fluidigm
CD1c/BDCA1	169Tm	AD5-8E7	Miltenyi
CD45RO	*170Er	UCHL1	Biologend
CD56	*171Yb	REA196	Miltenyi
CD15	172Yb	W6D3	Fluidigm
HLA-DR	173Yb	L243	Fluidigm
ROR gamma	*174Yb	REA278	Miltenyi
S100A8/9	*175Lu	CF-145	eBioscience
CD4	176Yb	RPA-T4	Fluidigm
CD16	209Bis	3G8	Fluidigm

IHC/IF			
Antigen	Experiment	Clone	Manufacturer
Keratin 17	IHC		
CD83	IHC	Polyclonal (ab205343)	Abcam
CD83	IF	HB15e	Novus
Wide spectrum keratin	IF	Polyclonal (ab9377)	Abcam
AE1/AE3/PCK26 Pan Keratin	IHC	Polyclonal (760-2595)	Roche
CD31	IF	C31/1395R	Novus
Gamma synuclein	IF	1H10D2	Abcam

**Table 1 – List of antibodies used.** Subtitles refer to the experiment in which each antibody was used. Antibodies that were custom conjugated are shown by an asterisk (\*) before the mass cytometry metal tags.

## **2.2 Generation of single cell suspensions from skin**

Surplus skin from breast reconstruction surgery was collected in accordance with the Newcastle and North Tyneside 1 Research Ethics Committee at the Royal Victoria Infirmary, Newcastle upon Tyne NHS Foundation Trust (Newcastle Dermatology Biobank - REC reference: 08/H0906/95+5). All work on skin tissue was done within class II biological safety cabinets using autoclave-sterilised equipment.

Skin was cut to approximately 3cm wide strips in 4°C PBS and then a 200µm whole skin layer was cut using a dermatome with a Pilling Wecprep blade and a .008 gauge Goulian guard.

### **2.2.1 Preparation of whole skin digest**

For whole skin digestion, following Section 2.2 a grid of slits was then cut into the whole skin sections to aid enzymatic access. Skin was then digested in a 10cm tissue culture dish overnight at 37°C, 5% CO<sub>2</sub> in RF-10 media with 1.6mg/ml type IV collagenase (Worthington, CLS-4). The media was then collected with a serological pipette, pipetted up and down over the remnants of skin, and filtered through a sterile 100µm cell strainer (BD Falcon, 352360). The tissue culture dish and strainer were washed through with RF-10 to collect any remaining cells. Cells were pelleted by centrifuging at 500g for 5 minutes. Supernatant was discarded and the pellet resuspended in 1ml RF-10 by gently pipetting up and down. Cells were then counted by taking off 10µl, mixing 1:1 with 0.4% trypan blue (Sigma, T8154) to stain dead cells and counting on a haemocytometer.

### **2.2.2 Optimisation of collagenase digestion of whole skin**

Skin was prepared as described in Section 2.2.1 with the following changes: Prior to cutting slits for enzymatic access, an 8mm diameter punch biopsy was used to cut volume-matched discs of 200µm thick whole skin. For each of the five dissociation timepoints to test, three punch biopsies were taken, totalling 30mm<sup>3</sup> of skin per timepoint ( $0.2 \times 3 \times \pi 4^2$ ). Three biopsies per tissue culture dish were treated with type IV collagenase and at 2, 4, 6, 8, 10 and 12 hours after adding the collagenase and

incubating, cells from one tissue culture dish were collected as described in Section 2.2.1, and stained for flow cytometry as described below.

### **2.2.3 Dermal and epidermal peeling**

For the generation of scRNA-seq data, CyTOF, flow cytometry experiments, IHC and whole mount staining skin was first treated with dispase and the epidermis and dermis separated to analyse separately.

Following Section 2.2 a grid of slits was cut into the skin sheets to aid enzymatic access, then the skin was treated with 2U/ml dispase II (Roche, 04942078001) in RPMI at 37°C for 1 hour. The epidermis was peeled from the dermis using forceps.

Dermis and epidermis were rinsed in PBS to remove dispase. For microscopy, these peeled sheets were used as described below. For the generation of single cell suspensions, both fragments were separately digested in a tissue culture dish at 37°C, 5% CO<sub>2</sub> in RF-10 media with 1.6 mg/ml type IV collagenase (Worthington, CLS-4) overnight and harvested as described in Section 2.2.1. Note that dermis dissolves leaving no visible remnants, whereas epidermis leaves visible sheets of stratum corneum.

### **2.2.4 Comparison of collagenase digestion between whole skin and peeled dermis and epidermis**

To match volumes of whole skin with the equivalent volume of peeled dermis and epidermis, for each time point six 8mm punch biopsy punches were taken from skin sheets prepared as in Section 2.2. Three punches per time point were kept in PBS at 4°C while three punches per time point were treated with dispase II and peeled, as described in 1.2.3. For each time point, three whole skin 8mm punches, three dermis 8mm punches and three epidermis 8mm punches were separately digested in 10cm tissue culture dishes at 37°C, 5% CO<sub>2</sub> in RF-10 media with 1.6 mg/ml type IV collagenase. After 2, 6, 12 and 16 hours, cells were collected as described in Section 2.2.1, and stained for flow cytometry as described below.

### **2.2.5 Freezing cells for short term storage**



Cells were pelleted by centrifuging at 500g for 5 minutes. Supernatant was removed and the pellet resuspended in 1ml freezing media, then made up to  $\sim 10^7$  cells per 1ml freezing media. The cell suspension was aliquoted into cryotubes, which were wrapped in bubble wrap to prevent flash freezing and stored in a  $-80^\circ\text{C}$  freezer.

## **2.3 Flow cytometry**

### **2.3.1 Flow cytometry analysis of cell suspensions**

Suspensions of whole skin, dermal or epidermal cells were resuspended in 100 $\mu\text{l}$  of flow buffer per  $10^7$  cells, transferred to polystyrene FACS tubes (BD Falcon, 352054) and stained with a cocktail containing 5 $\mu\text{l}$  of each antibody per  $10^7$  cells (as previously optimised in the lab) for 30 minutes at  $4^\circ\text{C}$  in the dark. Cells were washed in flow buffer by centrifuging at 500g for 5 minutes, then resuspended in 200 $\mu\text{l}$  of flow buffer per  $10^6$  cells. Immediately prior to analysis, cells were spiked with 1:10 DAPI (Sysmex Partec, 05-5005) added by volume and filtered through 35 $\mu\text{m}$  cell strainer caps (BD Falcon, 352235). Cells were then run through a Fortessa X20 for analysis.

### **2.3.2 FACS isolation of skin cells**

Dermal and epidermal cells were separately resuspended in 100 $\mu\text{l}$  of flow buffer per  $10^7$  cells, transferred to polypropylene FACS tubes (BD Falcon, 352063) and stained with a cocktail containing 5 $\mu\text{l}$  of each antibody per  $10^7$  cells for 30 minutes in  $4^\circ\text{C}$  in the dark. Cells were washed in flow buffer by centrifuging at 500g for 5 minutes, then resuspended in 1ml of flow buffer per  $2 \times 10^7$  cells. Immediately prior to sorting, cells were spiked with 1:10 DAPI by volume and filtered through 35 $\mu\text{m}$  cell strainer caps. Cells were then filtered using a 100 $\mu\text{m}$  cell strainer and sorted using a BD FACSAria Fusion Sorter with a 100 $\mu\text{m}$  fluidics nozzle. The Fusion Sorter was operated by a Flow Cytometry Core Facility (FCCF) core technician at all times. I devised and checked the gating and sorting strategies, and sorting was then carried out by the core technician.

Sorting was carried out into FACS tubes containing 500 $\mu\text{l}$  PBS. Prior to sorting, the sorter surfaces and centrifuge were cleaned with RNaseZap (ThermoFisher, AM9780). After

sorting, cells were centrifuged at 500g for 5 minutes and resuspended in <50µl PBS and counted using a haemocytometer.

## **2.4 Mass cytometry (CyTOF)**

All mass cytometry experiments were carried out using filter tips to avoid environmental metal contamination.

### **2.4.1 Mass cytometry analysis of cell suspensions**

The mass cytometry staining protocol used was developed by the FCCF staff members Drs G. Hulme, D. McDonald and A. Filby collaborating with Dr C. Lamb.

Suspensions of  $3 \times 10^6$  dermal or epidermal cells were incubated with 2.5µM Cell-ID Cisplatin (Fluidigm, 201064) made up in PBS for 5 minutes at room temperature before washing twice in wash buffer at 500g for 5 minutes. A master mix of cell surface-targeted metal-tagged antibodies was made up (**Table 1**) and cells were stained for 1 hour at room temperature, made up to 100µl wash buffer. After washing twice in PBS at 500g for 5 minutes, cells were fixed for 30 minutes at room temperature in a solution of FOXP3 fix-perm buffer (eBiosciences, 00-5523-00) with 1.6% formaldehyde (Polysciences, 18814). Cells were then washed twice in FOXP3 fix-perm buffer then stained with an intracellularly targeted antibody cocktail (**Table 1**) for 1 hour at room temperature. Cells were washed twice at 500g for 5 minutes in PBS, then incubated in Iridium intercalator (Fluidigm, 201192A) at 125nM in PBS for 1 hour. Cells were further fixed at 1.6% formaldehyde for 30 minutes at room temperature, washed twice in PBS and twice in distilled water. Cell pellets were then resuspended in 500µl of distilled water and 10µl was run on a BD Accuri cytometer to accurately measure the cell concentration. Cells were then made up to  $0.5 \times 10^6$  cells/ml in distilled water with 10% (v/v) EQ beads (Fluidigm, 201078) for analysis on the Helios mass cytometer (Fluidigm).

### **2.4.2 Metal tagged antibody conjugation**

Where pre-conjugated metal tagged antibodies were not available, antibodies were custom conjugated using carrier-free unconjugated antibodies and Maxpar Antibody

Labelling Kits (Fluidigm, 201141A-201176B). Custom conjugated antibodies are listed in **Table 1** with an asterisk. Conjugation was carried out as per the manufacturer's instructions as follows: The Maxpar polymer was spun briefly in a microcentrifuge then resuspended thoroughly in 95µl L-buffer, then 5µl of the specific metal solution was added and incubated for 30 minutes at 37°C on a heat block. This solution was then transferred to a 3kDa centrifugal filter (Millipore, UFC500396) and made up to 300µl with L-buffer before centrifuging for 12,000g for 25 minutes. The filtered waste was discarded, and the metal mixture resuspended in 400µl C-buffer and centrifuged at 12,000g for 30 minutes.

100µg of specific carrier-free unconjugated antibody was made up to 400µl in R-buffer in a 50kDa centrifugal filter (Millipore, UFC505096), then spun at 12,000g for 10 minutes. The filtered waste was discarded, and the antibody resuspended in 100µl 0.5M TCEP solution before incubating for 30 minutes at 37°C on a heat block. 300µl of C-buffer was added before centrifuging at 12,000g for 10 minutes. The filtered waste was discarded, the antibody resuspended in 400µl C-buffer and centrifuged for 12,000g for 10 minutes.

The metal was resuspended in 60µl C-buffer, then transferred to the antibody filter and mixed thoroughly before incubating for 90 minutes at 37°C on a heat block. 200µl W-buffer was added to this mixture and centrifuged at 12,000g for 10 minutes four times, being topped up with 400µl of W-buffer between each spin. The purified conjugated antibody was then made up to 100µl with W-buffer and 1µl tested on a NanoDrop spectrophotometer (ThermoFisher) at 280nm absorbance to check protein concentration. Antibodies were made up to 0.5mg/ml concentration using 0.05% sodium azide made up in W-buffer (Sigma, S2002).

#### **2.4.3 Antibody testing on beads**

To test the success of metal conjugation, beads were stained with each custom-conjugated antibody and run through the Helios mass cytometer. AbC Total Antibody Compensation positive beads (ThermoFisher, A10497) were used to test antibodies raised in rat and mouse, and UltraComp eBeads (ThermoFisher, 01-2222-41) were used

for recombinant human antibodies. Multiple antibodies were tested in a single bead tube, so to minimise the impact of isotope impurity and oxidation, metals with an isotope 1 or 16 atomic mass apart were stained in separate tubes. Two drops of beads were added to each polystyrene FACS tube and 125nM iridium intercalator (Fluidigm, 201192A) was added in 200µl PBS + 1% FCS to each tube and incubated at room temperature for 1h. Beads were washed once in PBS and twice in Milli-Q purified water, each at 2000g for 8 minutes, prior to running on the Helios mass cytometer. The Helios was operated by an FCCF core technician at all times. The presence of 191Ir/193Ir positive events with signal in the expected channels was used to confirm conjugation success.

#### **2.4.4 Antibody testing on cells**

To test that the antibody binding sites were not denatured past epitope recognition during the heating steps, custom conjugated antibodies were tested as a panel as described in Section 2.4.1, on whole skin cells.

#### **2.4.5 Antibody titration**

Both custom conjugated and pre-conjugated metal tagged antibodies were titrated to achieve optimal separation and minimise the effects of spillover. Multiple panels were devised to ensure no +/-1 or +16 channels were occupied so that spillover could be analysed from each channel, and each antibody was tested at three concentrations for staining (either “1:200, 1:100 and 1:50”, or where separation was worse during cell staining testing “1:100, 1:50 and 1:25” was used) using the method described in Section 2.4.1 on whole skin. Staining index was calculated as  $((\text{positive MFI} - \text{negative MFI}) / 2 \times \text{negative standard deviation})$ , and the highest value was chosen for the final staining concentration of each antibody. Antibodies with high background staining and spillover at their lowest titration were stained at 1:400. No further titration was required.

## **2.5 Immunohistochemistry (IHC)**

### **2.5.1 Whole mount immunofluorescence staining of dermis and epidermis**

Peeled dermis and epidermis sheets were cut to 1cm<sup>2</sup> and fixed in 2% formaldehyde (Polysciences, 18814) and 30% (w/v) sucrose in PBS for 24 hours at 4°C. Dermis and epidermis sheets were incubated in 300mM glycine for 24 hours at 4°C, washed in PBS twice for 10 minutes each on a gentle rocker, then blocked and permeabilized in PBS with 20% goat serum (R&D Systems, DY005) and 0.2% Triton X-100 (Sigma, T8787) for 24 hours at 4°C then washed in PBS with 0.1% Triton X-100 twice times for 10 minutes each on a gentle rocker. Primary antibodies were added in PBS with 20% goat serum and 0.1% Triton X-100 for 48 hours at 4°C then washed in PBS with 0.1% Triton X-100 five times for 10 minutes each on a gentle rocker. Secondary antibodies were added in PBS with 20% goat serum and 0.1% Triton X-100 for 24 hours then washed in PBS with 0.1% Triton X-100 five times for 10 minutes each on a gentle rocker.

For epidermal sheets, sheets were covered in 2 drops spectral DAPI (Perkin Elmer, FP1490) added to 500µl PBS for 30 minutes at room temperature. For dermal sheets, sheets were covered in 500µl of 0.1% DRAQ5 (Abcam, ab108410) in PBS for 30 minutes at room temperature.

Sheets were washed in PBS with 0.1% Triton X-100 three times for 10 minutes each on a gentle rocker, then mounted in Vectashield antifade mounting medium (Vector Laboratories, H-1000) and set for at least 24 hours before imaging. Slides were imaged using a Zeiss LSM800 Airyscan/Spinning disk Confocal Microscope and Zeiss ZEN Pro software (Zeiss, Germany).

For each experiment, a skin sheet was prepared in the same way but with only PBS with 20% goat serum and 0.1% Triton X-100 added for 48 hours, with no primary antibody. A second skin sheet was prepared in the same way but with no primary or secondary antibodies added. For each primary antibody (and for nuclear stains DAPI and DRAQ5), a further skin sheet was prepared and stained with only a single primary antibody and its secondary antibody. These were imaged to respectively confirm the lack of secondary-only staining caused by non-specific binding, to see the background fluorescence from the skin samples, and to confirm the lack of spillover into other channels where positive staining was found.

### **2.5.2 Immunohistochemistry on skin sections**

Sheets of whole skin, dermis and epidermis were prepared as Sections 2.2 and 2.2.3 and cut to 1cm<sup>2</sup> before fixation in 10% neutral-buffered formalin (Cellpath, BAF-6000-08A) for at least 24 hours. Fixed skin was sent to the Newcastle Molecular Pathology Node for paraffin embedding and slide sectioning. Sections were cut to standard 4µm thickness.

### **2.5.3 H&E staining**

Formalin-fixed paraffin embedded (FFPE) skin section slides were dewaxed in xylene (Fisher Scientific, 534056) for 5 minutes at room temperature. Slides were rehydrated in graded ethanol for 30 seconds at each of 99%, 95% and 70% ethanol (Fisher Scientific, BP28184) (diluted with water), and finally washed in running water. Slides were dipped in Mayer's Haematoxylin (Sigma, MSH16), water, Scotts tap water substitute (Sigma, S5134), Eosin (Sigma, HT110132) and water for 30 seconds each in sequence. Slides were dehydrated in graded ethanol for 30 seconds at each of 70%, 95% and 99% ethanol followed by 5 minutes in xylene. Excess xylene was carefully removed with tissue paper prior to cover slip mounting with DPX (Sigma, 06522).

### **2.5.4 Antibody staining**

Dual-colour chromogen staining was done by the Newcastle Molecular Pathology Node. Single colour chromogen staining was carried out as follows:

FFPE skin section slides were dewaxed in xylene for 5 minutes. Slides were rehydrated in graded ethanol for 30 seconds at each of 99%, 95% and 70% ethanol (diluted with water), and finally washed in running water. Slides were treated with hydrogen peroxide (made up to 0.3% v/v in water, Sigma, H1009) for 10 minutes and rinsed in water. Slides were submerged in citrate buffer in a pressure cooker until 2 minutes after max temperature and pressure had been reached. Slides were placed in TBS buffer for 5 minutes on a rocker.

Staining was done using a Vector Immpress Staining Kit (Vector Laboratories, MP-7800-15) containing 2.5% normal horse serum, peroxidase conjugated secondary antibody and DAB.

Slides were covered in 2.5% normal horse serum for 20 minutes at room temperature, then placed in primary antibody, diluted in TBS buffer, for 60 minutes at room temperature before washing twice for 5 minutes in TBS on a rocker. Slides were then stained using the secondary antibody for 30 minutes before washing twice for 5 minutes in TBS on a rocker. Slides were developed in DAB for 30 seconds, washed in running water, stained in Mayer's Haematoxylin for 30 seconds, washed in running water, stained in Scotts tap water substitute for 30 seconds, then washed in running water. Slides were dehydrated in graded ethanol for 30 seconds at each of 70%, 95% and 99% ethanol followed by 5 minutes in xylene. Excess xylene was carefully removed with tissue paper prior to cover slip mounting with DPX. Slides were imaged using a Zeiss Axioimager Microscope and Zeiss ZEN Pro software (Zeiss, Germany).

For each experiment, a slide was treated identically but treated with TBS buffer instead of primary antibody to confirm the lack of nonspecific staining.

## **2.6 Single cell RNA sequencing**

Library preparation was done by Emily Stephenson, and libraries were sent to the Wellcome Sanger Institute for sequencing. Cells were counted on a haemocytometer and loaded at 400-800 cells/ $\mu$ l with the aim of recovering 7000 live, single cells onto each channel of the Chromium chip (10x Genomics, Pleasanton, CA, USA) before droplet encapsulation on the Chromium Controller. Sequencing libraries were generated using the Single Cell 3' reagent kits as per the manufacturer's protocol. Libraries were sequenced using an Illumina HiSeq 4000 using v4 SBS chemistry to achieve a minimum depth of 50,000 raw reads per cell using the following parameters: Read1: 26 cycles, i7: 8 cycles, i5: 0 cycles; Read2: 98 cycles to generate 75bp paired end reads.

## **2.7 Data analysis**

### **2.7.1 Statistics and graphs**

Bar graphs, scatter plots and t tests were generated using GraphPad Prism 7.00 (GraphPad Software, La Jolla California USA).

### **2.7.2 Flow Analysis**

Flow cytometry and CyTOF analysis and layouts were produced using FlowJo\_V10 (FlowJo LLC, Ashland Oregon).

### **2.7.3 Mass cytometry clustering analysis**

Data from peeled, digested epidermis and dermis from 4 donors was clustered separately using the *cytokit* Bioconductor package version 1.6.1 (Chen et al., 2016). Data was downsampled to a maximum of 100,000 cells per experiment, transformed using the *cytofAsinh* option, clustered with *Rphenograph* and visualized as tSNE plots.

### **2.7.4 Microscopy imaging and analysis**

Zeiss ZEN Pro software (Zeiss, Germany) was used for imaging IHC and IF slides, as well as for tiling and Z-stack reconstruction of 3D models. ImageJ (NIH, Maryland) was used to enhance contrast in microscopy images, as well as for counting nuclei of tiled images.

### **2.7.5 Figure preparation**

Figures were prepared using Adobe Illustrator\_2018 (Adobe, California) for the generation and standardisation of legends, labels and axes text.

## **2.8 Single cell RNA sequencing data analysis**

scRNA-seq data was computationally analysed by Dr Peter Vegh, and the below analytical methods used are displayed for the purpose of following the experimental procedures.

### **2.8.1 Alignment and quality control of scRNA-seq data**

scRNA-seq data was quantified using the Cell Ranger Single-Cell Software Suite (version 2.0.2, 10x Genomics Inc) and aligned to the GRCh38 reference genome (official Cell



Ranger reference, version 1.2.0). Cells with under 200 genes detected or over 20% mitochondrial gene expression were removed. Genes expressed in fewer than 3 cells were also removed.

### **2.8.2 Doublet detection and exclusion**

Doublets were detected using a support vector machine (SVM) algorithm trained on our scRNA-seq data and simulated doublets. Simulated doublets were generated by randomly choosing pairs of cells from the same sequencing lane and combining their raw gene counts. The SVM was trained to identify simulated doublets using the SVC (support vector classifier) from the *svm* module in the *sklearn* package (version 0.19.1) in Python (v3.6.3). A grid search was applied during the training of the SVM models to optimise its hyperparameters using the *GridSearchCV* class in *sklearn*. Next, *Scrublet* (v0.2) was applied to remove further doublets, using an exclusion threshold suggested by the package (Wolock et al., 2019).

### **2.8.3 Data normalization and feature selection**

Data was normalized using the *NormalizeData* function in Seurat (v2.3.4) in R (v3.5.2) (Butler et al., 2018) (R Core Team 2018). Gene expression values were scaled and centred using the *ScaleData* function in Seurat. Highly variable genes were detected using the *FindVariableGenes* function in Seurat with minimum cut-off values 0.1 and 0.5 for expression and dispersion respectively.

### **2.8.4 Data embedding, visualization and clustering**

Principal components were calculated using *RunPCA* and adjusted for donor-to-donor variation using the Harmony package (v0.1.0). Dimensionality reduction and embedding was performed using Uniform Manifold Approximation and Projection (UMAP) by the *RunUMAP* function in Seurat with 20 PCs. The resultant k-nearest neighbours graph was clustered using the Louvain graph-based method.

### **2.8.5 Calculation of differential gene expression**

Differentially expressed genes were calculated using the Wilcoxon sum rank test on genes expressed in at least 30% of cells in either of the two populations compared, and

with a fold change cut-off of 0.25 (natural log scale). All  $p$ -values were adjusted for multiple testing using the Bonferroni correction. Initial annotation was performed by comparing these genes to published information of defined cell types, as well as using the FACS protein information coded for in the sequencing lanes. Following this, four major groups (lymphoid cells, APCs, keratinocytes, and other non-immune cells) were subsetted for higher resolution analysis using the methods from Sections 2.8.3 to 2.8.5.

### **2.8.6 Trajectory analysis**

Keratinocyte trajectory analysis was done using partition-based approximate graph abstraction (PAGA) in Scanpy v1.4 (sc.tl.paga) (Wolf et al., 2019). Diffusion pseudotime values were assigned to cells along the resultant differentiation pathways using Scanpy (sc.tl.dpt) (Wolf et al., 2018). Genes related to cell cycle were excluded from the analysis.

### **2.8.7 CellPhoneDB**

CellPhoneDB (Vento-Tormo et al., 2018) was used to identify significant ( $p < 0.05$ ) potential receptor-ligand interactions, using 1000 iterations of data permutations. A minimum threshold of 10% cells expressing a receptor or ligand in a given cell type was used.

**Chapter 3. Optimising the  
sampling of skin cell heterogeneity**



### 3.1 Chapter 3 Introduction

To construct a comprehensive single cell report of healthy adult skin cells which adequately captures the heterogeneity therein, the main challenges in experimental design to consider were comprehensive sampling and capturing biologically representative data.

Comprehensively sampling single cell heterogeneity requires a tissue dissociation method that can liberate the diverse cell types present. Skin requires dissociating to a single cell level, which requires cleavage of the cell surface adhesion molecules, collagens and other extracellular matrix components which hold these cells firmly in place. Universal dissociation is confounded by expression of different adhesion proteins, and in particular the stark difference between the dermal and epidermal extracellular matrices.

Skin digestion protocols are widely variable between studies. Trypsin (Cheng et al., 2018; Santegoets et al., 2008), collagenase (McGovern et al., 2014; Philippeos et al., 2018), pre-made enzyme blends (Tabib et al., 2018b; Kim et al., 2020) and collecting migrating cells without digestion are all common strategies to obtain single cell suspensions from skin tissue, with or without prior epidermal separation. Multiple protocols for epidermal separation are used, including dispase treatment (Kitano & Okada, 1983) and micro-dissection (Gulati et al., 2013). Historically, heat-separation was also employed for epidermal separation (Kassis & Søndergaard, 1982).

Botting *et al.* compared common skin dissociation protocols, and reported higher cell yields from epidermis treated with trypsin instead of type IV collagenase and the reverse in dermis (Botting et al., 2017). They also reported that trypsin cleaves many more common surface protein markers than type IV collagenase. Incubating skin for up to 48 hours at 37°C, 5% CO<sub>2</sub> and collecting the surrounding media without dissociation treatment is also commonly used to analyse the cells which migrate out of the skin, which is limited to DCs and LCs, and so would not account for stromal cells, macrophages or T cells (Botting et al., 2017).

The rarity of potential cell subsets is another issue to tackle. Villani *et al.* reported the cellular makeup of human PBMC using SmartSeq2 (Villani et al., 2017), and reported a previously undiscovered population at <0.1% of PBMC. Without the pre-selection required in plate sorting, which removed T cells and monocytes (the majority of PBMCs), finding this population in the 2,400 cells analysed would have been extremely improbable. As there would be no published marker profile for undiscovered cells in skin, erring on the side of large cell numbers would be key to avoid missing heterogeneity.

To hold biological relevance, the cell transcriptomes should mirror those *in vivo* as closely as possible. Any tissue digestion protocol, while absolutely necessary to analyse skin at a cellular level, will adversely impact experimental observations by changing cell phenotypes from steady state. Examples include cleavage of extracellular proteins and inducing phenotypic changes (Botting et al., 2017). Minimising or accounting for these effects is important to recapitulate the true phenotype and functions of these cells *in vivo*. Harsh digestion protocols are more likely to release a representative cell suspension, but risk accentuating these effects. Cells remaining outside of tissue also change due to the lack of reception of homeostatic signalling, although this can be offset at lower temperatures.

With these thoughts on sampling in mind, the chosen approach was to use a droplet based single cell separation approach to perform scRNA-seq, in order to sequence high numbers of cells with the aim of resolving clusters containing potential unknown rare cells that could otherwise be missed. Collagenase IV dissociation was used to balance high cell numbers (relative to DC migration or other enzyme blends) with lower effects on phenotype and function (relative to trypsin). The digestion method was optimised for the ideal treatment duration. A comprehensive sorting strategy was devised based on reported markers (Haniffa et al., 2012; Bertram et al., 2019) to further improve the chances of representing every cell type while avoiding removing cells through marker biases.

## 3.2 Results

### 3.2.1 Optimisation of tissue dissociation

To recapitulate *in vivo* skin as best as possible and to capture this heterogeneity while introducing as little bias as possible, the tissue dissociation conditions were first optimised in favour of high cell numbers, high variation in cell types released and high cell viability. In order to optimise the yield and viability of skin cells liberated through digestion, matched volumes of whole skin were incubated with type IV collagenase at increasing time points and analysed by flow cytometry for a single donor (**Figure 1**). Whole skin was first shaved to 200 $\mu$ m depth, sampling the epidermis and papillary dermis. This was chosen to sample the most leukocyte-rich and cellularly dense portion of the dermis (Wang et al, 3D atlas), while keeping the skin depth consistent between donors for each experiment, and to aid digestion by increasing the surface area to volume ratio of the samples. The 200 $\mu$ m sheet was volume-matched using an 8mm diameter punch biopsy. Three punches were used per time point, giving a total volume of 30mm<sup>3</sup> per time point.

Skin was collagenase IV digested for 2, 4, 6, 8 and 12 hours before staining with a broad panel of antibodies selected based on literature knowledge (Haniffa et al., 2012; Bertram et al., 2019) of skin cell markers, and analysing cell numbers and cell viability released by each time point by flow cytometry.

Figure 1

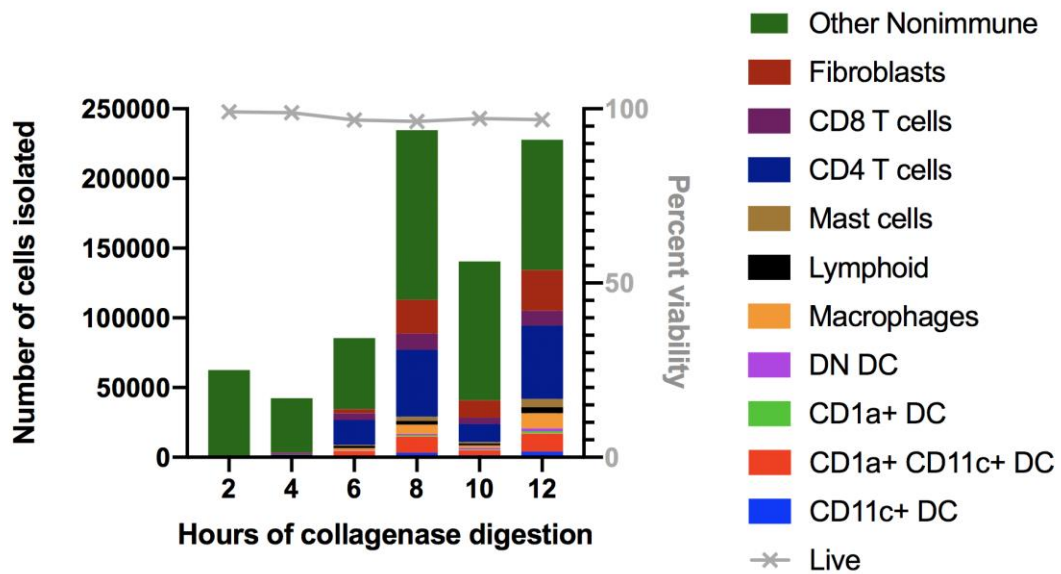


**Figure 1 – Optimisation of collagenase digestion duration.** Left axis: A stacked bar graph displaying the number of cells liberated and analysed by flow cytometry from 30mm<sup>3</sup> of whole skin treated with type IV collagenase at 37°C 5% CO<sub>2</sub> for set durations. Each colour represents cells from the flow gates shown in **Figure 2**. Right axis: The corresponding proportion of total live cells measured as the DAPI- gate as a percentage of the singlet cell gate in **Figure 2**, displayed as grey crosses. *n* = 1. DC = Dendritic cell; DN = double negative.



### 3.2.2 Overnight collagenase dissociation increases immune cell liberation with little effect on viability

Cell viability, as a measure of DAPI- cells, was at its highest between 2 and 6 hours of digestion (**Figure 1**). However, at 2 and 4 hours of digestion the vast majority of the cells released were CD45- nonimmune cells. These cell types had much higher viability than CD45+ cells across all digestion time points, and so the eventual release of less viable CD45+ immune cells will have weighted the total cell viability negatively at later time points. Cell viability plateaued after 4 hours, suggesting that collagenase digestion times between 6 and 12 hours have little effect on cell death.

The following cell types were identified: CD4 T cells, CD8 T cells, macrophages, mast cells, fibroblasts and DCs split by variable expression of CD1a and CD11c. The remaining denominations are “other nonimmune cells”, which should comprise CD45- CD73- endothelial cells, pericytes, keratinocytes and melanocytes. As well as “lymphoid”, which should comprise CD45+ HLA-DR- SSC<sup>low</sup> CD3- natural killer cells and B cells (**Figure 2**).

The total cell numbers released correlated largely with digestion time. Prior to 8 hours of digestion, relatively few cells were released. Between 8 and 12 hours there is less of a difference in total cell numbers, but there are noticeable differences in the amounts of rarer immune cell types released. Macrophages and dendritic cell subsets in particular are largely increased in number from 8 to 12 hours of digestion. This suggested that at least 12 hours of collagenase IV digestion would be more likely to sufficiently sample absolute skin cell heterogeneity.

It is notable that from the flow cytometry panel used, keratinocytes could not be reliably gated for. The epidermal immune cell subsets also cannot be reliably separated from their dermal counterparts. To approach these issues, epidermal separation was therefore used prior to collagenase digestion.

**Figure 2**

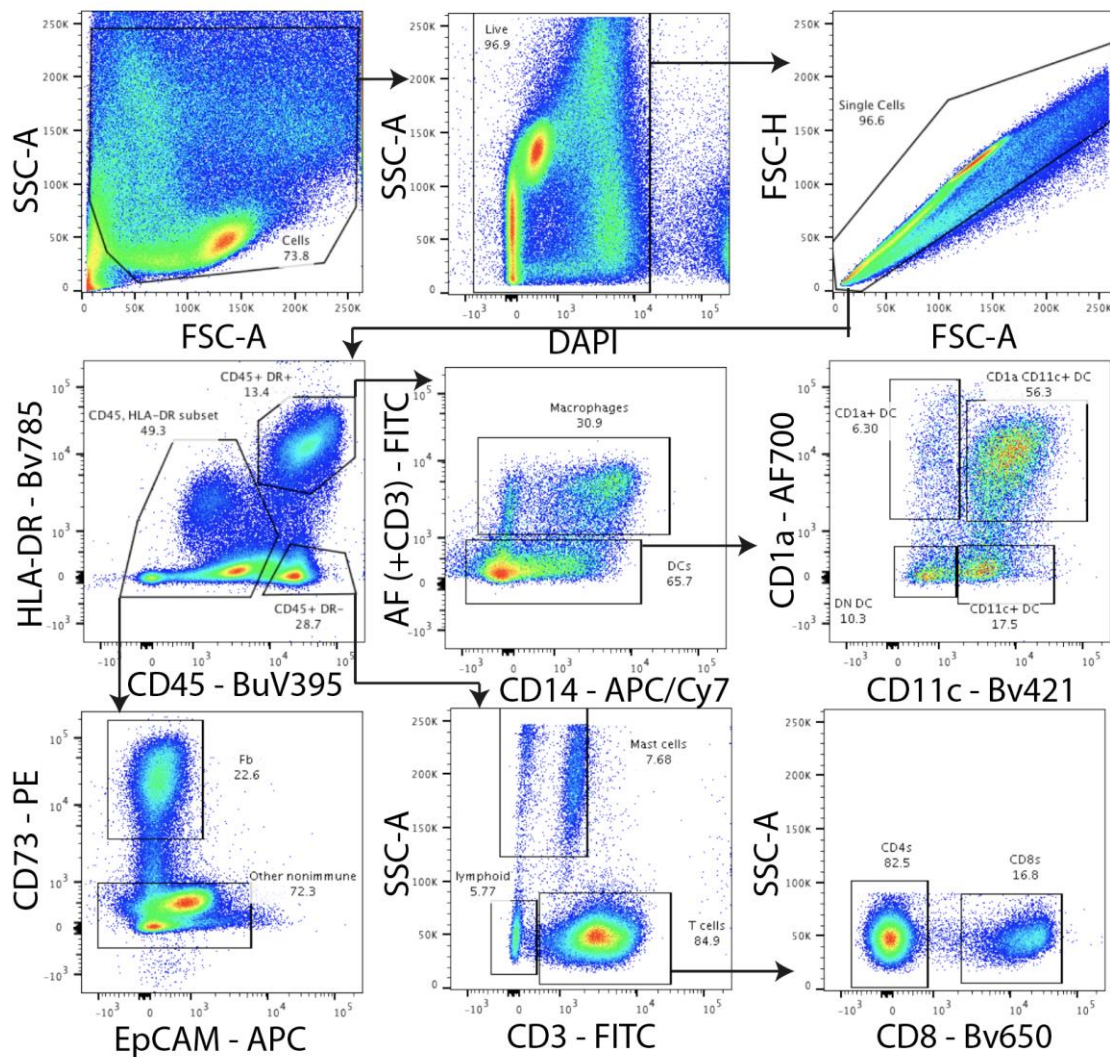


**Figure 2 – Gating strategy for the optimisation of collagenase digestion duration.** Skin from a single sample was treated with collagenase for 2, 4, 6, 8, 10 and 12 hours then stained with a broad cell type panel to analyse the frequency of different cell types present using flow cytometry. This gating strategy was used for all time points, with representative data shown from 12 hours of collagenase treatment. The name of each gate corresponding to the data in **Figure 1** is shown next to each gate, and the percentage of the parent gate found within each gate is displayed underneath this name. DC = Dendritic cell; DN = double negative; Fb = fibroblast.

### 3.2.3 Separation of dermis and epidermis leads to increased cell liberation by type IV collagenase

Efficient digestion relies on exposed surface area to allow enzymatic access. The apical surface of the epidermis is protected by the keratin heavy matrix making up the Stratum Corneum, and these keratins are not susceptible to type IV collagenase digestion. The Stratum Basale is held together by desmosomes and hemidesmosomes which include collagen type VII, a protein susceptible to type IV collagenase (Watanabe et al., 2018). Separating the epidermis from the dermis allows collagenase access through the basal layer, increasing epidermal cell liberation, and also allows for separation of the dermal and epidermal cell types without the need for additional flow cytometry antibodies; the size of the antibody panel used was already limited by the spectra available, on top of which there are no effective markers available with strong dermal-epidermal separation.

To compare cell liberation and viability after mechanical separation of the dermis and epidermis with unseparated whole skin, the above experiment was repeated, and a 1 hour dispase treatment step was used to digest the DEJ. Sample and volume matched whole skin, dermis and epidermis was then treated with type IV collagenase for 2, 6, 12 and 16 hours before flow cytometric analysis (**Figures 3-8**). At each time point the total cells liberated from the epidermis and dermis combined largely outnumbered those liberated from whole skin alone. Viability dropped more rapidly with time for dermis alone compared to whole skin, and the viability of epidermal cells released was much lower than both. However, the total number of viable cells released was greater after separation regardless. The low epidermal viability could possibly be caused by the release of dying suprabasal keratinocytes closer to terminal differentiation.

Treating skin with dispase and mechanically separating dermis from epidermis prior to tissue dissociation was chosen due to the benefits of increased cell numbers as well as the ability to barcode the tissue origin of each cell by sorting dermal and epidermal cells separately and sequencing them on different lanes. It is also unknown whether T cells found in the dermis and epidermis differ in a distinct way with which they could be computationally separated based on transcriptome alone.

Figure 3

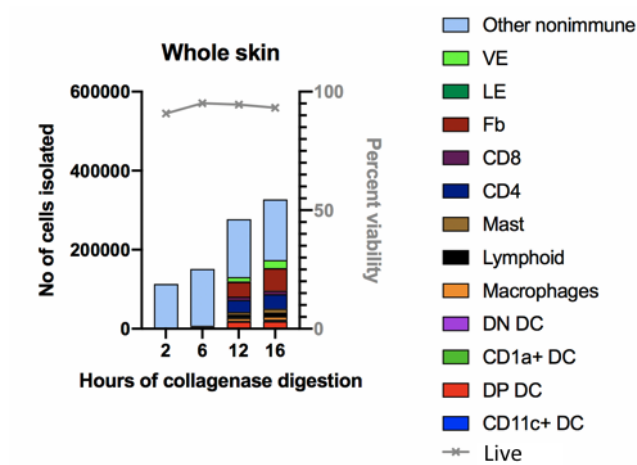


Figure 4

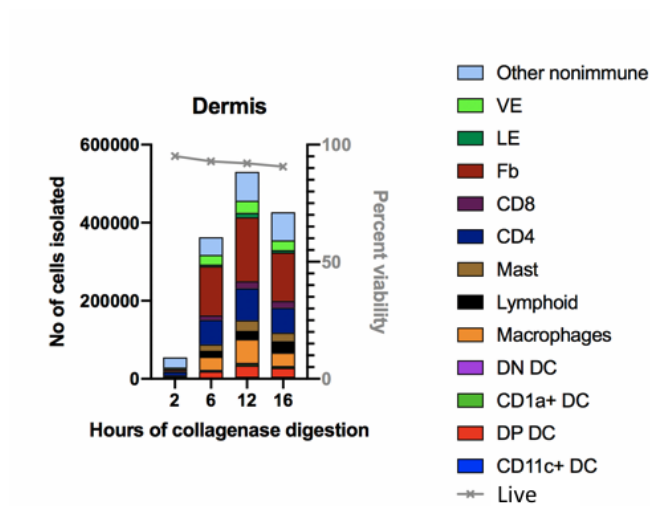
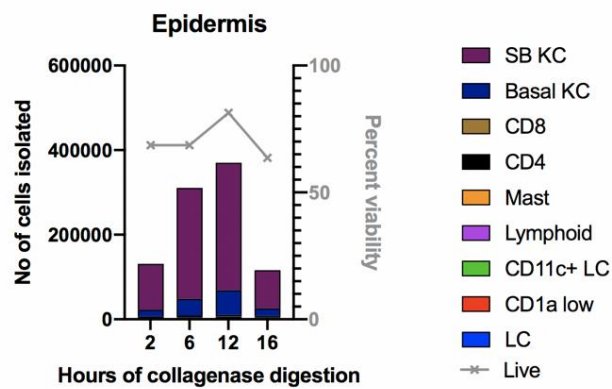


Figure 5



**Figure 3 – Comparison of collagenase digestion duration of whole skin.**

**Figure 4 – Comparison of collagenase digestion duration of dermis.**

**Figure 5 – Comparison of collagenase digestion duration of epidermis.**

Left axis: A stacked bar graph displaying the number of cells liberated and analysed by flow cytometry of skin treated with type IV collagenase at 37°C 5% CO<sub>2</sub> for 2, 6, 12 and 16 hours. Right axis: The corresponding proportion of total live cells measured as the DAPI- gate as a proportion of its parent gate in **Figure 2**, displayed as grey crosses. Data shown from a single repeat. Fb = fibroblast; LE = lymphatic endothelium; VE = vascular endothelium.

**Figure 3:** 30mm<sup>3</sup> of whole skin was treated with type IV collagenase for each timepoint. Each colour represents the cells captured in the flow gates shown in **Figure 6**.

**Figure 4:** Dermis peeled from 30mm<sup>3</sup> of whole skin after dispase treatment was treated with type IV collagenase for each timepoint. Each colour represents the cells captured in the flow gates shown in **Figure 7**.

**Figure 5:** Epidermis peeled from 30mm<sup>3</sup> of whole skin after dispase treatment was treated with type IV collagenase for each timepoint. Each colour represents the cells captured in the flow gates shown in **Figure 8**.

**Figure 6**

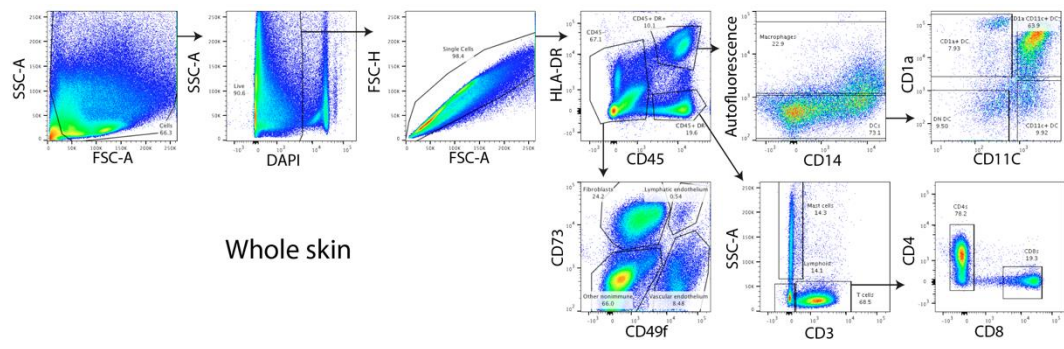


**Figure 7**

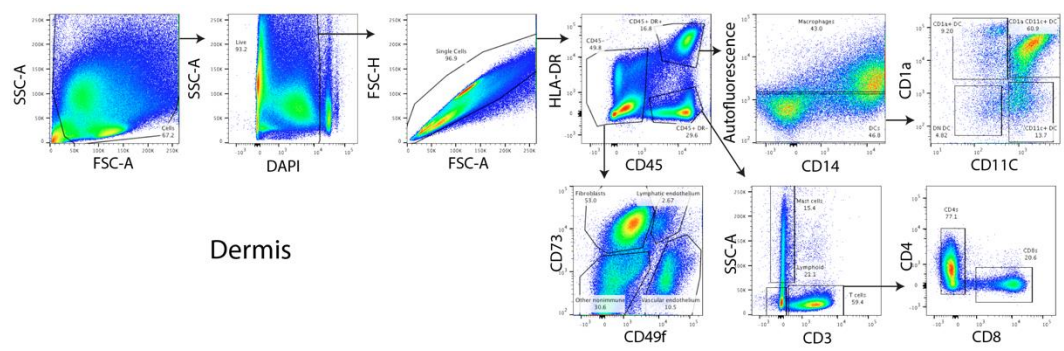


**Figure 8**

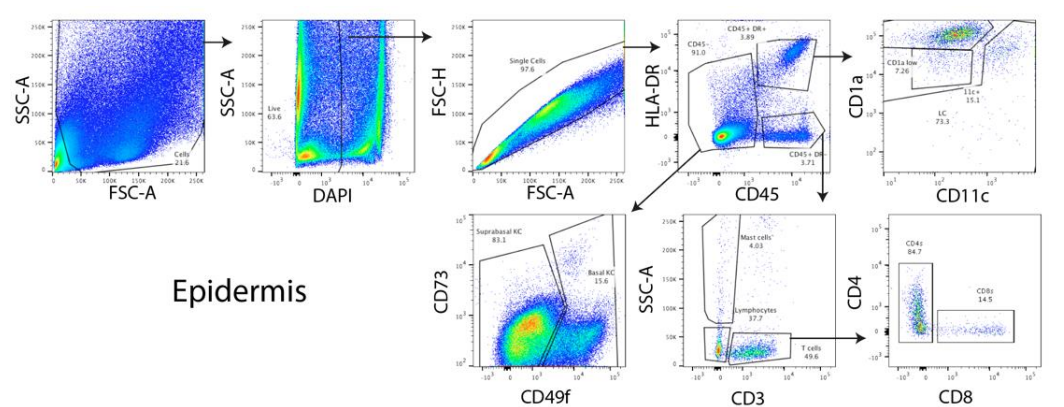


**Figure 6 – Gating strategy for the optimisation of whole skin collagenase digestion.**

**Figure 7 – Gating strategy for the optimisation of dermis collagenase digestion.**

**Figure 8 – Gating strategy for the optimisation of epidermis collagenase digestion.**

Skin from a single sample was punch biopsied, with equal volumes of skin being directly collagenase treated or dispase treated, peeled and the dermis and epidermis undergoing collagenase treatment. 2, 6, 12 and 16 hours of collagenase treatment were tested, and the resulting cells stained with a broad cell type panel to analyse the frequency of different cell types present using flow cytometry. The same gating strategy was used for each time point, and representative data is shown from 16 hours of collagenase treatment. The name of each gate is shown next to each gate, and the percentage of the parent gate found within each gate is displayed underneath this name. These gates correspond to the data in **Figures 3-5**.

**Figure 6:** 30mm<sup>3</sup> of whole skin was treated with type IV collagenase for each timepoint.

**Figure 7:** Dermis peeled from 30mm<sup>3</sup> of whole skin after dispase treatment was treated with type IV collagenase for each timepoint.

**Figure 8:** Epidermis peeled from 30mm<sup>3</sup> of whole skin after dispase treatment was treated with type IV collagenase for each timepoint.

### 3.2.4 FACS improves sampling of rare skin cell types

To further increase the sampling of rare cell types, FACS was employed prior to single cell sequencing, for a total of three donors (**Figures 9-10**). This enabled the removal of cellular debris, dead cells and doublets which would waste sequencing “real-estate” and contaminate the downstream data, as dead cells and doublets are difficult to remove computationally. By using a gating strategy with no gaps between gates, no biasing was introduced into the collection of cells for sequencing by excluding cells of potentially important specific protein expression, such as those far from the population median or cells within areas of poor separation, which can be difficult to label as positive or negative for a marker and are therefore often discarded (**Figures 9-10**).

The effect of this strategy, compared to loading equal numbers of dermal and epidermal cells without sampling, was to downsample the most common cell types: dermal fibroblasts and CD8 T cells as well as epidermal keratinocytes and melanocytes. Dermal endothelial cells were not affected, being sampled at the same rate pre- and post-sorting (**Table 2**). By sequencing relatively less of these common cell types much more immune cells could be sequenced. Cells from particularly uncommon gates were sampled at much higher rates than they otherwise would have been, allowing for capture of rare heterogeneity. For example, epidermal CD45+ HLA-DR+ CD11c+ cells were captured approximately 38 times more than their expected rate, and dermal CD45+ HLA-DR+ autofluorescent- CD14- CD11c- CD141- cells were captured at approximately a 10 times higher rate than without sorting (**Table 2**).



Figure 9

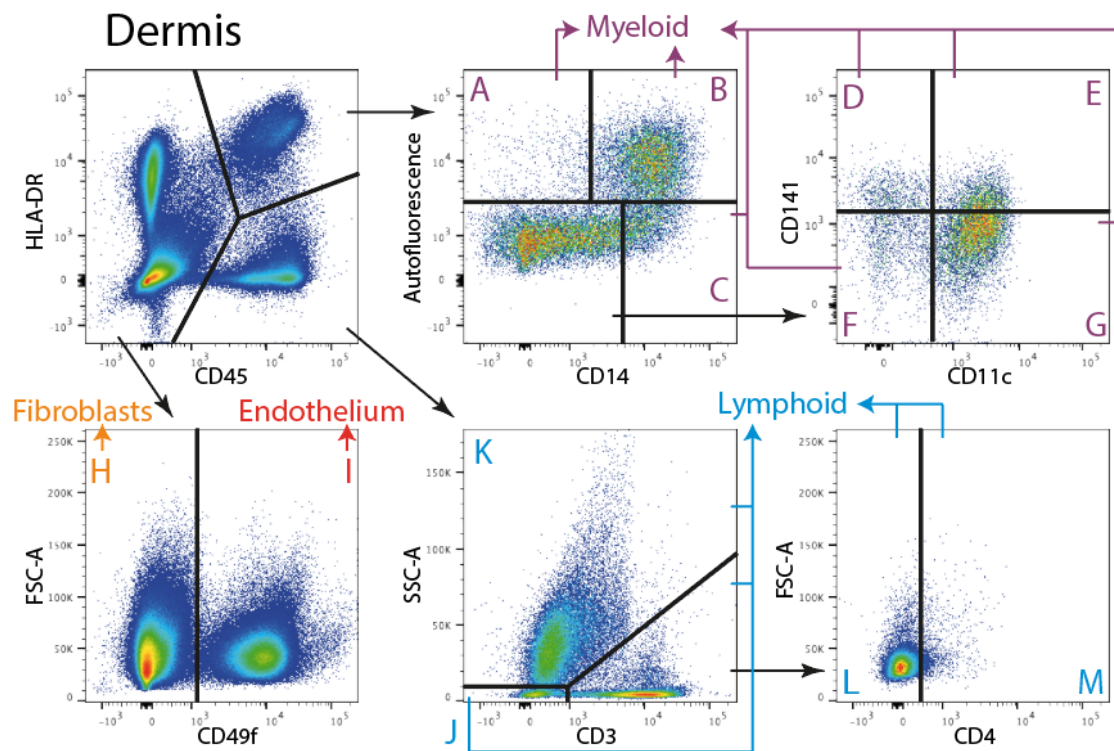
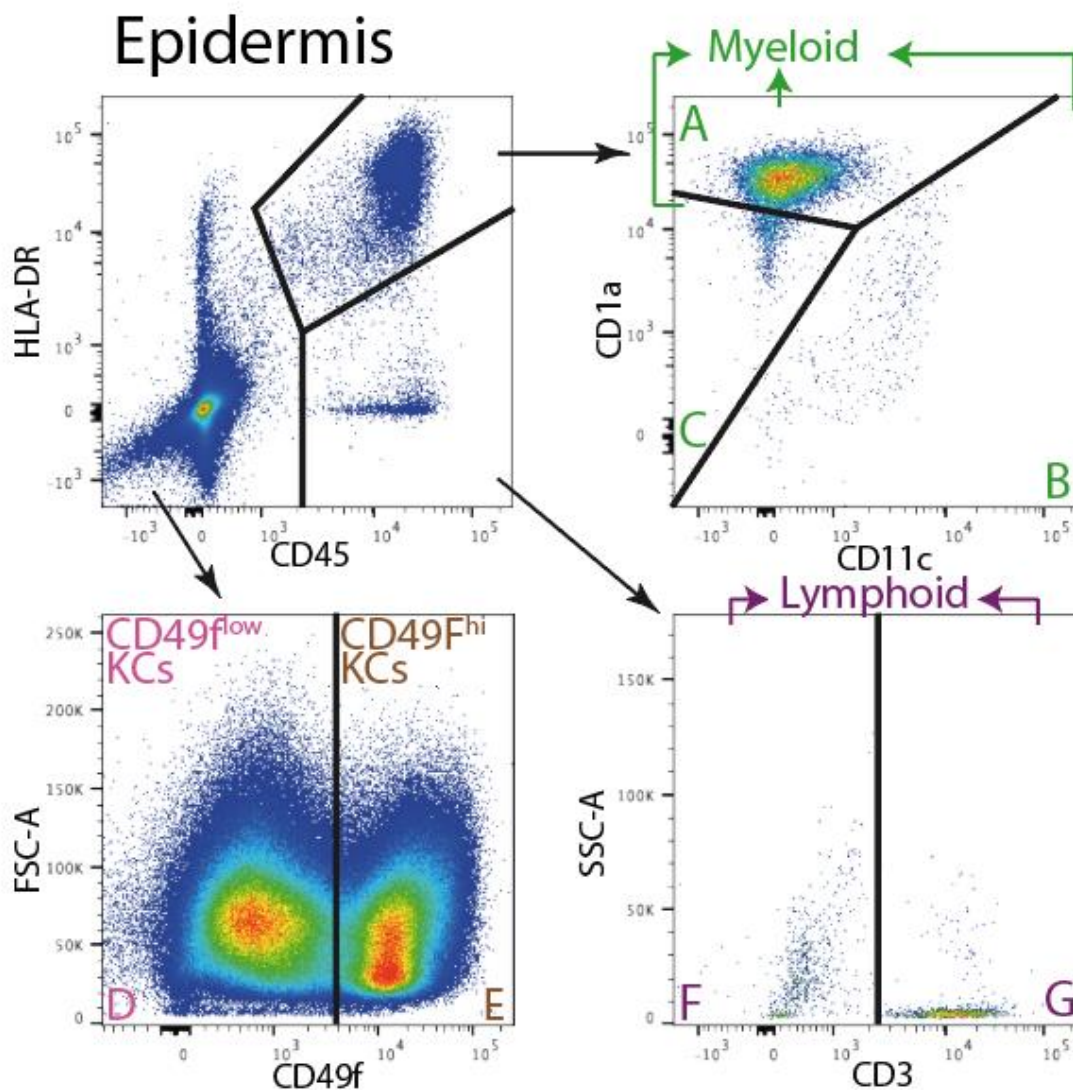


Figure 9 – Gating strategy for the sampling of dermal skin cell types for scRNA-seq.

Epidermis and dermis from 200 $\mu$ m sheets of skin were separated after 1 hour dispase treatment. Dermis was digested with collagenase overnight then stained with a broad cell type panel for flow sorting. Cells were sorted from each gate and combined into four broad categories: myeloid (purple), lymphoid (blue), fibroblasts (orange) and endothelium (red) as shown by arrows of the same colour. These labels represent the 10X lanes each gate was sequenced on, as shown in **Figure 18**. Gates are named A-M which refers to the statistics in **Table 2**. Representative data is shown from a one of  $n = 3$  donors.

Figure 10



**Figure 10 – Gating strategy for the sampling of epidermal skin cell types for scRNA-seq.**

Epidermis and dermis from 200 $\mu$ m sheets of skin were separated after 1 hour dispase treatment. Epidermis was digested with collagenase overnight then stained with a broad cell type panel for flow sorting. Cells were sorted from each gate and combined into four broad categories: myeloid (green), lymphoid (purple), CD49<sup>low</sup> KCs (pink) and CD49<sup>high</sup> KCs (brown) as shown by arrows of the same colour. These labels represent the 10X lanes each gate was sequenced on, as shown in **Figure 18**. Gates are named A-G which refers to the statistics in **Table 2**. Representative data is shown from a one of  $n = 3$  donors. KC = keratinocyte.

**Table 2**

Tissue	Dermis												
Droplet encapsulation lane	Myeloid							Fibroblasts	Endothelium	Lymphoid			
FACS gate	A	B	C	D	E	F	G	H	I	J	K	L	M
Percentage by loading unsampled	0.11	1.38	0.52	0.30	0.93	0.14	1.25	25.69	12.48	0.30	1.24	5.44	0.28
Percentage loaded after gating	1.28	2.30	1.96	1.40	1.69	1.55	2.30	12.50	12.50	3.34	3.39	3.39	2.39
Percentage upsampled	1161.34	167.44	378.17	468.10	182.34	1086.40	184.22	48.66	100.14	1103.00	272.64	62.35	842.45

Tissue	Epidermis						
Droplet encapsulation lane	Myeloid			CD49f low KCs	CD49f high KCs	Lymphoid	
FACS gate	A	B	C	D	E	F	G
Percentage by loading unsampled	0.80	0.05	0.09	30.93	17.79	0.06	0.29
Percentage loaded after gating	6.67	1.73	4.10	12.50	12.50	2.53	9.97
Percentage upsampled	836.37	3817.31	4604.19	40.42	70.27	4298.83	3498.30

**Table 2 – Sampling difference of skin cells with and without sorting.** Cells were sorted from dermis and epidermis using the **Figure 9-10** gating strategies to capture higher proportions of uncommon cell types. Columns represent the tissue and sorting gates. The “Percentage by loading unsampled” row shows the percentage of live single cells found in each gate, calculated as the mean of three samples and halved to account for equal loading of dermis to epidermis. The “Percentage loaded after gating” row shows the percentage of all 10X sequenced cells that originated from each gate, calculated as the mean of three samples. The “Percentage upsampled” row shows the percentage increase from the unsampled row to the gated row. Green numbers represent an increase in proportion, red numbers represent a decrease and yellow numbers represent gates for which the proportion has not changed by more than 5%. KC = keratinocyte.

### 3.2.5 Dissociation of human skin leads to loss of follicular structures

To investigate the effects of epidermal peeling on the structures found, skin was formalin fixed and paraffin embedded at various stages of the dissociation process, and slides H&E stained to aid in viewing morphology (**Figure 11**). Prior to cutting the skin to a uniform depth of 200µm, many structures can be seen, including hair follicles, associated sebaceous glands and endothelial vessels. The epidermis is easily recognisable by dark purple haematoxylin staining. The papillary dermis and reticular dermis are noticeably distinct, with eosin staining resulting in a much deeper hue of pink in the more collagen-rich reticular dermis. The increased cell density in the papillary vs reticular dermis is also visible through the blue nuclear staining.

While hair follicles are continuous with the epidermis, the vast majority of follicular keratinocytes are found deep in the reticular dermis where the bulb lies, much deeper than the 200µm depth used for dissociation. Sebaceous glands are also found deeper within the reticular dermis (**Figure 12**).

After cutting the 200µm thick skin graft, the reticular dermis can no longer be seen, as expected (**Figure 11**). The skin graft varies in thickness with the rising and falling of papilla. For example, in the image shown in **Figure 11**, this ranges from 258µm at the papillary trough to 402µm deep at the papillary peak. This may occur due to the papilla being squeezed through the graft knife. Some traces of hair follicle can still be seen after this cut is made, but the hair follicle bulbs containing the bulk of follicular cells are not seen (**Figure 11**).

After peeling the epidermis from the dermis, no epidermal structures can be seen in either tissue (**Figure 11**). It could be that the dispase separates hair follicles from the dermis, and the mechanical separation of the epidermis from the dermis breaks these structures from the epidermis, causing them to be lost during processing.

**Figure 11**

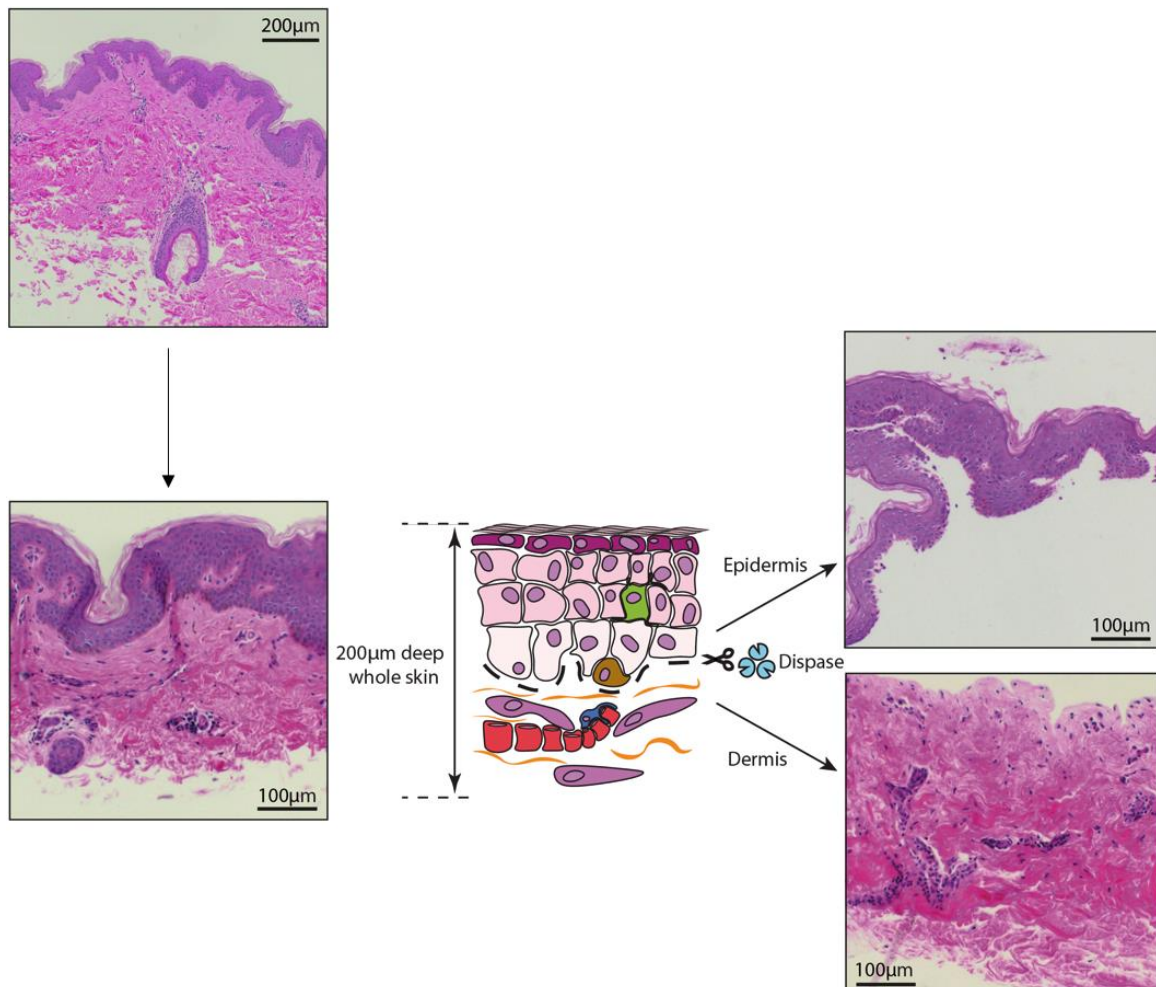


**Figure 11 – Hair follicles are lost during tissue processing.** Skin samples were collected from surgery, cut to 200µm depth using a dermatome, treated with dispase then peeled to separate dermis and epidermis. At each stage, ~1cm<sup>2</sup> of skin was formalin fixed for paraffin embedding, slides were sectioned and stained with H&E. **Top left:** Whole skin as received from surgery. **Bottom left:** Whole skin after cutting to 200µm depth. **Middle:** Schematic diagram of 200µm depth skin. **Top right:** Dispase separated epidermis. **Bottom right:** Dispase separated dermis. Scale bars represent the distance written above them. Representative images from one of  $n = 3$  samples shown.

**Figure 12**

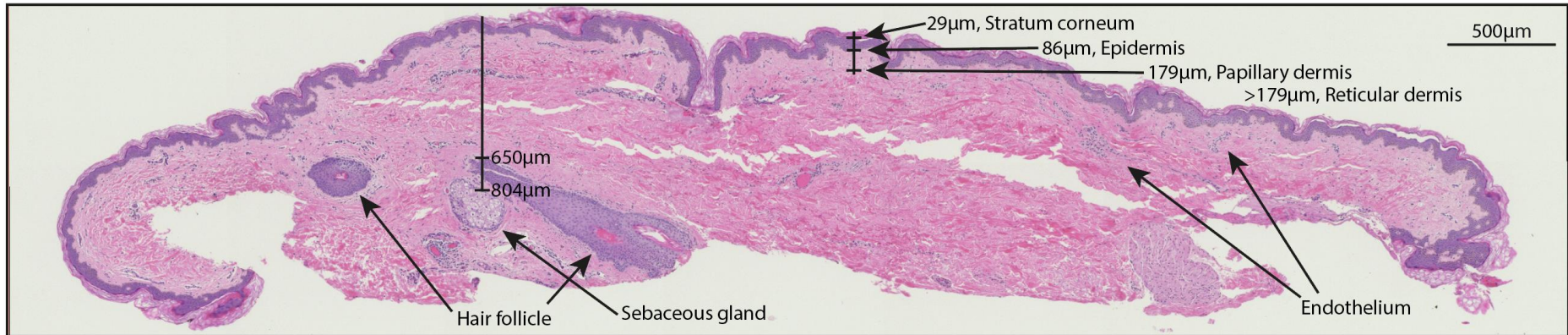


**Figure 12 – Hair follicle bulbs are found deep within the reticular dermis.** H&E stained slides from surgically removed skin (the top left panel of Figure 24) were imaged along their entire width by stitching tiled images and annotated with morphological features visible by H&E staining. Scale bar represents 500 $\mu$ m. Representative image from one of  $n = 3$  samples shown.

IHC staining for keratin 17, a marker of hair follicles, and haematoxylin was done on slides from each stage of dissociation to investigate whether hair follicle keratinocytes were detectable in the epidermal basal layer after mechanical separation (**Figures 13-16**). Hair follicles and sebaceous gland structures differentially stain positive for keratin 17 in the initial surgically removed skin, however after the skin graft cutting and mechanical separation of the epidermis, no positive cellular staining is seen (**Figures 15-16**).

### **3.2.6 Distorted distribution of basal and suprabasal keratinocytes**

Another interesting result is the ratio of basal to suprabasal cells found by flow cytometry (1:1.74, mean of 3 donors), as well as by CyTOF data shown in the next chapter (1:1.49, mean of 4 donors). In breast skin this ratio should be between 1:4 to 1:8 basal to suprabasal layers (Oltulu et al., 2018) (**Figure 12**). However, all live cells were liberated by enzymatic digestion, as evidenced by H&E staining of the epidermal material remaining after collagenase digestion, which shows that only the anuclear stratum corneum remains (**Figure 17**).

**Figure 13**

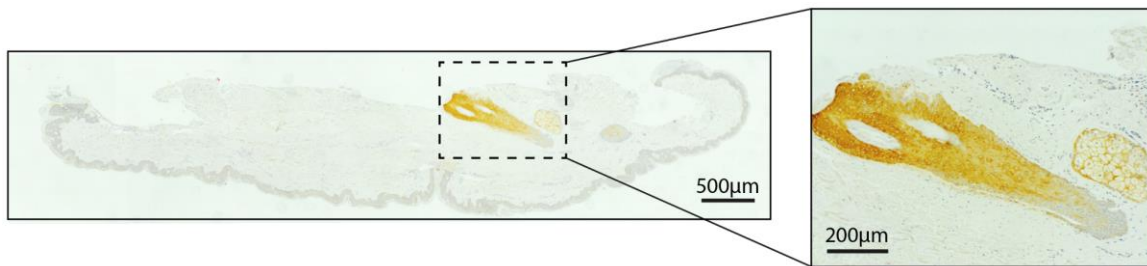


**Figure 14**

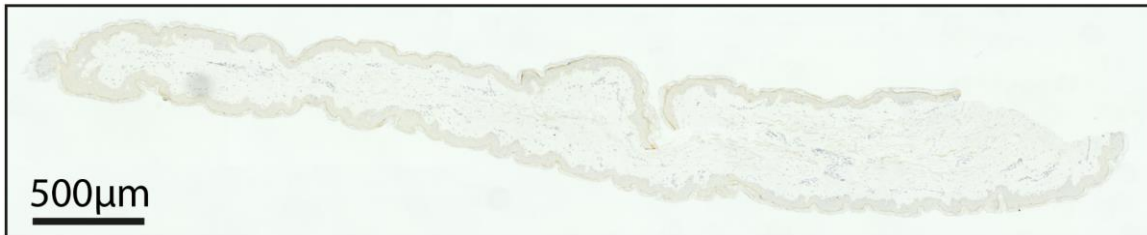


**Figure 15**



**Figure 16**

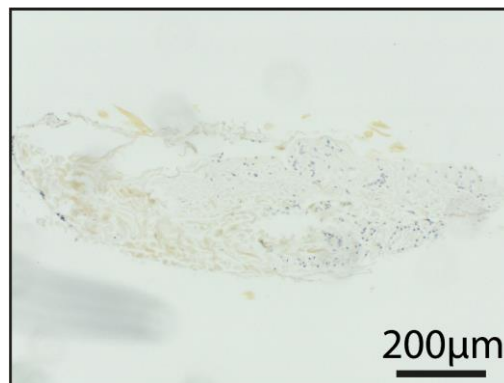


**Figure 13 – Follicular keratinocytes are present in surgically removed skin.**

**Figure 14 – Follicular keratinocytes are not present in 200µm depth skin.**

**Figure 15 – Follicular keratinocytes are not present in peeled epidermis.**

**Figure 16 – Follicular keratinocytes are not present in peeled dermis.**

FFPE skin slides were collected as in **Figure 11** and stained for keratin 17 (yellow) and haematoxylin. Scale bars represent the distance written above them. *n* = 1.



**Figure 17**

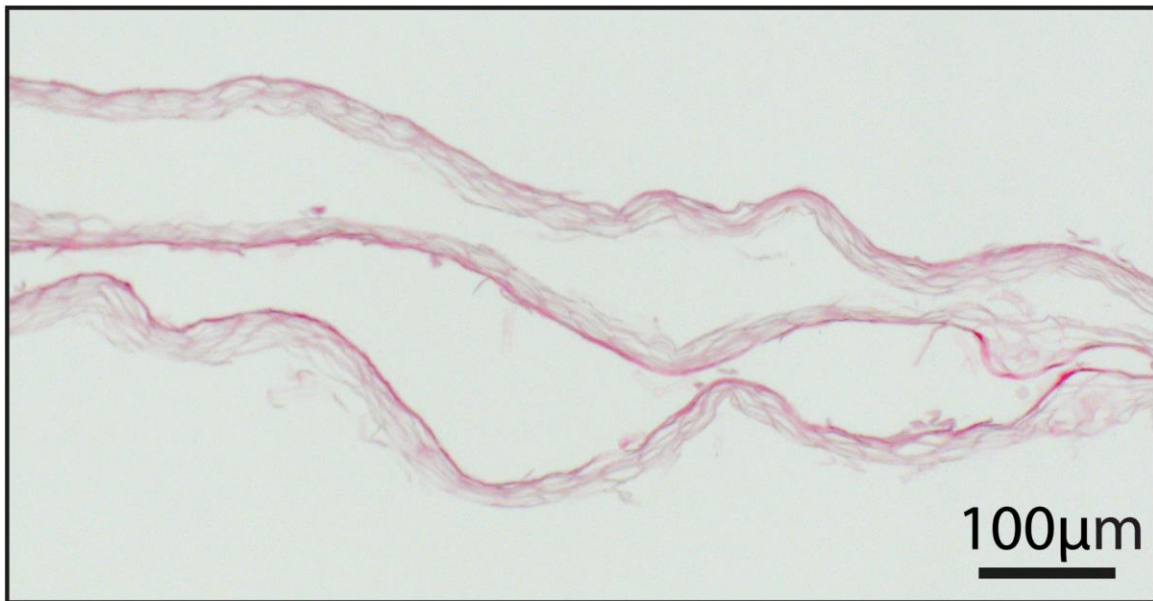


**Figure 17 – The stratum corneum alone remains after overnight epidermal collagenase digestion.** H&E staining of FFPE remnants of epidermis after 16 hours of collagenase digestion. Scale bar represents 100µm. Representative image from one of  $n = 2$  shown.

### 3.3 Discussion

Tissue dissociation is an inevitable concern when it comes to analysing cell suspensions from tissues. Every step in a dissociation protocol between collecting a sample and gaining data from it is time in which the cells are further from *in vivo* conditions, which can affect their expression profiles and phenotype. The overnight collagenase digestion used optimised the collection of the highest number of cells with an acceptably small viability loss, and without cleaving the protein markers needed for FACS. This is important as failing to capture rare heterogeneity cannot be retrospectively solved, as there is no way to definitively know if any unreported cell types or states exist and were not accounted for.

The optimisation results reveal that treating the epidermis for less time with type IV collagenase might have resulted in a higher yield, but keeping the conditions consistent across tissues was critical to comparatively analysing cells from dermis and epidermis (**Figures 3-5**). While trypsin digestion may also have liberated more epidermal cells, it has been reported to cleave many surface markers that would have hindered the FACS sampling of rarer immune cells (Botting et al., 2017). Cheng *et al.* analysed 92, 889 human epidermis cells from 12 samples using 10x, but the use of trypsin digestion liberated mostly keratinocytes with minimal immune cells (Cheng et al., 2018). Tabib *et al.* reported a much larger variety of cell types than Cheng *et al.* by using Miltenyi biotec's ready-made skin dissociation kit, but without epidermal peeling or sorting cells they also recovered few immune cells or keratinocytes (Tabib et al., 2018a).

It would be a helpful endeavour to compare transcriptome profiles under different dissociation conditions, to assess the level of inevitable transcriptome impact imparted from the dissociation method. Liberating single cells from tissue for scRNA-seq without any impact is currently impossible, but comparing data from shorter time courses of collagenase dissociation, as well as bulk data from immediately lysed tissue before and after dispase treatment could help to assess these impacts. Furthermore, the optimisation of dissociation presented in this thesis aimed only to ensure adequate variety and quantity in cells released, as well as to minimise cell death – a *de facto* marker of cell health and deviation from *in vivo* conditions. To refine the collagenase time point chosen, other biomarkers

which more directly assess the effects of *ex vivo* culture could have been assessed at each time point. For example, qPCR targeted for stress-response genes such as heat shock proteins could have more accurately determined the length of dissociation treatment at which optimal cell quality is maintained (Denisenko et al., 2020).

Having sampled only the papillary dermis and above, hair follicles and their associated cells, including arrector pili muscle cells, follicular stem cells and sebaceous gland cells, were not accounted for in this experiment. Hair follicle gene signatures have been previously reported as specific to mechanically separated reticular dermis, which Phillippeos *et al.* attribute to the placement of the follicular bulb deep within the reticular dermis (Phillippeos et al., 2018). Hair follicle cell states have been dissected with scRNA-seq in mouse, revealing previously unreported follicular populations, as well as the mixed contributions of both interfollicular epidermis (IFE) and follicular cells towards IFE wound healing (Joost et al., 2018, 2016). This approach was possible due to both the vastly increased density of hair follicles in murine skin compared to human as well as the authors use of Sca-1 bead enrichment to select for follicular cells. Investigation and validation of this heterogeneity within the cellular constituents of human hair follicles would be an interesting avenue to explore, and would likely require a specialised protocol such as microdissection to extract hair follicles at a high enough proportion for single cell capture.

Other than hair follicle structures, the remaining live cells appear to have been completely dissociated from skin as evidenced by H&E staining of the material left post digestion. However, less suprabasal keratinocytes were found by flow and mass cytometry than expected. This may be because cells in the basal layer will be more easily liberated by type IV collagenase due to the expression of collagen type VIII (COL7A1) that bind the cells to the DEJ, and as a result partially liberated clumps of suprabasal cells may have been filtered out (Watanabe et al., 2018). The more superficial cells in the suprabasal layers also begin to lose their nuclei and stop transcribing RNA, so it is likely that these cells would be lost to dead cell gating by flow, and would not be picked up by sequencing regardless, due to the lack of cytoplasmic RNA.

Another avenue for the expansion of this dataset is the comparison of skin from different sites. Breast skin was chosen due to the availability of sample with the aim of sequencing high cell numbers to interrogate potential rare populations, and this sample site was kept consistent within the experimental design. In particular, the number of immune cells found in skin varies widely with anatomical site, with higher concentrations of LCs and T cells found in back skin than in arm, abdomen or thigh skin (Del Duca et al., 2019). They can also differ functionally. For example, Bertram *et al.* report differences in HIV trafficking in LC subsets from anogenital skin (Bertram et al., 2019), and Del Duca *et al.* report heterogeneity of inflammatory marker expression by T cells and LCs across body sites (Del Duca et al., 2019). The number of layers of keratinocytes, and the density and diameter of hair follicles, also varies between anatomical sites, and with this likely comes differences in the keratinisation process (Oltulu et al., 2018; Otberg et al., 2004).

It is of note that the tissue dissociation optimisation presented here is therefore also specific to breast skin. Differences in epidermal thickness will particularly affect this processing method. The epidermis of dorsal hand skin can be more than twice as thick as that of breast, and as such would significantly reduce the amount of dermis sampled in the 200µm layer removed, and could possibly require harsher dissociation than overnight collagenase due to the lower surface area to volume ratio of the thicker epidermis (Oltulu et al., 2018). In terms of practicality, small skin samples will also be much more difficult to mechanically separate. These considerations mean that the optimised methods for high skin cell recovery would need to be worked up on skin from other body sites.

The optimised method of cell recovery from breast skin by using overnight treatment of type IV collagenase after dispase-assisted epidermal separation allowed for the liberation of high numbers of cells from both dermis and epidermis, with significant upsampling ratios of rare immune cells. These results ensured that skin heterogeneity would be adequately captured at a single cell level for scRNA-seq and mass cytometry.

**Chapter 4. Single cell analysis of the cellular  
composition of human skin**



## 4.1 Chapter 4 Introduction

Skin is highly cellularly diverse. It carries out vital functions as a barrier to infection, water loss and physical injury. These functions, and normal skin homeostasis, require this cellular heterogeneity and crosstalk between the diverse cell types in skin. Further understanding this intercellular heterogeneity is therefore of great interest. Skin is also a highly accessible organ. Healthy skin is commonly surgically removed, unlike most organs for which research samples are primarily resected due to disease, and is therefore a good model organ to profile healthy tissue.

Much of current skin knowledge is based on bulk skin experiments such as whole tissue sequencing, low parameter single cell experiments such as flow cytometry and microscopy (Haniffa et al., 2012; Wang et al., 2014) or the use of model systems, i.e. cultured cell lines or mammalian models (mostly murine) which, while useful, do not fully recapitulate the cellular landscape of human skin. Single cell RNA sequencing allows for both high dimensionality and analysis of single cell heterogeneity. Analysis of whole transcriptomes also addresses the bias introduced with selecting markers, and the issues inherent to transient changes in surface protein expression which can mask cell identity.

Therefore scRNA-seq was employed to generate a robust and comprehensive report of transcriptomes of the cell types present in healthy adult human skin, the heterogeneity within these cell types and to identify the transcriptomic markers which best identify each of these cells.

## 4.2 Results

### 4.2.1 Droplet based single cell sequencing of healthy human skin

Healthy adult human skin from the breast of female donors was dissociated after dispase-separation of epidermis and dermis, and FACS was employed to remove dead cells and doublets as well as upsample rare cell types (**Chapter 3, Figures 9-10**). A droplet based sequencing approach, specifically the 10x Genomics Chromium Controller, was then used to separate the FACS purified and sampled cells into barcoded single cells for sequencing (**Figure 18**). This high throughput approach allowed for the sequencing of

many more cells than a plate based approach, to better account for the cellular heterogeneity in human skin.

After sequencing and alignment, the sequencing data from all three donors was combined and processed as described in the methods by Dr Peter Vegh, a post-doctoral computational scientist in the Haniffa Lab. Single cell sequencing plots were generated in R and Python primarily by Dr Peter Vegh and Dr Gary Reynolds. Annotation of the scRNA-seq data and interpretation and generation of figures was carried out primarily by myself, as fully detailed in the declaration at the beginning of this thesis.

Single cell sequencing data consists of thousands of dimensions, which is impossible for a human to visualise and extremely time consuming for a computer to analyse. To simplify the data for visualisation and analysis, gene expression, which represents thousands of plottable axes in the data, are converted into principle components by PCA – tens of axes of sets of genes representing most of the variation within the data. This was then further simplified into two axes by uniform manifold approximation and projection (UMAP), and in parallel cells were grouped by similarity using Louvain clustering, and the resulting clusters annotated by matching gene expression to published gene and protein expression knowledge, along with the sequencing-lane-barcoded knowledge of the FACS gate origin and tissue origin (epidermis or dermis) of each cell.



**Figure 18**

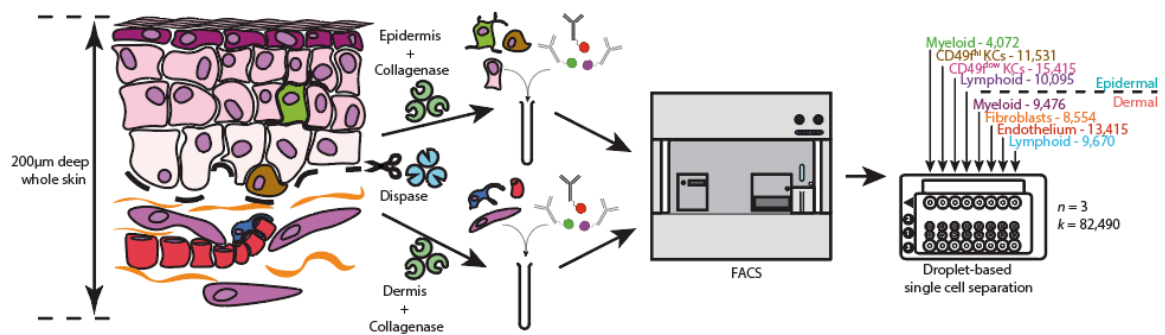


**Figure 18 – Experimental overview of 10X sequencing of healthy adult human skin.**

Skin from three donors was dispase treated and peeled to separate dermis and epidermis. Each tissue was collagenase digested and the cells stained with a broad cell type panel, then separated using FACS with the gating strategies shown in **Figures 9-10**. FACS enriched cells were loaded on the 10X Chromium Controller before sequencing. The coloured numbers are the final cell numbers analysed per lane by scRNA-seq.  $k$  = the total number of cells analysed post-QC from  $n = 3$  donors. KC = keratinocyte.

In total 82,490 cells passed QC, with an average of ~3000 genes per cell. Louvain clustering resulted in nineteen clusters at broad low resolution, done with the aim of segregating the cells into their cell types prior to breaking down the inter-cell-type heterogeneity (**Figures 19-22**). Sample mixing was done using Harmony (Korsunsky et al., 2018) to correct for differences caused by batch effect, and all three samples showed good mixing, with each of the nineteen clusters containing cells from each sample (**Figure 20** and **Table 3**). Average UMI and gene counts varied largely by sort gate, but these trends were consistent across each sample (**Figure 23**). For example, lymphoid cells (CD45+ HLA-DR-) in both the epidermis and dermis contained the lowest UMI and gene counts across all gates in each of the three samples, and nonimmune cells (fibroblasts, CD49<sup>low</sup> KCs and CD49<sup>high</sup> KCs) were the highest in each sample (**Figure 23**).

The top differentially expressed genes in each cluster highlights the cellular identity of each cluster, as well as providing the most rigorous RNA markers with which to identify these cells in future experiments (**Figure 24**).

In the epidermis, the following populations were identified: suprabasal keratinocytes expressing *KRT1* and lacking *ITGA6* expression, basal keratinocytes expressing *ITGA6*, *KRT5* and *KRT14*, melanocytes expressing *DCT* and *PMEL*, and epidermal APCs expressing MHC class II subtypes and *RNASE1* (Alam et al., 2011; Baxter & Pavan, 2003) (**Figures 19, 22** and **24**).

The dermal cell types found were: fibroblasts expressing *DCN* and *TNFAIP*, pericytes expressing *RGS5*, vascular endothelial cells expressing *PECAM1*, lymphatic endothelial cells expressing *CCL21*, schwann cells expressing *FGL2*, a subset of schwann cells expressing fibroblast genes like *LUM* called stromal schwann cells, plasma cells expressing immunoglobulin genes such as *IGKC*, pDCs expressing *GZMB* and dermal APCs expressing MHC class II subtypes (Zhang et al., 2018; Mitchell et al., 2008; Schenkel et al., 2002; Vaahtomeri et al., 2017; Gould et al., 2019; Jahrsdörfer et al., 2010) (**Figures 19, 22** and **24**).

**Figure 19**

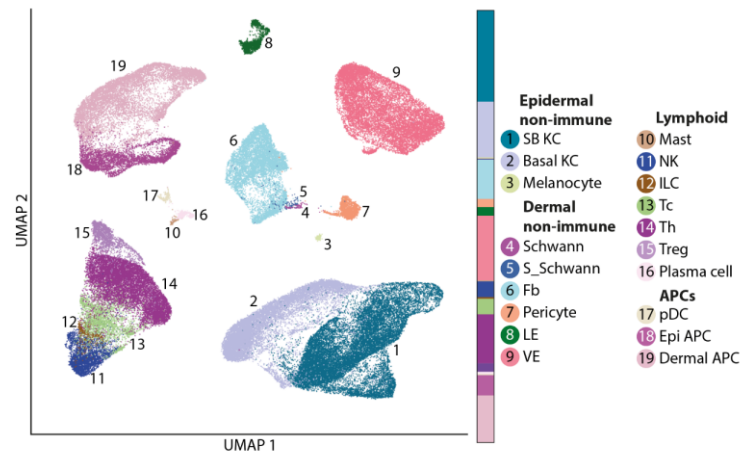


**Figure 20**

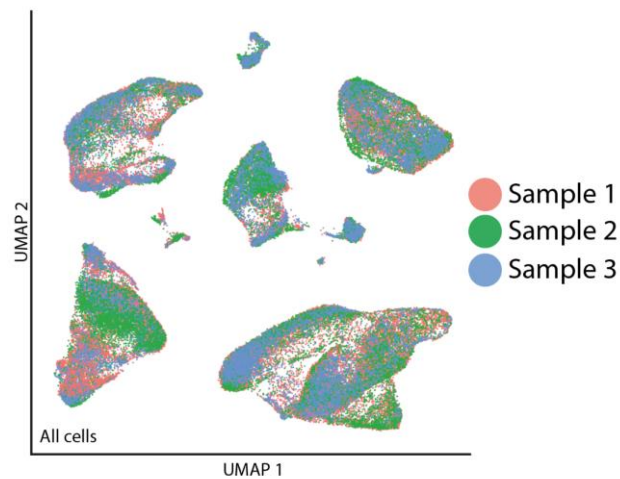


**Figure 19 – Broad cellular heterogeneity of healthy adult skin.** scRNA-seq data of skin cells that passed QC from  $n = 3$  donors was clustered and then UMAP coordinates were generated and plotted by Dr Peter Vegh. Clusters were manually annotated by comparing differentially expressed genes between clusters to the literature, as well by using the tissue and FACS gate origin of cells in each cluster. Each dot represents a single cell. Each colour represents a different cell type. The coloured bar between the UMAP and the legend represents the proportion of each annotated cell type. APC = antigen presenting cell; Epi = epidermal; Fb = fibroblast; ILC = innate lymphoid cell; KC = keratinocyte; LE = lymphatic endothelium; NK = Natural killer cell; pDC = plasmacytoid dendritic cell; S\_Schwann = Stromal Schwann cell; SB KC = suprabasal KC; Tc = cytotoxic T cell; Th = T helper cell; VE = vascular endothelium.

**Figure 20 – UMAP visualization of scRNA-seq analysis of healthy adult skin cells annotated by sample.** UMAP plot generated by Dr Peter Vegh. The same UMAP displayed in **Figure 19**, coloured by donor.

**Figure 21**

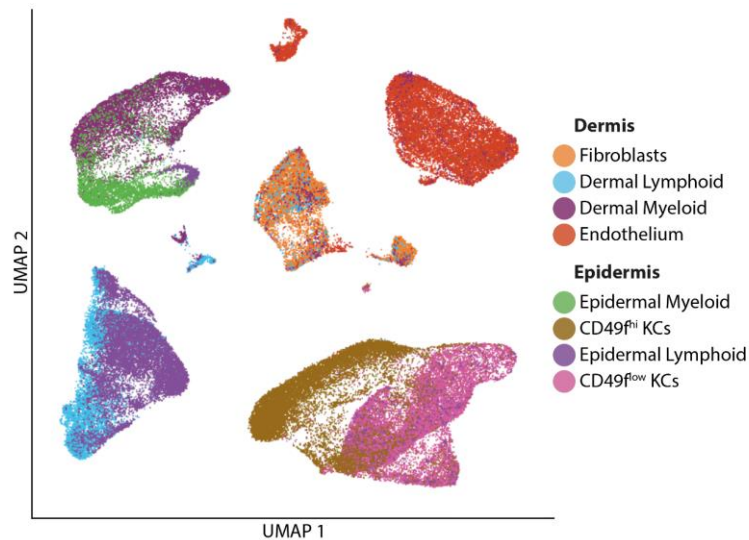


**Figure 22**

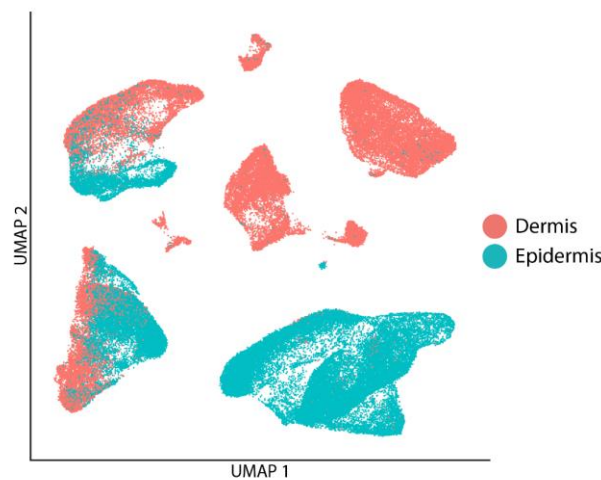


**Figure 21 – UMAP visualisation of scRNA-seq analysis of healthy adult skin cells annotated by 10x lane.** UMAP plot generated by Dr Peter Vegh. The same UMAP displayed in **Figure 19**, coloured by 10X lane. Labels refer to the lanes described in **Figures 9-10**.

**Figure 22 – UMAP visualisation of scRNA-seq analysis of healthy adult skin cells annotated by tissue.** The same UMAP displayed in **Figure 19**, but coloured by tissue of origin.

**Table 3**

Cluster	s1	s2	s3
CD83_KC	1071	951	122
DC1	49	78	75
DC2	259	76	96
F1	1325	1580	891
F2	981	443	628
F3	437	820	337
IL23_DC	311	224	232
ILC	185	51	49
KLF10_LC	178	60	29
LC1	484	126	306
LC2	648	149	320
LC3	773	135	337
LC4	100	170	64
LE1	158	185	174
LE2	293	535	283
Macrophage1	901	396	226
Macrophage2	598	212	148
Mast	161	4	27
Mel	114	98	32
mig_cDC	108	186	170
Mitotic_KC	274	119	143
moDC1	345	382	206
moDC2	889	901	461
moDC3	490	573	392
NK1	1509	282	244
NK2	525	71	143
NK3	118	72	44
pDC	117	109	14
Pericyte	461	693	435
Plasma_cell	150	221	17
Postmitotic_KC	9692	3449	2031
Premitotic_KC	5662	2682	1707
Schwann	29	45	7
Stroma_Schwann	40	69	18
Tc	1369	1035	569
Th	3820	3098	2416
Treg	999	268	354
VE1	3265	1810	968
VE2	2948	1936	1036
VE3	148	87	112

**Table 3 – Cell numbers per sample of detailed annotations of adult skin scRNA-seq data.** The broad annotations shown in **Figure 19** were subsetted into four groups (**APCs** – Epi APC, Dermal APC; **Lymphoid** – NK, ILC, Tc, Th, Treg; **Nonimmune** – Schwann, S\_Schwann, Fb, Pericyte, LE, VE, Melanocyte; **Keratinocytes** – SB KC, Basal KC). Each group was reanalysed to generate more detailed clusters and differentially expressed gene lists. Columns s1, s2 and s3 display the number of cells in each of the three samples found in each of these more detailed clusters. DC = dendritic cell; ILC = innate lymphoid cell; F = fibroblast; LC = Langerhans cell; LE = lymphatic endothelium; Mel = melanocyte; mig\_cDC = migratory conventional DC; moDC = monocyte-derived DC; NK = Natural killer cell; pDC = plasmacytoid DC; s = sample; Tc = cytotoxic T cell; Th = T helper cell; T reg = regulatory T cell; VE = vascular endothelium.

**Figure 23**

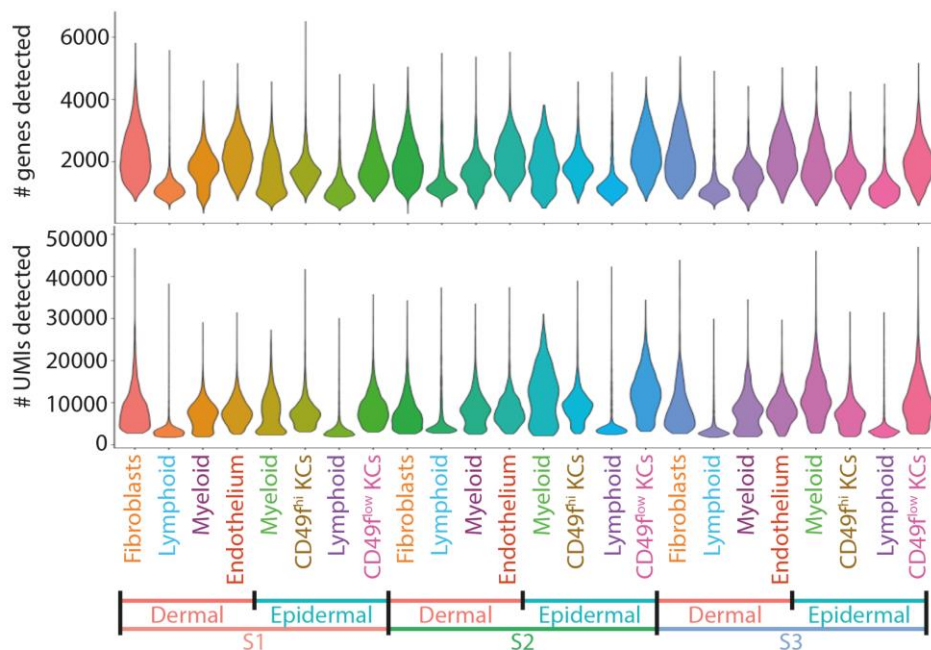


**Figure 23 – QC Violin plots of UMIs and genes found per cell in each 10x lane.** Violin plots generated by Dr Peter Vegh. Data metrics per sample and 10x lane. Unique molecular identifiers (UMIs) track the number of RNA molecules captured from each individual cell. Genes detected refer to the number of unique genes identified per cell, regardless of UMI count per gene. The width of each violin plot is related to the ratio of cells found at a particular Y coordinate. KC = keratinocyte.

**Figure 24**

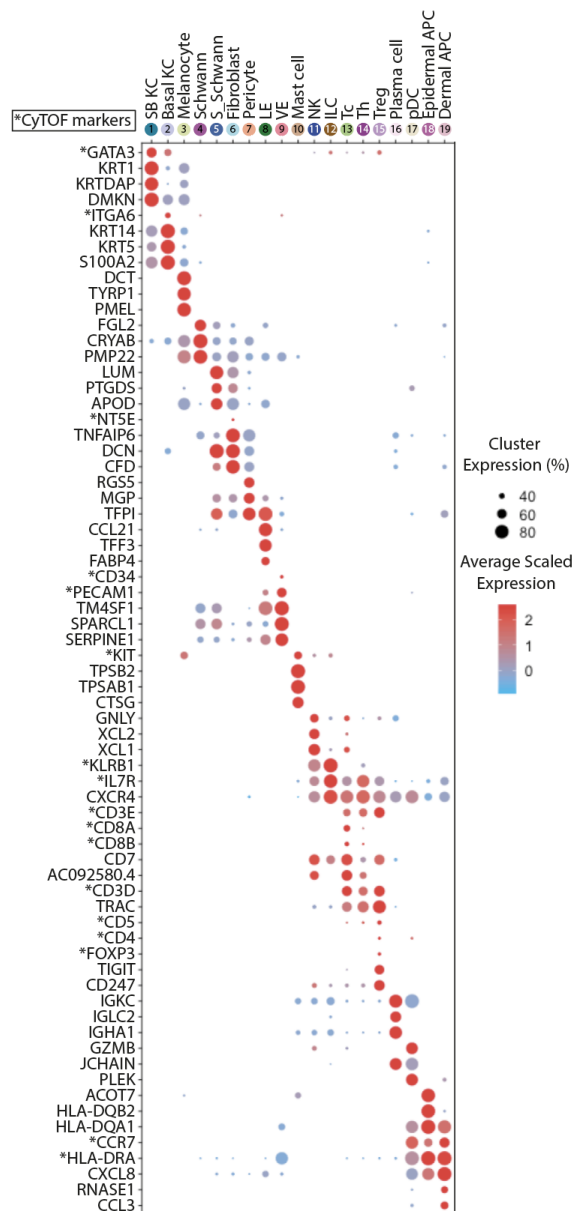


**Figure 24 – Top differentially expressed genes between the cell types in healthy adult skin.** Heatmap generated by Dr Peter Vegh. Differentially expressed genes were calculated for each cell type and plotted as a heatmap, alongside genes of protein markers used in for CyTOF (demarcated by a preceding asterisk (\*)) (**Figures 35-36** and **Table 1**). Cluster labels on the X axis correspond to those displayed in **Figure 19**. The radius of each circle corresponds to the percentage of cells within a cluster positively expressing each marker. The intensity of colour, from blue to red, corresponds to the relative average intensity of expression of cells within the cluster.

Across both tissue compartments the following cell types were identified: Cytotoxic T cells expressing *CD8A* and *CD8B*, helper T cells expressing *CD3D* and lacking *CD8A/B* expression, regulatory T cells expressing *TIGIT*, natural killer cells expressing *GNLY*, innate lymphoid cells expressing high levels of *IL7R* and mast cells expressing *KIT* (Joller et al., 2014; Veljkovic Vujaklija et al., 2013; Rafei-Shamsabadi et al., 2018; Cruse et al., 2014)(**Figures 19, 22 and 24**).

#### **4.2.2 Skin APCs are highly heterogeneous**

To further interrogate the heterogeneity found within the cell types of healthy adult human skin, the scRNA-seq data was split into four subsets: APCs, lymphoid cells, keratinocytes and the remaining nonimmune cells. Dr Gary Reynolds carried out higher resolution clustering on the APC fraction of the data, pulling out 14 clusters (**Figure 25**). Of mostly dermal cells: 4 DC clusters, 3 monocyte clusters and 2 macrophage clusters were found. Of mostly epidermal cells, 5 clusters of LCs were found. pDCs were also found but weren't included in the APC subset due to their stark transcriptional differences that would drive variable gene calculation towards splitting pDCs from the remaining APCs.

#### **4.2.3 DCs with dermal signatures isolated from the epidermis**

At both broad annotations and higher resolution clustering, dermal and epidermal APCs remain mostly distinct (**Figures 22 and 26**). However, some epidermal cells clustered together into dermal transcriptome identities. In particular, the moDC and migratory DC clusters contained cells isolated from the epidermis. This could suggest that these cells are able to migrate between the dermis and epidermis in healthy skin.

#### **4.2.4 Langerhans cells can display low HLA-DR protein expression**

The majority of the Langerhans cells were captured in the CD45+ HLA-DR+ gates and ran on the Epidermal Myeloid lane (**Figure 27**). However, most of the *KLF10*+ LCs and some of the LC1 cells were captured in Epidermal Lymphoid lane, meaning they fell into the CD45+ HLA-DR- gates (**Figures 10 and 27**). This is unexpected, as LCs classically express high levels of HLA-DR, and may mean that many studies isolating LCs in this manner do not account for, or misrepresent the rarity of, these particular subsets.



**Figure 25**

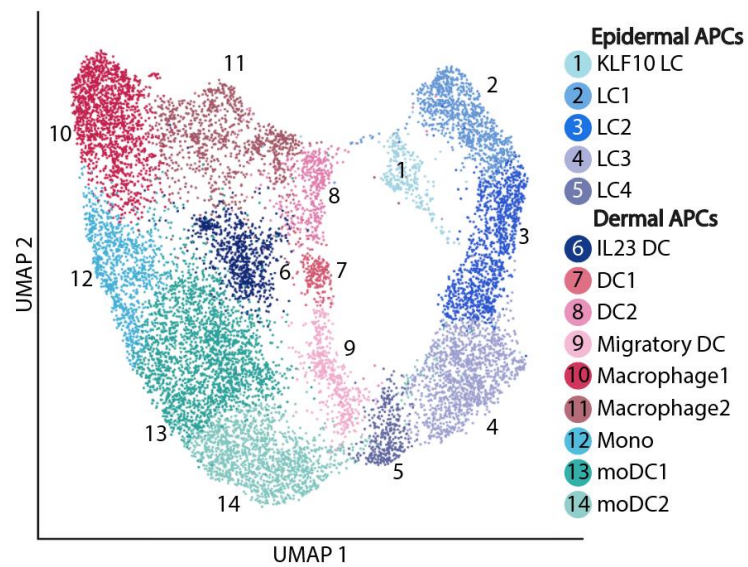


**Figure 25 – Heterogeneity of APC populations in healthy human skin.** UMAP plot generated by Dr Gary Reynolds. UMAP visualisation of antigen presenting cell (APC) populations found in epidermis and dermis. Colours represent cell types. DC = dendritic cells; LC = Langerhans cell; moDC = monocyte-derived DC; Mono = monocyte.

**Figure 26**

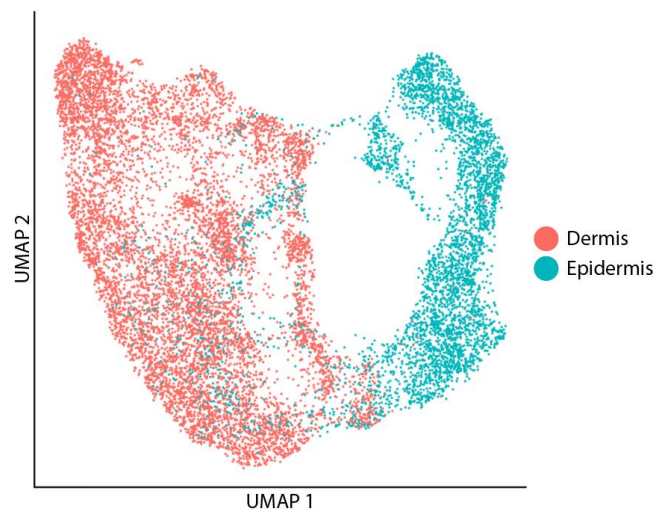


**Figure 26 – UMAP visualisation of scRNA-seq analysis of skin APC populations annotated by tissue.** UMAP plot generated by Dr Gary Reynolds. The same UMAP displayed in **Figure 25**, coloured by tissue.

**Figure 27**

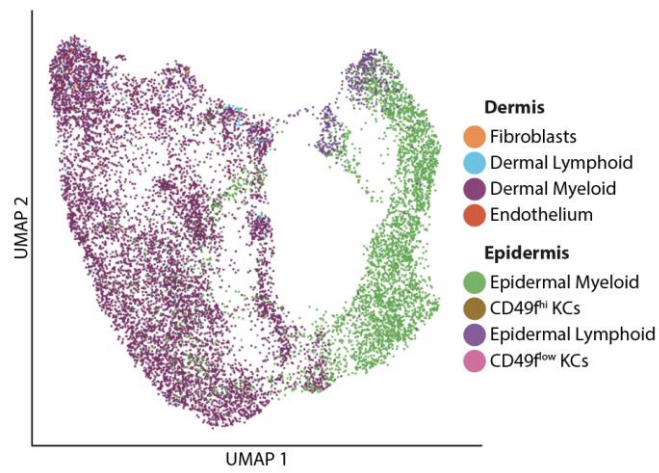


**Figure 27 – UMAP visualisation of scRNA-seq analysis of skin APC populations annotated by 10x lane. The same UMAP displayed in Figure 25, coloured by 10x lane.**

#### 4.2.5 Innate and adaptive lymphoid cell heterogeneity

Re-clustering the lymphoid cells at higher resolution revealed three clusters of NK cell (named NK1, NK2 and NK3) along with the helper, cytotoxic and regulatory T cell divisions and ILCs (**Figure 28**). Plasma cells and mast cells weren't included in the clustering and UMAP analysis due to their very different transcriptomes, which would drive the variable gene analysis towards separating them from the other lymphoid cells, rather than separating the heterogeneity within the lymphoid cells.

T cells did not form biologically meaningful distinct groupings further than the expected Tc, Th and Treg subsets, and rather separated primarily by their origin of epidermis or dermis (**Figure 29**). Interestingly, some expression of gamma-delta TCR genes (*TRGC1*, *TRGC2* and *TRDC*) was seen in the Tc cells, but these did not form a clear and distinct  $\nu\delta$  T cell cluster (**Figure 30**).

The four clusters of innate lymphoid cells could be split by expression of key killer cell functional genes (**Figure 31**). NK1 express high levels of *XCL1* and *XCL2*, as well as *KIT* which is not expressed in the other NK clusters. NK2 express the canonical NK receptor genes *KLRD1* and *KLRC1*, which are involved in initiating cytokine secretion upon immune challenge. NK3 are characterised by expression of the granzyme and perforin genes *GZMA*, *GZMB*, *GZMH* and *PRF1* and appear to be functionally active (**Figure 31**). Interestingly, the vast majority of epidermal NK cells were in the NK1 cluster (**Figure 29**). ILCs expressed high levels of the ILC receptor *IL7R* as well as *KLRB1*, and did not express the granzymes and killer genes expressed in the NK clusters. They may correspond to ILC3 phenotype due to expression of *KIT* (Bar-Ephraim et al., 2017).

**Figure 28**

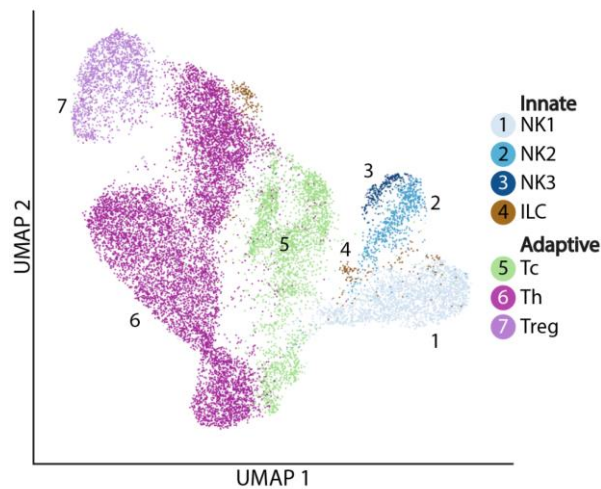


**Figure 28 – Lymphoid cell heterogeneity in healthy human skin.** UMAP plot generated by Dr Peter Vegh. UMAP visualisation of lymphoid cell populations found in epidermis and dermis. Colours represent cell types. ILC = innate lymphoid cell; NK = Natural Killer cell; Tc = cytotoxic T cell; Th = T helper cell; Treg = regulatory T cell.

**Figure 29**

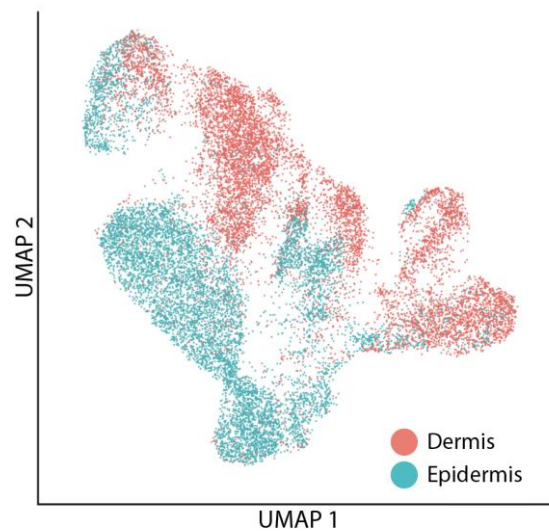


**Figure 29 – UMAP visualisation of scRNA-seq analysis of skin lymphoid cell populations annotated by tissue.** UMAP plot generated by Dr Peter Vegh. The same UMAP displayed in **Figure 28**, coloured by tissue.

**Figure 30**

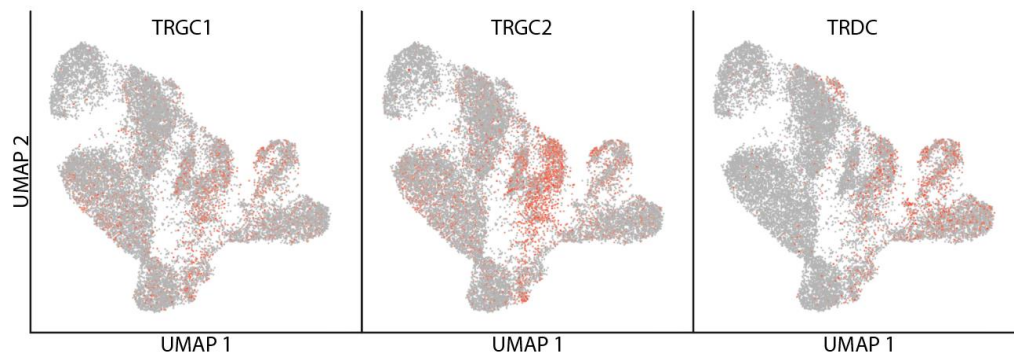


**Figure 30 – Gamma delta TCR expression in healthy skin.** Feature plots showing the expression of TCR genes on the UMAP shown in **Figure 28**. Relative expression is displayed from grey (no expression) to bright red (high expression).

**Figure 31**

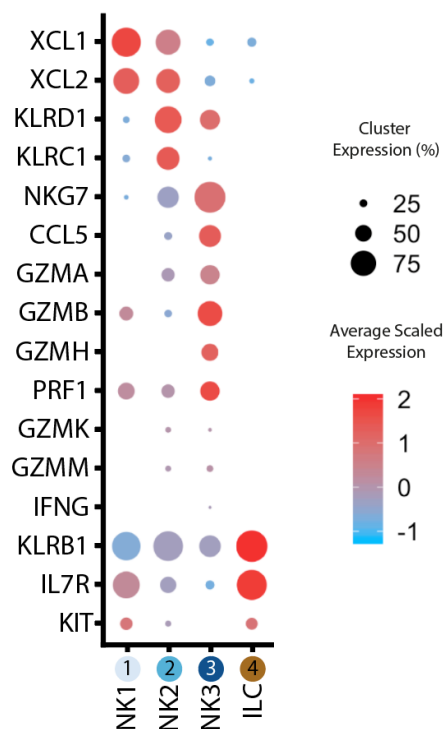


**Figure 31 – Functional gene variance in skin innate lymphoid cells.** Expression of genes reported in Natural Killer (NK) cells and Innate Lymphoid cells (ILCs) displayed as a heatmap. The radius of each circle corresponds to the percentage of cells within a cluster positively expressing each marker. The intensity of colour, from blue to red, corresponds to the relative average intensity of expression of cells within the cluster.

#### 4.2.6 Tissue microenvironmental differences affect lymphocyte transcription

As lymphoid cells were the only cells that clustered together regardless of dermal or epidermal origin, differential gene expression between the two compartments was interpreted to investigate the possible effects of microenvironmental cues. Tregs, helper T cells, cytotoxic T cells, NK1 and mast cells were found in both tissue compartments.

Differential gene expression between epidermal and dermal T cells revealed a number of genes upregulated in epidermal T cells. This included genes involved in TCR priming including *GADD45B*, *LMNA* and *TNFRSF18* as well as genes involved in tolerance such as *DUSP4*, *CD96* and *LY9* (**Figure 32**) (Bignon et al., 2015; Oukka et al., 2004; Stanko et al., 2018). Epidermal T cells may be more primed to respond to antigen presentation with either an immune response or tolerance due to the closer proximity to skin surface antigen challenge. To show that these expression differences weren't introduced by "soup effect", the introduction of noise in single cell sequencing data from free-floating RNA, dermal and epidermal NK1 were also compared, and the extent of differential expression of these genes was much lower than in the T cells (**Figure 32**).

Next, NK1 cells were compared across dermis and epidermis, as this was the only NK cluster with high cell numbers in both tissue compartments, revealing genes upregulated in each compartment. *XCL1* and *XCL2*, chemokines for XCR1, were both upregulated in epidermal NK1, suggesting a role in the potential trafficking of XCR1+ leukocytes into the epidermis (Matsuo, Kitahata, et al., 2018). Dermal NK1 expressed higher levels of functional killer genes such as *KLRB1*, *GNLY* and the anti-viral interferon-induced transmembrane proteins *IFITM1*, *IFITM2* and *IFITM3* (**Figure 33**) (Bailey et al., 2014). The gene expression profiles of NK cells in healthy skin may therefore vary to accommodate different functional roles the epidermis and dermis.

**Figure 32**

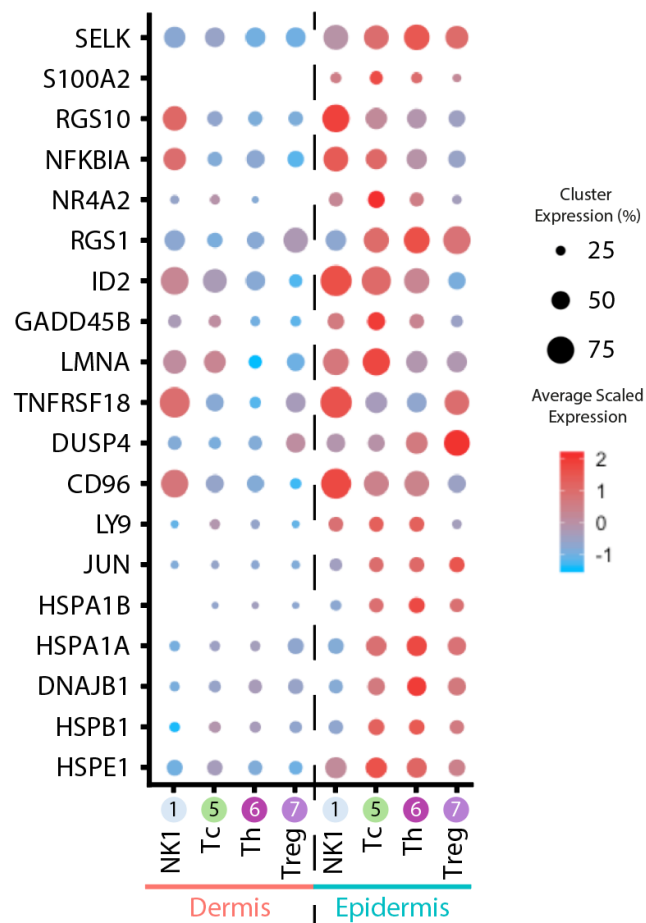


**Figure 32 – Tissue microenvironment-specific gene expression in skin T cells.** Heatmap displaying differentially expressed genes between dermal and epidermal T cells. NK1 cells are displayed as a control for tissue-wide gene expression differences. The radius of each circle corresponds to the percentage of cells within a cluster positively expressing each marker. The intensity of colour, from blue to red, corresponds to the relative average intensity of expression of cells within the cluster.

**Figure 33**

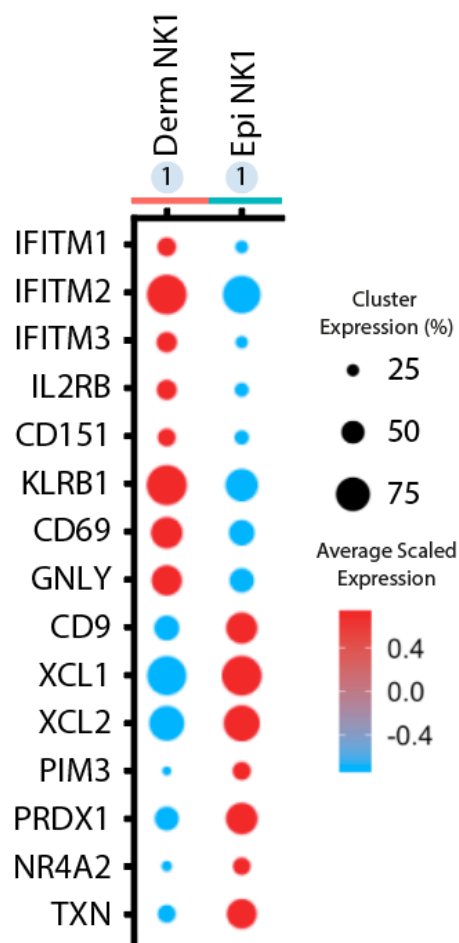


**Figure 33 – Tissue microenvironment-specific gene expression in skin NK cells.**

Heatmap displaying differentially expressed genes between dermal and epidermal NK cells. The radius of each circle corresponds to the percentage of cells within a cluster positively expressing each marker. The intensity of colour, from blue to red, corresponds to the relative average intensity of expression of cells within the cluster. Derm = Dermal; Epi = Epidermal.



#### 4.2.7 Epidermal mast cells are present at low numbers in healthy skin

Mast cells were also found in both the dermis and epidermis, identifiable by known mast cell markers including *KIT*, *CTSG* and *TPSAB1* (**Figure 34**) (Douaiher et al., 2014). These key functional receptors and mast cell granule proteases are expressed in both tissue compartments. However, differential gene expression analysis between the two clusters showed unique expression of some genes in each compartment. This includes pro-inflammatory *LXN* expression (Seed et al., 2019) in dermal mast cells, and anti-inflammatory *SOCS4* expression (Kedzierski et al., 2014) in epidermal mast cells which may suggest, counter to reports that epidermal mast cells are only seen during inflammation, that epidermal mast cells are present in healthy non-inflamed skin and are playing a more anti-inflammatory role than their dermal counterparts in steady state (**Figure 34**).

#### 4.2.8 Mass cytometric proteomic profiling of human skin

To compare the scRNA-seq data with protein expression profiling, Cytometry by Time of Flight (CyTOF/Mass Cytometry) was performed in parallel to sequencing. As only up to 40 protein markers can be used, CyTOF has much less resolving power than scRNA-seq, but the differences in RNA and protein expression are important to account for where possible regardless.

Dermal and epidermal cells were prepared in the same way as the scRNA-seq experiment, as detailed in methods, for four donors, and the cells were stained with a panel designed with the aim of capturing the phenotypes of all the major skin cell types (**Table 1**). The FCS files generated were gated to remove 191Ir<sup>-</sup> acellular debris, 195Pt<sup>+</sup> dead cells, QC beads (used to determine the efficiency of the CyTOF fluidics), and 133Cs<sup>+</sup> environmental contamination.

**Figure 34**

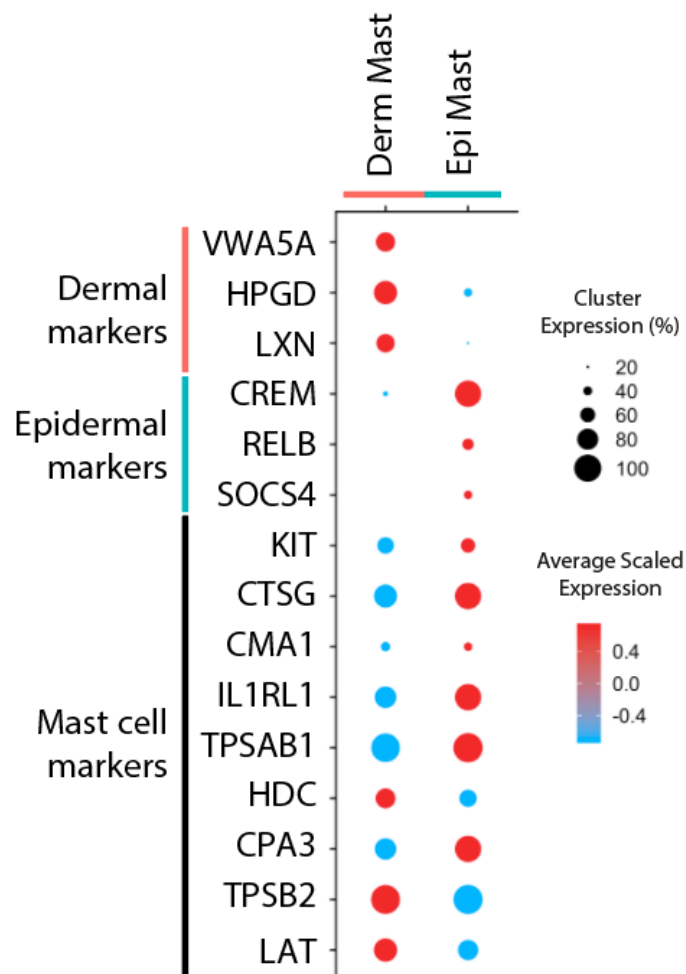


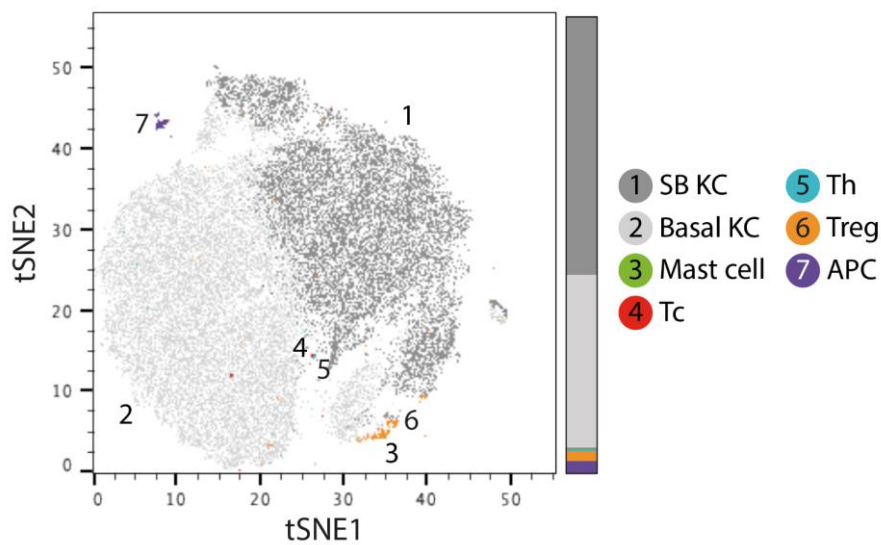
**Figure 34 – Tissue microenvironment-specific gene expression in skin mast cells.**

Heatmap displaying both known mast cell functional genes and differentially expressed genes between dermal and epidermal mast cells. Genes upregulated in the dermis or epidermis are labelled as dermal markers and epidermal markers respectively. Genes labelled as mast cell markers are known mast cell functional genes. The radius of each circle corresponds to the percentage of cells within a cluster positively expressing each marker. The intensity of colour, from blue to red, corresponds to the relative average intensity of expression of cells within the cluster. Derm = Dermal; Epi = Epidermal.

The remaining 1,959,717 live cells from four donors were processed using the cytofkit package in R. They were downsized to a maximum of 100,000 cells per tissue layer per donor to balance the cell numbers for comparison, as well as for computational practicality (for a total of 756,977 cells). They were then normalised, transformed using inverse hyperbolic sine transformation, clustered using PhenoGraph (Levine et al., 2015) and tSNE coordinates were generated for visualisation (**Figures 35-36**). The data from each donor was kept separate and the results of each donor were compared.

Clustering of the CyTOF data resulted in 21-41 clusters in each donor for epidermis, and between 28-44 clusters in each donor for dermis (**Figures 37-38**). Manual gating was then overlaid to determine the cell types present (**Figures 39-40**), and the relative proportions of each cell type were calculated, which is more accurate to the true mix of cell types found *in vivo* than the resampled scRNA-seq data (**Figures 35-36**, coloured stacked bars). The manually gated cells match the clusters well, but simplify multiple clusters into each cell type label (**Figures 37-38**). This is due to using high resolution with the aim of over-clustering to ensure that populations with few events were not erroneously integrated into larger clusters, and is also confounded by the inclusion of markers with little to no positive expression. These markers were not excluded from the clustering algorithm in order to avoid biasing the analysis, but the variation in negative expression contributes to biologically meaningless division of clusters.

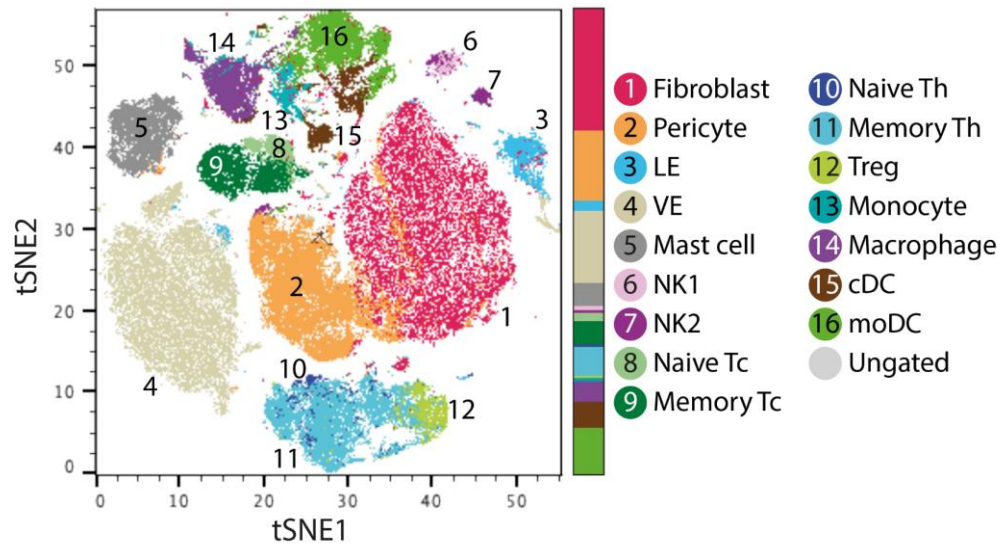
**Figure 35**



**Figure 35 – Protein expression heterogeneity of epidermal cells in healthy skin.**

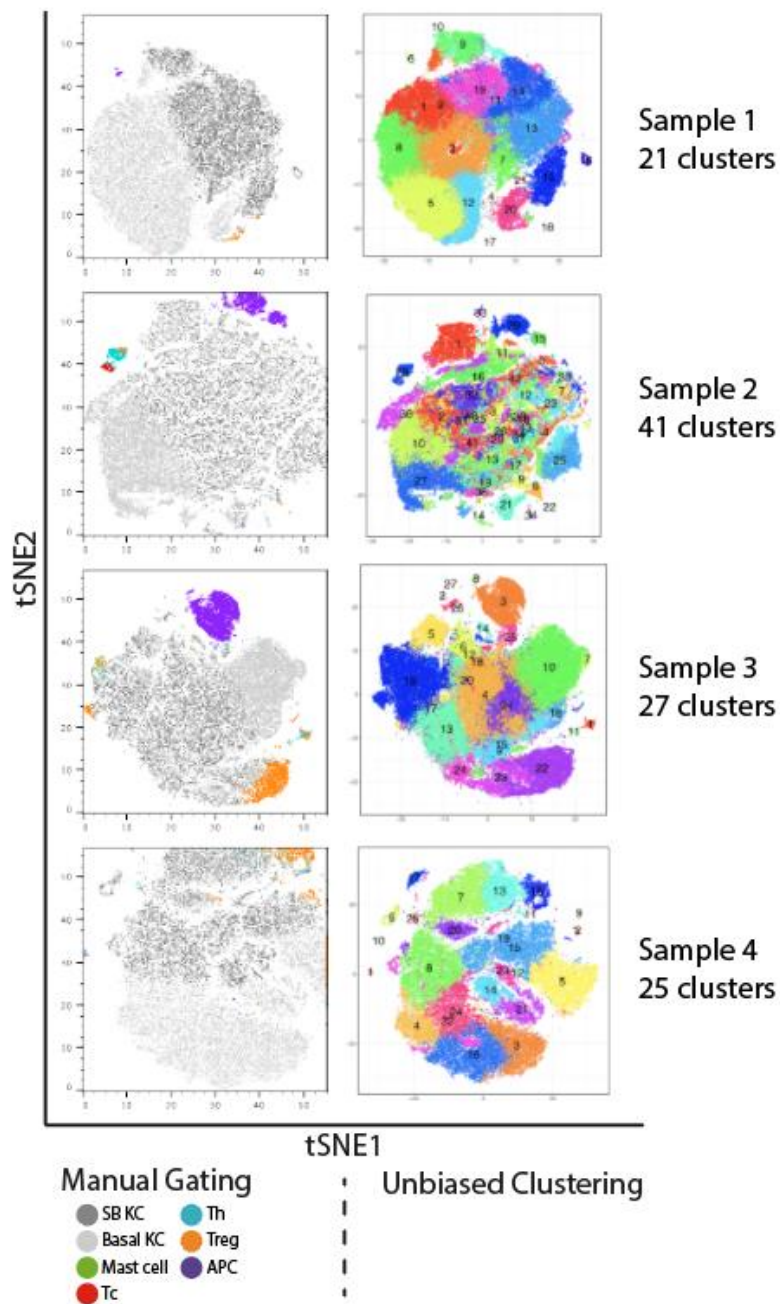
Epidermal cells collected after collagenase digestion were stained with antibodies against surface markers as well as cis-platin (live-dead separation) and an iridium intercalator (cell-debris separation), then fixed, permeabilised and stained with antibodies against intracellular and intranuclear markers for a total panel of 37 metal-conjugated antibodies for CyTOF. After Helios analysis, the live single cells were subsetted from the FCS file, downsampled to a maximum of 100,000 cells, clustered and tSNE coordinates were calculated. Cells were then manually gated (**Figure 39**) and this annotation was overlaid onto the tSNE visualization. Representative tSNE image from one of  $n = 4$  samples shown. The coloured bar represents the mean proportion of each gate from  $n = 4$  samples. APC = Antigen presenting cell; KC = keratinocyte; SB KC = suprabasal KC; Tc = cytotoxic T cell; Th = helper T cell; Treg = regulatory T cell.

**Figure 36**



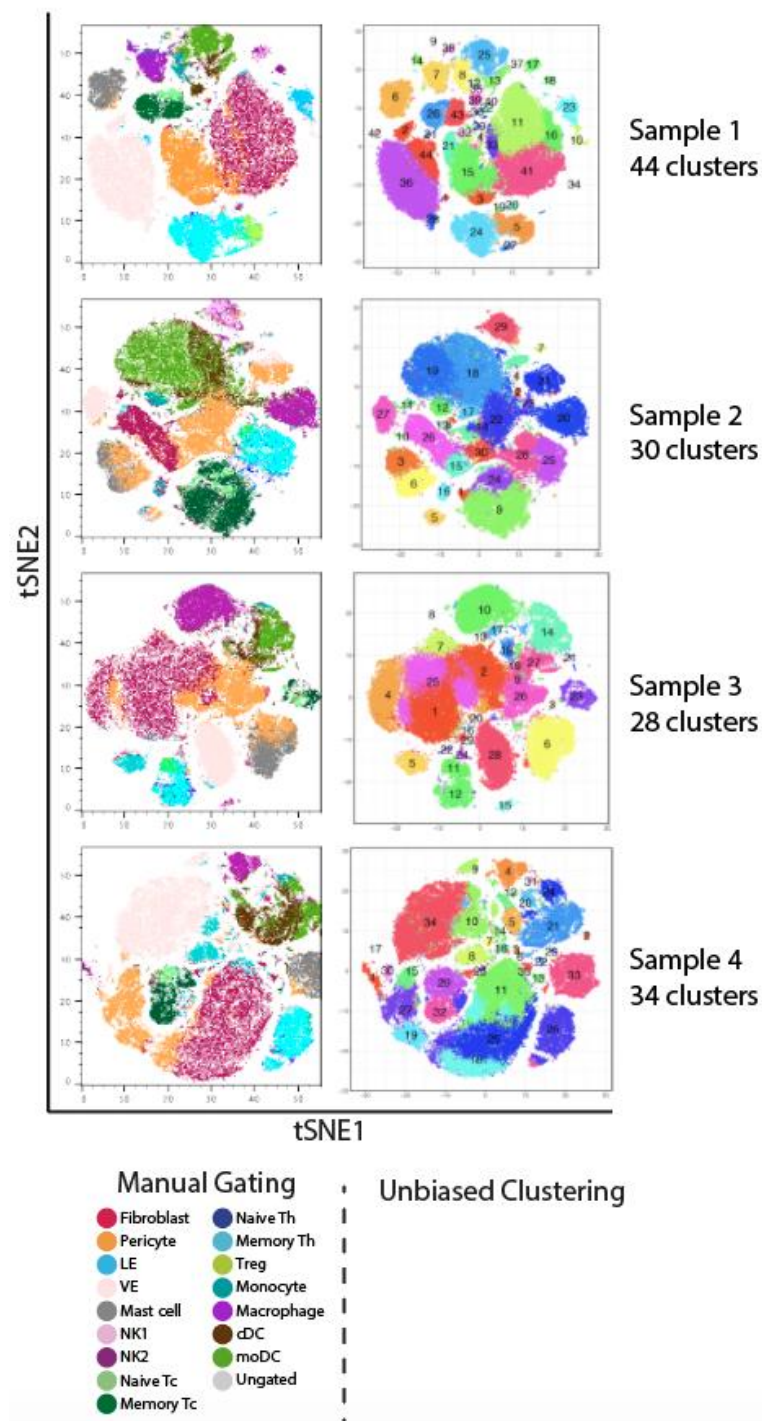
**Figure 36 – Protein expression heterogeneity of dermal cells in healthy skin.** Dermal cells collected after collagenase digestion were stained with antibodies against surface markers as well as cis-platin (live-dead separation) and an iridium intercalator (cell-debris separation), then fixed, permeabilised and stained with antibodies against intracellular and intranuclear markers for a total panel of 37 metal-conjugated antibodies for CyTOF. After Helios analysis, the live single cells were subsetted from the FCS file, downsampled to a maximum of 100,000 cells, clustered and tSNE coordinates were calculated. Cells were then manually gated (**Figure 40**) and this annotation was overlaid onto the tSNE visualization. Representative tSNE image from one of  $n = 4$  samples shown. The coloured bar represents the mean proportion of each gate from  $n = 4$  samples. cDC = conventional Dendritic cell; NK = NK cell; LE = lymphatic endothelium; moDC = monocyte-derived DC; Tc = cytotoxic T cell; Th = helper T cell; Treg = regulatory T cell; VE = vascular endothelium.

**Figure 37**



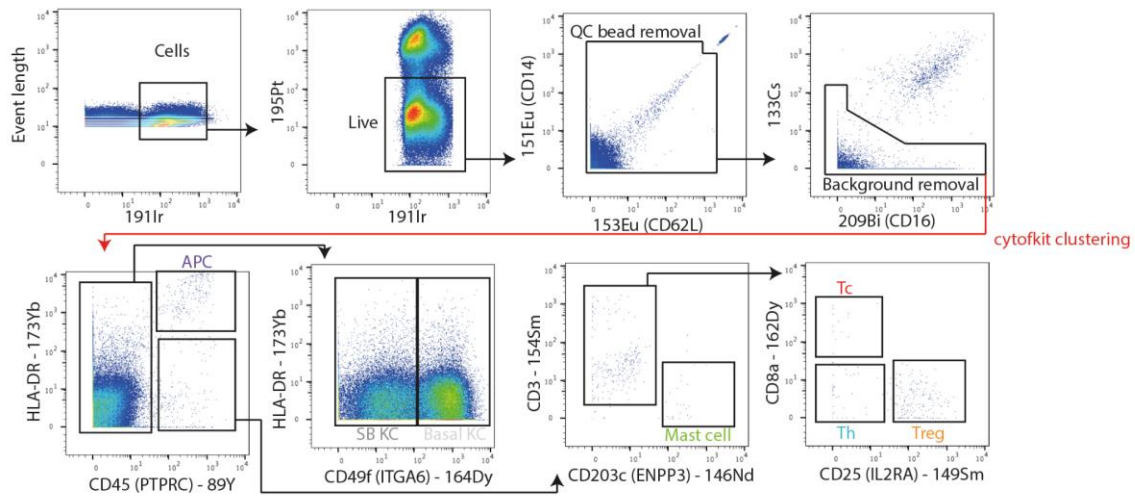
**Figure 37 – Manual gating versus clustering of epidermal CyTOF data.** Epidermal CyTOF data from **Figure 35**, expanded to show the plots from each of four samples. Left: tSNE plots annotated by overlaying a manual gating strategy (**Figure 39**). Right: tSNE plots annotated by automatic unbiased clustering. APC = antigen presenting cell; KC = keratinocyte; SB KC = suprabasal KC; Tc = cytotoxic T cell; Th = helper T cell; Treg = regulatory T cell.

Figure 38



**Figure 38 – Manual gating versus clustering of dermal CyTOF data.** Dermal CyTOF data from **Figure 36**, expanded to show the plots from each of four samples. Left: tSNE plots annotated by overlaying a manual gating strategy (**Figure 40**). Right: tSNE plots annotated by automatic unbiased clustering. cDC = conventional Dendritic cell; NK = NK cell; LE = lymphatic endothelium; moDC = monocyte-derived DC; Tc = cytotoxic T cell; Th = helper T cell; Treg = regulatory T cell; VE = vascular endothelium.

**Figure 39**



**Figure 39 – Gating strategy for CyTOF analysis of healthy adult epidermis cells.** The CyTOF data gating strategy used to annotate **Figure 35**. Representative image from one of  $n = 4$  samples shown. The red arrow represents the data that was downsampled and clustered using cytofkit. Before this arrow, brackets notate the presence of a marker in a channel which was also used for QC. After the red arrow, protein names for markers are written outside of brackets, and where they differ the corresponding gene names are written in brackets. APC = Antigen presenting cell; KC = keratinocyte; SB KC = suprabasal KC; Tc = cytotoxic T cell; Th = helper T cell; Treg = regulatory T cell.



**Figure 40**

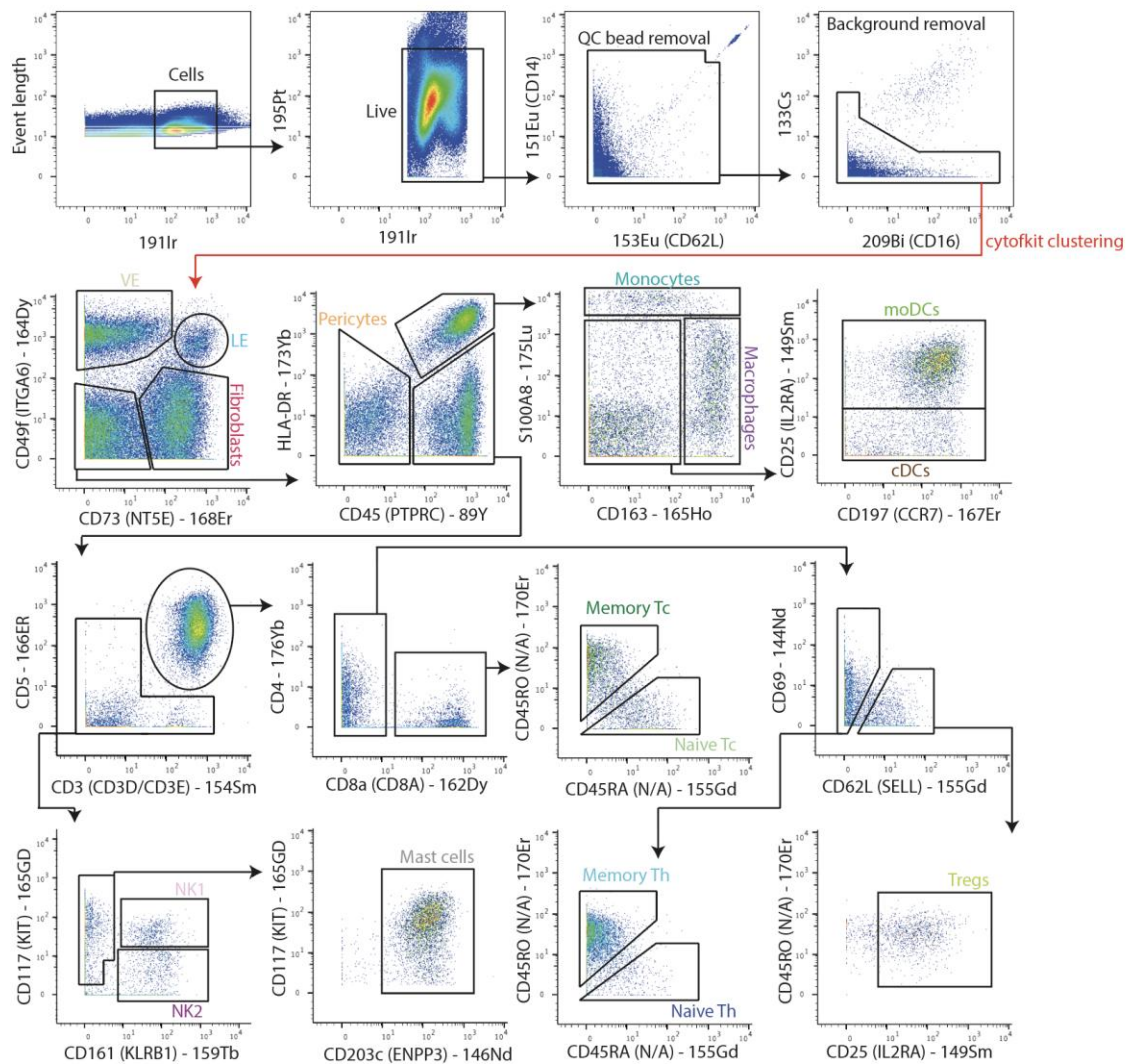


**Figure 40 – Gating strategy for CyTOF analysis of healthy adult dermis cells.** The CyTOF data gating strategy used to annotate **Figure 36**. Representative image from one of  $n = 4$  samples shown. The red arrow represents the data that was downsampled and clustered using cytofkit. Before this arrow, brackets denote the presence of a marker in a channel which was also used for QC. After the red arrow, protein names for markers are written outside of brackets, and where they differ the corresponding gene names are written in brackets. cDC = conventional Dendritic cell; NK = NK cell; LE = lymphatic endothelium; moDC = monocyte-derived DC; Tc = cytotoxic T cell; Th = helper T cell; Treg = regulatory T cell; VE = vascular endothelium.

With a minimum of 19 antibodies in the dermis and 8 antibodies in the epidermis, most of the same populations highlighted in **Figure 19** could be recapitulated in the dermis, with the exceptions of schwann cells, plasma cells, pDCs and ILCs. As schwann cells were isolated from the CD49f+ gate in the scRNA-seq data (**Figure 21**), they will be found in the vascular endothelial cell gate. Plasma cells are CD45+, HLA-DR- and otherwise marker negative in the context of this CyTOF panel and so will be found primarily within the ungated lymphoid cells which are double negative for KIT and KLRB1. ILCs express KLRB1 and so will likely be found within the NK2 gate. pDCs will likely be captured within the cDC gate due to their expression of CD45 and HLA-DR, and the lack of expression of the other APC markers used. NK1 and NK2 cells could be split by expression of KIT, while NK3 will likely fall in the NK2 KIT- gate as no antibodies for granzymes, which are markers necessary for their separation, were included in the panel. Protein expression also allowed for the identification of memory and naïve T cells by CD45RO and CD45RA respectively – post translational splicing modifications to CD45 that therefore could not be detected at RNA level (**Figure 36**) (Ganguly et al., 2016). This revealed that most dermal T cells found in healthy skin were CD45RO+ memory T cells, however in all 4 patients analysed naïve Tc cells were much more common than their Th counterparts.

In addition, pericytes were gated as marker negative, which will have inaccuracies introduced due to cells lacking expression of canonical markers falling here. In particular, fibroblasts lacking only CD73 expression will be found in this marker negative gate. The relative ratio of pericytes to fibroblasts is higher than that seen in the scRNA-seq data (1:4.68 by scRNA-seq, 1:1.74 by CyTOF), which suggests the extent of this gating contamination.

The epidermis was less well recapitulated, in part due to the overwhelming percentage of keratinocytes compared to immune cells. With the CyTOF panel used, melanocytes, NK cells and ILCs could not be gated for specifically. While melanocytes are found in the basal layer, they do not express CD49f, unlike basal keratinocytes. This is confirmed by the scRNA-seq data whereby melanocytes are primarily found within the lane loaded with CD49f- sorted cells (**Figure 21**). With no strongly positive markers for melanocytes in the panel, they will likely be found in the marker negative clusters identified as

suprabasal keratinocytes. NKs and ILCs were difficult to pull out due to the low numbers of lymphoid cells present in the epidermis relative to the total number of nonimmune cells. This is because the epidermis is much more cellular than the dermis, where most of the structure comes from ECM. They will likely be within the Th gate, as the weaker CD4 staining makes it more difficult to distinguish Th cells from NKs and ILCs.

CD45+ HLA-DR- CD3- CD203c+ epidermal mast cells could also be found by CyTOF, matching their gene expression by scRNA-seq (**Figure 39**). They were, however, much rarer than those found in the dermis, and so were likely highly upsampled by the FACS gating strategy used for capturing cells for scRNA-seq (**Figures 36-37**).

#### **4.2.9 Skin cells display mismatches in RNA and protein expression**

The unbiased clustering of CyTOF and transcriptomic data on cells treated under the same conditions allows for the validation of protein expression of the detected transcripts, and provides an insight into protein-RNA mismatches. For example, CD117 (the protein product of *KIT*. Gene and protein names are standardised in **Appendix Table 3**.) staining in the epidermis was not sufficient to detect melanocytes despite detection of *KIT* in melanocytes (**Figure 24**). *KIT* expression is reported as important to melanocyte differentiation and is expressed at protein level on immature precursors (Zocco & Blanpain, 2017; Wehrle-Haller, 2003). The presence of RNA without protein may suggest that mature differentiated melanocytes continue to transcribe *KIT* from their precursor programming without translating the CD117 protein. *CD4* RNA is detected at low levels in Tregs, and is almost absent in Th cells (**Figure 24**). This was unexpected, but matches the consistently low expression of CD4 protein found in both CyTOF and flow cytometry (**Figures 6-9**).

The archetypical T cell transcription factors *GATA3* and *FOXP3* were expectedly found in keratinocytes/Th/Treg and Treg cells respectively at RNA level, but were undetected at protein level and the cells may have required stimulation to actively translate these TFs (Zeitvogel et al., 2017; Lu et al., 2017)(**Figure 24**).

Interestingly, *ITGA6* RNA expression on basal keratinocytes and vascular endothelium is quite low, and is almost absent on LE cells, despite the fact that these cells were found almost exclusively by gating on positive expression for CD49f (the protein product of *ITGA6*), and this expression is confirmed by CyTOF (Figures 9-10, 24, 39-40). This could be caused by low turnover of the protein requiring little *ITGA6* transcription to maintain the protein expression. RNA expression of *ITGA6* is also seen in schwann cells but not stromal schwann cells, and both were captured by the CD49f+ sort gate (Figures 9 and 24).

In the endothelial fraction, CD73 is also highlighted as an efficient protein marker for lymphatic endothelial cells as well as fibroblasts, which can be further divided by LE CD49f expression (Figure 40). VE markers CD34 and CD31 are only found on CD49f+ CD73- cells, splitting the three cell types with variable expression of two markers. However, the high protein expression of CD73 on fibroblast and LE cells is not mirrored in the RNA data, with very few fibroblasts expressing high levels of *NT5E* (The gene for CD73) transcript (Figure 24).

### 4.3 Discussion

The optimisation of cell sampling was successful for comprehensively sequencing the cell types in skin. Overnight type IV collagenase followed by cell sorting and the high throughput of the 10x solution droplet encapsulation resulted in capturing most of the expected cell types at high numbers. The experimental design of separating dermis and epidermis, type IV collagenase digestion, FACS sampling and droplet separation scRNA-seq successfully generated an extensive transcriptomic profile of the cell types found in the top 200µm of healthy adult breast skin. In particular, pre-sorting the cells allowed for the capture of different phenotypes of skin DCs that would have likely been too rare to otherwise analyse. Sequencing 82,490 cells from 3 donors provided power to resolve clusters of uncommon cell types, including schwann cells and melanocytes.

The recovery of high numbers of cells from most skin cell types, and with good average gene counts of ~3000 per cell makes this a dataset a good resource for future human skin studies. The single cell sequencing data allows for the interpretation of cell-level

gene co-expression for any known deleterious mutation, providing a great resource for the investigation of cells involved in particular skin diseases. This human healthy data is also directly applicable to human disease, without the requirement of validating cross-species expression patterns. The data also crucially reveals the theoretically most efficient RNA markers for isolating specific skin cell types in future studies (**Figure 24**). Paired with the protein data of unbiased CyTOF clustering this gives an insight into which genes are strong markers at protein-level, which is more directly applicable to techniques such as FACS and IHC, and expanding on this data by validating each of the top markers at protein level would be a valuable avenue to expand on this study.

Of particular relevance to the wider scope of skin immunology literature are some of the transcriptome-proteome mismatches identified. The semi-unbiased FACS isolation strategy, which aimed to prevent expression-based exclusion of specific cells, uncovered LCs with a specific transcriptome profile (*KLF10*+ LCs and LC1) within the CD45+ HLA-DR- gate (**Figures 25 and 27**). A CD45 low LC population has been previously described by Bertram *et al.*, named CD33<sup>low</sup> cells, which may relate to these cells (Bertram *et al.*, 2019). The epidermal gating strategy used here did aim to capture these same cells as CD1a<sup>low</sup> CD11c- cells by using a relatively low HLA-DR gate for LCs, but even so further LCs were found in the CD45- gate (**Figure 10**). This is particularly important as LCs are classically considered to be HLA-DR+ and so these cells may be overlooked in studies considering them as such (Bertram *et al.*, 2019), although many studies of LCs use only CD1a or langerin expression as the definition of an LC (Patterson *et al.*, 2002; Greter *et al.*, 2012).

Epidermal DC migration occurs in human during inflammation, and has been shown in mouse at steady state (Ohl *et al.*, 2004) theoretically to maintain tolerance (Zaba *et al.*, 2009) The finding of transcriptomically dermal APCs in the epidermis could support this functionality in human, and is also in line with the finding of CD11c+ dermal-like DCs in the epidermis (Bertram *et al.*, 2019). Epidermal DC migration would be difficult to definitively prove in human, as transgenic organisms were required in mouse, or simply relied on langerin/CD207 expression, which can be seen in other tissues (Yoshino *et al.*, 2006; Eriksson & Singh, 2008; Stoitzner *et al.*, 2005).

This finding is unlikely to be due to contamination, as during peeling the epidermis is peeled away from the dermis, and then washed in PBS. For dermal APCs to contaminate the epidermis they would have to be loose individual cells, which should have been removed by PBS washing, or pieces of dermis remaining attached to the epidermis. However, the same level of epidermal cell contamination should then be seen in the dermal nonimmune cells, and this is not the case (**Figure 22**).

Capturing anti-inflammatory epidermal mast cells in healthy skin by both scRNA-seq and CyTOF is a novel finding, and could possibly represent a tolerogenic mechanism against allergy. In steady state mast cells migrate into the dermis before maturing, reportedly remaining close to blood vessels (Janssens et al., 2005). They reportedly infiltrate the epidermis during inflammation, and the presence of epidermal mast cells has even been used as a disease biomarker (Green et al., 1977; Sehra et al., 2016). They may not have been previously reported in healthy epidermis due to their scarcity: By CyTOF, only 0.09% (mean of  $n = 4$  to 2d.p.) of epidermal cells displayed the mast cell surface marker phenotype, and some of these may have even been other cells, for example CD117+ natural killer cells (**Figure 35**). Higher numbers were found by scRNA-seq, which may be due to the sorting strategy employed. Granulocytes are common in steady state circulation, but the surgically removed skin is removed from its blood supply, and the epidermis is avascular, so it is unlikely that these were an inflammatory artefact from tissue processing.

There are, however, gaps in this study. As described in the previous chapter, hair follicles and follicular cell types were not captured at single cell resolution by the scRNA-seq or CyTOF data. Similarly, Merkel cells were not found in this study. This also may be due to rarity, as Merkel cells are primarily found in touch-sensitive hairless skin such as hands and feet, and are also more common in murine skin (Halata et al., 2003). It would be particularly interesting to dissect the single cell transcriptome of Merkel cells in healthy skin as a comparison to the primary research target of these cells which is in disease: Merkel cell carcinoma. The possibility that they are generated in response to skin injury

in mice also provides an avenue for the analysis of heterogeneity between long lived and injury-induced Merkel cells (Wright et al., 2017).

With the exception of hair follicles and Merkel cells, the majority of skin cell types were accounted for by scRNA-seq and CyTOF, resulting in the successful categorisation of the cellular heterogeneity present in healthy human skin by protein and RNA.

**Chapter 5. Stromal cell heterogeneity  
within human skin**





## **5.1 Chapter 5 Introduction**

Skin is supported by an array of stromal cells. The dermis consists of fibroblasts connected by a collagenous extracellular matrix of their construction, which also anchors vascular and lymphatic vessels. The epidermis consists primarily of layers of keratinocytes with little interstitial space between them. These cells are responsible for holding the mechanical structure of skin, but also provide homeostatic functions and responses to perturbation, including inflammation and wound repair.

Nonimmune heterogeneity is widely reported at bulk level. Transcriptomic differences between venular and arteriolar dermal endothelium have been reported (Thiriot et al., 2017), and phenotypic differences are observed between papillary and reticular fibroblasts (Sorrell & Caplan, 2004). Additionally, different transitional states of both keratinocytes and fibroblasts are reported during wound healing versus tissue maintenance during homeostasis (Rognoni et al., 2018; Noguchi et al., 2014).

Despite using the moniker 'nonimmune', the skin stromal cells are also a vital part of the immune system. The vasculature brings immune cells into skin for surveillance during steady state, and this is crucially exacerbated during inflammatory response. Endothelial cells secrete a host of chemokines and express cell surface adhesion proteins to facilitate this extravasation into the dermis. Similarly, dermal lymphatics ensure skin lymphocytes circulate to lymph nodes for antigen presentation. In healthy epidermis, keratinocytes direct T cells through variable chemokine signalling, and can even initiate inflammatory responses via PRR and IFN-gamma induced MHC class II expression (Mansfield & Naik, 2020; Banerjee et al., 2004).

Delving into the stromal cell heterogeneity of skin could expand on the heterogeneity reported at bulk level, and uncovering the specific interactions between stromal and immune skin cells could provide insights into the skin immune system as a whole.

## **5.2 Results**

### **5.2.1 Cellular heterogeneity of the stromal cells within skin**

To interrogate the heterogeneity found within human skin nonimmune cells, two major subsets of the scRNA-seq data were created: keratinocytes, and the remaining nonimmune cells. These groups were selected by a combination prior knowledge of similarity and by their visualised relationships by UMAP (**Figure 41**). Of particular note, melanocytes fell closer to the dermal nonimmune cells, which may be due to their shared origins with schwann cells (Adameyko et al., 2009). Analysing keratinocytes separately also had the added biological relevance of allowing for keratinocyte trajectory analysis. Hence the division of nonimmune cells and keratinocytes, rather than separating dermal from epidermal nonimmune cells.

The melanocytes and dermal nonimmune cells were re-clustered, resulting in 12 groups: three fibroblast clusters named F1, F2 and F3; two lymphatic endothelial cell clusters named LE1 and LE2; three vascular endothelial cell clusters named VE1, VE2 and VE3; a cluster of pericytes; a melanocyte cluster and two schwann cell clusters named schwann cells and stroma schwann cells (**Figure 41**). These clusters showed good sample mixing, with cells from each of the three samples being found in each of the 12 clusters (**Figure 42**).

The 10x lane that each cell was run on provides an interesting look at the surface protein expression of these cells (**Figure 43**). As expected, most vascular and lymphatic cells fall in the endothelium gate, so are CD49f positive. Melanocytes are mostly CD49f low epidermal cells, and most fibroblasts fell within the CD45- CD49f- gate. Both clusters of schwann cells however were found in the CD49f positive endothelium lane. Some endothelial cells were found in the fibroblast gate and vice versa, which is likely due to the design of the gating strategy lacking gaps between populations to reduce selection bias.

**Figure 41**

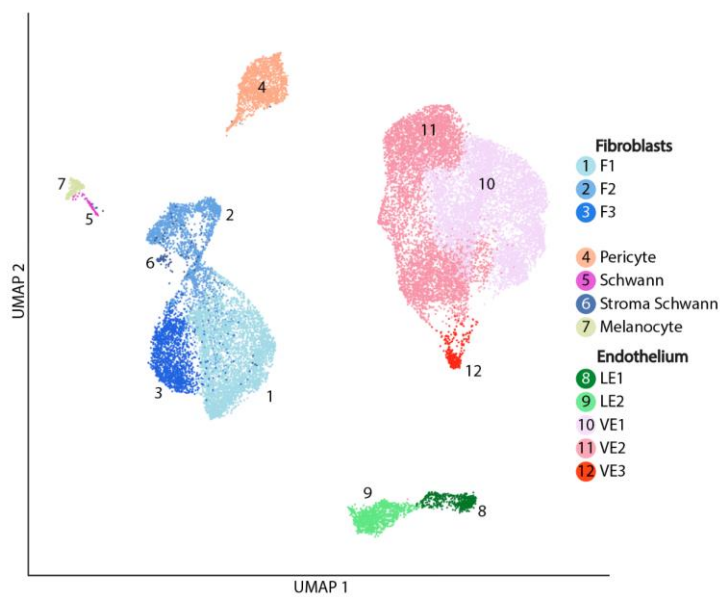


**Figure 41 – Heterogeneity of nonimmune cell populations in healthy human skin.**

Melanocytes and dermal nonimmune cells from three samples were re-clustered at higher resolution and then UMAP coordinates were generated and plotted by Dr Peter Vegh. Clusters were then manually annotated by comparing differentially expressed genes between clusters to the literature, as well by using the tissue and FACS gate origin of cells in each cluster. Each dot represents a single cell. Each colour represents a different cluster. F = fibroblast; LE = lymphatic endothelium; VE = vascular endothelium.

**Figure 42**

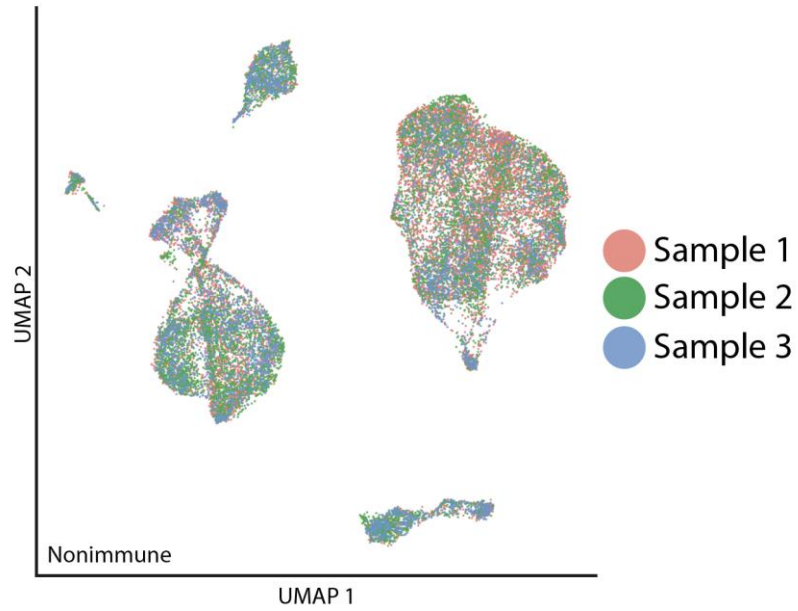


**Figure 42 – UMAP visualisation of scRNA-seq analysis of nonimmune cells annotated by sample.** UMAP plot generated by Dr Peter Vegh. The same UMAP displayed in **Figure 41**, coloured by sample.

**Figure 43**

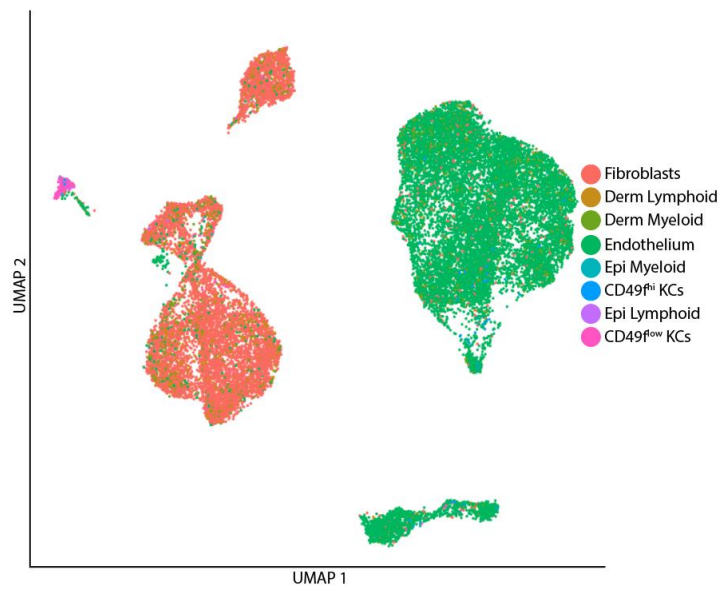


**Figure 43 – UMAP visualisation of scRNA-seq analysis of nonimmune cells annotated by 10x lane.** UMAP plot generated by Dr Peter Vegh. The same UMAP displayed in **Figure 41**, coloured by 10X lane. Labels refer to the lanes described in **Figures 9-10** and **18**.

### 5.2.2 Fibroblasts in human skin vary in immunomodulatory gene expression

The three fibroblast clusters (F1, F2 and F3) are distinguishable as fibroblasts by expression of fibroblast markers including *PTGES*, *PTGDS* and *NT5E* (**Figures 24, 44** and **Appendix Table 1**). The differentially expressed genes between these populations suggest differing functions of ECM production/remodelling and inflammation/immunomodulation. F1 fibroblasts express immunomodulatory cytokines including *TNFAIP*, *IL6* and *CXCL1*, as well as higher levels of stress related pro-inflammatory molecules *MT2A* and *PTGES*, suggesting an increased role in immune cell interaction (**Figure 44**). F2 fibroblasts display increased expression of genes involved in extracellular matrix production and remodelling including *MFAP5*, *MXRA8* and *PODN* (**Figure 44**). F3 fibroblasts share expression of the F1 cluster immunomodulatory markers, but also express high levels of the apoptosis-inducing molecule *CD82* and the CCR7-attracting chemokine *CCL19*. F3 fibroblasts also express genes associated with wound healing, for example *TNC* and *TGFB3* (**Figure 44**) (Lichtman et al., 2016; Trebault et al., 2007). The transcript expression of F1 and F2 fibroblasts are not exclusively geared towards inflammation or ECM maintenance respectively, and appear instead to be differential in their contributions to these key fibroblast functions. For example, F2 fibroblasts express the monocyte chemokines *CXCL3* and *CXCL12* at higher levels than F1 cells, and the F1 cluster expresses higher levels of the matrix metalloprotease *MMP2* (**Figure 44**).

### 5.2.3 Melanocyte and schwann cell transcriptome profiles

In spite of being dissociated from different tissue layers, melanocytes and schwann cells are found close together by their UMAP coordinates, the spatial relationship of which is related to transcriptomic relationship, and may be indicative of their shared origin from neural crest precursor cells (**Figure 41**). Melanocytes can be distinguished from the other nonimmune clusters by unique expression of markers including *PMEL*, *DCT*, *TYR*, *TYRP1* and *MLANA* (**Figure 44** and **Appendix Table 1**).

**Figure 44**

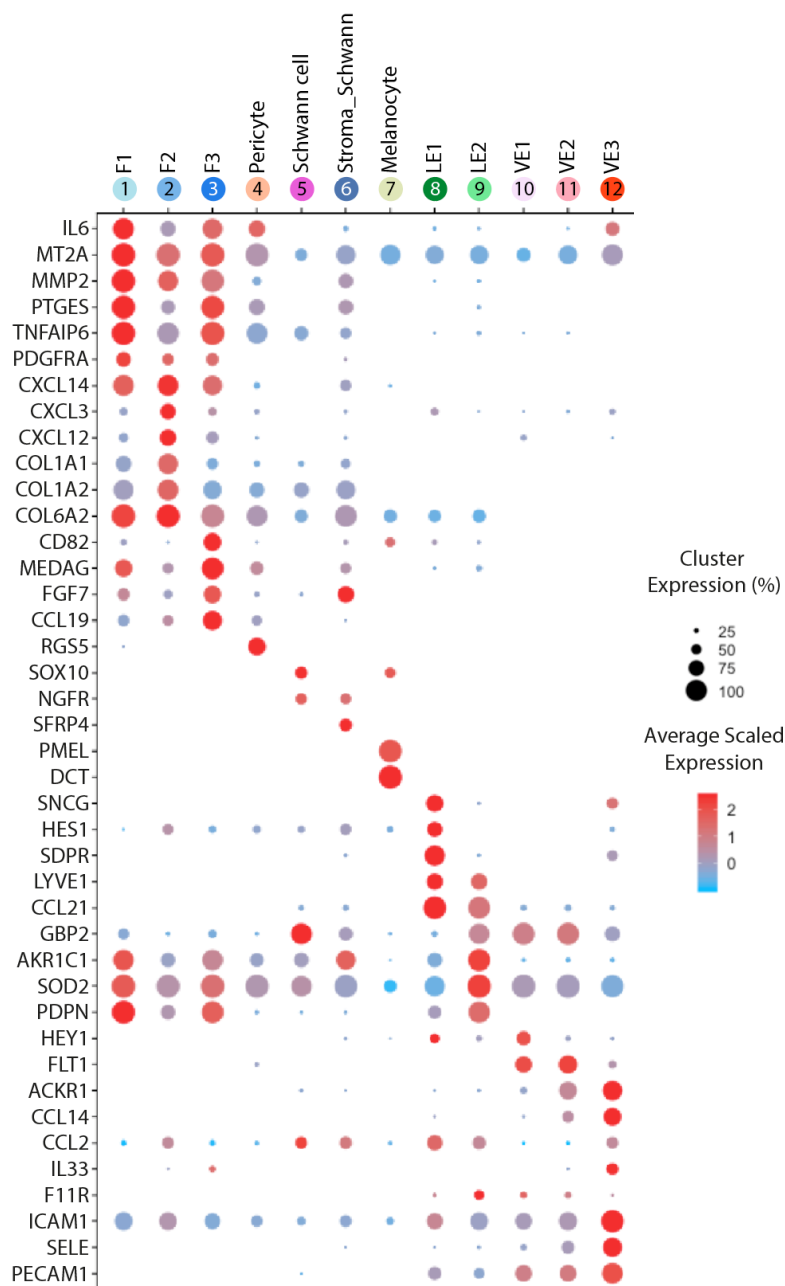


**Figure 44 – Top differentially expressed genes between the nonimmune cells in healthy skin.** Heatmap generated by Dr Peter Vegh. After clustering and annotating the nonimmune scRNA-seq data, differentially expressed genes were calculated and plotted as a heatmap. Cluster labels on the X axis correspond to those displayed in **Figure 41**. The radius of each circle corresponds to the percentage of cells within a cluster positively expressing each marker. The intensity of colour, from blue to red, corresponds to the relative average intensity of expression of cells within the cluster. F = fibroblast; LE = lymphatic endothelium; VE = vascular endothelium.



Schwann cells formed two distinct clusters, both identifiable by shared expression of the neurotrophin receptor *NGFR*. The first cluster, named schwann cells, also expresses high levels of *FLG2* as well as *SOX10*, an important regulator of myelination (**Figure 44** and **Appendix Table 1**)(Fujiwara et al., 2014). The other cluster expresses fibroblast markers, including *DCN*, *FGF7* and *MMP2*, and so was named stromal schwann cells (**Figure 44**). The unique gene expression profile of stromal schwann cells appears to closely match that of a skin cell cluster briefly described by Tabib *et al.* as a “rare fibroblast subset” (Tabib et al., 2018a)(named Cluster 7 in their Supplementary Figure S3).

#### 5.2.4 Heterogeneity of pericytes and lymphatic endothelial cells

Pericytes formed a single cluster expressing high levels of *RGS5*, *MCAM* and *PDGFRB* (**Figures 24, 44** and **Appendix Table 1**). Lymphatic endothelial cells formed two separate clusters, named LE1 and LE2 (**Figure 41**). Both clusters express the lymphatic markers *CCL21*, *LYVE1* and *PDPN*. However, LE1 expresses higher levels of *LYVE1* and lower levels of *PDPN* than LE2. This is in agreement with the reported difference in protein expression between initial lymphatics and the deeper collecting vessels (Wang et al., 2014) and so LE1 may be endothelial cells from initial lymphatic vessels, and LE2 cells from collecting vessels. LE1 also expresses higher levels of *CCL21*, a key chemokine which recruits CCR7+ APCs into the lymphatics, which further supports this distinction. Angiogenesis markers *SDPR* and *CCND1* are also found on LE1 cells, and LE2 differentially expresses *GBP2* and *SOD2* (**Figure 44** and **Appendix Table 1**).

#### 5.2.5 Three distinct clusters of vascular endothelial cells

Interestingly, a lot of heterogeneity is found within the vascular endothelial cells of the papillary dermis. Three clusters, named VE1, VE2 and VE3, are positive for blood vessel markers *PECAM1* and *CD34* and negative for the lymphatic vessel markers *CCL21* and *LYVE1* (**Figures 24** and **44**).

VE2 can be distinguished from VE1 by the expression of *ACKR1*, a nonspecific chemokine receptor. *ACKR1* has been shown to be expressed in post-capillary venules and not pre-capillary arterioles, demarcating the areas of endothelium where leukocyte trafficking primarily occurs (Thiriou et al., 2017). As the skin was cut to 200µm deep, excluding

anything deeper than papillary dermis, capillary endothelial cells should account for most, if not all, of the vascular endothelial cells present as the arteriolar and venular plexuses are found at over 1000 $\mu$ m depth (Braverman, 2000).

This could suggest that VE1 and VE2 represent the divide in capillary endothelial cells between the venular (ACKR1+, VE2) and arteriolar (ACKR1-, VE1) branch points (**Figure 45**). The ratio of VE2 to VE1 cells found by sequencing is approximately 1:1 (0.97:1, mean of  $n = 3$ ), as would be expected for a single dermal papilla capillary branch being halved at an imaginary midpoint. Furthermore, VE2 is higher in expression of the rolling adhesion proteins *SELE* and *SELP* and the hard adhesion molecule *ICAM1*, supporting the concept of *ACKR1* being selective of endothelial cells with leukocyte trafficking capabilities (**Figure 44** and **Appendix Table 1**).

To assess these key expression differences at protein level, flow cytometry was employed. Gating vascular endothelial cells as live, single CD45- CD73- CD49f+ CD34+ cells revealed ACKR1 positive and negative populations, with a ratio of 1.11:1 for ACKR1+ to ACKR1- cells, closely mirroring the ratio of VE2 to VE1 by scRNA-seq (**Figure 46**).

Next, expression of *SELP*, *SELE* and *ICAM1* was compared between the ACKR1+ population (VE2) and the ACKR1- population (VE1) (**Figures 46-47**). *SELE* and *SELP* expression appears to be mostly specific to ACKR1+ cells, as expected. *ICAM1* is seen on both VE1 and VE2, but with proportionally higher expression on VE2, which is mirrored in the scRNA-seq data. Plotting the ratio of cells positive for each adhesion molecule to cells negative for the same molecule shows a similar trend – that adhesion molecules are proportionally expressed more on ACKR1+ cells. However, this difference is only statistically significant ( $p < 0.05$ ) for *SELE* expression. The difference in *SELP* and *ICAM1* expression are not significant ( $p = 0.089$  and  $p = 0.222$  respectively) (**Figure 47**). Further repeats may be necessary to overcome the biological variability between donors.

Figure 45

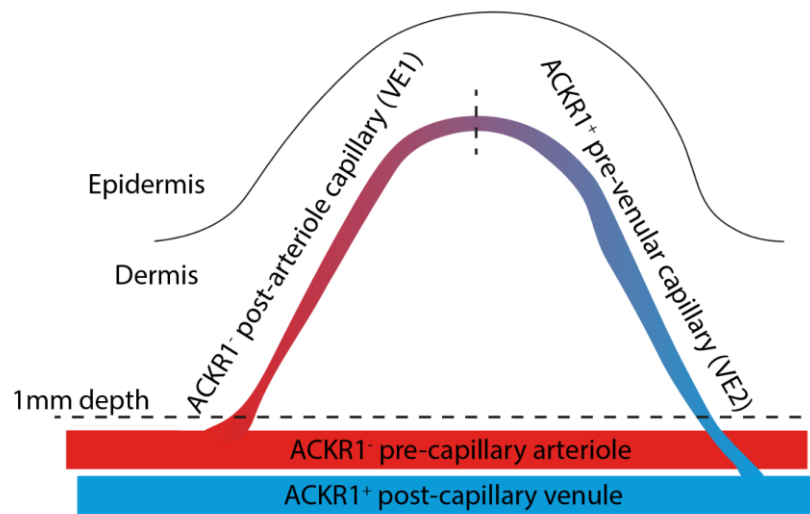


**Figure 45 – The potential morphology of VE1 and VE2 cells within a single dermal papilla.** ACKR1 expression is reportedly exclusive to post-capillary venules (blue), which occur below 1mm depth in skin, and its expression marks the transcriptional heterogeneity between endothelium with or without leukocyte trafficking capabilities. As the scRNA-seq data captures endothelium within 200µm depth, the split between ACKR1+/- clusters may represent the divide either side of the midpoint of the single capillary and its branches found within a dermal papilla (Braverman, 2000). VE = vascular endothelium.

Figure 46

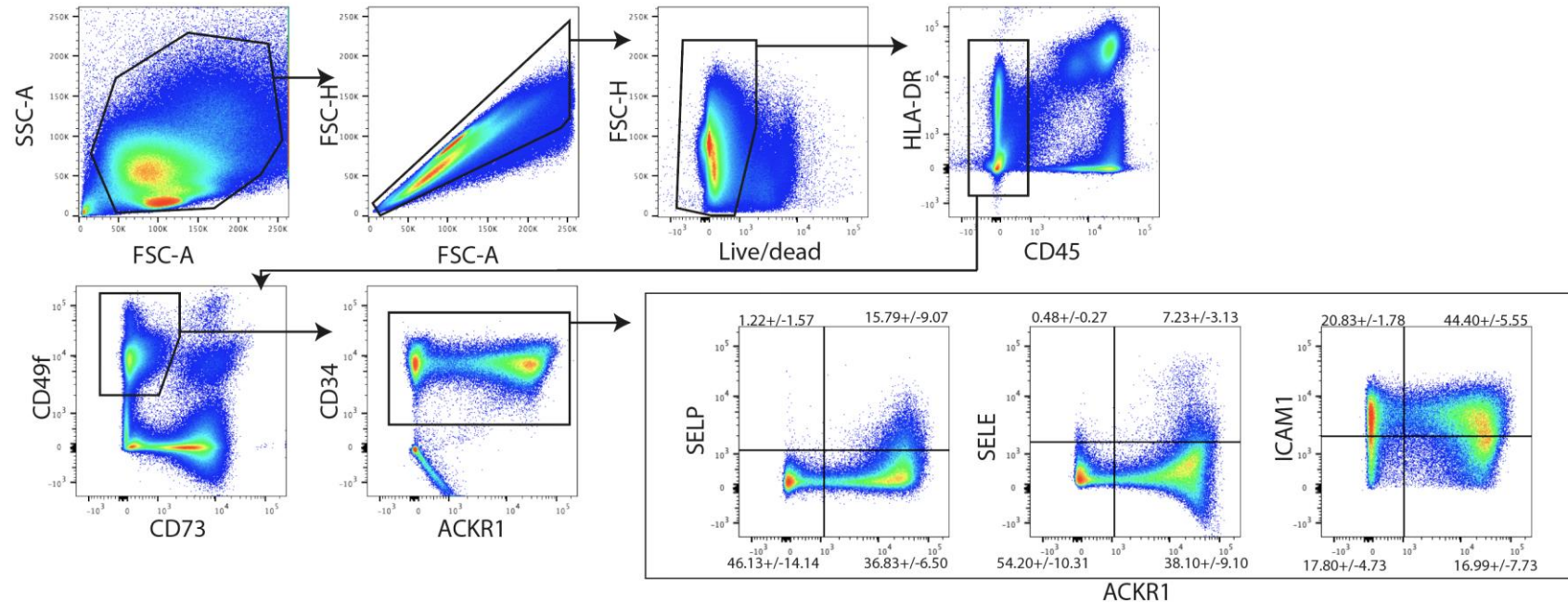
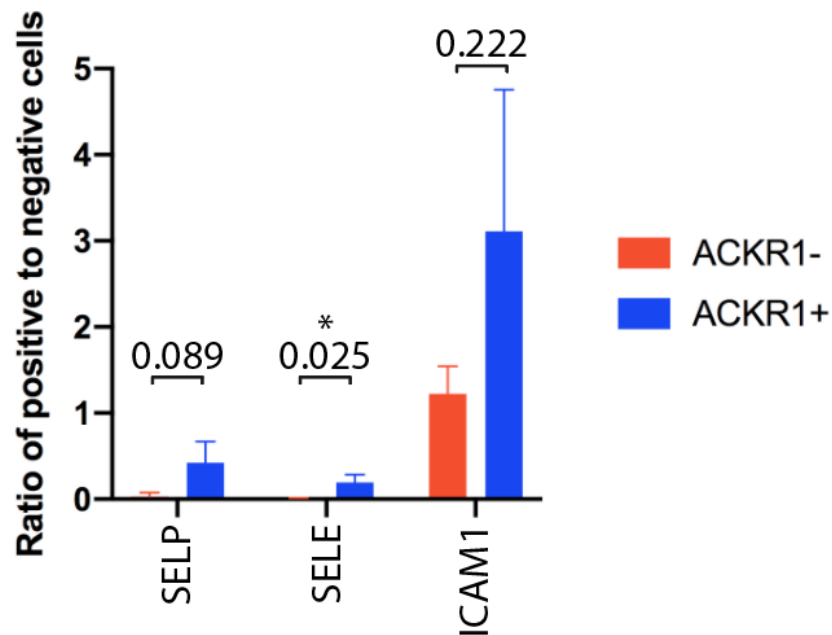


Figure 46 – Expression of endothelial adhesion markers is higher in ACKR1+ cells. Dermal cells were stained for markers to isolate vascular endothelial cells as well as antibodies against adhesion markers. Representative plots are shown from one of  $n = 3$  samples. The percentage of each quadrant is displayed as mean +/- SD of three samples.

Figure 47



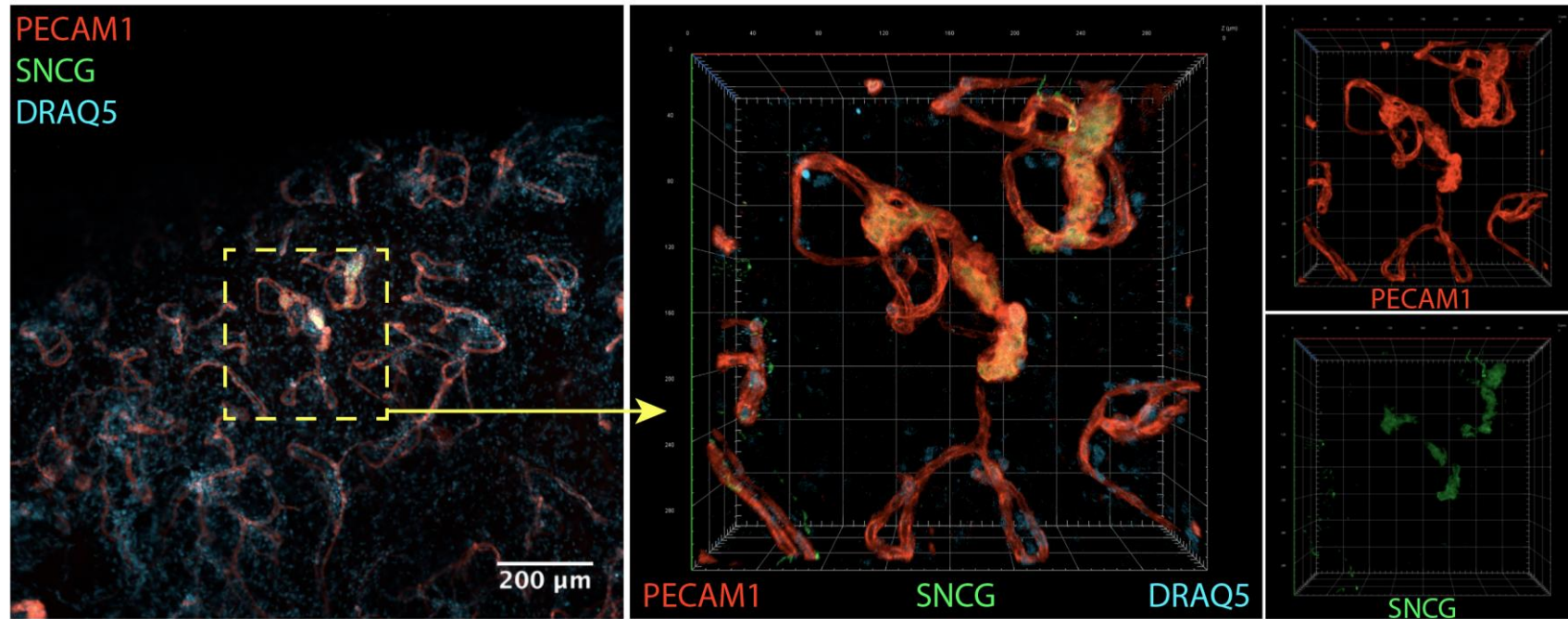
**Figure 47 – Vascular endothelial cell adhesion marker heterogeneity.** Bar graph displaying the ratio of vascular endothelial cells positive for each x axis marker to cells negative for that marker, using the data generated by the quadrant gates in **Figure 46**. Bars display the mean of 3 samples, error bars display the SD. Paired t tests were used between ACKR1+ and ACKR1- values to calculate p values shown above each pair. Asterisks show significance at  $p < 0.05$ .

### 5.2.6 Specialised leukocyte trafficking structures are present in healthy skin

A third population of vascular endothelial cells, VE3, was found at much lower numbers. VE3 makes up 2.82% (mean of  $n = 3$ ) of the vascular endothelial cells sequenced, and therefore is much rarer than VE1 and VE2. VE3, like VE2, is positive for *ACKR1* and as such is likely found in pre-venular capillary (Thiriot et al., 2017), and is characterised by much higher expression of adhesion markers, inflammatory cytokines and leukocyte-attracting chemokines such as *ICAM1*, *IL33* and *CCL23* respectively (**Figure 44** and **Appendix Table 1**).

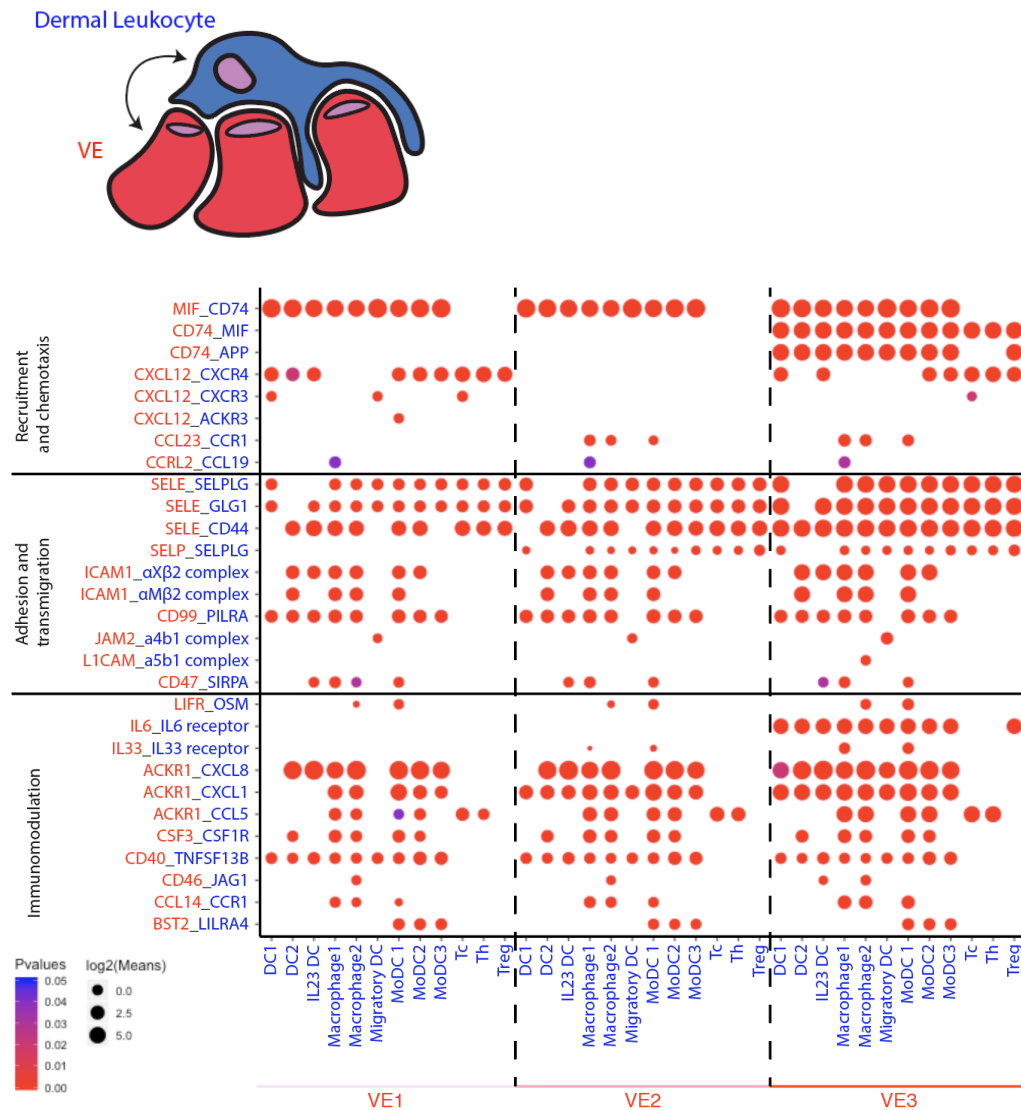
As VE3 appears to represent an endothelial cell with increased leukocyte extravasation capabilities, whole mount immunofluorescence staining was undertaken to determine whether this represented a specific type of capillary vessel or simply individual cells in a state of activation. CD31 (*PECAM1*) was used a classical marker of vascular endothelium and gamma synuclein (*SNCG*) as a marker for VE3 due to its specificity at transcript level by scRNA-seq (**Figure 44**). This staining revealed rare patches of SNCG+ vascular endothelium with a distinct distended morphology (**Figure 48**). PECAM1+ SNCG- vascular endothelium is a consistent diameter. Each PECAM1+ SNCG+ area found was much wider and less regularly structured. Notably, they were also connected to the thin PECAM1+ SNCG- vessels, so these structures appear to occur within VE2 vessels rather than forming their own capillary vessels.

Figure 48



**Figure 48 – Whole mount imaging of SNCG expression on dermal vasculature.** Peeled dermis was cut to roughly 1cm<sup>2</sup> squares and fixed and dehydrated overnight in formaldehyde and sucrose. Tissue was blocked, stained with primary antibodies to CD31 (PECAM1) and gamma synuclein (SNCG) then secondary fluorescent antibodies and DRAQ5 nuclear stain and then imaged using confocal microscopy. **Left:** Still image using 5x objective lens. **Middle:** 3D reconstruction of z-stack tiled images taken using 20x objective lens showing all three channels. Images were taken of the region in the dashed yellow square in the left panel. **Right:** Separate signals of PECAM1 (top) or SNCG (bottom) from middle panel. *n* = 3, representative images from a single sample.

**Figure 49**



**Figure 49 – Potential interactions between the vasculature and dermal leukocytes.**

Heatmap was plotted by Dr Peter Vegh. Heatmap showing expression of selected receptor-ligand pairs from CellPhoneDB between vascular endothelium clusters (red genes) and dermal leukocyte clusters (blue genes), as represented in the diagram above the heatmap. The radius of each circle corresponds to the averaged relative expression of both the receptor and ligand expressed in their relevant clusters. The intensity of colour, from blue to red, corresponds to the statistical significance of both genes being truly expressed. Genes were manually categorised by general function. VE = vascular endothelium; DC = dendritic cell; moDC = monocyte-derived DC; Tc = cytotoxic T cell; Th = helper T cell; Treg = regulatory T cell.



**Figure 50**

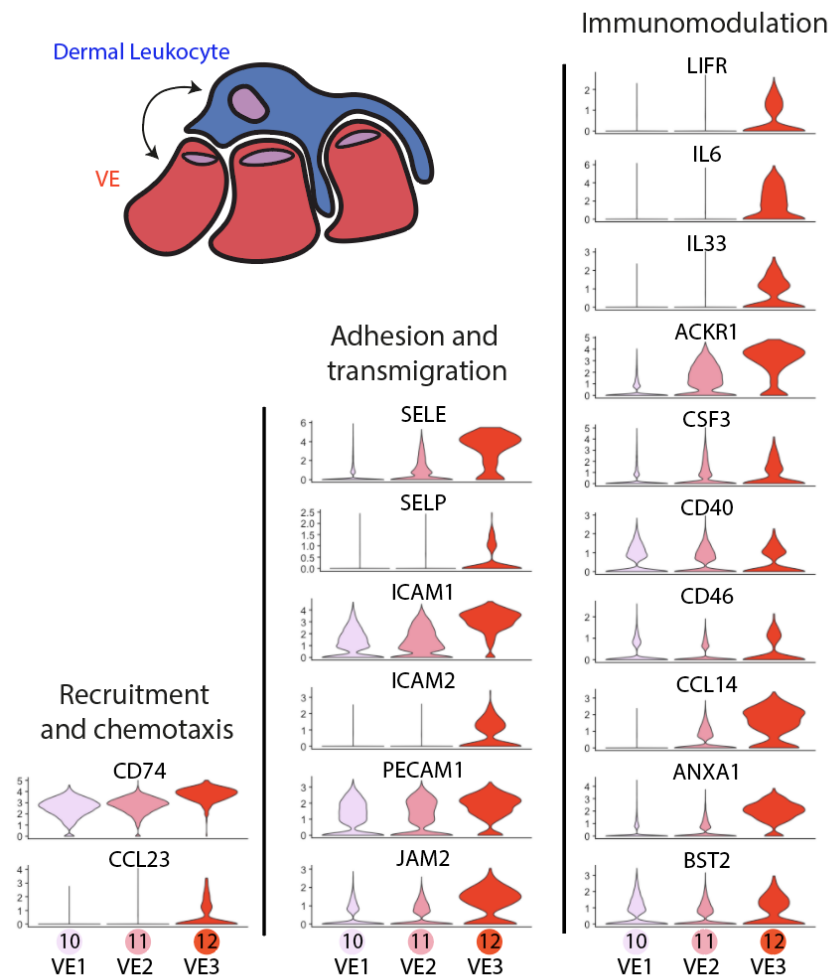


**Figure 50 – Heterogeneity in immunomodulatory gene expression between vascular endothelial cell clusters.** Violin plots showing the expression differences of the receptors and ligands in **Figure 49** across the three vascular endothelium (VE) clusters. The width of each violin plot is related to the ratio of cells found at a particular Y coordinate.

As this distended “leaky” appearance fit with the transcriptome profile of leukocyte trafficking, VE3 interactions with the immune system were next interrogated. CellPhoneDB, a database of receptors and their cognate ligands (Efremova et al., 2019), was used to evaluate the statistically significant interactions between each vascular endothelial cluster and dermal leukocytes (**Figure 49**). The genes with roles in endothelium:leukocyte interactions were grouped into three categories: those with roles in immunomodulation, such as inflammatory and tolerogenic cytokines; adhesion molecules and transmigration receptors; and recruitment receptors and chemokines. As predicted, VE3 appeared to have more interactions with leukocytes than VE1 or VE2, and this difference was accentuated by plotting the expression levels of each of the genes highlighted by CellPhoneDB as violin plots (**Figure 50**). The expression of basement membrane anchors and cell-cell adhesion proteins such as *COL4A1* and *ITGB1* was also decreased in VE3, which may facilitate the distended morphology of VE3 endothelium and aid in allowing leukocytes to pass between endothelial cells (**Figure 51**).

Figure 51

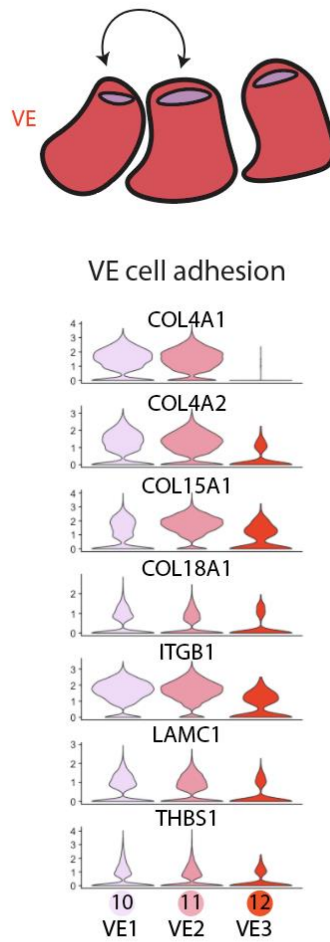


**Figure 51 – VE3 cells express lower levels of cell-cell adhesion proteins.** Violin plots showing the expression differences of selected receptor-ligand pairs from CellPhoneDB where both the receptor and cognate ligand are expressed on the same vascular endothelium (VE) cluster. The width of each violin plot is related to the ratio of cells found at a particular Y coordinate.

### 5.2.7 Keratinocyte heterogeneity follows keratinisation

Keratinocytes formed 8 clusters (**Figure 55**) which fell into four main groups: pre-proliferation KCs, post-proliferation KCs, proliferative KCs and a fourth group of KCs expressing various leukocyte markers including *CD83* (**Figure 52**). These groups showed good sample mixing with cells from each of the three samples falling into each cluster (**Figure 53**). Pre-proliferation KCs express transcripts for basal layer keratins including *KRT5* and *KRT14* (**Figure 54**). Most of these cells were found in the CD45- CD49f+ gate, which are also markers for basal layer keratinocytes (**Figure 21**).

Post-proliferation KCs include some cells expressing basal markers, but transition to express only suprabasal markers including *KRT1* and *KRT10* (**Figure 54**). The proliferating KCs include cells with both transcriptome profiles of basal and suprabasal genes, but are characterised by high expression of cell cycle progression markers such as *CDK1*, *MKI67* and *HMMR* (**Figure 54** and **Appendix Table 2**).

**Figure 52**

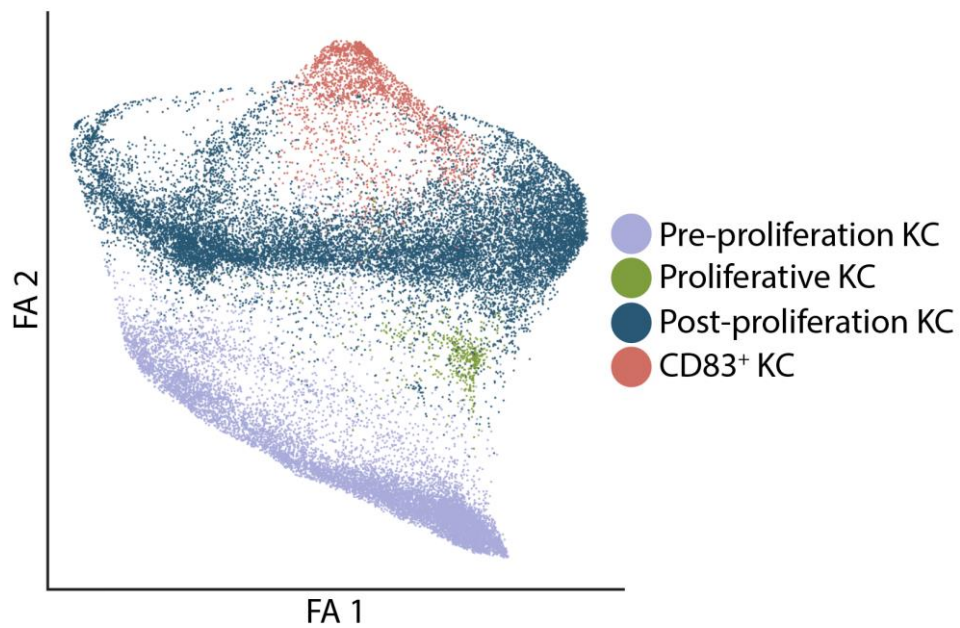


**Figure 52 – Force-directed graph visualization of scRNA-seq analysis of keratinocytes.**

Keratinocytes from three samples were re-clustered at higher resolution and then force atlas (FA) coordinates were generated and plotted by Dr Peter Vegh. Cells in close proximity follow a trajectory of changing transcriptomes. Clusters were then manually annotated and combined by comparing differentially expressed genes between clusters to the literature. Each dot represents a single cell. Each colour represents a different cluster. KC = Keratinocyte.

**Figure 53**

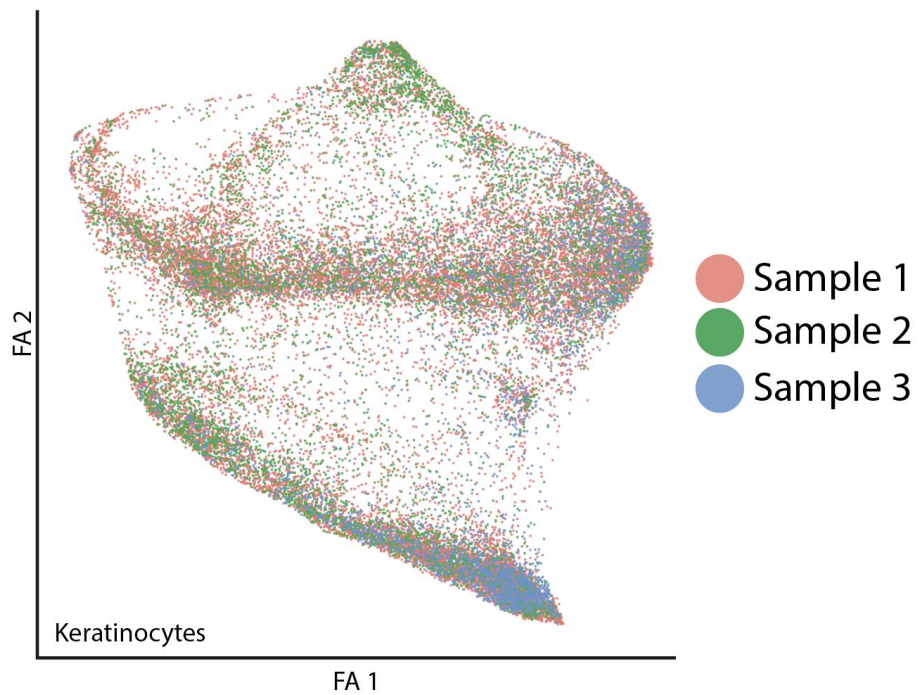


**Figure 53 – Force-directed graph visualization of scRNA-seq analysis of keratinocytes annotated by sample.** FA plot generated by Dr Peter Vegh. The same FA plot displayed in **Figure 52**, but coloured by the sample.

**Figure 54**

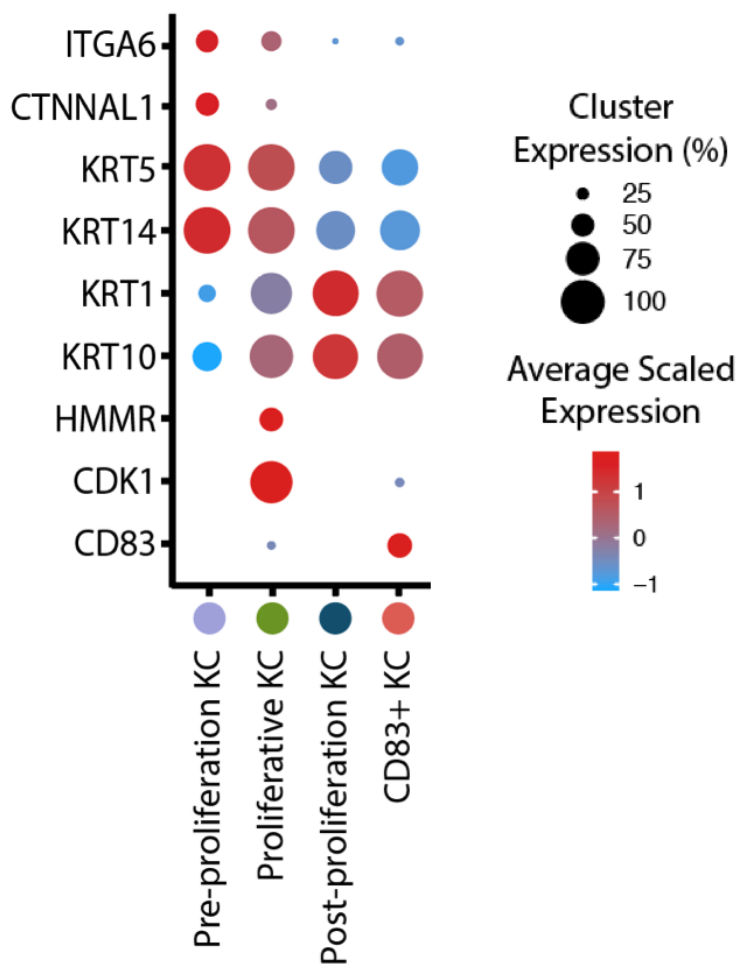


**Figure 54 – Keratinocyte subset markers in healthy adult skin.** Heatmap generated by Dr Peter Vegh. After annotating the keratinocyte data, differentially expressed genes and selected genes from literature were plotted as a heatmap. Cluster labels on the X axis correspond to those displayed in **Figure 52**. The radius of each circle corresponds to the percentage of cells within a cluster positively expressing each marker. The intensity of colour, from blue to red, corresponds to the relative average intensity of expression of cells within the cluster. KC = keratinocyte.

### 5.2.8 Distinct differentiation pathway of lamellar body-producing KCs

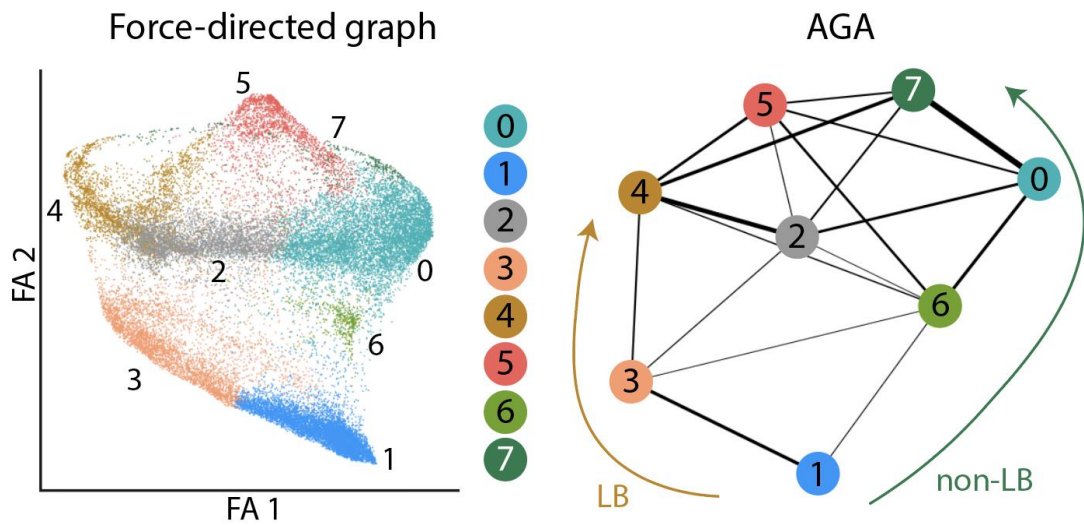
Trajectory analysis was run by Dr Peter Vegh using Force-directed graph (FDG) and PAGA in order to interrogate the differentiation process of keratinocytes from the basal layer to the stratum corneum (**Figure 55**). This revealed two differentiation trajectories linking the basal and corneal layers. By probing the differentially expressed genes between the two pathways, I interpreted a possible biological explanation for the divide. One arm (non-LB) shows a direct transition from undifferentiated basal keratinocytes to the suprabasal layers, transitioning from expression of basal genes, e.g. *KRT5* and *KRT14*, to suprabasal genes like *KRT1* and *KRT10*, and finally to terminal differentiation markers including *IVL* and *PERP*. The other arm shows this same well categorised trajectory, but becomes enriched for transcripts involved in lamellar body generation, including *ABCA12*, *CKPA4* and *CLIP1*, in the post-proliferation KCs (**Figure 56**). Both pathways appear to converge at the terminally differentiated cells (Cluster 7, **Figure 56**).

### 5.2.9 CD83+ Inflammatory keratinocytes reside in healthy skin

The fourth group of keratinocytes, CD83+ KCs, express suprabasal transcripts as well as inflammatory markers including the activated APC marker *CD83*, the T cell homing chemokine *CCL20*, the intercellular adhesion marker *ICAM1*, the inflammatory bradykinin receptor *BDKRB1* and the inflammatory cytokine *TNF* (**Figure 57**). The presence of these genes suggests that these cells may have an inflammatory or immunomodulatory function.

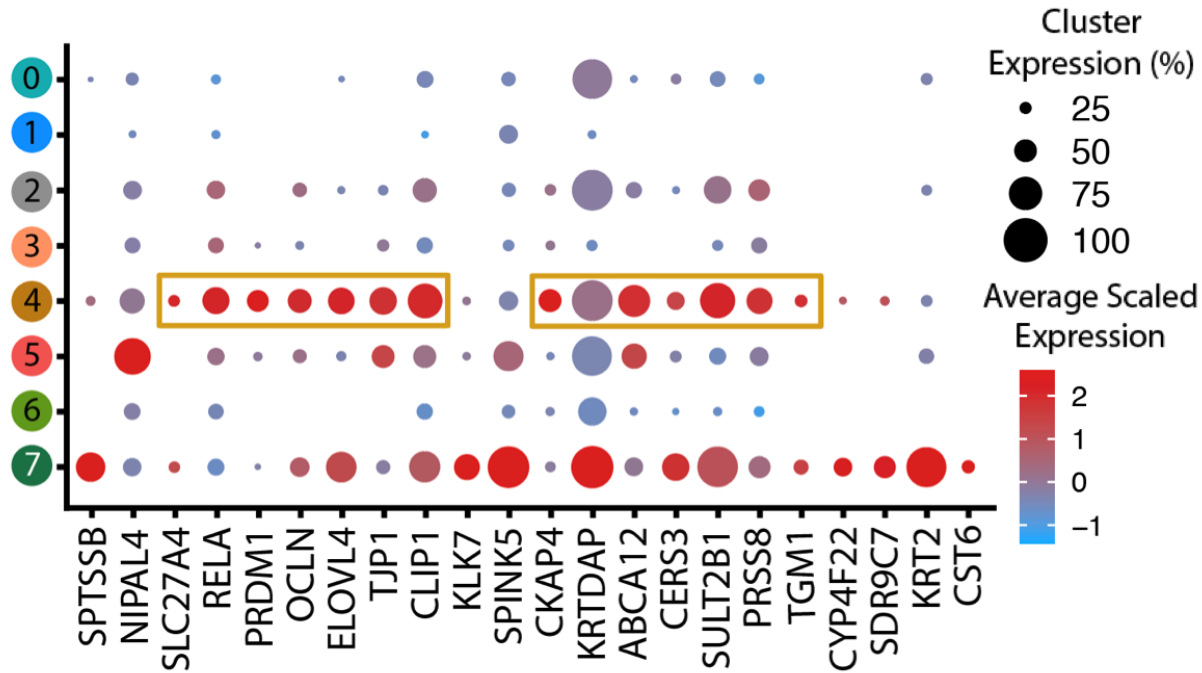


Figure 55



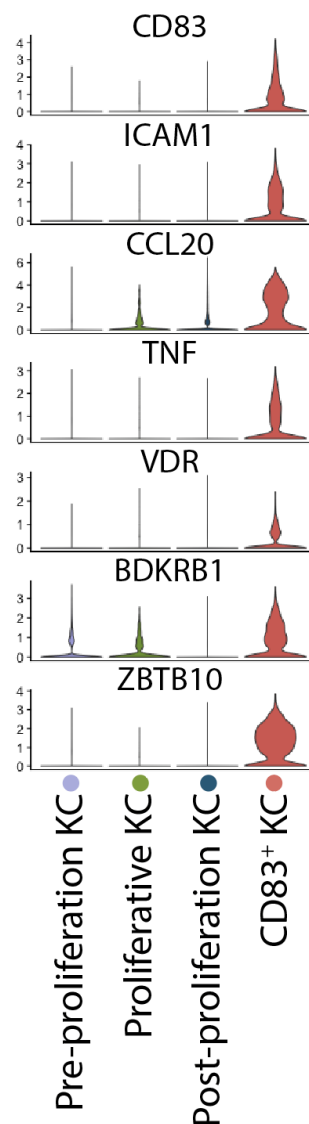
**Figure 55 – Trajectory visualization of adult skin keratinocytes.** Force atlas (FA) and approximate graph abstraction (AGA) plots generated by Dr Peter Vegh. **Left:** The same FA plot displayed in **Figure 52**, but coloured by detailed clustering. Cells in close proximity follow a trajectory of changing transcriptomes. **Right:** AGA plot of the same keratinocyte clusters. Thicker lines represent closer connections between clusters. Arrows indicate the annotation of two differentiation pathways from basal to suprabasal keratinocytes. LB = Lamellar body expressing; non-LB = non-lamellar body expressing.

Figure 56



**Figure 56 – Expression of lamellar body-related genes in specific keratinocyte clusters.** Heatmap generated by Dr Peter Vegh. Keratinocyte clusters as shown in **Figure 55** were plotted on the Y axis. The brown boxes highlight the high expression of lamellar body related genes in the LB pathway. The radius of each circle corresponds to the percentage of cells within a cluster positively expressing each marker. The intensity of colour, from blue to red, corresponds to the relative average intensity of expression of cells within the cluster.

**Figure 57**

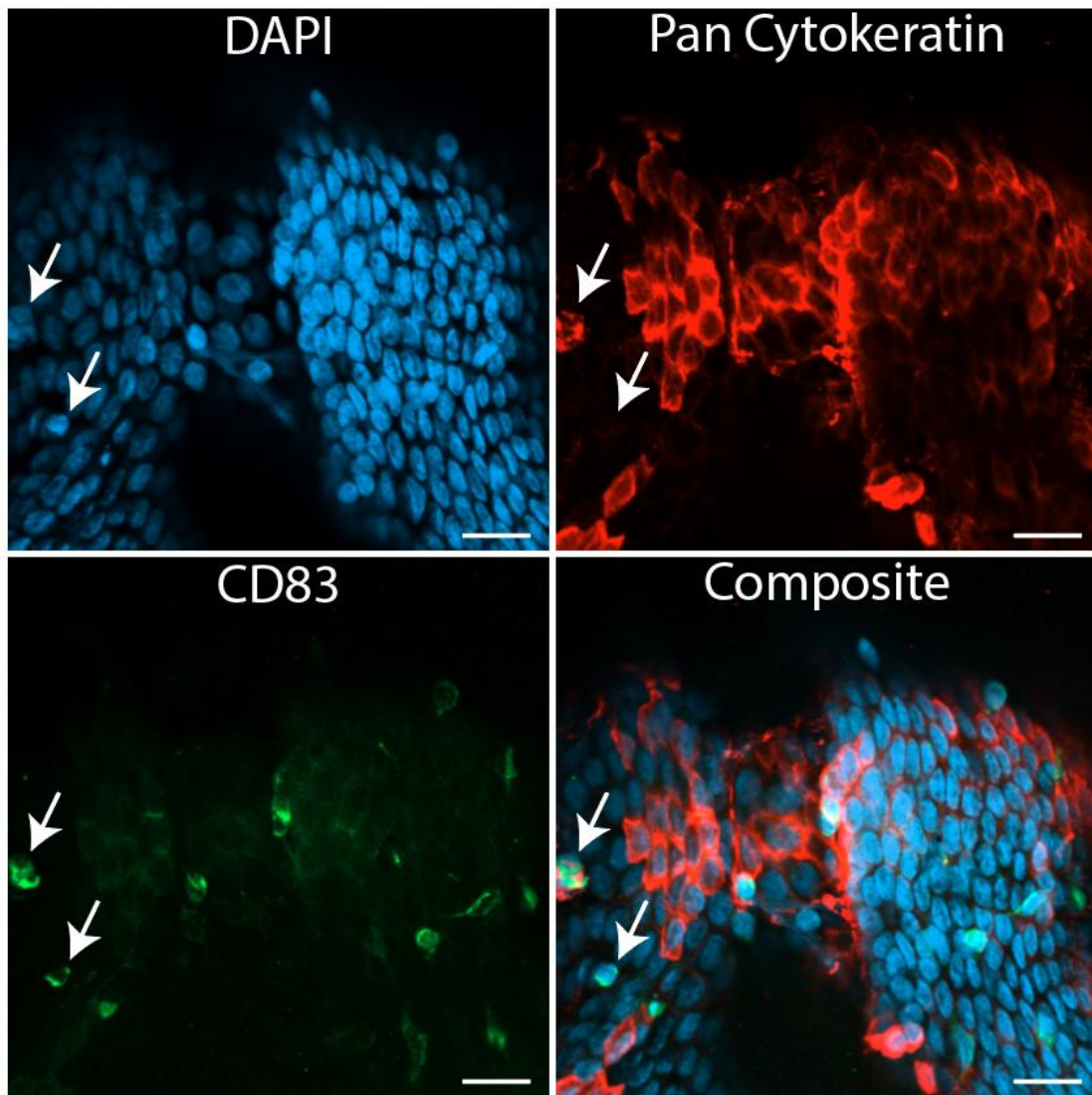


**Figure 57 – CD83+ KCs express higher levels of immunomodulatory genes.** Violin plots showing the top immunomodulatory differentially expressed genes between CD83+ KCs and the other keratinocyte subsets. The width of each violin plot is related to the ratio of cells found at a particular Y coordinate. X axis labels refer to the annotations shown in **Figure 52**. KC = keratinocyte.

Whole mount immunofluorescence staining for CD83 was employed to determine if these cells are present prior to cell dissociation and incubation at 37°C, which may affect cell activation, as well as to validate the protein expression of this marker. Dual staining with a pan-keratin antibody was used to distinguish these cells from LCs, which may also express CD83. Keratin- CD83+ LCs were found, as well as Keratin+ CD83+ keratinocytes (**Figure 58**). The double positive cells were rarer than expected from the scRNA-seq data, and the papillary folds of the epidermis made scalable quantification of these cells difficult by whole mount staining. Therefore, IHC staining of skin slides was undertaken to quantify these cells.

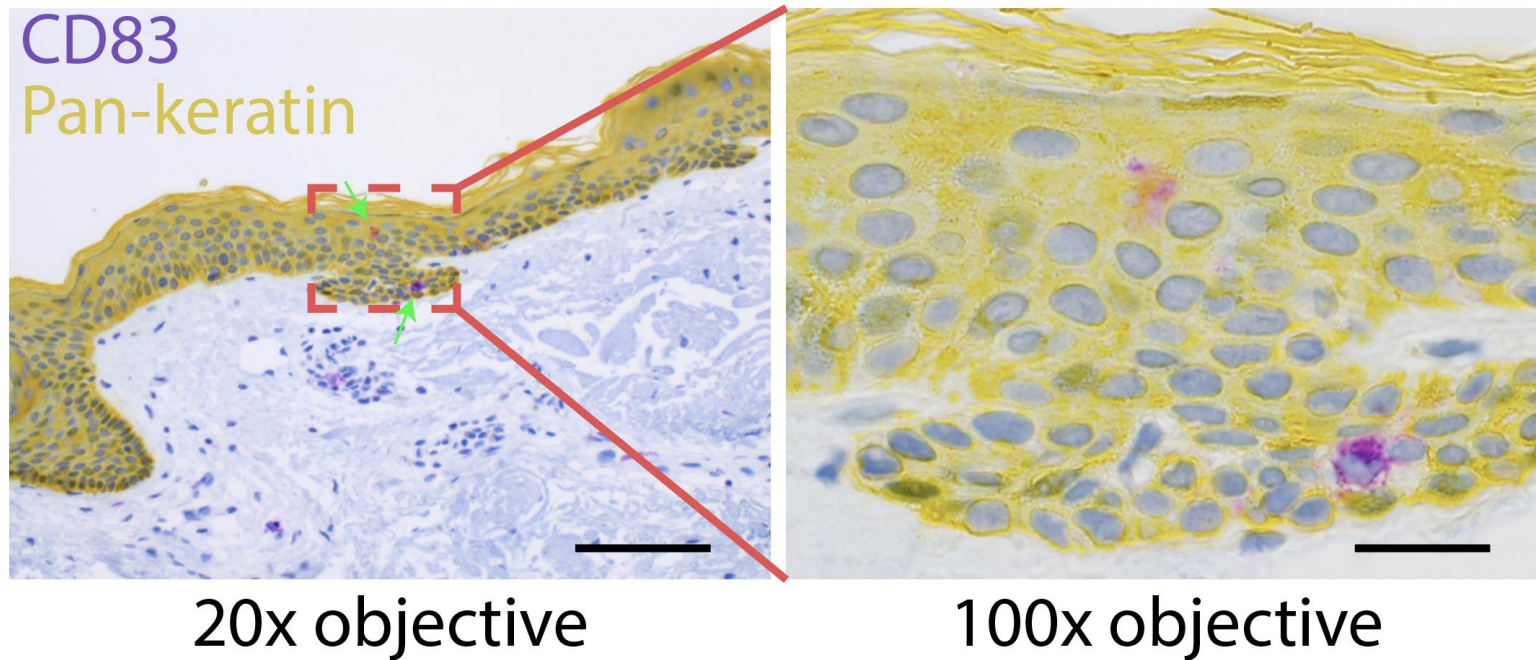
Dual staining of CD83 and pan-keratin showed dual positive cells in the interfollicular epidermis, consistent with the whole mount staining (**Figure 59**). Dual positive cells were also found within hair follicles (Data not shown). Quantification was possible by counting CD83+ keratin+ cells as a percentage of all pan-keratin positive nuclei, giving the relative proportion of CD83+ keratinocytes (**Figure 60**). This came to 0.14 +/- 0.04% (mean +/- SD,  $n = 3$ ) CD83+ keratinocytes, much lower than the 7.56 +/- 5.18% (mean +/- SD,  $n = 3$ ) of keratinocytes found in the scRNA-seq inflammatory CD83+ keratinocyte cluster. This may be due to multiple reasons. CD83 may be translated at a much lower rate than it is transcribed in these cells, leading to the marker poorly recapitulating their presence in tissue. There may also be a protein-RNA mismatch in these cells if they are transcriptionally primed to respond to inflammation, but do not express inflammatory proteins at steady state. This result may also be due to the effects of tissue dissociation increasing the proportion of inflammatory cells seen as the cells respond to tissue damage, which would be seen far less, if at all, in sections from tissue which was rapidly fixed in formaldehyde after excision.

Figure 58



**Figure 58 – Whole mount imaging of CD83 expression on keratinocytes.** Peeled epidermis was cut to roughly 1cm<sup>2</sup> squares and fixed and dehydrated overnight in formaldehyde and sucrose. Tissue was blocked, stained with primary antibodies to CD83) and pan cytokeratin then secondary fluorescent antibodies and DAPI nuclear stain and then imaged using confocal microscopy. The top white arrow shows a CD83+ keratin+ keratinocyte. The bottom white arrow shows a CD83+ keratin- Langerhans cell. Scale bars represent 20µm. *n* = 3, representative images from a single sample.

Figure 59



**Figure 59 – In situ visualization of CD83+ keratinocytes in healthy adult skin.** Slides of healthy adult skin were stained by the Newcastle Molecular Pathology Node for CD83 (purple) and pan-keratin (yellow). Green arrows show double positive cells. Scale bars represent 100 $\mu$ m on the left panel and 20 $\mu$ m on the right panel. Representative images shown from one of  $n = 3$  samples.

Figure 60

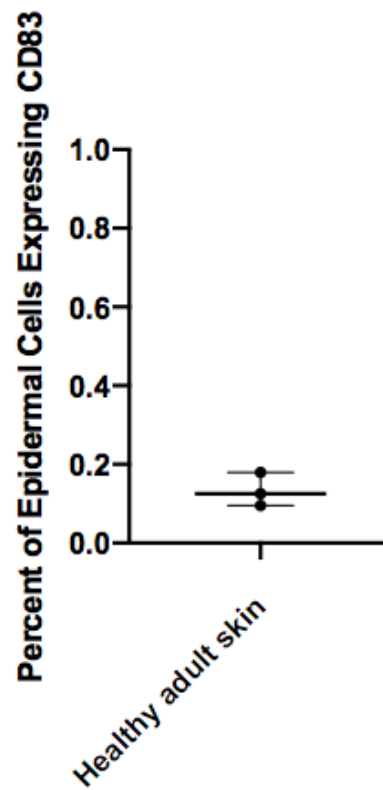


Figure 60 – Percentage of CD83+ keratinocytes found in healthy adult epidermis.

Nuclei of keratin+ (yellow) cells were counted on slides from  $n = 3$  samples in Figure 59. The number of CD83+ keratin+ cells in each slide are shown as a percentage of keratin+ cells.

### 5.2.10 CD83+ keratinocytes may interact with epidermal T cells

Epidermal T cells were revealed to be more immunologically primed than dermal T cells in **Chapter 4** (Figure 32). As the main epidermal microenvironmental signals likely come from keratinocytes, investigation of the possible interactions between CD83+ keratinocytes and epidermal T cells was carried out. CellPhoneDB was used, comparing interactions of the four main groups of keratinocytes with epidermal Tc, Th and Treg cells (**Figure 61**). Many of the statistically significant immunomodulatory interactions are specific to CD83+ KCs, which can further be seen by comparing the expression of the receptors and ligands from these interactions which are expressed by the keratinocytes (**Figure 62**). In particular, the interactions which are not also found between dermal nonimmune and dermal immune cells may contribute to the tissue-specific microenvironmental cues for priming epidermal T cells (**Figure 63**). These epidermal-specific interactions include CD83+ keratinocyte *CCL20* expression, which may attract Th/Treg and Tc cells by their expression of *CCR6* and *CXCR3* respectively. Expression of the adhesion molecules *CDH1* and *ICAM4* may provide specific adherence to epidermal T cells via expression of integrin complexes  $\alpha E\beta 7$  and  $\alpha L\beta 2$  respectively. Furthermore, expression of *LTB* receptor on CD83+ KCs may allow for increased anti-viral activity, and secretion of *TNF* may mediate T cell apoptosis in return (Koroleva et al., 2018).



**Figure 61**

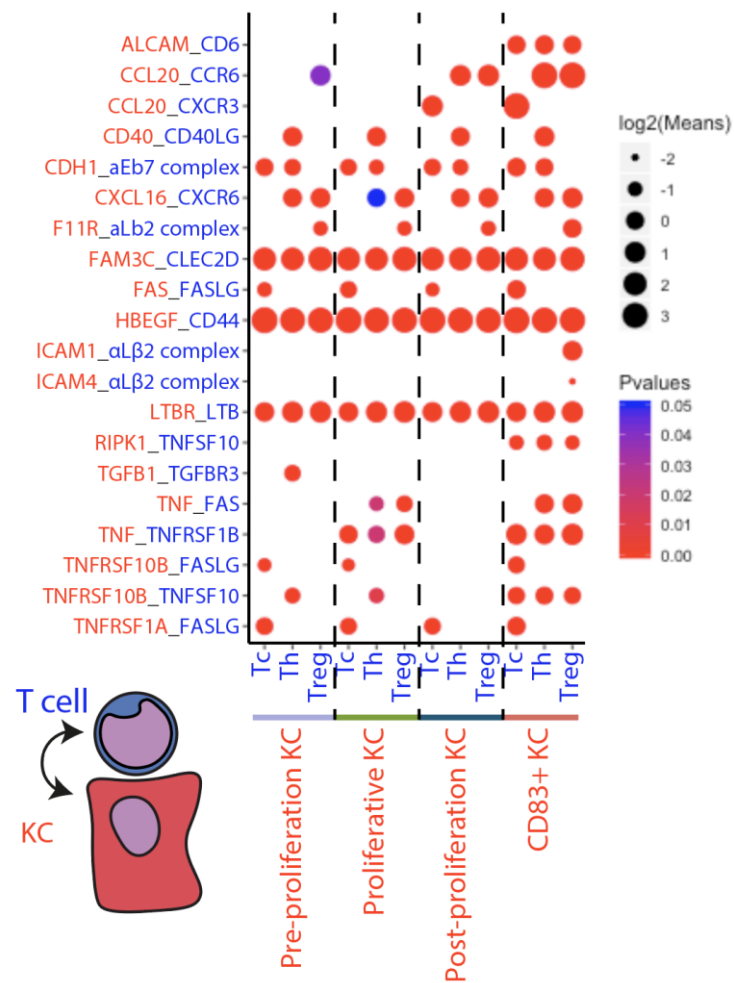


**Figure 61 – Potential interactions between CD83+ keratinocytes and epidermal T cells.**

Heatmap was plotted by Dr Peter Vegh. Heatmap showing expression of selected receptor-ligand pairs from CellPhoneDB between keratinocyte clusters (red genes) and epidermal T cell clusters (blue genes), as shown in the diagram below the heatmap. The radius of each circle corresponds to the averaged relative expression of both the receptor and ligand expressed in their relevant clusters. The intensity of colour, from blue to red, corresponds to the statistical significance of both genes being truly expressed. KC = keratinocyte; Tc = cytotoxic T cell; Th = helper T cell; Treg = regulatory T cell.

**Figure 62**

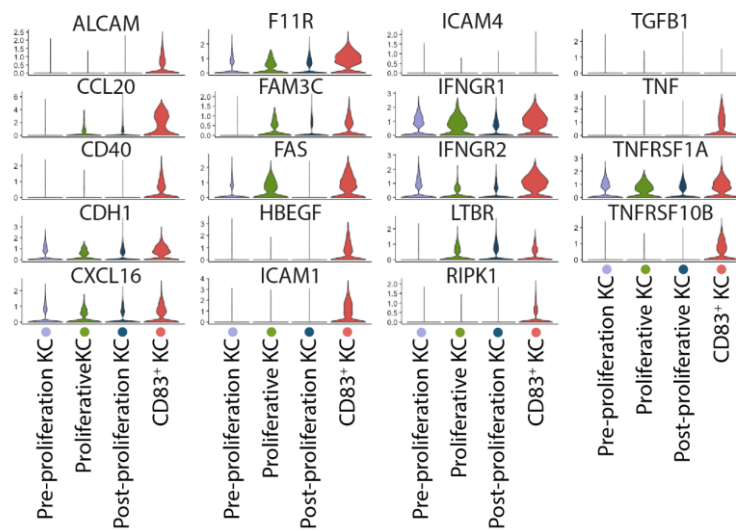


**Figure 62 – CD83+ keratinocytes express higher levels of T cell interacting genes.** Violin plots showing the expression differences of the receptors and ligands in **Figure 61** across the four keratinocyte clusters shown in **Figure 52**. The width of each violin plot is related to the ratio of cells found at a particular Y coordinate. Keratinocyte = KC.

**Figure 63**

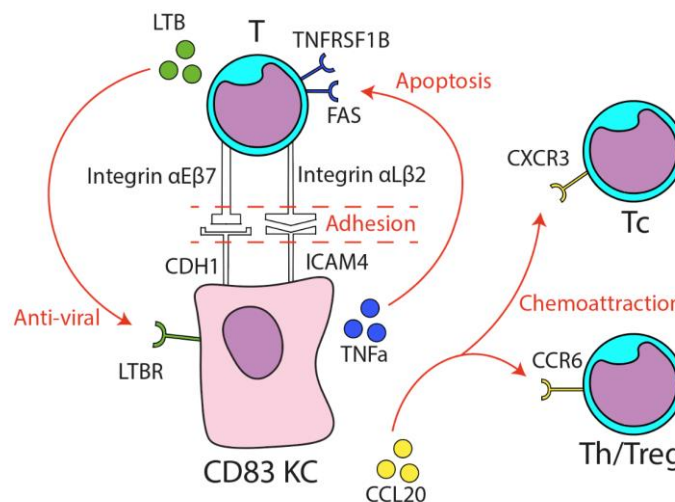


**Figure 63 – Diagram representing the receptor-ligand interactions between CD83 KCs and T cells that are unique to the epidermis.** Of the gene pairs shown in **Figures 61** and **62**, interactions that were not also found in any dermal nonimmune and T cell interactions are represented schematically, with their potential functions shown in red.

### 5.3 Discussion

In depth clustering of the stromal cells within skin was successfully able to identify heterogeneity between cell states. Fibroblast heterogeneity is often reported between papillary and reticular fibroblasts (Philippeos et al., 2018; Janson et al., 2012) although this wasn't recapitulated at single cell level by Tabib *et al.* (Tabib et al., 2018a). Tabib *et al.* do report heterogeneity of inflammatory and ECM maintenance genes within healthy skin fibroblasts, however the reported transcript markers do not match the F1, F2 and F3 clusters presented here. Hagai *et al.* show that dermal fibroblast immune functional gene expression (as opposed to transcription factors and other regulators) is not well conserved across species, including inflammatory cytokine expression (Hagai et al., 2018). This is postulated as an evolutionary advantage enabling adaptation of innate immunity (Hagai et al., 2018). This functional gene expression in fibroblasts may also be highly biologically variable between individuals or body sites, which could explain the difference in findings between this study and other papers.

VE3 structures appear to be analogous to high endothelial venules (HEVs), sharing similar morphology and gene expression. HEVs are specialised vascular structures found in the post-capillary veins of lymphoid organs, with the appearance of a swollen vessel (Mionnet et al., 2011). These vessels express many of the leukocyte adhesion markers expressed by VE3 (Veerman et al., 2019; Pollheimer Jürgen et al., 2013, p.33), and in particular IL33, which is also expressed almost exclusively in VE3 within this data set, is a marker of HEVs and was first isolated as an HEV-specific nuclear protein (Miller, 2011). HEVs facilitate leukocyte extravasation into lymph nodes, even outside of inflammatory conditions, in order to aid immune surveillance and antigen sampling during steady state homeostasis and infection (Mionnet et al., 2011), therefore VE3 structures may also facilitate this function in skin.

The finding of gamma synuclein (*SNCG*) positive vascular endothelial cells is particularly interesting in healthy skin. While *SNCG* was chosen as a marker of VE3 due to its high specificity rather than its functional relevance, interestingly it has been proposed to alter cytoskeletal morphology by decreasing microtubule rigidity (Zhang et al., 2011), which could be postulated as a function of *SNCG* expression in VE3 to aid in leukocytes

physically passing through endothelial cells during transmigration, and could also account for the distended appearance of these structures by microscopy (**Figure 48**). It should be noted that *SNCG* was expressed only on VE3 and LE1 cells. The discussed functionality of the gene would fit *CCL21*<sup>high</sup> initial lymphatic capillaries as well. In order to distinguish the *SNCG*+*CD31*+ structures found by whole mount staining as vascular, morphology was observed. *SNCG*+ vessel sections were continuous with <10µm wide vasculature, and did not approach the 50-100µm diameter previously observed in dermal lymphatics by Wang *et al.* (Wang *et al.*, 2014).

Another functional link between *SNCG* expression and the probable leukocyte extravasation functions of VE3 comes from the reported links between high expression of *SNCG* and cancer metastases (Surguchov *et al.*, 2001; Shao *et al.*, 2018). Data from a single cell study into malignant melanoma tissue by Tirosh *et al.* also reveals high levels of *SNCG*, which was exclusive to endothelial cells (Tirosh *et al.*, 2016). Taken together with the findings in this study, this could provide a linking mechanism whereby an increase in VE3 phenotype within endothelium could possibly facilitate excessive cellular extravasation, leading to an increased likelihood of metastasis. Investigating this possibility directly by comparing this scRNA-seq data with a large dataset of melanoma endothelium for the presence of VE3 signatures could further substantiate this theory.

VE2 appears to represent pre-venular capillary, as supported by the co-expression of *ACKR1* with adhesion markers by flow cytometry, as well as the 50:50 split of *ACKR1* expression on vascular endothelial cells. However, whole mount staining for *ACKR1*, *PECAM1* and *SNCG* together would be required to confirm the proposed spatial arrangement of cells with VE1, VE2 and VE3 transcriptomes. As protein expression doesn't necessarily match RNA expression, using FACS to isolate these *ACKR1*+ endothelial cells within the top 200µm of skin, and sequencing them to confirm that they match the VE2 expression profile could also confirm that these are the same cells as found by protein expression.

No specific surface markers were identified for VE3, making it difficult to perform functional studies on them. Sorting and comparing the three subsets of VE using a

leukocyte adhesion assay to quantitatively compare endothelial adhesion properties would be an interesting way to interrogate their leukocyte transmigration capabilities in healthy skin (Wilhelmsen et al., 2013; Lamberti et al., 2014). However, many of the markers exclusive to VE3 cells are intracellular, so live unfixed unpermeabilised cells cannot be sorted using these proteins. The strong cell surface markers for VE3, mostly leukocyte adhesion markers, are also expressed on VE2 at lower levels by transcript. A clear distinction between low and high expressing populations could not be seen in the flow data, and so sorting and sequencing of “buckets” of variable expression for these markers would likely be required to identify and confirm a valid sorting strategy for VE3 cells.

Trajectory analysis of keratinocytes inferred the existence of two differentiation trajectories, differing by development of lamellar bodies or not. Heterogeneity among keratinocytes with respect to lamellar body production has previously been reported at protein level by Raymond *et al.*, who used density gradient centrifugation to separate bulk keratinocytes into an LB-enriched fraction and a LB-low fraction (Raymond et al., 2008). Mass spectrometry on these fractions revealed a large number of proteins differentially expressed between the two, many of which match up to those found in this study, for example *CLIP1* and *ABCA12* among many others (Raymond et al., 2008). It is particularly interesting that the two keratinocyte trajectories infer that lamellar body expression could be decided in the basal layer, and that these basal cells differentiate into LB expressing suprabasal keratinocytes.

The water-retaining properties of the epidermis are provided by lamellar body secretion, and as such many of these secreted proteins are found continuously across the epidermis. They are reported as such in healthy skin, and discontinuous expression of these proteins is seen in disease conditions, in particular ichthyosis: a dry skin condition strongly linked with dysregulation of lamellar body proteins such as *ABCA12* (Thomas et al., 2006; Elias et al., 2017). It is of note that the scRNA-seq results suggest that this continuous barrier may be maintained by only a fraction of keratinocytes in adult skin, and this may provide some insight into how to more selectively approach treatment for diseases such as ichthyosis.

It is important to note that lamellar body production and secretion is upregulated as an injury response in order to stem water loss from an epidermal wound. The triggering mechanism for this is linked to the loss of an extracellular calcium gradient, normally from low extracellular calcium in the basal layer to high in the suprabasal layer (Menon et al., 1994). This system could have been perturbed as the skin for scRNA-seq was digested in calcium-free media, although it would be difficult to maintain a gradient throughout digestion. As all skin cells were subject to the same methods and only some expressed transcripts for LB-associated proteins, this suggests that this heterogeneity could be genuine. Staining for proteins which would not be secreted, such as transcription factors, would be a good way to validate this heterogeneity within unperturbed skin.

The exact mechanics of keratinocyte differentiation throughout adulthood, and the maintenance and location of epidermal stem cells with proliferative ability is still a topic for debate, with supporting experimental evidence towards different theories. It is therefore of note that the finding of mitotic keratinocytes within this dataset, as well as the trajectories plotted, do not necessarily support either the hierarchical or stochastic models of keratinocyte division, as these mitotic cells could be the transit amplifying cells or be basal progenitor keratinocytes which have stochastically entered a division cycle (Roshan et al., 2016).

CD83 KCs express *CCL20*, secretion of which in keratinocytes is a well reported marker of psoriasis (Harper et al., 2009). Further comparison between the *CCL20*-expressing CD83+ keratinocytes found in healthy skin with psoriatic keratinocytes would be interesting to explore the possibility of this cell state being linked to inflammatory keratinocytes in disease. Cheng *et al.* report, using scRNA-seq, a healthy skin keratinocyte subset enriched for cell-cell communication genes across multiple skin sites, which may be related to the finding of CD83+ KCs (Cheng et al., 2018).

The spatial location of CD83+ keratinocytes could be important information when considering the cells they might interact with. Transcriptomically they are mostly

suprabasal, yet some cells in the cluster express basal keratins. This is supported by the IHC staining, as most of the CD83+ keratin+ epidermal cells were found in the stratum spinosum. Spatial mapping of CD83+ keratinocytes and T cells together may help to delineate the possibility of interaction, as epidermal T cells are found closer to the basement membrane (Clark et al., 2006). While this staining was used to validate the expression of CD83 in the IFE (the epidermal area best matching the cells in the scRNA-seq data), it is interesting that CD83+ keratinocytes were also found, at similarly rare numbers, in both the infundibulum region and bulb of hair follicles. As these regions were not captured for scRNA-seq, it isn't known whether or not keratinocytes with a similar inflammatory transcriptome profile are present therein. However, hair follicles are known to be sites of increased immunomodulation and Tregs are specifically guided to the infundibulum by keratinocytes during development, so it would be interesting to explore the similarities and differences between CD83 expressing keratinocytes in the IFE and in hair follicle regions (Scharschmidt et al., 2017). Particularly, microdissection and scRNA-seq of human hair follicles could provide a comparison between these cells and provide a clearer picture of the single cell heterogeneity involved in follicular T cell trafficking.

Tamoutounour *et al.* report MHC class II+ keratinocytes in both the IFE and infundibulum which play a role in modulating steady state homeostatic T cell response to commensal microbes (Tamoutounour et al., 2019). In mice these keratinocytes were shown to express *Ccl20* and *Icam1*, which are differentially expressed in CD83+ KCs. It would be advantageous to functionally compare these cells, and ascertain whether or not human CD83+ KCs interact with the microbiome. This could be investigated computationally by aligning the human and mouse datasets, or experimentally by following a similar protocol to Tamoutounour *et al.* and repeating the staining done in **Figure 59** after topical culture of commensal bacteria (Tamoutounour et al., 2019).

Investigation of the heterogeneity present in the stromal cells of healthy human skin has expanded on what is known about stromal interaction with the skin's immune system, in particular by identifying different states of immunomodulatory fibroblasts, HEV-like VE3 cells and inflammatory gene signatures in CD83+ keratinocytes. These findings could

have widespread implications for inflammatory skin diseases which involve immune infiltration and stromal interactions in skin.



## **Chapter 6. Summarising Discussion**



## **6.1 Chapter 6 Introduction**

Skin is composed of a wide array of distinct cell types with corroborating functions that provide mechanical, water and immunological barrier properties. Skin is highly cellularly heterogeneous, and much of this heterogeneity is masked when analysing skin cells or tissue in bulk. Segregating cell identities via single- or double-digit parameter protein analysis also poses problems as low parameter analysis can be subject to bias, whereby cells that are distinct by expression of unreported markers go overlooked, and surface proteins can be regularly expressed and sequestered. Much of human skin research correlates with findings in mouse skin, but there remain to be features unique to either human or mouse. Characterising skin cell heterogeneity by performing scRNA-seq on human skin aimed to overcome these issues and provide an unbiased comprehensive resource of human skin cell transcriptome profiles.

In this study a combination of FACS and droplet based scRNA-seq was employed to comprehensively analyse the cellular heterogeneity of healthy adult human skin. CyTOF was run in parallel to compare known protein expression with single cell transcriptomes. The dissociation method was optimised to provide a balance of high cell numbers and low cell death. Single cell sequencing successfully recapitulated the heterogeneity within most skin cell types, providing a strong reference dataset for future skin studies, and also revealed previously unreported findings including steady state epidermal mast cells, HEV-like vessels in non-lymphoid tissue, multiple states of NKs, fibroblasts and lymphatic endothelium.

## **6.2 The novelty of findings from skin single cell analysis**

### **6.2.1 Relevance of optimisation to future skin studies**

In order to minimise the chances of missing a rare cell type or infrequent transitional state, durations of skin dissociation were compared using flow cytometry. Separation of dermis and epidermis was deemed as necessary to recover any meaningful epidermal data, as epidermal nonimmune cells were otherwise liberated at very low numbers and, with some exceptions, epidermal immune cell profiles would have been impossible to accurately separate from dermal immune cell profiles. Type IV collagenase was chosen

based on published comparisons of common skin dissociation techniques (Botting et al., 2017), and 12-16 hours of digestion (The range between which gave a good practical variance for experiments by dissociating skin overnight) gave many more total cells, and much more variance in the immune cell phenotypes released, than 2-10 hours of dissociation.

Much of published skin research using single cell analysis, particularly flow cytometry, uses varied dissociation methods across different labs. Multiple studies have been carried out comparing the common methods more extensively, and though there is general agreement between these studies in regards to the benefits and costs of using specific treatments, there yet remains to be one unifying 'ideal' method of skin dissociation used in the field (Gunawan et al., 2016; Botting et al., 2017; Waise et al., 2019). The optimisation presented in this thesis is very specific to epidermis and papillary dermis in human breast skin. It may be that skin dense in hair follicles or sweat glands, such as scalp or armpit skin respectively, requires different dissociation conditions. Additionally, while breast skin provides a highly accessible model, it accounts for a relatively low proportion of the skin covering any one human. It may also have site specific features, such as metabolic differences caused by the higher levels of subcutaneous fat (Schautz et al., 2011). It is worth considering, then, that while the optimisation performed here was robust for this study, it would still be beneficial for future skin studies to include their own more targeted dissociation optimisation.

It could also be said that this study aimed to refine a dissociation protocol which balances the effects on all skin cell types, whereas the previous study by Botting *et al.* focusses on APCs, and Waise *et al.* focus on fibroblasts (Botting et al., 2017; Waise et al., 2019). One aim of this thesis was to empower skin researchers to focus on the specific cells relevant to their research questions. If this was successful in doing so, then more future studies should hopefully be able to focus on their cells of interest, and their dissociation methods should therefore be tailored to these particular cells.

### **6.2.2 Capture of rare cell types for comprehensive sequencing**

Employing FACS prior to both bulk and single cell sequencing is common in order to remove dead cells and doublets, which is a very valuable technique in order to reduce noise in the data. It is also widely used to select for cell types of interest, which can provide beneficial focus to a study but can also introduce bias whereby cells of interest which don't match the reported surface phenotype are unaccounted for, and continue to go unreported (Philippeos et al., 2018; Haniffa et al., 2012). The use of contiguous gates within this study, encompassing all skin cells, reduced the sampling bias to only events removed based on low size and granularity (acellular debris), high DAPI uptake (dead and dying cells) and non-uniform ratio of forward scatter area vs height (cell doublets). This is not a perfect strategy, as the possibility remains of losing cells with unusual properties, for example extremely small cells, cells that facilitate DAPI uptake, cells that display autofluorescence in the DAPI channel or pairs of cell types that naturally adhere at high rates *in vivo*. These risks were deemed unavoidable, as without these steps high levels of noise would be introduced into the data. This gating strategy allowed for efficient enrichment of rare cell types, and was inspired by the contiguous gating strategy employed by Villani *et al.* in order to avoid monocyte oversampling from PBMCs (Villani et al., 2017). Adapting this further to resample more populations than could be assigned to individual sequencing lanes successfully resulted in the capture of previously unreported levels of heterogeneity within human skin.

Unlike the optimised dissociation protocol, I believe that this strategy could be more widely applicable to many studies. As mentioned, similar strategies of contiguous gating have been used in the past, but resampling cells based on diverse cell type markers is not widely performed. This strategy could greatly aid skin research where there is an interest in cellular diversity, or in studies aiming to comprehensively profile other tissues. This strategy does, however, muddy the analysis of cell proportions which could be particularly disadvantageous for quantitative comparisons of cells in disease states.

H&E analysis of skin at various stages of the dissociation process confirmed that all cells within the top 200µm of skin were being liberated, with the exceptions of hair follicles and anuclear corneocytes. This is an important observation, especially as hair follicle cell states are missing from other recent human skin scRNA-seq studies (Tabib et al., 2018a).

This knowledge necessitates a different approach for capturing hair follicle cells in future studies. One possible approach is the microdissection of individual hair follicles (Limbu & Higgins, 2020).

Combining the approach of dissociating high cell numbers from large skin samples and sorting to capture rare cells with the high throughput of droplet based scRNA-seq resulted in a dataset that met the aims of this study as a comprehensive view of the cellular heterogeneity within healthy adult skin. As well as providing a useful reference dataset for future studies, detailed annotation revealed some interesting findings, including the presence of epidermal mast cells and NK cell heterogeneity in healthy skin.

### **6.2.3 Proteomic profiling of human skin by CyTOF**

CytoTOF was undertaken using a panel of markers selected from known protein expression in skin, and amalgamating APC, lymphoid and nonimmune markers into one panel allowed for a more comprehensive look at skin protein expression than previously published panels which were focussed on one compartment (Alcántara-Hernández et al., 2017; Guo et al., 2019). The comparison of CyTOF and scRNA-seq datasets gave insight into protein-RNA mismatches of these known markers, and in particular revealed the lack of RNA expression of some nonimmune cell markers, including *ITGA6/CD49f* and *NT5E/CD73*. This could provide insights into protein stability and tissue longevity of these cells, as these cells express high protein levels but do not continue to transcribe the relevant genes. The CyTOF data also provided a comparison of accurate cell type proportions, something that was obfuscated by the FACS strategy in the scRNA-seq data. Following on from this work, it would be valuable to design additional CyTOF panels in order to investigate and validate the expression of many of the genes that have been mentioned as functionally relevant and interesting in this study.

While not fully explored as part of this thesis outside of a comparison to scRNA-seq data, this proteomic characterisation data is useful in and of itself. There are few studies integrating the immune and nonimmune cells of human skin by protein expression, and none with high parameter techniques such as CyTOF. CyTOF has been used to analyse skin dendritic cells as well as blood T cells from psoriatic patients, in two separate

studies (Alcántara-Hernández et al., 2017; Guo et al., 2019). Analysing all skin cell types in a single panel allows for the evaluation of markers that can be used to pick out a single cell type from all of skin, which is very useful for downstream studies of particular cells. This condensing of panels allows for future experiments to be done with flow cytometry, which has marked advantages over CyTOF in my opinion. Firstly, cells are not destroyed and so can be sorted for further experiments. And secondly, flow antibodies are more widely accessible in a wider variety of pre-conjugated fluorophores. This makes it more practical to add to and change marker panels as new protein expression information is learned.

#### **6.2.4 Focussed analysis of cellular heterogeneity in scRNA-seq data**

scRNA-seq analysis centres around interpretation of variable gene expression. In order to look at the variable gene expression within specific subsets of cells, without masking these subtle differences with the much more variable expression differences between subsets, the data was split into four parts: keratinocytes, other nonimmune cells, APCs and lymphoid cells.

scRNA-seq resulted in a broad dataset with many findings, both entirely unreported or previously unconfirmed at single cell level, that would be interesting to explore in further detail by validating both protein expression and the functional validity of these findings. While this work was targeted at broadly interrogating many aspects of skin, experimental investigation of the novel findings could have sustained a large body of work in each compartment alone. In the interest of generating a more concise report, specific scRNA-seq results were chosen for further validation.

#### **6.2.5 Dermal nonimmune and vascular heterogeneity**

Analysis of the nonimmune cells in particular unveiled heterogeneity within dermal fibroblasts, schwann cells, lymphatic endothelial cells and vascular endothelial cells. The vasculature was particularly intriguing as the three clusters appeared to correspond to functionally and spatially distinct cells that could be tested for with staining. Flow cytometry analysis of dermal vascular endothelial cells supported the idea that dermal capillaries mirror the expression differences in larger vessels (venules and arterioles),

with ACKR1 and other leukocyte adhesion molecules being specifically co-expressed. This could be of particular relevance to inflammatory skin diseases. Knowing the transcriptome expression of capillaries with extravasation capabilities provides many theoretical target genes to investigate in regards to slowing excessive trafficking of immune cells into diseased skin.

Furthermore, whole mount staining for SNCG, a transcript marker uniquely expressed on VE3 among all vascular endothelial cells, revealed strikingly morphologically distinct structures within the dermal vascular capillaries. These enlarged, distended looking sections of vessel were found at similar rarity to VE3 by scRNA-seq, in skin that was fixed very quickly after surgery, having only gone through one hour of dispase treatment. Assuming these are the same cells as highlighted in the VE3 cluster by scRNA-seq, they are transcribing high levels of chemokines, adhesion molecules and immunomodulatory genes involved in leukocyte transmigration. The appearance and functional gene expression patterns of VE3 closely mirror lymphoid tissue vascular microstructures called HEVs, which facilitate steady state immune surveillance by passing leukocytes into lymph nodes and increasing T cell-DC interaction frequency. VE3 structures could be contributing to non-lymphoid tissue in a similar way, and it would be interesting to both functionally validate this increased extravasation capability as well as to look for VE3-like structures in other non-lymphoid tissue immune barriers, such as the gut. The existence of this structure could be vitally important if the link to cancer metastases discussed in Section 5.3 was further explored, as it could provide opportunities for pre-emptive diagnostic methods targeted at VE3. Even without this exploration, targeting VE3 could be useful in any studies into the movement of skin immune cells.

### **6.2.6 Keratinocyte heterogeneity and immunomodulation**

Trajectory analysis of the keratinocyte compartment computationally recapitulated the known keratinisation differentiation pathway from basal to suprabasal cells. It also revealed a distinct transcriptional trajectory for lamellar body production. This could be particularly useful to dissect further for research into ichthyoses, as well looking into the role of lamellar bodies in wound responses.



The keratinocyte sub-clustering also revealed a cluster of keratinocytes expressing inflammatory transcripts. While this didn't form a clear singular trajectory, it did appear as though cells from both LB trajectory arms (primarily suprabasal KCs) fed into this CD83+ KC cluster. It would be of interest to determine whether these cells are actively surveilling healthy skin, or if they represent an inflammatory state that any keratinocyte can become under the right conditions, which is something that is already reported in the literature (Juráňová et al., 2017). IHC staining lent evidence towards both, as cells expressing both keratin and CD83 were present in the epidermis of skin fixed within minutes of surgical removal, meaning these cells were likely not expressing CD83 in response to wounding or collagenase digestion, but they were much less common by protein staining than by scRNA-seq. Direct spatial interrogation of RNA expression, for example RNAScope staining or spatial transcriptomics, could further elucidate this. The presence of these cells could be very important for the understanding of T cell priming and tolerance in healthy skin. They may also provide a link to inflammatory keratinocytes in disease states. If the inflammatory gene signatures in healthy CD83+ keratinocytes can become accentuated in diseases like psoriasis, this knowledge could provide gene targets to investigate for the prevention of unregulated psoriatic inflammation.

### **6.3 Single cell sequencing publications**

When this project was conceived in early 2016, single cell RNA sequencing was a growing field and there were no published uses of this technology analysing skin. Since then, multiple skin scRNA-seq works have been published. This study primarily achieved novelty by both taking a broad scope and interrogating biological meaning – as many of these studies are either broad but purely computational and do not delve into skin biology, or are very focussed and do not analyse the interactions between stromal cells and immune cells.

However, these studies represent an enormous combined dataset, with skin dissociated using multiple different methods, and many different findings reported. Many of the same findings will be given different nomenclature across different studies, something

which is increasingly common with single cell analysis whereby clusters are often given semi-unbiased names (such as celltype1, celltype2 and so on) to avoid locking in a suggestive name before new information comes to light about the cell type.

Alternatively, there will be genuinely inconsistent findings across studies as well due to variables such as donor-donor differences and dissociation protocol differences.

Forming a consensus of the clusters identified across these papers would be a powerful way to consolidate all of these findings. As of now, it can be very difficult to work out the relationship between, for example, *SFRP2/DPP4* fibroblasts highlighted by Tabib *et al.* and *PRG4* fibroblasts identified by Philippeos *et al.* simply by reading these papers (Tabib *et al.*, 2018a; Philippeos *et al.*, 2018). Even scouring extensive supplementary heatmaps may not reveal a straightforward answer, as marker overlap between studies is far from perfect, possibly due to the aforementioned introduced variables. A large scale computational study in which as many published skin scRNA-seq datasets as possible are analysed in parallel, but still kept related to their original annotations (in particular where functional validation has been carried out), would be a monumental task but one that could solidify the landscape of skin cell heterogeneity.

#### **6.4 The power of investigative scRNA-seq**

The ultimate aim of an encyclopaedic scRNA-seq study is to fully categorise the transcriptomes of all cells in a tissue. This study demonstrates that this technique can reveal novel findings as well as solidify *a priori* knowledge from bulk experiments. However, it also shows that the technology isn't yet on par with the goal of fully categorising all heterogeneity within a tissue. Here, around 5,000-10,000 UMIs were sequenced per cell, capturing an average of the 3,000 most highly expressed genes per cell. Mammalian cells can express more than 50,000 individual transcripts, meaning this likely underrepresents the mRNA in each cell by a significant margin (Marinov *et al.*, 2014). It is possible that this could result in the concealment of heterogeneity of functionally important genes which are transcribed at low levels. scRNA-seq also suffers from the need to validate protein expression for any gene the expression of which may be deemed relevant to a functional hypothesis.

scRNA-seq is still a rapidly developing field. Early studies, between 2009-2012, were able to attain high transcriptome coverage in low cell numbers (Tang et al., 2009; Ramsköld et al., 2012). This study, initiated in 2016, was able to balance lower coverage with high cell numbers. In 2019, Hughes *et al.* developed a method to increase transcriptome coverage without sacrificing as much in terms of cell numbers (Hughes et al., 2019). There are also different single cell capture reagents available with unique benefits. 10x Genomics offers a TCR profiling kit that can provide information on T cell clonality, but even this enriches only alpha and beta chain TCR genes and doesn't capture gamma or delta chain expression. In 5-10 years time, it seems likely that further advances in scRNA-seq technologies will allow for even more transcriptome coverage and more single cells at more practical costs. This study was carried out using the cutting edge approaches of 2016, and it is probable that repeating the experimental pipeline presented here using the technology of 2026 will uncover even more novelties of skin cell heterogeneity.

## **6.5 Further work**

To take this work further, I have since been involved in a wider team effort within the Haniffa Lab expanding on and comparing this healthy adult dataset to foetal skin as well as adult psoriasis and eczema skin. Many of the interesting findings in this study stem from finding features that are in accordance with inflammatory responses at low amounts in healthy skin, and so looking at inflammatory skin conditions by scRNA-seq provides an opportunity to investigate the possibility of certain cell states, such as VE3, F3 and CD83+ KCs, being the healthy counterparts to inflammatory cells, with their differentiation pathway being exaggerated in disease. Some of the findings from this work include the absence of specific lamellar body-expressing KCs in early foetal skin and an increase in VE3 cells in both inflammatory skin conditions.

Spatial mapping of the cell clusters found by scRNA-seq would be a good next step in expanding on an atlas of cell states in healthy adult skin. As the scope of this study was

quite broad, there remain many questions that could be expanded on spatially, such as the confirmation of the proposed spatial arrangement of VE1 and VE2 cells.

Protein staining is useful as confirming that a cell expresses a protein is necessary to draw functional conclusions about how that cell might use that protein. By IHC, ~1-4 proteins can be stained for at once. By imaging mass cytometry, this increases to a theoretical limit of 40+, but as of writing this a practical limit of closer to 20 is more reasonable (Tanner et al., 2013; Baharlou et al., 2019). In all cases these analyse much fewer parameters than sequencing, and cell identification must rely on uniquely expressed markers to accurately identify specific cells. Crucially, protein staining alone as a validation of sequencing data must also rely on the dangerous assumption that RNA and protein expression is matched, both on the positive and negative cells – something that could be overcome with an intermediate step of extensive plate-based sequencing, using indexing data to match protein expression patterns to sequencing clusters.

Directly interrogating spatial RNA expression has the potential to overcome these issues. For example, staining with RNA-specific antibodies using RNAScope or using spatial transcriptome sequencing techniques could provide useful information. Finding specific cell states in close proximity could help to confirm possible interactions. For example, are *CCL19*-expressing F3 cells actively recruiting *CCR7*<sup>+</sup> leukocytes in healthy skin? Such validation could also help to confirm that no specific cell subsets failed to be dissociated for the scRNA-seq experiments.

A single skin slide from one donor was run and processed using Spatial Transcriptomics, whereby a tissue section is attached to a chip covered in 100µm diameter spots, each of which contains RNA probes and unique barcodes (Ståhl et al., 2016). The tissue is lysed on the chip and RNA from each spot is sequenced as the bulk collection of all cells that fell on that area. In theory, this shows RNA expression in situ, and could help to spatially decode the heterogeneity revealed in this study. Ultimately, this line of experimentation wasn't continued as the wide diameter spots meant that only 1-2 spots represented the 200µm depth accounted for in the scRNA-seq data, and so the result was close to representing bulk sequencing of separated epidermis and dermis. Higher resolution

solutions are continually being developed, which could provide great insights into the arrangement of cells in skin (Burgess, 2019).

Experimental perturbations on VE3 may be able to delineate more about its purpose and ontogeny. One difficulty in scRNA-seq analysis is that similar cells forming distinct subsets of unique origins are difficult to tell apart from identical cells in different activation states, or different phases of differentiation. Cells in both circumstances should express similar key functional transcriptomic markers with a transitional range of differentially expressed genes. To investigate whether VE3 represents a permanent structure present from development, or an activated response to inflammatory challenge, one possible experiment would be to try to challenge VE3. TNF $\alpha$  has been shown to upregulate many of the adhesion molecules expressed by VE3, including ICAM1 and SELE (Yang et al., 2009; Makó et al., 2010). TGF $\beta$  reportedly upregulates SNCG expression in tumours, which may be driving a VE3 phenotype in the tumour vasculature (Shao et al., 2018). If a time course of TNF $\alpha$  or TGF $\beta$  treatment of dermal sections was able to increase the numbers of VE3 cells present, this would suggest that VE3 forms as an activated inflammatory state. This could be measured by flow cytometric analysis of SNCG+ vascular cells in treated and untreated dermis. If a statistically significant increase in quantity was not seen, however, the reverse would not be proven as there may be other inflammatory signals required for VE3 activation. Confirmation of VE3-like cells in murine skin, followed by lineage tracing experiments tracking SNCG expression in developing mice skin, could be useful to interrogate VE3 as a fixed cell type in this case.

Expanding on the datasets collected is possible on multiple fronts. As discussed in **Chapter 3**, hair follicles and their related glands and structures as well as Merkel cells and their innervating neurons would need to be captured to fully encompass the cell types in human skin. In addition, this study was limited to epidermis and papillary dermis. The reticular dermis is less cellular, and physically separating it to dissociate and sequence independently would allow for an interesting comparison between the cells found there and the papillary dermal cells analysed in this study.

Collecting skin from different sites would also greatly expand on this work. This study represents a near-comprehensive analysis of cell states in breast skin, and site-specific differences in both stromal and immune cells are widely reported at bulk level.

Consolidating these differences in one high-parameter dataset with scRNA-seq and CyTOF would improve on the resource aspect of this data, providing future skin studies with site-specific data which is crucial for certain studies, for example anogenital skin in research into HIV transfer, or sun-exposed vs non-sun-exposed skin in cancer studies.

Differences in patient demographics are another source of potential investigation. To avoid seeing large biological differences within the relatively small sample size of this study, only skin from females, collected in the North East of England, was sequenced. However, ethnicity and sex innately have marked effects on skin, and ageing and environmental factors such as sun exposure continue to affect the composition and phenotype of skin cells throughout life (Dao & Kazin, 2007; Solé-Boldo et al., 2020; Martincorena et al., 2015).

Thoroughly investigating patient demographics with single cell techniques would require a vast sample cohort, but also incredible computational power. scRNA-seq data analysis in particular becomes very computationally demanding and time consuming with high cell numbers, and analysing high cell numbers in each of tens-to-hundreds of patients in parallel would currently be very impractical. Another solution to demographic-based questions in scRNA-seq findings would be to take a targeted approach. The specific result(s) of interest, found in one patient group by scRNA-seq, could be validated using more scalable experimental techniques within other patient groups of interest.

While the effects of tissue dissociation were investigated and minimised here, a more in depth look at the exact effects of this process on skin cell transcription could help to normalise for (or at least understand) the differences between skin cells *in vivo* and skin cells in their analysed state post-dissociation. Firstly, only one sample per experiment was run for most of the optimisation experiments. Repeating these at least three times total would allow for the calculation of statistical significance and ensure that the results weren't outliers. Secondly, the ideal experiment would be to sequence skin dissociated

for different durations, with multiple donors at each duration, and compare the transcriptomic differences. scRNA-seq or CyTOF would be impossible to perform without dissociation, but the tissue can be directly lysed to undergo bulk sequencing, which can be deconvoluted using scRNA-seq data, although such techniques can struggle to identify rare cell types, especially if these cells express no unique markers, or if transcription of these markers are sensitive to dissociation effects. Spatial transcriptomics would provide another possibility as a compromise between bulk and single cell sequencing of “unperturbed” skin.

## **6.6 Concluding remarks**

The cellular diversity of skin is vital for its ability to protect against immunological challenges, maintain tolerance to self and inert antigens, and respond to physical damage. This study was able to comprehensively categorise healthy skin cells in a semi-unbiased manner by both transcript and protein expression, providing an invaluable reference for the study of skin diseases and their specific cellular deviations from health. In particular, definitive RNA and protein marker characterisation of skin cells will allow for much more targeted analysis of populations of interest. This study also highlighted previously unreported cell types in healthy skin: the presence non-lymphoid HEV-like vessels in the dermis, a rare subset of epidermal mast cells and potentially immunomodulatory keratinocytes. The scRNA-seq data also displayed high levels of heterogeneity within keratinocytes, fibroblasts, dermal APCs, LCs, schwann cells, NK cells and vascular and lymphatic endothelial cells. These results constitute a significant contribution to the pool of knowledge in this field. Building upon this framework by further investigating the functional roles of the cells identified, categorising hair follicles and Merkel cells, contrasting patient demographics and integrating other skin single cell datasets could re-determine the way in which skin cells are analysed and interpreted going forward.

## 7 Appendix tables

Appendix Table 1

Gene	Cluster	p_val	p_val_adj	FC	pct.1	pct.2
TNFAIP6	F1	0	0	12.07701033	0.999	0.345
THBS2	F1	0	0	9.139773447	0.993	0.235
SERPINE2	F1	0	0	7.655962455	0.93	0.286
STC1	F1	0	0	7.058463987	0.727	0.301
PTGES	F1	0	0	6.856350275	0.997	0.249
MMP2	F1	0	0	6.026928253	0.998	0.259
PTX3	F1	0	0	5.811789942	0.444	0.067
MT1X	F1	0	0	5.614997982	0.88	0.322
IL6	F1	0	0	5.384974766	0.904	0.286
AKR1C1	F1	0	0	5.177622277	0.89	0.392
G0S2	F1	0	0	4.996891006	0.794	0.438
PDPN	F1	0	0	4.946624222	0.981	0.257
MT2A	F1	0	0	4.906508534	0.999	0.786
COMP	F1	0	0	4.859774548	0.544	0.069
DCN	F1	0	0	4.857275516	0.989	0.309
PLIN2	F1	0	0	4.845230611	0.922	0.503
CFD	F1	0	0	4.544779134	0.968	0.296
CD44	F1	0	0	4.511398952	0.997	0.37
COL6A2	F1	0	0	4.374495221	0.999	0.358
CRISPLD2	F1	0	0	4.367825926	0.976	0.238
NAMPT	F1	0	0	4.344654886	0.996	0.781
CTSL	F1	0	0	4.323252206	0.945	0.422
IGFBP4	F1	0	0	4.292129023	0.969	0.391
AKR1C2	F1	0	0	4.275432156	0.778	0.244
CEMIP	F1	0	0	4.226899799	0.654	0.111
GREM1	F1	0	0	4.117239982	0.684	0.096
ADAMT5	F1	0	0	4.099964115	0.664	0.068
CXCL14	F1	0	0	3.838872348	0.893	0.217
GLUL	F1	0	0	3.830049779	0.917	0.585
CP	F1	0	0	3.765961572	0.825	0.133
COL1A1	F2	0	0	17.04066191	0.871	0.196
COL1A2	F2	0	0	9.634031749	0.898	0.28
COL3A1	F2	0	0	9.188583877	0.819	0.211
CXCL3	F2	0	0	9.041058049	0.68	0.208
SFRP2	F2	0	0	9.00582815	0.769	0.173
PTGDS	F2	0	0	8.505071008	0.768	0.236
CXCL12	F2	0	0	8.280744951	0.724	0.231



MT1M	F2	0	0	7.174043136	0.791	0.205
DCN	F2	0	0	6.94409887	0.992	0.364
HSPA1A	F2	0	0	6.774176173	0.837	0.532
CCDC80	F2	0	0	6.758430057	0.932	0.306
MT1E	F2	0	0	6.642733344	0.765	0.178
HSPA1B	F2	0	0	6.638511849	0.766	0.273
CFD	F2	0	0	6.242307816	0.966	0.351
PLAC9	F2	0	0	5.953643913	0.75	0.152
TPPP3	F2	0	0	5.536965223	0.657	0.113
CXCL2	F2	0	0	5.289597048	0.673	0.318
S100A4	F2	0	0	5.183238204	0.933	0.391
MFAP4	F2	0	0	5.122282856	0.864	0.225
SERPINF1	F2	0	0	4.897063255	0.896	0.26
SEPP1	F2	0	0	4.846551391	0.814	0.269
TSC22D3	F2	0	0	4.838582745	0.856	0.298
FBLN1	F2	0	0	4.78751356	0.714	0.17
APOE	F2	0	0	4.665701445	0.491	0.135
DPT	F2	0	0	4.609801233	0.879	0.208
LUM	F2	0	0	4.5066534	0.845	0.266
CXCL14	F2	0	0	4.47479844	0.898	0.272
GEM	F2	0	0	4.36839009	0.779	0.276
CTSK	F2	0	0	4.299703355	0.904	0.262
COL6A1	F2	0	0	4.216100939	0.971	0.376
CCL19	F3	0	0	21.26528073	0.828	0.193
IGFBP5	F3	0	0	6.800469652	0.835	0.251
FGF7	F3	0	0	4.43137731	0.76	0.167
MEDAG	F3	0	0	4.282088463	0.942	0.282
CD82	F3	0	0	3.755577973	0.779	0.112
TNFAIP6	F3	0	0	3.315545653	0.998	0.411
CRISPLD2	F3	0	0	3.28846467	0.95	0.314
TNC	F3	0	0	3.277036986	0.63	0.126
C3	F3	0	0	3.218764334	0.794	0.168
CEMIP	F3	0	0	3.141452497	0.692	0.163
SERPINE2	F3	0	0	3.132526448	0.913	0.353
PTGES	F3	0	0	3.099446194	0.984	0.325
TGFB3	F3	0	0	2.990080291	0.59	0.1
TUBB2B	F3	0	0	2.965600395	0.647	0.18
CD44	F3	0	0	2.742652287	0.997	0.433
PTGS2	F3	0	0	2.70739641	0.649	0.186
PRDX6	F3	0	0	2.667608988	0.941	0.71
EDNRB	F3	0	0	2.613099988	0.727	0.253
C1S	F3	0	0	2.609683766	0.967	0.343

APOE	F3	0	0	2.605061035	0.728	0.125
CXCL14	F3	0	0	2.531935697	0.838	0.289
CTSL	F3	0	0	2.500153428	0.944	0.475
BNIP3L	F3	0	0	2.486558244	0.971	0.746
MT1X	F3	0	0	2.473817956	0.846	0.381
TMEM176B	F3	0	0	2.439862801	0.728	0.184
CFH	F3	0	0	2.425986604	0.941	0.349
MT1A	F3	0	0	2.40532425	0.609	0.197
CYP1B1	F3	0	0	2.346135809	0.718	0.212
IL6	F3	0	0	2.345757152	0.858	0.352
AXL	F3	0	0	2.342593661	0.807	0.261
RGS5	Pericyte	0	0	18.64537522	0.762	0.039
MGP	Pericyte	0	0	7.238671695	0.79	0.438
NDUFA4L2	Pericyte	0	0	6.714125441	0.731	0.048
TFPI	Pericyte	0	0	5.478454534	0.909	0.54
KCNE4	Pericyte	0	0	5.072996593	0.755	0.093
NR2F2	Pericyte	0	0	4.699060562	0.673	0.131
KCNJ8	Pericyte	0	0	4.636718646	0.598	0.015
PDGFRB	Pericyte	0	0	4.305616983	0.864	0.212
GJA4	Pericyte	0	0	4.302113279	0.638	0.044
CPE	Pericyte	0	0	4.106765345	0.654	0.073
LURAP1L	Pericyte	0	0	3.989245094	0.619	0.051
C11orf96	Pericyte	0	0	3.658131178	0.675	0.096
HIPK2	Pericyte	0	0	3.446498884	0.661	0.175
CYP26B1	Pericyte	0	0	3.161539263	0.542	0.118
SSTR2	Pericyte	0	0	3.158846028	0.487	0.027
SNHG15	Pericyte	0	0	3.086471412	0.74	0.418
PI15	Pericyte	0	0	3.077537651	0.305	0.008
VEGFA	Pericyte	0	0	2.917523448	0.681	0.27
ZFHX3	Pericyte	0	0	2.906521782	0.588	0.104
TPM2	Pericyte	0	0	2.900582527	0.54	0.124
EDNRB	Pericyte	0	0	2.893515073	0.729	0.253
ZNF503	Pericyte	0	0	2.713766992	0.567	0.144
PROCR	Pericyte	0	0	2.67648698	0.553	0.186
SMIM3	Pericyte	0	0	2.638875012	0.649	0.156
CALD1	Pericyte	0	0	2.627235251	0.97	0.768
CHN1	Pericyte	0	0	2.622943726	0.435	0.078
CLMN	Pericyte	0	0	2.5034239	0.459	0.011
CRYAB	Pericyte	0	0	2.468551136	0.678	0.239
PRRX1	Pericyte	0	0	2.375959359	0.631	0.191
SH3PXD2A	Pericyte	0	0	2.353498493	0.656	0.243
CDH19	Schwann	0	0	8.051749806	0.79	0.003

NRXN1	Schwann	0	0	7.397381699	0.728	0.001
ANK3	Schwann	0	0	6.327759946	0.667	0.004
MYOT	Schwann	0	0	5.193800166	0.556	0.001
CADM2	Schwann	0	0	4.124918583	0.531	0.007
COL28A1	Schwann	0	0	4.054130387	0.667	0.001
S100B	Schwann	0	0	3.971816176	0.321	0.004
ITGB8	Schwann	0	0	3.865815509	0.543	0.013
SLITRK6	Schwann	0	0	3.573965206	0.519	0.001
CADM4	Schwann	0	0	3.443702583	0.63	0.02
FOXD3-AS1	Schwann	0	0	3.344356283	0.531	0.003
FIGN	Schwann	0	0	3.1343144	0.519	0.006
SOX10	Schwann	0	0	2.922821964	0.543	0.005
MAL	Schwann	0	0	2.721143821	0.321	0.003
GFRA3	Schwann	0	0	2.59077766	0.309	0
XKR4	Schwann	0	0	2.504580273	0.358	0.002
ERBB3	Schwann	0	0	2.385438437	0.358	0.005
ART3	Schwann	0	0	2.133572804	0.309	0.001
SLC35F1	Schwann	0	0	1.899552698	0.309	0.002
NTM	Schwann	5.53E-303	1.29E-298	4.38482911	0.568	0.017
PCSK2	Schwann	5.12E-300	1.19E-295	2.906220649	0.444	0.01
IQGAP2	Schwann	1.73E-276	4.03E-272	2.801206063	0.494	0.014
SSUH2	Schwann	1.64E-250	3.83E-246	2.296571231	0.346	0.007
GPM6B	Schwann	2.29E-246	5.34E-242	9.297041666	0.926	0.061
NGFR	Schwann	3.68E-244	8.58E-240	3.597730568	0.506	0.016
PLP1	Schwann	1.29E-234	3.00E-230	6.368680228	0.741	0.038
SEMA3C	Schwann	8.17E-229	1.90E-224	4.471026421	0.679	0.033
GPR155	Schwann	7.11E-190	1.66E-185	3.534128922	0.58	0.029
MPZ	Schwann	7.63E-163	1.78E-158	11.98441232	0.321	0.01
COL8A1	Schwann	3.68E-131	8.58E-127	2.301120433	0.321	0.012
SFRP4	Stromal_Schwann	0	0	10.8015825	0.551	0.019
NGFR	Stromal_Schwann	0	0	3.156125895	0.488	0.016
CLDN1	Stromal_Schwann	1.95E-239	4.55E-235	3.169207105	0.409	0.016
P2RY14	Stromal_Schwann	7.32E-224	1.71E-219	2.557378236	0.394	0.016
C2orf40	Stromal_Schwann	6.91E-192	1.61E-187	2.11651273	0.323	0.013
GPC3	Stromal_Schwann	2.73E-151	6.36E-147	3.271408382	0.535	0.046
SLC22A3	Stromal_Schwann	3.05E-133	7.10E-129	1.845190491	0.354	0.022
MTSS1	Stromal_Schwann	2.69E-122	6.27E-118	2.458940397	0.504	0.05
INHBA	Stromal_Schwann	7.76E-112	1.81E-107	2.482125677	0.346	0.026
HGF	Stromal_Schwann	1.73E-109	4.03E-105	2.162221132	0.37	0.029
ABCA8	Stromal_Schwann	1.19E-98	2.77E-94	2.897389371	0.449	0.049
LUM	Stromal_Schwann	2.05E-89	4.78E-85	15.32410296	0.945	0.313
MFAP5	Stromal_Schwann	1.01E-87	2.37E-83	3.361388694	0.528	0.073

DKK3	Stromal_Schwann	1.38E-82	3.22E-78	2.577803889	0.559	0.089
IGFBP6	Stromal_Schwann	1.78E-78	4.14E-74	5.524663417	0.598	0.11
CYP1B1	Stromal_Schwann	5.62E-76	1.31E-71	11.36144604	0.803	0.244
PLEKHA4	Stromal_Schwann	3.31E-67	7.73E-63	2.898774023	0.63	0.139
TGFBI	Stromal_Schwann	4.34E-63	1.01E-58	4.404832904	0.685	0.18
NOV	Stromal_Schwann	6.41E-58	1.49E-53	2.306356898	0.323	0.041
PDGFRL	Stromal_Schwann	8.13E-57	1.90E-52	2.430482642	0.535	0.109
DCN	Stromal_Schwann	8.32E-57	1.94E-52	2.807786554	1	0.416
LRRN4CL	Stromal_Schwann	1.75E-56	4.08E-52	2.091702489	0.378	0.057
PRRX1	Stromal_Schwann	2.68E-56	6.24E-52	3.333002765	0.724	0.218
FGF7	Stromal_Schwann	2.54E-55	5.91E-51	5.390987116	0.709	0.205
PTGDS	Stromal_Schwann	3.42E-50	7.98E-46	9.255883864	0.756	0.28
APOD	Stromal_Schwann	8.10E-45	1.89E-40	36.74191335	0.835	0.44
CHRD1	Stromal_Schwann	1.09E-44	2.55E-40	2.181977387	0.472	0.104
LTBP4	Stromal_Schwann	3.81E-43	8.88E-39	2.903540649	0.78	0.361
MATN2	Stromal_Schwann	4.16E-43	9.70E-39	1.799343695	0.362	0.067
LSP1	Stromal_Schwann	3.28E-42	7.64E-38	1.662657193	0.307	0.048
DCT	Melanocyte	0	0	82.61034845	0.988	0
TYRP1	Melanocyte	0	0	47.99542911	0.947	0
PMEL	Melanocyte	0	0	39.56373908	0.967	0.007
MLANA	Melanocyte	0	0	35.74107086	0.984	0.001
CAPN3	Melanocyte	0	0	11.68848078	0.893	0.005
CYB561A3	Melanocyte	0	0	10.59804392	0.832	0.071
PLP1	Melanocyte	0	0	8.368797148	0.893	0.032
QPCT	Melanocyte	0	0	8.08184621	0.861	0.117
TYR	Melanocyte	0	0	6.509830994	0.75	0
GPM6B	Melanocyte	0	0	6.288758218	0.779	0.056
CHCHD6	Melanocyte	0	0	6.2748146	0.709	0.033
KRT1	Melanocyte	0	0	6.221240054	0.766	0.039
MFSD12	Melanocyte	0	0	6.186074991	0.75	0.052
PCSK2	Melanocyte	0	0	6.151651996	0.783	0.003
NSG1	Melanocyte	0	0	6.015767952	0.791	0.002
TFAP2A	Melanocyte	0	0	5.882201008	0.754	0.006
BCAN	Melanocyte	0	0	5.787947343	0.742	0.001
TRPM1	Melanocyte	0	0	5.443524288	0.746	0
SFN	Melanocyte	0	0	5.376778933	0.795	0.069
DMKN	Melanocyte	0	0	5.293600773	0.807	0.035
STXBP6	Melanocyte	0	0	4.02691734	0.73	0.043
FRZB	Melanocyte	0	0	3.901811254	0.561	0.017
SLCO4A1-AS1	Melanocyte	0	0	3.749466724	0.602	0.006
KRTDAP	Melanocyte	0	0	3.736026755	0.635	0.029

RAB38	Melanocyte	0	0	3.725073464	0.643	0.022
FXYD3	Melanocyte	0	0	3.68968717	0.574	0.005
CRABP1	Melanocyte	0	0	3.67467313	0.48	0.019
MIA	Melanocyte	0	0	3.55002793	0.488	0.005
KRT17	Melanocyte	0	0	3.446357986	0.676	0.045
KIT	Melanocyte	0	0	3.406209955	0.594	0.006
CCL21	LE1	0	0	36.579416	0.967	0.222
TFF3	LE1	0	0	27.56395513	0.975	0.082
SDPR	LE1	0	0	8.537278725	0.867	0.032
FABP4	LE1	0	0	6.493791424	0.64	0.081
LYVE1	LE1	0	0	5.67995764	0.692	0.067
EFEMP1	LE1	0	0	5.369110772	0.816	0.219
SNCG	LE1	0	0	5.365495877	0.739	0.045
MMRN1	LE1	0	0	5.342780511	0.787	0.074
LAPTM5	LE1	0	0	4.522067176	0.779	0.1
CHRD1	LE1	0	0	2.916030767	0.602	0.094
IGF1	LE1	0	0	2.508052666	0.424	0.03
UCP2	LE1	0	0	2.32297169	0.391	0.011
PDE1A	LE1	0	0	2.054385393	0.387	0.016
CRACR2B	LE1	0	0	1.866015238	0.335	0.017
SCNN1B	LE1	0	0	1.820518507	0.308	0.011
PROX1	LE1	2.21E-258	5.14E-254	2.537780348	0.495	0.079
FXYD6	LE1	1.09E-254	2.54E-250	2.376729019	0.503	0.084
TFPI	LE1	1.96E-250	4.57E-246	3.87259123	0.992	0.556
FLT4	LE1	1.51E-235	3.52E-231	1.753177916	0.325	0.037
HES1	LE1	5.23E-233	1.22E-228	7.201088287	0.654	0.162
ADIRF	LE1	2.11E-231	4.92E-227	6.282208368	0.938	0.567
CLDN5	LE1	7.71E-213	1.80E-208	3.809675538	0.936	0.399
FABP5	LE1	3.31E-201	7.72E-197	2.922868392	0.832	0.293
HSPA1A	LE1	1.22E-198	2.84E-194	9.146164961	0.915	0.551
RAMP2	LE1	7.55E-179	1.76E-174	3.77656577	0.793	0.33
CCND1	LE1	9.61E-172	2.24E-167	2.662317454	0.584	0.162
ARL4A	LE1	9.69E-168	2.26E-163	3.622832473	0.853	0.436
HSPA1B	LE1	2.02E-163	4.72E-159	6.859993041	0.739	0.307
GADD45B	LE1	2.01E-161	4.68E-157	6.982039541	0.957	0.754
ECSCR.1	LE1	1.81E-160	4.23E-156	2.85918206	0.894	0.465
CCL21	LE2	0	0	12.02136532	0.931	0.204
FABP4	LE2	0	0	10.85876777	0.628	0.067
MMRN1	LE2	0	0	7.737375363	0.838	0.053
AKR1C3	LE2	0	0	5.223892704	0.907	0.509
FABP5	LE2	0	0	5.189222386	0.816	0.28
ANGPT2	LE2	0	0	4.919836368	0.89	0.441

TFF3	LE2	0	0	4.751773918	0.85	0.064
STMN1	LE2	0	0	4.439261787	0.943	0.385
LYVE1	LE2	0	0	4.241353062	0.691	0.051
TFPI	LE2	0	0	4.031197823	0.981	0.545
EGLN3	LE2	0	0	4.024765519	0.859	0.298
CNKSR3	LE2	0	0	3.944603338	0.86	0.271
AKR1C1	LE2	0	0	3.923799163	0.943	0.45
CLDN5	LE2	0	0	3.810925205	0.913	0.386
NRP2	LE2	0	0	3.616308137	0.736	0.172
PROX1	LE2	0	0	3.562433963	0.619	0.062
PPFIBP1	LE2	0	0	3.379544426	0.889	0.362
CARHSP1	LE2	0	0	3.262138738	0.874	0.475
IRF8	LE2	0	0	3.202624084	0.672	0.101
SNCA	LE2	0	0	3.051509865	0.664	0.092
NUPR1	LE2	0	0	3.003777358	0.976	0.699
SCN3B	LE2	0	0	2.97822545	0.619	0.036
ARL4A	LE2	0	0	2.954498398	0.875	0.424
CD200	LE2	0	0	2.94029674	0.877	0.368
PLA1A	LE2	0	0	2.756594047	0.5	0.013
COX17	LE2	0	0	2.747199187	0.86	0.493
TGFB2	LE2	0	0	2.740498485	0.627	0.025
HEBP1	LE2	0	0	2.734183331	0.839	0.398
C16orf62	LE2	0	0	2.652599216	0.657	0.113
CHRD1	LE2	0	0	2.573816004	0.628	0.08
EMCN	VE1	0	0	4.4751932	0.956	0.377
PLS3	VE1	0	0	3.507352316	0.964	0.511
CYP1A1	VE1	0	0	3.505113585	0.471	0.121
CX3CL1	VE1	0	0	3.495485106	0.614	0.225
SPARCL1	VE1	0	0	3.354468197	0.989	0.576
HEY1	VE1	0	0	3.114718182	0.607	0.128
RCAN1	VE1	0	0	3.022621637	0.96	0.551
ENG	VE1	0	0	2.767292876	0.872	0.597
TAGLN	VE1	0	0	2.716730379	0.452	0.196
IFI27	VE1	0	0	2.684363324	0.957	0.602
MRPL33	VE1	0	0	2.621214604	0.956	0.595
RBP7	VE1	0	0	2.608931603	0.475	0.131
PNP	VE1	0	0	2.555337478	0.885	0.46
PLVAP	VE1	0	0	2.547462808	0.876	0.387
CD200	VE1	0	0	2.514174096	0.746	0.269
SPRY1	VE1	0	0	2.499568095	0.831	0.58
TSPAN13	VE1	0	0	2.447236514	0.695	0.27
ADGRL4	VE1	0	0	2.418685683	0.857	0.331

STK38L	VE1	0	0	2.385710453	0.61	0.254
MYL9	VE1	0	0	2.374380202	0.714	0.388
CD83	VE1	0	0	2.284138406	0.528	0.194
SOX17	VE1	0	0	2.271459115	0.597	0.223
SGK1	VE1	0	0	2.261424434	0.688	0.397
MYCBP2	VE1	0	0	2.242233955	0.844	0.506
CALCRL	VE1	0	0	2.224308088	0.774	0.333
MTUS1	VE1	0	0	2.216323215	0.484	0.217
MCTP1	VE1	0	0	2.213904868	0.839	0.335
MYLK	VE1	0	0	2.177794109	0.727	0.315
PKIG	VE1	0	0	2.173386705	0.897	0.649
PLK2	VE1	0	0	2.168395564	0.447	0.176
ACKR1	VE2	0	0	4.15347959	0.762	0.15
SERPINE1	VE2	0	0	4.090638477	0.954	0.568
HLA-DRB1	VE2	0	0	3.722493614	0.989	0.517
TM4SF1	VE2	0	0	3.091981868	1	0.563
HLA-DQA1	VE2	0	0	3.015197808	0.709	0.177
EDN1	VE2	0	0	2.78828737	0.444	0.178
FABP5	VE2	0	0	2.727977	0.5	0.239
UPP1	VE2	0	0	2.694008344	0.951	0.478
NCOA7	VE2	0	0	2.619760423	0.857	0.6
HLA-DQB1	VE2	0	0	2.612968092	0.844	0.272
CAV1	VE2	0	0	2.512104753	0.988	0.767
CYR61	VE2	0	0	2.508957582	0.766	0.496
HLA-DRB5	VE2	0	0	2.462262871	0.892	0.348
TMEM173	VE2	0	0	2.400436325	0.884	0.453
COL15A1	VE2	0	0	2.396656757	0.924	0.462
SELE	VE2	0	0	2.331816508	0.546	0.132
CD74	VE2	0	0	2.319751613	0.987	0.579
HLA-DRA	VE2	0	0	2.306768867	0.937	0.431
PRSS23	VE2	0	0	2.273642494	0.822	0.334
EGFL7	VE2	0	0	2.268909875	0.654	0.242
C10orf10	VE2	0	0	2.249843197	0.908	0.459
PDLIM1	VE2	0	0	2.233343356	0.972	0.72
PIM3	VE2	0	0	2.222104285	0.868	0.507
ESAM	VE2	0	0	2.213954371	0.908	0.432
SLCO4A1	VE2	0	0	2.191209329	0.82	0.292
PLVAP	VE2	0	0	2.18316196	0.878	0.39
ACTN1	VE2	0	0	2.168561796	0.976	0.577
ZNF385D	VE2	0	0	2.124636381	0.876	0.392
CLDN5	VE2	0	0	2.10746063	0.694	0.316
ETS2	VE2	0	0	2.09610904	0.961	0.581

AQP1	VE3	0	0	6.790659202	0.928	0.209
SDPR	VE3	5.16E-269	1.20E-264	2.247503835	0.458	0.044
SNCG	VE3	1.33E-267	3.11E-263	2.663031273	0.493	0.054
RNASE1	VE3	1.84E-262	4.30E-258	3.42070776	0.622	0.096
HLA-DMA	VE3	3.00E-243	6.98E-239	3.3112151	0.666	0.123
CCL14	VE3	5.12E-238	1.19E-233	4.377189552	0.758	0.17
SELE	VE3	3.67E-225	8.55E-221	18.76593531	0.818	0.228
CD34	VE3	1.11E-203	2.60E-199	3.483016383	0.775	0.201
CYTL1	VE3	6.86E-203	1.60E-198	2.237366181	0.357	0.037
IL33	VE3	8.37E-199	1.95E-194	2.361762522	0.516	0.078
ACKR1	VE3	1.62E-186	3.78E-182	9.968142915	0.839	0.297
RAMP3	VE3	3.28E-183	7.65E-179	2.663719901	0.536	0.096
CD74	VE3	2.64E-176	6.15E-172	4.574791729	0.997	0.677
HLA-DRA	VE3	3.29E-167	7.67E-163	4.636888694	0.971	0.553
CTGF	VE3	1.05E-164	2.45E-160	3.863035685	0.651	0.152
HSPA1B	VE3	1.24E-164	2.88E-160	4.100736478	0.85	0.308
HLA-DPA1	VE3	1.03E-163	2.41E-159	4.198004698	0.916	0.416
PDK4	VE3	3.14E-154	7.31E-150	3.882178158	0.646	0.166
ADIRF	VE3	5.58E-145	1.30E-140	4.842436775	0.928	0.57
ICAM1	VE3	4.13E-140	9.62E-136	4.939901762	0.957	0.727
HSPA1A	VE3	1.21E-134	2.81E-130	4.530594242	0.914	0.553
GNG11	VE3	2.24E-134	5.22E-130	3.219935081	0.98	0.619
SCARB1	VE3	4.13E-134	9.62E-130	2.013030958	0.366	0.058
HLA-DPB1	VE3	4.57E-131	1.06E-126	3.633871055	0.873	0.469
RND1	VE3	4.32E-130	1.01E-125	4.880807592	0.798	0.33
ITM2A	VE3	6.62E-124	1.54E-119	2.956733676	0.839	0.364
RAMP2	VE3	4.45E-119	1.04E-114	3.139159886	0.798	0.333
ICAM2	VE3	3.82E-117	8.90E-113	2.471436098	0.507	0.128
BCAM	VE3	2.53E-113	5.90E-109	2.817770383	0.83	0.392

**Appendix Table 1 – Detailed nonimmune cluster differentially expressed genes.**

Differentially expressed genes calculated by Dr Peter Vegh. The top 30 differentially expressed genes per cluster between all nonimmune cells, using the annotations in **Figure 41**. FC = Expression fold change between the cluster and all other nonimmune cells. pct1 = The percentage of cells in the cluster expressing the gene. pct2 = The percentage of all nonimmune cells expressing the gene. p\_val = p value; p\_val\_adj = adjusted p value.



**Appendix Table 2**

Gene	Cluster	p_val	p_val_adj	FC	pct.1	pct.2
IER2	CD83_KC	0	0	6.675290753	0.993	0.759
EIF5	CD83_KC	0	0	6.332748961	0.983	0.58
RSRP1	CD83_KC	0	0	5.698293897	0.974	0.599
NR4A2	CD83_KC	0	0	5.639839976	0.744	0.142
EGR1	CD83_KC	0	0	5.551869024	0.882	0.494
TRA2B	CD83_KC	0	0	5.519836487	0.99	0.644
IRF1	CD83_KC	0	0	5.307507862	0.972	0.502
RSRC2	CD83_KC	0	0	5.153803431	0.997	0.757
HIST1H4C	CD83_KC	0	0	5.139470069	0.884	0.264
CCL20	CD83_KC	0	0	5.066553803	0.664	0.297
PPP1R10	CD83_KC	0	0	5.061975711	0.875	0.24
BAZ1A	CD83_KC	0	0	4.966619981	0.983	0.746
CLK1	CD83_KC	0	0	4.878709984	0.988	0.665
DNAJA1	CD83_KC	0	0	4.851498222	0.974	0.598
YME1L1	CD83_KC	0	0	4.745463508	0.893	0.327
ARID4B	CD83_KC	0	0	4.451682476	0.909	0.374
TUBB4B	CD83_KC	0	0	4.438752845	0.982	0.691
GPBP1	CD83_KC	0	0	4.234178678	0.974	0.599
WSB1	CD83_KC	0	0	4.232163917	0.973	0.562
NCOA7	CD83_KC	0	0	4.193773592	0.828	0.413
DDX39A	CD83_KC	0	0	4.077378239	0.927	0.338
ZBTB10	CD83_KC	0	0	4.034030347	0.751	0.118
ID3	CD83_KC	0	0	4.032075101	0.766	0.233
TRA2A	CD83_KC	0	0	3.99445965	0.931	0.389
FOS	CD83_KC	0	0	3.986961074	0.944	0.606
ARL5B	CD83_KC	0	0	3.962181335	0.957	0.497
KMT2E	CD83_KC	0	0	3.927524952	0.944	0.484
NR4A1	CD83_KC	0	0	3.925421846	0.961	0.58
NR1D1	CD83_KC	0	0	3.865609836	0.978	0.705
SERTAD1	CD83_KC	0	0	3.770099493	0.925	0.432
STMN1	Mitotic_KC	0	0	7.615204598	0.927	0.134
CDK1	Mitotic_KC	0	0	4.530656035	0.899	0.046
UBE2C	Mitotic_KC	0	0	4.510343314	0.765	0.023
NUSAP1	Mitotic_KC	0	0	3.504960505	0.864	0.106
TOP2A	Mitotic_KC	0	0	3.476584412	0.711	0.009
CENPW	Mitotic_KC	0	0	3.270965208	0.866	0.109
CENPF	Mitotic_KC	0	0	3.215735055	0.646	0.01
KIAA0101	Mitotic_KC	0	0	2.900758825	0.619	0.019
ANLN	Mitotic_KC	0	0	2.791121462	0.709	0.023

PRC1	Mitotic_KC	0	0	2.777128876	0.782	0.07
TK1	Mitotic_KC	0	0	2.612459886	0.567	0.015
AURKB	Mitotic_KC	0	0	2.504323908	0.646	0.006
CDKN3	Mitotic_KC	0	0	2.44928279	0.619	0.012
CCNB2	Mitotic_KC	0	0	2.430372849	0.616	0.012
BIRC5	Mitotic_KC	0	0	2.376682196	0.597	0.016
MKI67	Mitotic_KC	0	0	2.347879186	0.612	0.006
ASPM	Mitotic_KC	0	0	2.245544856	0.502	0.007
ZWINT	Mitotic_KC	0	0	2.227122032	0.659	0.022
TPX2	Mitotic_KC	0	0	2.155984031	0.612	0.02
MAD2L1	Mitotic_KC	0	0	2.143847678	0.655	0.028
PBK	Mitotic_KC	0	0	2.138242766	0.578	0.004
KIF20B	Mitotic_KC	0	0	2.138228628	0.567	0.074
CCNB1	Mitotic_KC	0	0	2.134911078	0.422	0.022
CDC20	Mitotic_KC	0	0	2.054791759	0.437	0.012
HMMR	Mitotic_KC	0	0	2.044355914	0.489	0.007
NUF2	Mitotic_KC	0	0	1.959228717	0.562	0.007
SMC2	Mitotic_KC	0	0	1.910217021	0.64	0.066
TROAP	Mitotic_KC	0	0	1.899066874	0.466	0.004
UBE2T	Mitotic_KC	0	0	1.879126356	0.537	0.027
RRM2	Mitotic_KC	0	0	1.874875573	0.401	0.004
KRTDAP	Postmitotic_KC	0	0	12.07245251	0.95	0.346
SPRR1B	Postmitotic_KC	0	0	8.774331158	0.678	0.221
SBSN	Postmitotic_KC	0	0	8.370798971	0.871	0.328
KRT1	Postmitotic_KC	0	0	6.921164425	0.98	0.483
LYPD3	Postmitotic_KC	0	0	5.574193703	0.849	0.336
CALML5	Postmitotic_KC	0	0	5.565261774	0.563	0.135
KRT10	Postmitotic_KC	0	0	3.882492055	0.964	0.686
CD24	Postmitotic_KC	0	0	3.594958356	0.449	0.128
FABP5	Postmitotic_KC	0	0	3.226072342	0.34	0.099
KRT16	Postmitotic_KC	0	0	3.187894067	0.722	0.487
SULT2B1	Postmitotic_KC	0	0	2.947868244	0.531	0.165
LAMTOR4	Postmitotic_KC	0	0	2.889885878	0.929	0.677
CA2	Postmitotic_KC	0	0	2.866888359	0.631	0.364
CSTA	Postmitotic_KC	0	0	2.750305071	0.808	0.528
TMEM40	Postmitotic_KC	0	0	2.512458945	0.623	0.19
PRSS3	Postmitotic_KC	0	0	2.457717342	0.62	0.254
DEFB1	Postmitotic_KC	0	0	2.4121537	0.726	0.259
MSMO1	Postmitotic_KC	0	0	2.340249893	0.533	0.166
DBI	Postmitotic_KC	0	0	2.220742054	0.791	0.504
CSTB	Postmitotic_KC	0	0	2.213359297	0.912	0.675
NUPR1	Postmitotic_KC	0	0	2.119078376	0.921	0.685

GLTP	Postmitotic_KC	0	0	2.0327077	0.539	0.241
APOE	Postmitotic_KC	0	0	2.007094286	0.684	0.258
DYNLL1	Postmitotic_KC	0	0	1.998058258	0.92	0.712
RHOV	Postmitotic_KC	0	0	1.951431194	0.749	0.248
TMEM45B	Postmitotic_KC	0	0	1.910089422	0.347	0.042
TSC22D1	Postmitotic_KC	0	0	1.879918063	0.728	0.515
CTNNBIP1	Postmitotic_KC	0	0	1.822574733	0.5	0.221
PKP1	Postmitotic_KC	0	0	1.714431264	0.694	0.422
KCNK7	Postmitotic_KC	0	0	1.706763455	0.453	0.099
KRT15	Premitotic_KC	0	0	11.38496611	0.816	0.093
POSTN	Premitotic_KC	0	0	6.84303572	0.765	0.053
KRT5	Premitotic_KC	0	0	5.837743857	0.998	0.719
COL17A1	Premitotic_KC	0	0	5.348815699	0.94	0.237
DST	Premitotic_KC	0	0	3.54687091	0.881	0.402
ZFP36L2	Premitotic_KC	0	0	3.134501964	0.845	0.581
CYR61	Premitotic_KC	0	0	2.950208896	0.469	0.205
S100A6	Premitotic_KC	0	0	2.94661124	0.868	0.419
IFITM3	Premitotic_KC	0	0	2.839256501	0.69	0.2
PDLIM1	Premitotic_KC	0	0	2.802099834	0.869	0.486
ITGB1	Premitotic_KC	0	0	2.74922679	0.758	0.247
SOX4	Premitotic_KC	0	0	2.666276033	0.317	0.113
SYT8	Premitotic_KC	0	0	2.634834147	0.71	0.252
TGFBI	Premitotic_KC	0	0	2.433934559	0.725	0.309
GADD45A	Premitotic_KC	0	0	2.42658929	0.729	0.374
BGN	Premitotic_KC	0	0	2.352650512	0.596	0.179
LAMB3	Premitotic_KC	0	0	2.290895499	0.642	0.212
EFEMP1	Premitotic_KC	0	0	2.253835889	0.51	0.066
RND3	Premitotic_KC	0	0	2.211151886	0.821	0.598
ITGA2	Premitotic_KC	0	0	2.173046282	0.486	0.138
ASS1	Premitotic_KC	0	0	2.076950189	0.47	0.039
CAV2	Premitotic_KC	0	0	2.059749637	0.793	0.522
WNT3	Premitotic_KC	0	0	2.049212056	0.493	0.073
CTNNAL1	Premitotic_KC	0	0	2.028828361	0.482	0.015
DCN	Premitotic_KC	0	0	1.957127966	0.514	0.193
IL1R2	Premitotic_KC	0	0	1.872429324	0.308	0.103
ASPN	Premitotic_KC	0	0	1.846601996	0.327	0.042
GDPD2	Premitotic_KC	0	0	1.840814075	0.398	0.029
COL7A1	Premitotic_KC	0	0	1.812454056	0.39	0.066
ITGA6	Premitotic_KC	0	0	1.807363037	0.463	0.123

**Appendix Table 2 – Detailed keratinocyte cluster differentially expressed genes.**

Differentially expressed genes calculated by Dr Peter Vegh. The top 30 differentially

expressed genes per cluster between all keratinocytes, using the annotations in **Figure 52**. FC = Expression fold change between the cluster and all other keratinocytes. pct1 = The percentage of cells in the cluster expressing the gene. pct2 = The percentage of all keratinocytes expressing the gene. p\_val = p value; p\_val\_adj = adjusted p value.

**Appendix Table 3**

Gene symbol	Gene name	HCNG ID	Alternate protein name
ABCA12	ATP binding cassette subfamily A member 12	HGNC:14637	
AC092580.4	N/A	N/A	
ACKR1	atypical chemokine receptor 1 (Duffy blood group)	HGNC:4035	
ACOT7	acyl-CoA thioesterase 7	HGNC:24157	
AKR1C1	aldo-keto reductase family 1 member C1	HGNC:384	
ALCAM	activated leukocyte cell adhesion molecule	HGNC:400	
APLNR	apelin receptor	HGNC:339	
APOD	apolipoprotein D	HGNC:612	
APP	amyloid beta precursor protein	HGNC:620	
ATOH1	atonal bHLH transcription factor 1	HGNC:797	
ATXN1	ataxin 1	HGNC:10548	SCA1
AXL	AXL receptor tyrosine kinase	HGNC:905	
BDKRB1	bradykinin receptor B1	HGNC:1029	
BST2	bone marrow stromal cell antigen 2	HGNC:1119	
CADM1	cell adhesion molecule 1	HGNC:5951	
CCL1	C-C motif chemokine ligand 1	HGNC:10609	
CCL14	C-C motif chemokine ligand 14	HGNC:10612	
CCL19	C-C motif chemokine ligand 19	HGNC:10617	
CCL2	C-C motif chemokine ligand 2	HGNC:10618	
CCL20	C-C motif chemokine ligand 20	HGNC:10619	
CCL21	C-C motif chemokine ligand 21	HGNC:10620	
CCL23	C-C motif chemokine ligand 23	HGNC:10622	
CCL27	C-C motif chemokine ligand 27	HGNC:10626	
CCL3	C-C motif chemokine ligand 3	HGNC:10627	
CCL5	C-C motif chemokine ligand 5	HGNC:10632	
CCR10	C-C motif chemokine receptor 10	HGNC:4474	
CCR2	C-C motif chemokine receptor 2	HGNC:1603	
CCR4	C-C motif chemokine receptor 4	HGNC:1605	
CCR7	C-C motif chemokine receptor 7	HGNC:1608	
CCRL2	C-C motif chemokine receptor like 2	HGNC:1612	
CD14	CD14 molecule	HGNC:1628	
CD151	CD151 molecule (Raph blood group)	HGNC:1630	
CD19	CD19 molecule	HGNC:1633	
CD1A	CD1a molecule	HGNC:1634	
CD1C	CD1c molecule	HGNC:1636	
CD207	CD207 molecule	HGNC:17935	Langerin
CD247	CD247 molecule	HGNC:1677	PD-L1
CD33	CD33 molecule	HGNC:1659	
CD34	CD34 molecule	HGNC:1662	
CD3D	CD3d molecule	HGNC:1673	CD3
CD3E	CD3e molecule	HGNC:1674	CD3
CD4	CD4 molecule	HGNC:1678	
CD40	CD40 molecule	HGNC:11919	
CD40LG	CD40 ligand	HGNC:11935	
CD44	CD44 molecule (Indian blood group)	HGNC:1681	
CD46	CD46 molecule	HGNC:6953	
CD47	CD47 molecule	HGNC:1682	
CD5	CD5 molecule	HGNC:1685	
CD6	CD6 molecule	HGNC:1691	
CD69	CD69 molecule	HGNC:1694	
CD7	CD7 molecule	HGNC:1695	
CD74	CD74 molecule	HGNC:1697	
CD82	CD82 molecule	HGNC:6210	
CD83	CD83 molecule	HGNC:1703	
CD8A	CD8a molecule	HGNC:1706	CD8
CD8B	CD8b molecule	HGNC:1707	CD8

CD9	CD9 molecule	HGNC:1709	
CD96	CD96 molecule	HGNC:16892	
CD99	CD99 molecule (Xg blood group)	HGNC:7082	
CDH1	cadherin 1	HGNC:1748	E-cadherin
CDH2	cadherin 2	HGNC:1759	N-cadherin
CDK1	cyclin dependent kinase 1	HGNC:1722	
CERS3	ceramide synthase 3	HGNC:23752	
CFD	complement factor D	HGNC:2771	
CKAP4	cytoskeleton associated protein 4	HGNC:16991	
CLEC2D	C-type lectin domain family 2 member D	HGNC:14351	
CLEC4C	C-type lectin domain family 4 member C	HGNC:13258	CD303
CLEC6A	C-type lectin domain containing 6A	HGNC:14556	
CLEC7A	C-type lectin domain containing 7A	HGNC:14558	
CLEC9A	C-type lectin domain containing 9A	HGNC:26705	
CLIP1	CAP-Gly domain containing linker protein 1	HGNC:10461	
CMA1	chymase 1	HGNC:2097	
COL15A1	collagen type XV alpha 1 chain	HGNC:2192	
COL18A1	collagen type XVIII alpha 1 chain	HGNC:2195	
COL1A1	collagen type I alpha 1 chain	HGNC:2197	
COL1A2	collagen type I alpha 2 chain	HGNC:2198	
COL4A1	collagen type IV alpha 1 chain	HGNC:2202	
COL4A2	collagen type IV alpha 2 chain	HGNC:2203	
COL6A2	collagen type VI alpha 2 chain	HGNC:2212	
COL7A1	collagen type VII alpha 1 chain	HGNC:2214	
CPA3	carboxypeptidase A3	HGNC:2298	
CREM	cAMP responsive element modulator	HGNC:2352	
CRYAB	crystallin alpha B	HGNC:2389	
CSF1R	colony stimulating factor 1 receptor	HGNC:2433	CD115
CSF2	colony stimulating factor 2	HGNC:2434	GMCSF
CSF3	colony stimulating factor 3	HGNC:2438	GCSF
CST6	cystatin E/M	HGNC:2478	
CTNNAL1	catenin alpha like 1	HGNC:2512	
CTSG	cathepsin G	HGNC:2532	
CXCL1	C-X-C motif chemokine ligand 1	HGNC:4602	
CXCL12	C-X-C motif chemokine ligand 12	HGNC:10672	
CXCL14	C-X-C motif chemokine ligand 14	HGNC:10640	
CXCL16	C-X-C motif chemokine ligand 16	HGNC:16642	
CXCL3	C-X-C motif chemokine ligand 3	HGNC:4604	
CXCL8	C-X-C motif chemokine ligand 8	HGNC:6025	
CXCR1	C-X-C motif chemokine receptor 1	HGNC:6026	
CXCR3	C-X-C motif chemokine receptor 3	HGNC:4540	
CXCR4	C-X-C motif chemokine receptor 4	HGNC:2561	
CXCR6	C-X-C motif chemokine receptor 6	HGNC:16647	
CYP4F22	cytochrome P450 family 4 subfamily F member 22	HGNC:26820	
DCN	decorin	HGNC:2705	
DCT	dopachrome tautomerase	HGNC:2709	
DLK1	delta like non-canonical Notch ligand 1	HGNC:2907	
DMKN	dermokine	HGNC:25063	
DNAJB1	DnaJ heat shock protein family (Hsp40) member B1	HGNC:5270	
DPP4	dipeptidyl peptidase 4	HGNC:3009	
DUSP4	dual specificity phosphatase 4	HGNC:3070	
ELOVL4	ELOVL fatty acid elongase 4	HGNC:14415	
ENPP3	ectonucleotide pyrophosphatase/phosphodiesterase 3	HGNC:3358	CD203c
EPCAM	epithelial cell adhesion molecule	HGNC:11529	EpCAM
F11R	F11 receptor	HGNC:14685	
F13A1	coagulation factor XIII A chain	HGNC:3531	FXIIIA
FABP4	fatty acid binding protein 4	HGNC:3559	
FAM3C	FAM3 metabolism regulating signaling molecule C	HGNC:18664	
FAS	Fas cell surface death receptor	HGNC:11920	
FASLG	Fas ligand	HGNC:11936	

FCER1A	Fc fragment of IgE receptor Ia	HGNC:3609	FCεR1
FCGR3A	CD151 molecule (Raph blood group)	HGNC:1630	CD16
FGF7	fibroblast growth factor 7	HGNC:3685	
FGL2	fibrinogen like 2	HGNC:3696	
FLG	filaggrin	HGNC:3748	
FLG2	filaggrin family member 2	HGNC:33276	
FLT1	fms related receptor tyrosine kinase 1	HGNC:3763	
FLT3	fms related receptor tyrosine kinase 3	HGNC:3765	CD135
FOXP3	forkhead box P3	HGNC:6106	
FUT4	fucosyltransferase 4	HGNC:4015	CD15
GADD45B	growth arrest and DNA damage inducible beta	HGNC:4096	
GATA3	GATA binding protein 3	HGNC:4172	
GBP2	guanylate binding protein 2	HGNC:4183	
GLG1	golgi glycoprotein 1	HGNC:4316	
GPLY	granulysin	HGNC:4414	
GZMA	granzyme A	HGNC:4708	
GZMB	granzyme B	HGNC:4709	
GZMH	granzyme H	HGNC:4710	
GZMK	granzyme K	HGNC:4711	
GZMM	granzyme M	HGNC:4712	
HBEGF	heparin binding EGF like growth factor	HGNC:3059	
HDC	histidine decarboxylase	HGNC:4855	
HES1	hes family bHLH transcription factor 1	HGNC:5192	
HEY1	hes related family bHLH transcription factor with YRPW motif 1	HGNC:4880	
HLA-DQA1	major histocompatibility complex, class II, DQ alpha 1	HGNC:4942	
HLA-DQB2	major histocompatibility complex, class II, DQ beta 2	HGNC:4945	
HLA-DRA	major histocompatibility complex, class II, DR alpha	HGNC:4947	
HMMR	hyaluronan mediated motility receptor	HGNC:5012	
HPGD	15-hydroxyprostaglandin dehydrogenase	HGNC:5154	
HSPA1A	heat shock protein family A (Hsp70) member 1A	HGNC:5232	
HSPA1B	heat shock protein family A (Hsp70) member 1B	HGNC:5233	
HSPB1	heat shock protein family B (small) member 1	HGNC:5246	
HSPE1	heat shock protein family E (Hsp10) member 1	HGNC:5269	
HSPG2	heparan sulfate proteoglycan 2	HGNC:5273	
ICAM1	intercellular adhesion molecule 1	HGNC:5344	
ICAM4	intercellular adhesion molecule 4 (Landsteiner-Wiener blood group)	HGNC:5347	
ID2	inhibitor of DNA binding 2	HGNC:5361	
IFITM1	interferon induced transmembrane protein 1	HGNC:5412	
IFITM2	interferon induced transmembrane protein 2	HGNC:5413	
IFITM3	interferon induced transmembrane protein 3	HGNC:5414	
IFNA1	interferon alpha 1	HGNC:5417	IFN alpha
IFNG	interferon gamma	HGNC:5438	IFN gamma
IGHA1	immunoglobulin heavy constant alpha 1	HGNC:5478	
IGKC	immunoglobulin kappa constant	HGNC:5716	
IGLC2	immunoglobulin lambda constant 2	HGNC:5856	
IL10	interleukin 10	HGNC:5962	
IL12A	interleukin 12A	HGNC:5969	
IL13	interleukin 13	HGNC:5973	
IL15	interleukin 15	HGNC:5977	
IL18	interleukin 18	HGNC:5986	
IL1A	interleukin 1 alpha	HGNC:5991	
IL1B	interleukin 1 beta	HGNC:5992	
IL1RL1	interleukin 1 receptor like 1	HGNC:5998	
IL22	interleukin 22	HGNC:14900	
IL2RA	interleukin 2 receptor subunit alpha	HGNC:6008	CD25
IL2RB	interleukin 2 receptor subunit beta	HGNC:6009	
IL33	interleukin 33	HGNC:16028	
IL34	interleukin 34	HGNC:28529	
IL3RA	interleukin 3 receptor subunit alpha	HGNC:6012	CD123

IL4	interleukin 4	HGNC:6014	
IL5	interleukin 5	HGNC:6016	
IL6	interleukin 6	HGNC:6018	
IL7R	interleukin 7 receptor	HGNC:6024	
ITGA6	integrin subunit alpha 6	HGNC:6142	CD49f
ITGAE	integrin subunit alpha E	HGNC:6147	CD103
ITGAM	integrin subunit alpha M	HGNC:6149	CD11b
ITGAX	integrin subunit alpha X	HGNC:6152	CD11c
ITGB1	integrin subunit beta 1	HGNC:6153	CD29
ITGB4	integrin subunit beta 4	HGNC:6158	CD104
IVL	involucrin	HGNC:6187	
JAG1	jagged canonical Notch ligand 1	HGNC:6188	
JAM2	junctional adhesion molecule 2	HGNC:14686	
JCHAIN	joining chain of multimeric IgA and IgM	HGNC:5713	
JUN	Jun proto-oncogene, AP-1 transcription factor subunit	HGNC:6204	
KIT	KIT proto-oncogene, receptor tyrosine kinase	HGNC:6342	CD117
KLF10	Kruppel like factor 10	HGNC:11810	
KLK7	kallikrein related peptidase 7	HGNC:6368	
KLRB1	killer cell lectin like receptor B1	HGNC:6373	CD161
KLRC1	killer cell lectin like receptor C1	HGNC:6374	CD159a
KLRD1	killer cell lectin like receptor D1	HGNC:6378	CD94
KRT1	keratin 1	HGNC:6412	
KRT10	keratin 10	HGNC:6413	
KRT14	keratin 14	HGNC:6416	
KRT17	keratin 17	HGNC:6427	
KRT2	keratin 2	HGNC:6439	
KRT5	keratin 5	HGNC:6442	
KRTDAP	keratinocyte differentiation associated protein	HGNC:16313	
L1CAM	L1 cell adhesion molecule	HGNC:6470	
LAMC1	laminin subunit gamma 1	HGNC:6492	
LAT	linker for activation of T cells	HGNC:18874	
LGR5	leucine rich repeat containing G protein-coupled receptor 5	HGNC:4504	
LIFR	LIF receptor subunit alpha	HGNC:6597	
LILRA4	leukocyte immunoglobulin like receptor A4	HGNC:15503	
LMNA	lamin A/C	HGNC:6636	
LSP1	lymphocyte specific protein 1	HGNC:6707	
LTB	lymphotoxin beta	HGNC:6711	
LTBR	lymphotoxin beta receptor	HGNC:6718	
LUM	lumican	HGNC:6724	
LXN	latexin	HGNC:13347	
LY9	lymphocyte antigen 9	HGNC:6730	
LYVE1	lymphatic vessel endothelial hyaluronan receptor 1	HGNC:14687	
MBP	myelin basic protein	HGNC:6925	
MEDAG	mesenteric estrogen dependent adipogenesis	HGNC:25926	
MGP	matrix Gla protein	HGNC:7060	
MIF	macrophage migration inhibitory factor	HGNC:7097	
MKI67	marker of proliferation Ki-67	HGNC:7107	
MMP2	matrix metalloproteinase 2	HGNC:7166	
MPZ	myelin protein zero	HGNC:7225	
MT2A	metallothionein 2A	HGNC:7406	
NCAM1	neural cell adhesion molecule 1	HGNC:7656	CD56
NFKBIA	NFKB inhibitor alpha	HGNC:7797	
NGFR	nerve growth factor receptor	HGNC:7809	p75NTR
NIPAL4	NIPA like domain containing 4	HGNC:28018	
NKG7	natural killer cell granule protein 7	HGNC:7830	
NOS2	nitric oxide synthase 2	HGNC:7873	iNOS
NR4A2	nuclear receptor subfamily 4 group A member 2	HGNC:7981	
NRP1	neuropilin 1	HGNC:8004	CD304
NT5E	5'-nucleotidase ecto	HGNC:8021	CD73
OCLN	occludin	HGNC:8104	



OSM	oncostatin M	HGNC:8506	
PDGFB	platelet derived growth factor subunit B	HGNC:8800	
PDGFRA	platelet derived growth factor receptor alpha	HGNC:8803	
PDPN	podoplanin	HGNC:29602	
PECAM1	platelet and endothelial cell adhesion molecule 1	HGNC:8823	CD31
PERP	p53 apoptosis effector related to PMP22	HGNC:17637	
PILRA	paired immunoglobulin like type 2 receptor alpha	HGNC:20396	
PIM3	Pim-3 proto-oncogene, serine/threonine kinase	HGNC:19310	
PLEK	pleckstrin	HGNC:9070	
PMEL	premelanosome protein	HGNC:10880	
PMP22	peripheral myelin protein 22	HGNC:9118	
PPARG	peroxisome proliferator activated receptor gamma	HGNC:9236	
PRDM1	PR/SET domain 1	HGNC:9346	
PRDX1	peroxiredoxin 1	HGNC:9352	
PRF1	perforin 1	HGNC:9360	
PRSS8	serine protease 8	HGNC:9491	
PTGDR2	prostaglandin D2 receptor 2	HGNC:4502	CD294
PTGDS	prostaglandin D2 synthase	HGNC:9592	
PTGES	prostaglandin E synthase	HGNC:9599	
PTPRC	protein tyrosine phosphatase receptor type C	HGNC:9666	CD45
RELA	RELA proto-oncogene, NF-kB subunit	HGNC:9955	
RELB	RELB proto-oncogene, NF-kB subunit	HGNC:9956	
RGS1	regulator of G protein signaling 1	HGNC:9991	
RGS10	regulator of G protein signaling 10	HGNC:9992	
RGS5	regulator of G protein signaling 5	HGNC:10001	
RIPK1	receptor interacting serine/threonine kinase 1	HGNC:10019	
RNASE1	ribonuclease A family member 1, pancreatic	HGNC:10044	
RORC	RAR related orphan receptor C	HGNC:10260	ROR gamma
S100A2	S100 calcium binding protein A2	HGNC:10492	
S100A8	S100 calcium binding protein A8	HGNC:10498	
S100A9	S100 calcium binding protein A9	HGNC:10499	
SCD	stearyl-CoA desaturase	HGNC:10571	
SDPR	caveolae associated protein 2	HGNC:10690	Cavin2
SDR9C7	short chain dehydrogenase/reductase family 9C member 7	HGNC:29958	
SELE	selectin E	HGNC:10718	
SELK	selenoprotein K	HGNC:30394	
SELL	selectin L	HGNC:10720	
SELP	selectin P	HGNC:10721	
SELPLG	selectin P ligand	HGNC:10722	
SERPINE1	serpin family E member 1	HGNC:8583	
SFRP2	secreted frizzled related protein 2	HGNC:10777	
SFRP4	secreted frizzled related protein 4	HGNC:10778	
SIGLEC6	sialic acid binding Ig like lectin 6	HGNC:10875	
SIGLEC8	sialic acid binding Ig like lectin 8	HGNC:10877	
SIRPA	signal regulatory protein alpha	HGNC:9662	
SLC27A4	solute carrier family 27 member 4	HGNC:10998	
SNCG	synuclein gamma	HGNC:11141	
SOCS4	suppressor of cytokine signaling 4	HGNC:19392	
SOD2	superoxide dismutase 2	HGNC:11180	
SOX10	SRY-box transcription factor 10	HGNC:11190	
SPARCL1	SPARC like 1	HGNC:11220	
SPINK5	serine peptidase inhibitor Kazal type 5	HGNC:15464	
SPTSSB	serine palmitoyltransferase small subunit B	HGNC:24045	
SULT2B1	sulfotransferase family 2B member 1	HGNC:11459	
TBX21	T-box transcription factor 21	HGNC:11599	TBET
TCF4	transcription factor 4	HGNC:11634	E2-2
TFF3	trefoil factor 3	HGNC:11757	
TFPI	tissue factor pathway inhibitor	HGNC:11760	
TGFB1	transforming growth factor beta 1	HGNC:11766	
TGFB3	transforming growth factor beta receptor 3	HGNC:11774	

TGM1	transglutaminase 1	HGNC:11777	
THBD	thrombomodulin	HGNC:11784	CD141
THBS1	thrombospondin 1	HGNC:11785	
THY1	Thy-1 cell surface antigen	HGNC:11801	CD90
TIGIT	T cell immunoreceptor with Ig and ITIM domains	HGNC:26838	
TJP1	tight junction protein 1	HGNC:11827	
TLR7	toll like receptor 7	HGNC:15631	
TLR9	toll like receptor 9	HGNC:15633	
TM4SF1	transmembrane 4 L six family member 1	HGNC:11853	
TNF	tumor necrosis factor	HGNC:11892	TNF alpha
TNFAIP6	TNF alpha induced protein 6	HGNC:11898	
TNFRSF10B	TNF receptor superfamily member 10b	HGNC:11905	
TNFRSF18	TNF receptor superfamily member 18	HGNC:11914	
TNFRSF1A	TNF receptor superfamily member 1A	HGNC:11916	
TNFRSF1B	TNF receptor superfamily member 1B	HGNC:11917	
TNFSF10	TNF superfamily member 10	HGNC:11925	
TPSAB1	tryptase alpha/beta 1	HGNC:12019	
TPSB2	tryptase beta 2	HGNC:14120	
TRAC	T cell receptor alpha constant	HGNC:12029	
TRDC	T cell receptor delta constant	HGNC:12253	
TRGC1	T cell receptor gamma constant 1	HGNC:12275	
TRGC2	T cell receptor gamma constant 2	HGNC:12276	
TXN	thioredoxin	HGNC:12435	
TYR	tyrosinase	HGNC:12442	
TYRP1	tyrosinase related protein 1	HGNC:12450	
VCAM1	vascular cell adhesion molecule 1	HGNC:12663	
VDR	vitamin D receptor	HGNC:12679	
VEGFA	vascular endothelial growth factor A	HGNC:12680	
VWASA	von Willebrand factor A domain containing 5A	HGNC:6658	
XCL1	X-C motif chemokine ligand 1	HGNC:10645	
XCL2	X-C motif chemokine ligand 2	HGNC:10646	
XCR1	X-C motif chemokine receptor 1	HGNC:1625	
ZBTB10	zinc finger and BTB domain containing 10	HGNC:30953	

**Appendix Table 3 – Gene symbols listed with standardised nomenclature.** A list of all genes mentioned within the text and figures of this thesis. Gene names and HCNID's are taken from the HUGO Gene Nomenclature Committee database (accessed via <https://www.genenames.org/>). Alternate protein names are shown where the protein product of a gene is referred to by a different name or symbol within this thesis.

## 8 References

- Adameyko, I., Lallemand, F., Aquino, J.B., Pereira, J.A., Topilko, P., Müller, T., Fritz, N., Beljajeva, A., Mochii, M., Liste, I., Usoskin, D., Suter, U., Birchmeier, C. & Ernfors, P. (2009) Schwann Cell Precursors from Nerve Innervation Are a Cellular Origin of Melanocytes in Skin. *Cell*. 139 (2), 366–379.
- Akiyama, M., Sugiyama-Nakagiri, Y., Sakai, K., McMillan, J.R., Goto, M., Arita, K., Tsuji-Abe, Y., Tabata, N., Matsuoka, K., Sasaki, R., Sawamura, D. & Shimizu, H. (2005) Mutations in lipid transporter ABCA12 in harlequin ichthyosis and functional recovery by corrective gene transfer. *The Journal of clinical investigation*. 115 (7), 1777–1784.
- Alam, H., Sehgal, L., Kundu, S.T., Dalal, S.N. & Vaidya, M.M. (2011) Novel function of keratins 5 and 14 in proliferation and differentiation of stratified epithelial cells. *Molecular biology of the cell*. 22 (21), 4068–4078.
- Alcántara-Hernández, M., Leylek, R., Wagar, L.E., Engleman, E.G., Keler, T., Marinkovich, M.P., Davis, M.M., Nolan, G.P. & Idoyaga, J. (2017) High-Dimensional Phenotypic Mapping of Human Dendritic Cells Reveals Interindividual Variation and Tissue Specialization. *Immunity*. 47 (6), 1037-1050.e6.
- Apostolidis, S.A., Stifano, G., Tabib, T., Rice, L.M., Morse, C.M., Kahaleh, B. & Lafyatis, R. (2018) Single Cell RNA Sequencing Identifies HSPG2 and APLNR as Markers of Endothelial Cell Injury in Systemic Sclerosis Skin. *Frontiers in Immunology*. 92191.
- Ashina, K., Tsubosaka, Y., Nakamura, T., Omori, K., Kobayashi, K., Hori, M., Ozaki, H. & Murata, T. (2015) Histamine Induces Vascular Hyperpermeability by Increasing Blood Flow and Endothelial Barrier Disruption In Vivo. *PloS one*. 10 (7), e0132367–e0132367.
- Astarita, J.L., Acton, S.E. & Turley, S.J. (2012) Podoplanin: emerging functions in development, the immune system, and cancer. *Frontiers in immunology*. 3283–283.
- Baharlou, H., Canete, N.P., Cunningham, A.L., Harman, A.N. & Patrick, E. (2019) Mass Cytometry Imaging for the Study of Human Diseases—Applications and Data Analysis Strategies. *Frontiers in Immunology*. 102657.
- Bailey, C.C., Zhong, G., Huang, I.-C. & Farzan, M. (2014) IFITM-Family Proteins: The Cell's First Line of Antiviral Defense. *Annual review of virology*. 1261–283.
- Balan, S. & Dalod, M. (2016) 'In Vitro Generation of Human XCR1+ Dendritic Cells from CD34+ Hematopoietic Progenitors', in Elodie Segura & Nobuyuki Onai (eds.) *Dendritic Cell Protocols*. [Online]. New York, NY: Springer New York. pp. 19–37.
- Balato, A., Unutmaz, D. & Gaspari, A.A. (2009) Natural Killer T Cells: An Unconventional T-Cell Subset with Diverse Effector and Regulatory Functions. *Journal of Investigative Dermatology*. 129 (7), 1628–1642.

- Banerjee, G., Damodaran, A., Devi, N., Dharmalingam, K. & Raman, G. (2004) Role of Keratinocytes in Antigen Presentation and Polarization of Human T Lymphocytes. *Scandinavian Journal of Immunology*. 59 (4), 385–394.
- Bar-Ephraim, Y.E. (Yotam E.), Cornelissen, F., Papazian, N., Konijn, T., Hoogenboezem, R., Sanders, M., Westerman, B.A. (Bart A.), Gönültas, M. (Mehmet), Kwekkeboom, J., den Haan, J.M.M., Reijmers, R., Mebius, R. & Cupedo, T. (2017) Cross-Tissue Transcriptomic Analysis of Human Secondary Lymphoid Organ-Residing ILC3s Reveals a Quiescent State in the Absence of Inflammation. *Cell Reports*. 21 (3), 823–833.
- Bautista-Hernández, L.A., Gómez-Olivares, J.L., Buentello-Volante, B. & Bautista-de Lucio, V.M. (2017) Fibroblasts: The Unknown Sentinels Eliciting Immune Responses Against Microorganisms. *European journal of microbiology & immunology*. 7 (3), 151–157.
- Baxter, L.L. & Pavan, W.J. (2003) Pmel17 expression is Mitf-dependent and reveals cranial melanoblast migration during murine development. *Gene Expression Patterns*. 3 (6), 703–707.
- Behrens, D.T., Villone, D., Koch, M., Brunner, G., Sorokin, L., Robenek, H., Bruckner-Tuderman, L., Bruckner, P. & Hansen, U. (2012) The Epidermal Basement Membrane Is a Composite of Separate Laminin- or Collagen IV-containing Networks Connected by Aggregated Perlecan, but Not by Nidogens. *Journal of Biological Chemistry*. 287 (22), 18700–18709.
- Belkaid, Y. & Harrison, O.J. (2017) Homeostatic Immunity and the Microbiota. *Immunity*. 46 (4), 562–576.
- Bergers, G. & Song, S. (2005) The role of pericytes in blood-vessel formation and maintenance. *Neuro-oncology*. 7 (4), 452–464.
- Bertram, K.M., Botting, R.A., Baharlou, H., Rhodes, J.W., Rana, H., Graham, J.D., Patrick, E., Fletcher, J., Plasto, T.M., Truong, N.R., Royle, C., Doyle, C.M., Tong, O., Nasr, N., Barnouti, L., Kohout, M.P., Brooks, A.J., Wines, M.P., Haertsch, P., et al. (2019) Identification of HIV transmitting CD11c+ human epidermal dendritic cells. *Nature Communications*. 10 (1), 2759.
- Bigley, V., McGovern, N., Milne, P., Dickinson, R., Pagan, S., Cookson, S., Haniffa, M. & Collin, M. (2015) Langerin-expressing dendritic cells in human tissues are related to CD1c+ dendritic cells and distinct from Langerhans cells and CD141<sup>high</sup> XCR1+ dendritic cells. *Journal of leukocyte biology*. 97 (4), 627–634.
- Bignon, A., Régent, A., Klipfel, L., Desnoyer, A., de la Grange, P., Martinez, V., Lortholary, O., Dalloul, A., Mouthon, L. & Balabanian, K. (2015) DUSP4-mediated accelerated T-cell senescence in idiopathic CD4 lymphopenia. *Blood*. 125 (16), 2507.
- Bitoun, E., Chavanas, S., Irvine, A.D., Lonie, L., Bodemer, C., Paradisi, M., Hamel-Teillac, D., Ansai, S., Mitsuhashi, Y., Taïeb, A., de Prost, Y., Zambruno, G., Harper, J.I. &

- Hovnanian, A. (2002) Netherton Syndrome: Disease Expression and Spectrum of SPINK5 Mutations in 21 Families. *Journal of Investigative Dermatology*. 118 (2), 352–361.
- Blanpain, C. & Fuchs, E. (2006) Epidermal stem cells of the skin. *Annual review of cell and developmental biology*. 22339–373.
- Bodnar, R.J., Rodgers, M.E., Chen, W.C.W. & Wells, A. (2013) Pericyte regulation of vascular remodeling through the CXC receptor 3. *Arteriosclerosis, thrombosis, and vascular biology*. 33 (12), 2818–2829.
- Bodnar, R.J., Satish, L., Yates, C.C. & Wells, A. (2016) Pericytes: A newly recognized player in wound healing. *Wound repair and regeneration : official publication of the Wound Healing Society [and] the European Tissue Repair Society*. 24 (2), 204–214.
- Boiocchi, L., Lonardi, S., Vermi, W., Fisogni, S. & Facchetti, F. (2013) BDCA-2 (CD303): a highly specific marker for normal and neoplastic plasmacytoid dendritic cells. *Blood*. 122 (2), 296–297.
- Bonnans, C., Chou, J. & Werb, Z. (2014) Remodelling the extracellular matrix in development and disease. *Nature reviews. Molecular cell biology*. 15 (12), 786–801.
- Botting, R.A., Bertram, K.M., Baharlou, H., Sandgren, K.J., Fletcher, J., Rhodes, J.W., Rana, H., Plasto, T.M., Wang, X.M., Lim, J.J.K., Barnouti, L., Kohout, M.P., Papadopoulos, T., Merten, S., Olbourne, N., Cunningham, A.L., Haniffa, M. & Harman, A.N. (2017) Phenotypic and functional consequences of different isolation protocols on skin mononuclear phagocytes. *Journal of leukocyte biology*. 101 (6), 1393–1403.
- Braverman, I.M. (2000) The Cutaneous Microcirculation. *Journal of Investigative Dermatology Symposium Proceedings*. 5 (1), 3–9.
- Breton, G., Zheng, S., Valieris, R., Tojal da Silva, I., Satija, R. & Nussenzweig, M.C. (2016) Human dendritic cells (DCs) are derived from distinct circulating precursors that are precommitted to become CD1c+ or CD141+ DCs. *The Journal of experimental medicine*. 213 (13), 2861–2870.
- Burgess, D.J. (2019) Spatial transcriptomics coming of age. *Nature Reviews Genetics*. 20 (6), 317–317.
- Butler, A., Hoffman, P., Smibert, P., Papalexi, E. & Satija, R. (2018) Integrating single-cell transcriptomic data across different conditions, technologies, and species. *Nature Biotechnology*. 36411.
- Butovsky, O., Jedrychowski, M.P., Moore, C.S., Cialic, R., Lanser, A.J., Gabriely, G., Koeglsperger, T., Dake, B., Wu, P.M., Doykan, C.E., Fanek, Z., Liu, L., Chen, Z., Rothstein, J.D., Ransohoff, R.M., Gygi, S.P., Antel, J.P. & Weiner, H.L. (2014)

Identification of a unique TGF- $\beta$ -dependent molecular and functional signature in microglia. *Nature Neuroscience*. 17 (1), 131–143.

- Campbell, K.S. & Purdy, A.K. (2011) Structure/function of human killer cell immunoglobulin-like receptors: lessons from polymorphisms, evolution, crystal structures and mutations. *Immunology*. 132 (3), 315–325.
- Carpentier, S., Vu Manh, T.-P., Chelbi, R., Henri, S., Malissen, B., Haniffa, M., Ginhoux, F. & Dalod, M. (2016) Comparative genomics analysis of mononuclear phagocyte subsets confirms homology between lymphoid tissue-resident and dermal XCR1+ DCs in mouse and human and distinguishes them from Langerhans cells. *Journal of Immunological Methods*. 43235–49.
- Cella, M., Fuchs, A., Vermi, W., Facchetti, F., Otero, K., Lennerz, J.K.M., Doherty, J.M., Mills, J.C. & Colonna, M. (2009) A human natural killer cell subset provides an innate source of IL-22 for mucosal immunity. *Nature*. 457 (7230), 722–725.
- Chakraborty, S., Zawieja, S., Wang, W., Zawieja, D.C. & Muthuchamy, M. (2010) Lymphatic system: a vital link between metabolic syndrome and inflammation. *Annals of the New York Academy of Sciences*. 1207 Suppl 1 (Suppl 1), E94–E102.
- Chen, H., Lau, M.C., Wong, M.T., Newell, E.W., Poidinger, M. & Chen, J. (2016) Cytokit: A Bioconductor Package for an Integrated Mass Cytometry Data Analysis Pipeline. *PLOS Computational Biology*. 12 (9), e1005112.
- Cheng, J.B., Sedgewick, A.J., Finnegan, A.I., Harirchian, P., Lee, J., Kwon, S., Fassett, M.S., Golovato, J., Gray, M., Ghadially, R., Liao, W., Perez White, B.E., Mauro, T.M., Mully, T., Kim, E.A., Sbitany, H., Neuhaus, I.M., Grekin, R.C., Yu, S.S., et al. (2018) Transcriptional Programming of Normal and Inflamed Human Epidermis at Single-Cell Resolution. *Cell Reports*. 25 (4), 871–883.
- Chopra, K., Calva, D., Sosin, M., Tadisina, K.K., Banda, A., De La Cruz, C., Chaudhry, M.R., Legesse, T., Drachenberg, C.B., Manson, P.N. & Christy, M.R. (2015) A Comprehensive Examination of Topographic Thickness of Skin in the Human Face. *Aesthetic Surgery Journal*. 35 (8), 1007–1013.
- Chorro, L., Sarde, A., Li, M., Woollard, K.J., Chambon, P., Malissen, B., Kissenpfennig, A., Barbaroux, J.-B., Groves, R. & Geissmann, F. (2009) Langerhans cell (LC) proliferation mediates neonatal development, homeostasis, and inflammation-associated expansion of the epidermal LC network. *The Journal of Experimental Medicine*. 206 (13), 3089–3100.
- Chu, C.-C., Di Meglio, P. & Nestle, F.O. (2011) Harnessing dendritic cells in inflammatory skin diseases. *Seminars in immunology*. 23 (1), 28–41.
- Cicha, I., Beronov, K., Ramirez, E.L., Osterode, K., Goppelt-Struebe, M., Raaz, D., Yilmaz, A., Daniel, W.G. & Garlich, C.D. (2009) Shear stress preconditioning modulates endothelial susceptibility to circulating TNF- $\alpha$  and monocytic cell recruitment in a simplified model of arterial bifurcations. *Atherosclerosis*. 207 (1), 93–102.

- Cichorek, M., Wachulska, M., Stasiewicz, A. & Tymińska, A. (2013) Skin melanocytes: biology and development. *Postepy dermatologii i alergologii*. 30 (1), 30–41.
- Cisse, B., Caton, M.L., Lehner, M., Maeda, T., Scheu, S., Locksley, R., Holmberg, D., Zweier, C., den Hollander, N.S., Kant, S.G., Holter, W., Rauch, A., Zhuang, Y. & Reizis, B. (2008) Transcription factor E2-2 is an essential and specific regulator of plasmacytoid dendritic cell development. *Cell*. 135 (1), 37–48.
- Clark, R.A., Chong, B., Mirchandani, N., Brinster, N.K., Yamanaka, K., Dowgiert, R.K. & Kupper, T.S. (2006) The Vast Majority of CLA<sup>+</sup> T Cells Are Resident in Normal Skin. *The Journal of Immunology*. 176 (7), 4431.
- Clingen, P.H., Berneburg, M., Petit-Frère, C., Woollons, A., Lowe, J.E., Arlett, C.F. & Green, M.H.L. (2001) Contrasting effects of an ultraviolet B and an ultraviolet A tanning lamp on interleukin-6, tumour necrosis factor- $\alpha$  and intercellular adhesion molecule-1 expression. *British Journal of Dermatology*. 145 (1), 54–62.
- Collin, M.P., Hart, D.N.J., Jackson, G.H., Cook, G., Cavet, J., Mackinnon, S., Middleton, P.G. & Dickinson, A.M. (2006) The fate of human Langerhans cells in hematopoietic stem cell transplantation. *The Journal of Experimental Medicine*. 203 (1), 27–33.
- Cook-Mills, J.M., Marchese, M.E. & Abdala-Valencia, H. (2011) Vascular cell adhesion molecule-1 expression and signaling during disease: regulation by reactive oxygen species and antioxidants. *Antioxidants & redox signaling*. 15 (6), 1607–1638.
- Coombe, L., Warren, R.L., Jackman, S.D., Yang, C., Vandervalk, B.P., Moore, R.A., Pleasance, S., Coope, R.J., Bohlmann, J., Holt, R.A., Jones, S.J.M. & Birol, I. (2016) Assembly of the Complete Sitka Spruce Chloroplast Genome Using 10X Genomics' GemCode Sequencing Data. *PloS one*. 11 (9), e0163059–e0163059.
- Cose, S., Brammer, C., Khanna, K., Masopust, D. & Lefrançois, L. (2006) Evidence that a significant number of naive T cells enter non-lymphoid organs as part of a normal migratory pathway. *European journal of immunology*. 361423–33.
- Cruse, G., Metcalfe, D.D. & Olivera, A. (2014) Functional deregulation of KIT: link to mast cell proliferative diseases and other neoplasms. *Immunology and allergy clinics of North America*. 34 (2), 219–237.
- Dao, H. & Kazin, R.A. (2007) Gender differences in skin: A review of the literature. *Gender Medicine*. 4 (4), 308–328.
- Deckers, J., Hammad, H. & Hoste, E. (2018) Langerhans Cells: Sensing the Environment in Health and Disease. *Frontiers in immunology*. 993–93.
- Deho', L., Leoni, C., Brodie, T.M., Montagner, S., De Simone, M., Polletti, S., Barozzi, I., Natoli, G. & Monticelli, S. (2014) Two Functionally Distinct Subsets of Mast Cells

Discriminated By IL-2–Independent CD25 Activities. *The Journal of Immunology*. 193 (5), 2196.

Del Duca, E., Pavel, A.B., Dubin, C., Song, T., Wallace, E.B., Peng, X., Estrada, Y.D., Xu, H., Maari, C., Jack, C., St-Cyr Proulx, E., Krueger, J.G., Bissonnette, R. & Guttman-Yassky, E. (2019) Major Differences in Expression of Inflammatory Pathways in Skin from Different Body Sites of Healthy Individuals. *Journal of Investigative Dermatology*. 139 (10), 2228–2232.e10.

Demyanets Svitlana, Konya Viktoria, Kastl Stefan P., Kaun Christoph, Rauscher Sabine, Niessner Alexander, Pentz Richard, Pfaffenberger Stefan, Rychli Kathrin, Lemberger Christof E., de Martin Rainer, Heinemann Akos, Huk Ihor, Gröger Marion, Maurer Gerald, Huber Kurt & Wojta Johann (2011) Interleukin-33 Induces Expression of Adhesion Molecules and Inflammatory Activation in Human Endothelial Cells and in Human Atherosclerotic Plaques. *Arteriosclerosis, Thrombosis, and Vascular Biology*. 31 (9), 2080–2089.

Denisenko, E., Guo, B.B., Jones, M., Hou, R., de Kock, L., Lassmann, T., Poppe, D., Clément, O., Simmons, R.K., Lister, R. & Forrest, A.R.R. (2020) Systematic assessment of tissue dissociation and storage biases in single-cell and single-nucleus RNA-seq workflows. *Genome Biology*. 21 (1), 130.

Dijkstra, D., Stark, H., Chazot, P.L., Shenton, F.C., Leurs, R., Werfel, T. & Gutzmer, R. (2008) Human Inflammatory Dendritic Epidermal Cells Express a Functional Histamine H4 Receptor. *Journal of Investigative Dermatology*. 128 (7), 1696–1703.

Dorschner, R.A., Pestonjamas, V.K., Tamakuwala, S., Ohtake, T., Rudisill, J., Nizet, V., Agerberth, B., Gudmundsson, G.H. & Gallo, R.L. (2001) Cutaneous Injury Induces the Release of Cathelicidin Anti-Microbial Peptides Active Against Group A Streptococcus. *Journal of Investigative Dermatology*. 117 (1), 91–97.

Douaiher, J., Succar, J., Lancerotto, L., Gurish, M.F., Orgill, D.P., Hamilton, M.J., Krilis, S.A. & Stevens, R.L. (2014) Development of mast cells and importance of their tryptase and chymase serine proteases in inflammation and wound healing. *Advances in immunology*. 122211–252.

Driskell, R.R., Lichtenberger, B.M., Hoste, E., Kretschmar, K., Simons, B.D., Charalambous, M., Ferron, S.R., Herault, Y., Pavlovic, G., Ferguson-Smith, A.C. & Watt, F.M. (2013) Distinct fibroblast lineages determine dermal architecture in skin development and repair. *Nature*. 504 (7479), 277–281.

Durand, M. & Segura, E. (2015) The known unknowns of the human dendritic cell network. *Frontiers in immunology*. 6129–129.

Eckhart, L., Lippens, S., Tschachler, E. & Declercq, W. (2013) Cell death by cornification. *Biochimica et Biophysica Acta (BBA) - Molecular Cell Research*. 1833 (12), 3471–3480.



- Efremova, M., Vento-Tormo, M., Teichmann, S.A. & Vento-Tormo, R. (2019) CellPhoneDB v2.0: Inferring cell-cell communication from combined expression of multi-subunit receptor-ligand complexes. *bioRxiv*. 680926.
- Elias, M.S., Long, H.A., Newman, C.F., Wilson, P.A., West, A., McGill, P.J., Wu, K.C., Donaldson, M.J. & Reynolds, N.J. (2017) Proteomic analysis of filaggrin deficiency identifies molecular signatures characteristic of atopic eczema. *The Journal of allergy and clinical immunology*. 140 (5), 1299–1309.
- Eriksson, A.U. & Singh, R.R. (2008) Cutting edge: migration of langerhans dendritic cells is impaired in autoimmune dermatitis. *Journal of immunology (Baltimore, Md. : 1950)*. 181 (11), 7468–7472.
- Escobedo, N. & Oliver, G. (2017) The Lymphatic Vasculature: Its Role in Adipose Metabolism and Obesity. *Cell metabolism*. 26 (4), 598–609.
- Fahey, T.J., III, Turbeville, T. & McIntyre, K. (1995) Differential TNF Secretion by Wound Fibroblasts Compared to Normal Fibroblasts in Response to LPS. *Journal of Surgical Research*. 58 (6), 759–764.
- Feingold, K.R. (2012) Lamellar Bodies: The Key to Cutaneous Barrier Function. *Journal of Investigative Dermatology*. 132 (8), 1951–1953.
- Feng, D., Nagy, J.A., Pyne, K., Dvorak, H.F. & Dvorak, A.M. (1998) Neutrophils emigrate from venules by a transendothelial cell pathway in response to FMLP. *The Journal of experimental medicine*. 187 (6), 903–915.
- Frohman, M., Agerberth, B., Ahangari, G., Ståhle-Bäckdahl, M., Lidén, S., Wigzell, H. & Gudmundsson, G.H. (1997) The Expression of the Gene Coding for the Antibacterial Peptide LL-37 Is Induced in Human Keratinocytes during Inflammatory Disorders. *Journal of Biological Chemistry*. 272 (24), 15258–15263.
- Fuchs, A., Vermi, W., Lee, J.S., Lonardi, S., Gilfillan, S., Newberry, R.D., Cella, M. & Colonna, M. (2013) Intraepithelial type 1 innate lymphoid cells are a unique subset of IL-12- and IL-15-responsive IFN- $\gamma$ -producing cells. *Immunity*. 38 (4), 769–781.
- Fuchs, E. (1995) Keratins and the Skin. *Annual Review of Cell and Developmental Biology*. 11 (1), 123–154.
- Fujisawa, H., WANG, B., KONDO, S., SHIVJI, G.M. & SAUDER, D.N. (1997) Costimulation with Ultraviolet B and Interleukin-1 $\alpha$  Dramatically Increase Tumor Necrosis Factor- $\alpha$  Production in Human Dermal Fibroblasts. *Journal of Interferon & Cytokine Research*. 17 (5), 307–313.
- Fujiwara, S., Hoshikawa, S., Ueno, T., Hirata, M., Saito, T., Ikeda, T., Kawaguchi, H., Nakamura, K., Tanaka, S. & Ogata, T. (2014) SOX10 Transactivates S100B to Suppress Schwann Cell Proliferation and to Promote Myelination. *PLOS ONE*. 9 (12), e115400.

- Furio, L., Briotet, I., Journeaux, A., Billard, H. & Péguet-Navarro, J. (2010) Human Langerhans Cells Are More Efficient Than CD14–CD1c+ Dermal Dendritic Cells at Priming Naive CD4+ T Cells. *Journal of Investigative Dermatology*. 130 (5), 1345–1354.
- Ganguly, K., Giddaluru, J., August, A. & Khan, N. (2016) Post-transcriptional Regulation of Immunological Responses through Riboclustering. *Frontiers in immunology*. 7161–161.
- Gebhardt, T., Whitney, P.G., Zaid, A., Mackay, L.K., Brooks, A.G., Heath, W.R., Carbone, F.R. & Mueller, S.N. (2011) Different patterns of peripheral migration by memory CD4+ and CD8+ T cells. *Nature*. 477 (7363), 216–219.
- Ghazizadeh, S. & Taichman, L.B. (2001) Multiple classes of stem cells in cutaneous epithelium: a lineage analysis of adult mouse skin. *The EMBO journal*. 20 (6), 1215–1222.
- Giesen, C., Wang, H.A.O., Schapiro, D., Zivanovic, N., Jacobs, A., Hattendorf, B., Schüffler, P.J., Grolimund, D., Buhmann, J.M., Brandt, S., Varga, Z., Wild, P.J., Günther, D. & Bodenmiller, B. (2014) Highly multiplexed imaging of tumor tissues with subcellular resolution by mass cytometry. *Nature Methods*. 11 (4), 417–422.
- Ginhoux, F. & Guilliams, M. (2016) Tissue-Resident Macrophage Ontogeny and Homeostasis. *Immunity*. 44 (3), 439–449.
- Gober, M.D., Fischelevich, R., Zhao, Y., Unutmaz, D. & Gaspari, A.A. (2008) Human natural killer T cells infiltrate into the skin at elicitation sites of allergic contact dermatitis. *The Journal of investigative dermatology*. 128 (6), 1460–1469.
- Goebeler, M., Yoshimura, T., Toksoy, A., Ritter, U., Bröcker, E.-B. & Gillitzer, R. (1997) The Chemokine Repertoire of Human Dermal Microvascular Endothelial Cells and Its Regulation by Inflammatory Cytokines. *Journal of Investigative Dermatology*. 108 (4), 445–451.
- Goleva, E., Berdyshev, E. & Leung, D.Y. (2019) Epithelial barrier repair and prevention of allergy. *The Journal of clinical investigation*. 129 (4), 1463–1474.
- Gomez Perdiguero, E., Klapproth, K., Schulz, C., Busch, K., Azzoni, E., Crozet, L., Garner, H., Trouillet, C., de Bruijn, M.F., Geissmann, F. & Rodewald, H.-R. (2015) Tissue-resident macrophages originate from yolk-sac-derived erythro-myeloid progenitors. *Nature*. 518 (7540), 547–551.
- Gonçalves, N.P., Mohseni, S., El Soury, M., Ulrichsen, M., Richner, M., Xiao, J., Wood, R.J., Andersen, O.M., Coulson, E.J., Raimondo, S., Murray, S.S. & Vægter, C.B. (2019) Peripheral Nerve Regeneration Is Independent From Schwann Cell p75(NTR) Expression. *Frontiers in cellular neuroscience*. 13235–235.

- Goodwin, S., McPherson, J.D. & McCombie, W.R. (2016) Coming of age: ten years of next-generation sequencing technologies. *Nature Reviews Genetics*. 17 (6), 333–351.
- Gould, T.W., Dominguez, B., de Winter, F., Yeo, G.W., Liu, P., Sundararaman, B., Stark, T., Vu, A., Degen, J.L., Lin, W. & Lee, K.-F. (2019) Glial cells maintain synapses by inhibiting an activity-dependent retrograde protease signal. *PLoS Genetics*. 15 (3), e1007948.
- Green, R.M., Cordero, A. & Winkelmann, R.K. (1977) Epidermal Mast Cells. *Archives of Dermatology*. 113 (2), 166–169.
- Greter, M., Lelios, I., Pelczar, P., Hoeffel, G., Price, J., Leboeuf, M., Kündig, T.M., Frei, K., Ginhoux, F., Merad, M. & Becher, B. (2012) Stroma-derived interleukin-34 controls the development and maintenance of langerhans cells and the maintenance of microglia. *Immunity*. 37 (6), 1050–1060.
- Grice, E.A. & Segre, J.A. (2011) The skin microbiome. *Nature reviews. Microbiology*. 9 (4), 244–253.
- Griffin, J.W. & Thompson, W.J. (2008) Biology and pathology of nonmyelinating Schwann cells. *Glia*. 56 (14), 1518–1531.
- Guilliams, M., Ginhoux, F., Jakubzick, C., Naik, S.H., Onai, N., Schraml, B.U., Segura, E., Tussiwand, R. & Yona, S. (2014) Dendritic cells, monocytes and macrophages: a unified nomenclature based on ontogeny. *Nature reviews. Immunology*. 14 (8), 571–578.
- Gulati, N., Krueger, J.G., Suárez-Fariñas, M. & Mitsui, H. (2013) Creation of differentiation-specific genomic maps of human epidermis through laser capture microdissection. *The Journal of investigative dermatology*. 133 (11), 2640–2642.
- Gunawan, M., Jardine, L. & Haniffa, M. (2016) 'Isolation of Human Skin Dendritic Cell Subsets', in Elodie Segura & Nobuyuki Onai (eds.) *Dendritic Cell Protocols*. [Online]. New York, NY: Springer New York. pp. 119–128.
- Guo, R., Zhang, T., Meng, X., Lin, Z., Lin, J., Gong, Y., Liu, X., Yu, Y., Zhao, G., Ding, X., Chen, X. & Lu, L. (2019) Lymphocyte mass cytometry identifies a CD3-CD4+ cell subset with a potential role in psoriasis. *JCI insight*. 4 (6), e125306.
- Gurish, M.F. & Austen, K.F. (2012) Developmental Origin and Functional Specialization of Mast Cell Subsets. *Immunity*. 37 (1), 25–33.
- Gurish, M.F., Ghildyal, N., Arm, J., Austen, K.F., Avraham, S., Reynolds, D. & Stevens, R.L. (1991) Cytokine mRNA are preferentially increased relative to secretory granule protein mRNA in mouse bone marrow-derived mast cells that have undergone IgE-mediated activation and degranulation. *The Journal of Immunology*. 146 (5), 1527.

- Hagai, T., Chen, X., Miragaia, R.J., Rostom, R., Gomes, T., Kunowska, N., Henriksson, J., Park, J.-E., Proserpio, V., Donati, G., Bossini-Castillo, L., Vieira Braga, F.A., Naamati, G., Fletcher, J., Stephenson, E., Vegh, P., Trynka, G., Kondova, I., Dennis, M., et al. (2018) Gene expression variability across cells and species shapes innate immunity. *Nature*. 563 (7730), 197–202.
- Halata, Z., Grim, M. & Bauman, K.I. (2003) Friedrich Sigmund Merkel and his “Merkel cell”, morphology, development, and physiology: Review and new results. *The Anatomical Record Part A: Discoveries in Molecular, Cellular, and Evolutionary Biology*. 271A (1), 225–239.
- Halprin, K.M. (1972) EPIDERMAL “TURNOVER TIME”—A RE-EXAMINATION. *British Journal of Dermatology*. 86 (1), 14–19.
- Hambleton, S., Salem, S., Bustamante, J., Bigley, V., Boisson-Dupuis, S., Azevedo, J., Fortin, A., Haniffa, M., Ceron-Gutierrez, L., Bacon, C.M., Menon, G., Trouillet, C., McDonald, D., Carey, P., Ginhoux, F., Alsina, L., Zumwalt, T.J., Kong, X.-F., Kumararatne, D., et al. (2011) IRF8 Mutations and Human Dendritic-Cell Immunodeficiency. *New England Journal of Medicine*. 365 (2), 127–138.
- Haniffa, M., Ginhoux, F., Wang, X.-N., Bigley, V., Abel, M., Dimmick, I., Bullock, S., Grisotto, M., Booth, T., Taub, P., Hilkens, C., Merad, M. & Collin, M. (2009) Differential rates of replacement of human dermal dendritic cells and macrophages during hematopoietic stem cell transplantation. *The Journal of experimental medicine*. 206 (2), 371–385.
- Haniffa, M., Gunawan, M. & Jardine, L. (2015) Human skin dendritic cells in health and disease. *Journal of dermatological science*. 77 (2), 85–92.
- Haniffa, M., Shin, A., Bigley, V., McGovern, N., Teo, P., See, P., Wasan, P.S., Wang, X.-N., Malinarich, F., Malleret, B., Larbi, A., Tan, P., Zhao, H., Poidinger, M., Pagan, S., Cookson, S., Dickinson, R., Dimmick, I., Jarrett, R.F., et al. (2012) Human tissues contain CD141hi cross-presenting dendritic cells with functional homology to mouse CD103+ nonlymphoid dendritic cells. *Immunity*. 37 (1), 60–73.
- Hansen, L., Schmidt-Christensen, A., Gupta, S., Fransén-Pettersson, N., Hannibal, T.D., Reizis, B., Santamaria, P. & Holmberg, D. (2015) E2-2 Dependent Plasmacytoid Dendritic Cells Control Autoimmune Diabetes. *PLOS ONE*. 10 (12), e0144090.
- Harman, A.N., Bye, C.R., Nasr, N., Sandgren, K.J., Kim, M., Mercier, S.K., Botting, R.A., Lewin, S.R., Cunningham, A.L. & Cameron, P.U. (2013) Identification of Lineage Relationships and Novel Markers of Blood and Skin Human Dendritic Cells. *The Journal of Immunology*. 190 (1), 66.
- Harper, E.G., Guo, C., Rizzo, H., Lillis, J.V., Kurtz, S.E., Skorcheva, I., Purdy, D., Fitch, E., Iordanov, M. & Blauvelt, A. (2009) Th17 cytokines stimulate CCL20 expression in keratinocytes in vitro and in vivo: implications for psoriasis pathogenesis. *The Journal of investigative dermatology*. 129 (9), 2175–2183.

- Hashimoto, D., Chow, A., Noizat, C., Teo, P., Beasley, M.B., Leboeuf, M., Becker, C.D., See, P., Price, J., Lucas, D., Greter, M., Mortha, A., Boyer, S.W., Forsberg, E.C., Tanaka, M., van Rooijen, N., García-Sastre, A., Stanley, E.R., Ginhoux, F., et al. (2013) Tissue-resident macrophages self-maintain locally throughout adult life with minimal contribution from circulating monocytes. *Immunity*. 38 (4), 792–804.
- Heideveld, E. & van den Akker, E. (2017) Digesting the role of bone marrow macrophages on hematopoiesis. *European Macrophage and Dendritic Cell Society (EMDS) Special Issue: Monocytes, dendritic cells and macrophages - basic research and pathophysiological aspects*. 222 (6), 814–822.
- Hellstrom, M., Kaln, M., Lindahl, P., Abramsson, A. & Betsholtz, C. (1999) Role of PDGF-B and PDGFR-beta in recruitment of vascular smooth muscle cells and pericytes during embryonic blood vessel formation in the mouse. *Development*. 126 (14), 3047.
- Hoeffel, G., Wang, Y., Greter, M., See, P., Teo, P., Malleret, B., Leboeuf, M., Low, D., Oller, G., Almeida, F., Choy, S.H.Y., Grisotto, M., Renia, L., Conway, S.J., Stanley, E.R., Chan, J.K.Y., Ng, L.G., Samokhvalov, I.M., Merad, M., et al. (2012) Adult Langerhans cells derive predominantly from embryonic fetal liver monocytes with a minor contribution of yolk sac-derived macrophages. *The Journal of Experimental Medicine*. 209 (6), 1167–1181.
- Hollander, L., Han, H., De Winter, M., Svensson, L., Masich, S., Daneholt, B. & Norlén, L. (2015) Skin Lamellar Bodies are not Discrete Vesicles but Part of a Tubuloreticular Network. *Acta dermato-venereologica*. 96.
- Homey, B., Alenius, H., Müller, A., Soto, H., Bowman, E.P., Yuan, W., McEvoy, L., Lauerma, A.I., Assmann, T., Bünemann, E., Lehto, M., Wolff, H., Yen, D., Marxhausen, H., To, W., Sedgwick, J., Ruzicka, T., Lehmann, P. & Zlotnik, A. (2002) CCL27–CCR10 interactions regulate T cell-mediated skin inflammation. *Nature Medicine*. 8 (2), 157–165.
- Hong, S., Dissing-Olesen, L. & Stevens, B. (2016) New insights on the role of microglia in synaptic pruning in health and disease. *Current opinion in neurobiology*. 36128–134.
- Horsley, V., O’Carroll, D., Tooze, R., Ohinata, Y., Saitou, M., Obukhanych, T., Nussenzweig, M., Tarakhovskiy, A. & Fuchs, E. (2006) Blimp1 defines a progenitor population that governs cellular input to the sebaceous gland. *Cell*. 126 (3), 597–609.
- Hughes, T.K., Wadsworth, M.H., Gierahn, T.M., Do, T., Weiss, D., Andrade, P.R., Ma, F., de Andrade Silva, B.J., Shao, S., Tsoi, L.C., Ordovas-Montanes, J., Gudjonsson, J.E., Modlin, R.L., Love, J.C. & Shalek, A.K. (2019) Highly Efficient, Massively-Parallel Single-Cell RNA-Seq Reveals Cellular States and Molecular Features of Human Skin Pathology. *bioRxiv*. 689273.

- Hunger, R.E., Sieling, P.A., Ochoa, M.T., Sugaya, M., Burdick, A.E., Rea, T.H., Brennan, P.J., Belisle, J.T., Blauvelt, A., Porcelli, S.A. & Modlin, R.L. (2004) Langerhans cells utilize CD1a and langerin to efficiently present nonpeptide antigens to T cells. *The Journal of clinical investigation*. 113 (5), 701–708.
- Jahrsdörfer, B., Vollmer, A., Blackwell, S.E., Maier, J., Sontheimer, K., Beyer, T., Mandel, B., Lunov, O., Tron, K., Nienhaus, G.U., Simmet, T., Debatin, K.-M., Weiner, G.J. & Fabricius, D. (2010) Granzyme B produced by human plasmacytoid dendritic cells suppresses T-cell expansion. *Blood*. 115 (6), 1156–1165.
- Jaitley, S. & Saraswathi, T. (2012) Pathophysiology of Langerhans cells. *Journal of oral and maxillofacial pathology : JOMFP*. 16 (2), 239–244.
- Jaks, V., Barker, N., Kasper, M., van Es, J.H., Snippert, H.J., Clevers, H. & Toftgård, R. (2008) Lgr5 marks cycling, yet long-lived, hair follicle stem cells. *Nature Genetics*. 40 (11), 1291–1299.
- Janson, D.G., Saintigny, G., van Adrichem, A., Mahé, C. & El Ghalbzouri, A. (2012) Different Gene Expression Patterns in Human Papillary and Reticular Fibroblasts. *Journal of Investigative Dermatology*. 132 (11), 2565–2572.
- Janssens, A.S., Heide, R., den Hollander, J.C., Mulder, P.G.M., Tank, B. & Oranje, A.P. (2005) Mast cell distribution in normal adult skin. *Journal of clinical pathology*. 58 (3), 285–289.
- Johansen, C., Funding, A.T., Otkjaer, K., Kragballe, K., Jensen, U.B., Madsen, M., Binderup, L., Skak-Nielsen, T., Fjording, M.S. & Iversen, L. (2006) Protein Expression of TNF- $\alpha$  in Psoriatic Skin Is Regulated at a Posttranscriptional Level by MAPK-Activated Protein Kinase 2. *The Journal of Immunology*. 176 (3), 1431.
- Joller, N., Lozano, E., Burkett, P.R., Patel, B., Xiao, S., Zhu, C., Xia, J., Tan, T.G., Sefik, E., Yajnik, V., Sharpe, A.H., Quintana, F.J., Mathis, D., Benoist, C., Hafler, D.A. & Kuchroo, V.K. (2014) Treg cells expressing the coinhibitory molecule TIGIT selectively inhibit proinflammatory Th1 and Th17 cell responses. *Immunity*. 40 (4), 569–581.
- Jones, P.H., Simons, B.D. & Watt, F.M. (2007) Sic Transit Gloria: Farewell to the Epidermal Transit Amplifying Cell? *Cell Stem Cell*. 1 (4), 371–381.
- Joost, S., Jacob, T., Sun, X., Annusver, K., La Manno, G., Sur, I. & Kasper, M. (2018) Single-Cell Transcriptomics of Traced Epidermal and Hair Follicle Stem Cells Reveals Rapid Adaptations during Wound Healing. *Cell Reports*. 25 (3), 585-597.e7.
- Joost, S., Zeisel, A., Jacob, T., Sun, X., La Manno, G., Lonnerberg, P., Linnarsson, S. & Kasper, M. (2016) Single-Cell Transcriptomics Reveals that Differentiation and Spatial Signatures Shape Epidermal and Hair Follicle Heterogeneity. *Cell systems*. 3 (3), 221-237.e9.

- Juráňová, J., Franková, J. & Ulrichová, J. (2017) The role of keratinocytes in inflammation. *Journal of Applied Biomedicine*. 15 (3), 169–179.
- Kadowaki, N., Ho, S., Antonenko, S., Malefyt, R.W., Kastelein, R.A., Bazan, F. & Liu, Y.J. (2001) Subsets of human dendritic cell precursors express different toll-like receptors and respond to different microbial antigens. *The Journal of experimental medicine*. 194 (6), 863–869.
- Kaminska, R., Helisalmi, P., Harvima, R.J., Horsmanheimo, M., Harvima, I.T. & Naukkarinen, A. (1999) Focal Dermal–Epidermal Separation and Fibronectin Cleavage in Basement Membrane by Human Mast Cell Trypsin. *Journal of Investigative Dermatology*. 113 (4), 567–573.
- Kassis, V. & Søndergaard, J. (1982) Heat-separation of normal human skin for epidermal and dermal prostaglandin analysis. *Archives of Dermatological Research*. 273 (3), 301–306.
- Kedzierski, L., Linossi, E.M., Kolesnik, T.B., Day, E.B., Bird, N.L., Kile, B.T., Belz, G.T., Metcalf, D., Nicola, N.A., Kedzierska, K. & Nicholson, S.E. (2014) Suppressor of cytokine signaling 4 (SOCS4) protects against severe cytokine storm and enhances viral clearance during influenza infection. *PLoS pathogens*. 10 (5), e1004134–e1004134.
- Kim, B.S. (2015) Innate lymphoid cells in the skin. *The Journal of investigative dermatology*. 135 (3), 673–678.
- Kim, B.S., Miyagawa, F., Cho, Y.-H., Bennett, C.L., Clausen, B.E. & Katz, S.I. (2009) Keratinocytes function as accessory cells for presentation of endogenous antigen expressed in the epidermis. *The Journal of investigative dermatology*. 129 (12), 2805–2817.
- Kim, B.S., Siracusa, M.C., Saenz, S.A., Noti, M., Monticelli, L.A., Sonnenberg, G.F., Hepworth, M.R., Van Voorhees, A.S., Comeau, M.R. & Artis, D. (2013) TSLP elicits IL-33-independent innate lymphoid cell responses to promote skin inflammation. *Science translational medicine*. 5 (170), 170ra16-170ra16.
- Kim, D., Kobayashi, T., Voisin, B., Jo, J.-H., Sakamoto, K., Jin, S.-P., Kelly, M., Pasięka, H.B., Naff, J.L., Meyerle, J.H., Ikpeama, I.D., Fahle, G.A., Davis, F.P., Rosenzweig, S.D., Alejo, J.C., Pittaluga, S., Kong, H.H., Freeman, A.F. & Nagao, K. (2020) Targeted therapy guided by single-cell transcriptomic analysis in drug-induced hypersensitivity syndrome: a case report. *Nature Medicine*.
- Kim, Young Hee, Kim, Young Hye, Shin, Y.K., Jo, Y.R., Park, D.K., Song, M.-Y., Yoon, B.-A., Nam, S.H., Kim, J.H., Choi, B.-O., Shin, H.Y., Kim, S.W., Kim, S.H., Hong, Y.B., Kim, J.K. & Park, H.T. (2019) p75 and neural cell adhesion molecule 1 can identify pathologic Schwann cells in peripheral neuropathies. *Annals of Clinical and Translational Neurology*. 6 (7), 1292–1301.

- Kitano, Y. & Okada, N. (1983) Separation of the epidermal sheet by dispase. *British Journal of Dermatology*. 108 (5), 555–560.
- Knepper, T.C., Montesion, M., Russell, J.S., Sokol, E.S., Frampton, G.M., Miller, V.A., Albacker, L.A., McLeod, H.L., Eroglu, Z., Khushalani, N.I., Sondak, V.K., Messina, J.L., Schell, M.J., DeCaprio, J.A., Tsai, K.Y. & Brohl, A.S. (2019) The Genomic Landscape of Merkel Cell Carcinoma and Clinicogenomic Biomarkers of Response to Immune Checkpoint Inhibitor Therapy. *Clinical Cancer Research*. 25 (19), 5961.
- Kobayashi, T., Voisin, B., Kim, D.Y., Kennedy, E.A., Jo, J.-H., Shih, H.-Y., Truong, A., Doebel, T., Sakamoto, K., Cui, C.-Y., Schlessinger, D., Moro, K., Nakae, S., Horiuchi, K., Zhu, J., Leonard, W.J., Kong, H.H. & Nagao, K. (2019) Homeostatic Control of Sebaceous Glands by Innate Lymphoid Cells Regulates Commensal Bacteria Equilibrium. *Cell*. 176 (5), 982-997.e16.
- Koroleva, E.P., Fu, Y.-X. & Tumanov, A.V. (2018) Lymphotoxin in physiology of lymphoid tissues - Implication for antiviral defense. *Cytokine*. 10139–47.
- Korsunsky, I., Fan, J., Slowikowski, K., Zhang, F., Wei, K., Baglaenko, Y., Brenner, M., Loh, P.-R. & Raychaudhuri, S. (2018) Fast, sensitive, and accurate integration of single cell data with Harmony. *bioRxiv*. 461954.
- Lamberti, G., Prabhakarapandian, B., Garson, C., Smith, A., Pant, K., Wang, B. & Kiani, M.F. (2014) Bioinspired microfluidic assay for in vitro modeling of leukocyte-endothelium interactions. *Analytical chemistry*. 86 (16), 8344–8351.
- Lawrance, W., Banerji, S., Day, A.J., Bhattacharjee, S. & Jackson, D.G. (2016) Binding of Hyaluronan to the Native Lymphatic Vessel Endothelial Receptor LYVE-1 Is Critically Dependent on Receptor Clustering and Hyaluronan Organization. *The Journal of biological chemistry*. 291 (15), 8014–8030.
- Le, N., Nagarajan, R., Wang, J.Y.T., Araki, T., Schmidt, R.E. & Milbrandt, J. (2005) Analysis of congenital hypomyelinating Egr2Lo/Lo nerves identifies Sox2 as an inhibitor of Schwann cell differentiation and myelination. *Proceedings of the National Academy of Sciences of the United States of America*. 102 (7), 2596–2601.
- Lechler, T. & Fuchs, E. (2005) Asymmetric cell divisions promote stratification and differentiation of mammalian skin. *Nature*. 437 (7056), 275–280.
- Lee, J., Rabbani, C.C., Gao, H., Steinhart, M.R., Woodruff, B.M., Pflum, Z.E., Kim, A., Heller, S., Liu, Y., Shipchandler, T.Z. & Koehler, K.R. (2020) Hair-bearing human skin generated entirely from pluripotent stem cells. *Nature*.
- Levine, J.H., Simonds, E.F., Bendall, S.C., Davis, K.L., Amir, E.D., Tadmor, M.D., Litvin, O., Fienberg, H.G., Jager, A., Zunder, E.R., Finck, R., Gedman, A.L., Radtke, I., Downing, J.R., Pe'er, D. & Nolan, G.P. (2015) Data-Driven Phenotypic Dissection of AML Reveals Progenitor-like Cells that Correlate with Prognosis. *Cell*. 162 (1), 184–197.



- Ley K & Gaehtgens P (1991) Endothelial, not hemodynamic, differences are responsible for preferential leukocyte rolling in rat mesenteric venules. *Circulation Research*. 69 (4), 1034–1041.
- Lichtman, M.K., Otero-Vinas, M. & Falanga, V. (2016) Transforming growth factor beta (TGF- $\beta$ ) isoforms in wound healing and fibrosis. *Wound Repair and Regeneration*. 24 (2), 215–222.
- Limbu, S. & Higgins, C.A. (2020) 'Isolating Dermal Papilla Cells from Human Hair Follicles Using Microdissection and Enzyme Digestion', in Natalia V. Botchkareva & Gillian E. Westgate (eds.) *Molecular Dermatology: Methods and Protocols*. [Online]. New York, NY: Springer US. pp. 91–103.
- Liu, K., Victora, G.D., Schwickert, T.A., Guermonprez, P., Meredith, M.M., Yao, K., Chu, F.-F., Randolph, G.J., Rudensky, A.Y. & Nussenzweig, M. (2009) In vivo analysis of dendritic cell development and homeostasis. *Science (New York, N.Y.)*. 324 (5925), 392–397.
- Lovászi, M., Szegedi, A., Zouboulis, C.C. & Törőcsik, D. (2017) Sebaceous-immunobiology is orchestrated by sebum lipids. *Dermato-endocrinology*. 9 (1), e1375636–e1375636.
- Lu, L., Barbi, J. & Pan, F. (2017) The regulation of immune tolerance by FOXP3. *Nature Reviews Immunology*. 17 (11), 703–717.
- Luecken, M.D. & Theis, F.J. (2019) Current best practices in single-cell RNA-seq analysis: a tutorial. *Molecular systems biology*. 15 (6), e8746–e8746.
- Lundberg, K., Albrekt, A.-S., Nelissen, I., Santegoets, S., de Gruijl, T.D., Gibbs, S. & Lindstedt, M. (2013) Transcriptional profiling of human dendritic cell populations and models—unique profiles of in vitro dendritic cells and implications on functionality and applicability. *PloS one*. 8 (1), e52875–e52875.
- Mackenzie, I.C. (1970) Relationship between Mitosis and the Ordered Structure of the Stratum Corneum in Mouse Epidermis. *Nature*. 226 (5246), 653–655.
- MacLeod, A.S., Hemmers, S., Garijo, O., Chabod, M., Mowen, K., Witherden, D.A. & Havran, W.L. (2013) Dendritic epidermal T cells regulate skin antimicrobial barrier function. *The Journal of clinical investigation*. 123 (10), 4364–4374.
- Macosko, E.Z., Basu, A., Satija, R., Nemesh, J., Shekhar, K., Goldman, M., Tirosh, I., Bialas, A.R., Kamitaki, N., Martersteck, E.M., Trombetta, J.J., Weitz, D.A., Sanes, J.R., Shalek, A.K., Regev, A. & McCarroll, S.A. (2015) Highly Parallel Genome-wide Expression Profiling of Individual Cells Using Nanoliter Droplets. *Cell*. 161 (5), 1202–1214.
- Maiti, R., Duan, M., Danby, S.G., Lewis, R., Matcher, S.J. & Carré, M.J. (2020) Morphological parametric mapping of 21 skin sites throughout the body using

optical coherence tomography. *Journal of the Mechanical Behavior of Biomedical Materials*. 102103501.

Makó, V., Czúcz, J., Weiszhar, Z., Herczenik, E., Matkó, J., Prohászka, Z. & Cervenak, L. (2010) Proinflammatory activation pattern of human umbilical vein endothelial cells induced by IL-1 $\beta$ , TNF- $\alpha$ , and LPS. *Cytometry Part A*. 77A (10), 962–970.

Mansfield, K. & Naik, S. (2020) Unraveling Immune-Epithelial Interactions in Skin Homeostasis and Injury. *The Yale journal of biology and medicine*. 93 (1), 133–143.

Maricich, S.M., Wellnitz, S.A., Nelson, A.M., Lesniak, D.R., Gerling, G.J., Lumpkin, E.A. & Zoghbi, H.Y. (2009) Merkel cells are essential for light-touch responses. *Science (New York, N.Y.)*. 324 (5934), 1580–1582.

Marinov, G.K., Williams, B.A., McCue, K., Schroth, G.P., Gertz, J., Myers, R.M. & Wold, B.J. (2014) From single-cell to cell-pool transcriptomes: stochasticity in gene expression and RNA splicing. *Genome research*. 24 (3), 496–510.

Martincorena, I., Roshan, A., Gerstung, M., Ellis, P., Van Loo, P., McLaren, S., Wedge, D.C., Fullam, A., Alexandrov, L.B., Tubio, J.M., Stebbings, L., Menzies, A., Widaa, S., Stratton, M.R., Jones, P.H. & Campbell, P.J. (2015) High burden and pervasive positive selection of somatic mutations in normal human skin. *Science*. 348 (6237), 880.

Matsuo, K., Kitahata, K., Kawabata, F., Kamei, M., Hara, Y., Takamura, S., Oiso, N., Kawada, A., Yoshie, O. & Nakayama, T. (2018) A Highly Active Form of XCL1/Lymphotactin Functions as an Effective Adjuvant to Recruit Cross-Presenting Dendritic Cells for Induction of Effector and Memory CD8<sup>+</sup> T Cells. *Frontiers in Immunology*. 92775.

Matsuo, K., Nagakubo, D., Komori, Y., Fujisato, S., Takeda, N., Kitamatsu, M., Nishiwaki, K., Quan, Y.-S., Kamiyama, F., Oiso, N., Kawada, A., Yoshie, O. & Nakayama, T. (2018) CCR4 Is Critically Involved in Skin Allergic Inflammation of BALB/c Mice. *Journal of Investigative Dermatology*. 138.

Matsushima, H., Yamada, N., Matsue, H. & Shimada, S. (2004) TLR3-, TLR7-, and TLR9-Mediated Production of Proinflammatory Cytokines and Chemokines from Murine Connective Tissue Type Skin-Derived Mast Cells but Not from Bone Marrow-Derived Mast Cells. *The Journal of Immunology*. 173 (1), 531.

McEver, R.P. & Zhu, C. (2010) Rolling cell adhesion. *Annual review of cell and developmental biology*. 26363–396.

McGovern, N., Schlitzer, A., Gunawan, M., Jardine, L., Shin, A., Poyner, E., Green, K., Dickinson, R., Wang, X.-N., Low, D., Best, K., Covins, S., Milne, P., Pagan, S., Aljefri, K., Windebank, M., Miranda-Saavedra, D., Larbi, A., Wasan, P.S., et al. (2014) Human dermal CD14<sup>+</sup> cells are a transient population of monocyte-derived macrophages. *Immunity*. 41 (3), 465–477.

- Mellman, I. & Steinman, R.M. (2001) Dendritic Cells: Specialized and Regulated Antigen Processing Machines. *Cell*. 106 (3), 255–258.
- Menon, G.K., Price, L.F., Bommannan, B., Elias, P.M. & Feingold, K.R. (1994) Selective Obliteration of the Epidermal Calcium Gradient Leads to Enhanced Lamellar Body Secretion. *Journal of Investigative Dermatology*. 102 (5), 789–795.
- Merad, M., Manz, M.G., Karsunky, H., Wagers, A., Peters, W., Charo, I., Weissman, I.L., Cyster, J.G. & Engleman, E.G. (2002) Langerhans cells renew in the skin throughout life under steady-state conditions. *Nature Immunology*. 3 (12), 1135–1141.
- Miao, Z., Moreno, P., Huang, N., Papatheodorou, I., Brazma, A. & Teichmann, S.A. (2020) Putative cell type discovery from single-cell gene expression data. *Nature Methods*. 17 (6), 621–628.
- Miller, A.M. (2011) Role of IL-33 in inflammation and disease. *Journal of inflammation (London, England)*. 8 (1), 22–22.
- Mionnet, C., Sanos, S.L., Mondor, I., Jorquera, A., Laugier, J.-P., Germain, R.N. & Bajénoff, M. (2011) High endothelial venules as traffic control points maintaining lymphocyte population homeostasis in lymph nodes. *Blood*. 118 (23), 6115–6122.
- Mitchell, T.S., Bradley, J., Robinson, G.S., Shima, D.T. & Ng, Y.-S. (2008) RGS5 expression is a quantitative measure of pericyte coverage of blood vessels. *Angiogenesis*. 11 (2), 141–151.
- Morioka, K., Arai, M. & Ihara, S. (2011) Steady and temporary expressions of smooth muscle actin in hair, vibrissa, arrector pili muscle, and other hair appendages of developing rats. *Acta histochemica et cytochemica*. 44 (3), 141–153.
- Morrison, K.M., Miesegaes, G.R., Lumpkin, E.A. & Maricich, S.M. (2009) Mammalian Merkel cells are descended from the epidermal lineage. *Developmental biology*. 336 (1), 76–83.
- Myles, I.A., Fontecilla, N.M., Valdez, P.A., Vithayathil, P.J., Naik, S., Belkaid, Y., Ouyang, W. & Datta, S.K. (2013) Signaling via the IL-20 receptor inhibits cutaneous production of IL-1 $\beta$  and IL-17A to promote infection with methicillin-resistant *Staphylococcus aureus*. *Nature immunology*. 14 (8), 804–811.
- Naik, S., Bouladoux, N., Wilhelm, C., Molloy, M.J., Salcedo, R., Kastenmuller, W., Deming, C., Quinones, M., Koo, L., Conlan, S., Spencer, S., Hall, J.A., Dzutsev, A., Kong, H., Campbell, D.J., Trinchieri, G., Segre, J.A. & Belkaid, Y. (2012) Compartmentalized control of skin immunity by resident commensals. *Science (New York, N.Y.)*. 337 (6098), 1115–1119.
- Nestle, F.O., Conrad, C., Tun-Kyi, A., Homey, B., Gombert, M., Boyman, O., Burg, G., Liu, Y.-J. & Gilliet, M. (2005) Plasmacytoid predendritic cells initiate psoriasis through

- interferon-alpha production. *The Journal of experimental medicine*. 202 (1), 135–143.
- Nishimura, E.K., Jordan, S.A., Oshima, H., Yoshida, H., Osawa, M., Moriyama, M., Jackson, I.J., Barrandon, Y., Miyachi, Y. & Nishikawa, S.-I. (2002) Dominant role of the niche in melanocyte stem-cell fate determination. *Nature*. 416 (6883), 854–860.
- Noguchi, F., Nakajima, T., Inui, S., Reddy, J.K. & Itami, S. (2014) Alteration of skin wound healing in keratinocyte-specific mediator complex subunit 1 null mice. *PLoS one*. 9 (8), e102271–e102271.
- Novak, N., Allam, J.-P., Hagemann, T., Jenneck, C., Laffer, S., Valenta, R., Kochan, J. & Bieber, T. (2004) Characterization of FcεRI-bearing CD123+ blood dendritic cell antigen-2+ plasmacytoid dendritic cells in atopic dermatitis. *Journal of Allergy and Clinical Immunology*. 114 (2), 364–370.
- Novak, N., Kraft, S., Haberstrok, J., Geiger, E., Allam, P. & Bieber, T. (2002) A Reducing Microenvironment Leads to the Generation of FcεRI<sup>high</sup> Inflammatory Dendritic Epidermal Cells (IDEC). *Journal of Investigative Dermatology*. 119 (4), 842–849.
- Novak, N., Valenta, R., Bohle, B., Laffer, S., Haberstrok, J., Kraft, S. & Bieber, T. (2004) FcεRI engagement of Langerhans cell-like dendritic cells and inflammatory dendritic epidermal cell-like dendritic cells induces chemotactic signals and different T-cell phenotypes in vitro. *Journal of Allergy and Clinical Immunology*. 113 (5), 949–957.
- O’Carroll, S.J., Kho, D.T., Wiltshire, R., Nelson, V., Rotimi, O., Johnson, R., Angel, C.E. & Graham, E.S. (2015) Pro-inflammatory TNFα and IL-1β differentially regulate the inflammatory phenotype of brain microvascular endothelial cells. *Journal of Neuroinflammation*. 12 (1), 131.
- O’Flanagan, C.H., Campbell, K.R., Zhang, A.W., Kabeer, F., Lim, J.L.P., Biele, J., Eirew, P., Lai, D., McPherson, A., Kong, E., Bates, C., Borkowski, K., Wiens, M., Hewitson, B., Hopkins, J., Pham, J., Ceglia, N., Moore, R., Mungall, A.J., et al. (2019) Dissociation of solid tumor tissues with cold active protease for single-cell RNA-seq minimizes conserved collagenase-associated stress responses. *Genome Biology*. 20 (1), 210.
- Ohl, L., Mohaupt, M., Czeloth, N., Hintzen, G., Kiafard, Z., Zwirner, J., Blankenstein, T., Henning, G. & Förster, R. (2004) CCR7 Governs Skin Dendritic Cell Migration under Inflammatory and Steady-State Conditions. *Immunity*. 21 (2), 279–288.
- Okabe, Y. & Medzhitov, R. (2016) Tissue biology perspective on macrophages. *Nature Immunology*. 17 (1), 9–17.
- Oltulu, P., Ince, B., Kokbudak, N., Findik, S. & Kilinc, F. (2018) Measurement of Epidermis, Dermis, and Total Skin Thicknesses from Six Different Body Regions with a new Ethical Histometric Technique. *Turkish Journal of Plastic Surgery*. 26 (2), 56+.

- Ong, S.-M., Teng, K., Newell, E., Chen, H., Chen, J., Loy, T., Yeo, T.-W., Fink, K. & Wong, S.-C. (2019) A Novel, Five-Marker Alternative to CD16–CD14 Gating to Identify the Three Human Monocyte Subsets. *Frontiers in Immunology*. 101761.
- Oren, A., Ganz, T., Liu, L. & Meerloo, T. (2003) In human epidermis,  $\beta$ -defensin 2 is packaged in lamellar bodies. *Experimental and Molecular Pathology Special Issue: University of California, Los Angeles Department of Pathology*. 74 (2), 180–182.
- Otberg, N., Richter, H., Schaefer, H., Blume-Peytavi, U., Sterry, W. & Lademann, J. (2004) Variations of Hair Follicle Size and Distribution in Different Body Sites. *Journal of Investigative Dermatology*. 122 (1), 14–19.
- Otsuka, M., Egawa, G. & Kabashima, K. (2018) Uncovering the Mysteries of Langerhans Cells, Inflammatory Dendritic Epidermal Cells, and Monocyte-Derived Langerhans Cell-Like Cells in the Epidermis. *Frontiers in immunology*. 91768–1768.
- Oukka, M., Wein, M.N. & Glimcher, L.H. (2004) *Schnurri-3* (KRC) Interacts with c-Jun to Regulate the IL-2 Gene in T Cells. *The Journal of Experimental Medicine*. 199 (1), 15.
- Ouwehand, K., Scheper, R.J., de Gruijl, T.D. & Gibbs, S. (2010) Epidermis-to-dermis migration of immature Langerhans cells upon topical irritant exposure is dependent on CCL2 and CCL5. *European Journal of Immunology*. 40 (7), 2026–2034.
- Pardo, J., Balkow, S., Anel, A. & Simon, M.M. (2002) Granzymes are essential for natural killer cell-mediated and perfacilitated tumor control. *European Journal of Immunology*. 32 (10), 2881–2886.
- Patterson, B.K., Landay, A., Siegel, J.N., Flener, Z., Pessis, D., Chaviano, A. & Bailey, R.C. (2002) Susceptibility to human immunodeficiency virus-1 infection of human foreskin and cervical tissue grown in explant culture. *The American journal of pathology*. 161 (3), 867–873.
- Philippeos, C., Telerman, S.B., Oulès, B., Pisco, A.O., Shaw, T.J., Elgueta, R., Lombardi, G., Driskell, R.R., Soldin, M., Lynch, M.D. & Watt, F.M. (2018) Spatial and Single-Cell Transcriptional Profiling Identifies Functionally Distinct Human Dermal Fibroblast Subpopulations. *The Journal of investigative dermatology*. 138 (4), 811–825.
- Picelli, S., Björklund, Å.K., Faridani, O.R., Sagasser, S., Winberg, G. & Sandberg, R. (2013) Smart-seq2 for sensitive full-length transcriptome profiling in single cells. *Nature Methods*. 10 (11), 1096–1098.
- Picelli, S., Faridani, O.R., Björklund, Å.K., Winberg, G., Sagasser, S. & Sandberg, R. (2014) Full-length RNA-seq from single cells using Smart-seq2. *Nature Protocols*. 9 (1), 171–181.
- Plantinga, M., Guilliams, M., Vanheerswynghels, M., Deswarte, K., Branco-Madeira, F., Toussaint, W., Vanhoutte, L., Neyt, K., Killeen, N., Malissen, B., Hammad, H. &

- Lambrecht, B.N. (2013) Conventional and Monocyte-Derived CD11b+ Dendritic Cells Initiate and Maintain T Helper 2 Cell-Mediated Immunity to House Dust Mite Allergen. *Immunity*. 38 (2), 322–335.
- Pober, J.S., Merola, J., Liu, R. & Manes, T.D. (2017) Antigen Presentation by Vascular Cells. *Frontiers in immunology*. 81907–1907.
- Pollheimer Jürgen, Bodin Johanna, Sundnes Olav, Edelmann Reidunn J., Skånland Sigrid S., Sponheim Jon, Brox Mari Johanna, Sundlisæter Eirik, Loos Tamara, Vatn Morten, Kasprzycka Monika, Wang Junbai, Küchler Axel M., Taskén Kjetil, Haraldsen Guttorm & Hol Johanna (2013) Interleukin-33 Drives a Proinflammatory Endothelial Activation That Selectively Targets Nonquiescent Cells. *Arteriosclerosis, Thrombosis, and Vascular Biology*. 33 (2), e47–e55.
- Potten, C.S. (1981) 'Cell Replacement in Epidermis (Keratopoiesis) via Discrete Units of Proliferation', in G.H. Bourne, J.F. Danielli, & K.W. Jeon (eds.) *International Review of Cytology*. [Online]. Academic Press. pp. 271–318.
- Puhlmann, M., Weinreich, D.M., Farma, J.M., Carroll, N.M., Turner, E.M. & Alexander, H.R., Jr (2005) Interleukin-1beta induced vascular permeability is dependent on induction of endothelial tissue factor (TF) activity. *Journal of translational medicine*. 337–37.
- Qing, Z., Sandor, M., Radvany, Z., Sewell, D., Falus, A., Potthoff, D., Muller, W.A. & Fabry, Z. (2001) Inhibition of Antigen-Specific T Cell Trafficking into the Central Nervous System via Blocking PECAM1/CD31 Molecule. *Journal of Neuropathology & Experimental Neurology*. 60 (8), 798–807.
- Rafei-Shamsabadi, D.A., van de Poel, S., Dorn, B., Kunz, S., Martin, S.F., Klose, C.S.N., Arnold, S.J., Tanriver, Y., Ebert, K., Diefenbach, A., Halim, T.Y.F., McKenzie, A.N.J. & Jakob, T. (2018) Lack of Type 2 Innate Lymphoid Cells Promotes a Type I-Driven Enhanced Immune Response in Contact Hypersensitivity. *The Journal of investigative dermatology*. 138 (9), 1962–1972.
- Ramsköld, D., Luo, S., Wang, Y.-C., Li, R., Deng, Q., Faridani, O.R., Daniels, G.A., Khrebtukova, I., Loring, J.F., Laurent, L.C., Schroth, G.P. & Sandberg, R. (2012) Full-length mRNA-Seq from single-cell levels of RNA and individual circulating tumor cells. *Nature biotechnology*. 30 (8), 777–782.
- Raymond, A.-A., de Peredo, A.G., Stella, A., Ishida-Yamamoto, A., Bouyssie, D., Serre, G., Monsarrat, B. & Simon, M. (2008) Lamellar Bodies of Human Epidermis. *Molecular & Cellular Proteomics*. 7 (11), 2151.
- Reynolds, G. & Haniffa, M. (2015) Human and Mouse Mononuclear Phagocyte Networks: A Tale of Two Species? *Frontiers in immunology*. 6330–330.
- Rhodes, J.W., Tong, O., Harman, A.N. & Turville, S.G. (2019) Human Dendritic Cell Subsets, Ontogeny, and Impact on HIV Infection. *Frontiers in Immunology*. 101088.

- Rinkevich, Y., Walmsley, G.G., Hu, M.S., Maan, Z.N., Newman, A.M., Drukker, M., Januszky, M., Krampitz, G.W., Gurtner, G.C., Lorenz, H.P., Weissman, I.L. & Longaker, M.T. (2015) Skin fibrosis. Identification and isolation of a dermal lineage with intrinsic fibrogenic potential. *Science (New York, N.Y.)*. 348 (6232), aaa2151–aaa2151.
- Rnjak-Kovacina, J. & Weiss, A. (2013) 'The Role of Elastin in Wound Healing and Dermal Substitute Design', in *Dermal Replacements in General, Burn, and Plastic Surgery: Tissue Engineering in Clinical Practice*. [Online]. pp. 57–66.
- Rognoni, E., Pisco, A.O., Hiratsuka, T., Sipilä, K.H., Belmonte, J.M., Mobasser, S.A., Philippeos, C., Dilão, R. & Watt, F.M. (2018) Fibroblast state switching orchestrates dermal maturation and wound healing. *Molecular systems biology*. 14 (8), e8174–e8174.
- Roshan, A., Murai, K., Fowler, J., Simons, B.D., Nikolaidou-Neokosmidou, V. & Jones, P.H. (2016) Human keratinocytes have two interconvertible modes of proliferation. *Nature cell biology*. 18 (2), 145–156.
- Sa, S.M., Valdez, P.A., Wu, J., Jung, K., Zhong, F., Hall, L., Kasman, I., Winer, J., Modrusan, Z., Danilenko, D.M. & Ouyang, W. (2007) The Effects of IL-20 Subfamily Cytokines on Reconstituted Human Epidermis Suggest Potential Roles in Cutaneous Innate Defense and Pathogenic Adaptive Immunity in Psoriasis. *The Journal of Immunology*. 178 (4), 2229.
- Saalbach, A., Janik, T., Busch, M., Herbert, D., Anderegg, U. & Simon, J.C. (2015) Fibroblasts support migration of monocyte-derived dendritic cells by secretion of PGE2 and MMP-1. *Experimental Dermatology*. 24 (8), 598–604.
- Sabat, R., Wolk, K., Loyal, L., Döcke, W.-D. & Ghoreschi, K. (2019) T cell pathology in skin inflammation. *Seminars in Immunopathology*. 41 (3), 359–377.
- Sahoo, P.K., Smith, D.S., Perrone-Bizzozero, N. & Twiss, J.L. (2018) Axonal mRNA transport and translation at a glance. *Journal of Cell Science*. 131 (8), jcs196808.
- Salzer, J.L. (2015) Schwann cell myelination. *Cold Spring Harbor perspectives in biology*. 7 (8), a020529–a020529.
- Sanchez Rodriguez, R., Pauli, M.L., Neuhaus, I.M., Yu, S.S., Arron, S.T., Harris, H.W., Yang, S.H.-Y., Anthony, B.A., Sverdrup, F.M., Krow-Lucal, E., MacKenzie, T.C., Johnson, D.S., Meyer, E.H., Löhr, A., Hsu, A., Koo, J., Liao, W., Gupta, R., Debbaneh, M.G., et al. (2014) Memory regulatory T cells reside in human skin. *The Journal of clinical investigation*. 124 (3), 1027–1036.
- Santegoets, S.J.A.M., Gibbs, S., Kroeze, K., van de Ven, R., Scheper, R.J., Borrebaeck, C.A., de Gruijl, T.D. & Lindstedt, M. (2008) Transcriptional profiling of human skin-resident Langerhans cells and CD1a+ dermal dendritic cells: differential activation states suggest distinct functions. *Journal of Leukocyte Biology*. 84 (1), 143–151.

- Sawa, Y., Sugimoto, Y., Ueki, T., Ishikawa, H., Sato, A., Nagato, T. & Yoshida, S. (2007) Effects of TNF- $\alpha$  on Leukocyte Adhesion Molecule Expressions in Cultured Human Lymphatic Endothelium. *Journal of Histochemistry & Cytochemistry*. 55 (7), 721–733.
- Scharschmidt, T.C., Vasquez, K.S., Pauli, M.L., Leitner, E.G., Chu, K., Truong, H.-A., Lowe, M.M., Sanchez Rodriguez, R., Ali, N., Laszik, Z.G., Sonnenburg, J.L., Millar, S.E. & Rosenblum, M.D. (2017) Commensal Microbes and Hair Follicle Morphogenesis Coordinately Drive Treg Migration into Neonatal Skin. *Cell host & microbe*. 21 (4), 467-477.e5.
- Schautz, B., Later, W., Heller, M., Müller, M.J. & Bosy-Westphal, A. (2011) Associations between breast adipose tissue, body fat distribution and cardiometabolic risk in women: cross-sectional data and weight-loss intervention. *European Journal of Clinical Nutrition*. 65 (7), 784–790.
- Schenkel, A.R., Mamdouh, Z., Chen, X., Liebman, R.M. & Muller, W.A. (2002) CD99 plays a major role in the migration of monocytes through endothelial junctions. *Nature Immunology*. 3 (2), 143–150.
- Schepeler, T., Page, M.E. & Jensen, K.B. (2014) Heterogeneity and plasticity of epidermal stem cells. *Development (Cambridge, England)*. 141 (13), 2559–2567.
- Schneider, C., Nobs, S.P., Kurrer, M., Rehrauer, H., Thiele, C. & Kopf, M. (2014) Induction of the nuclear receptor PPAR- $\gamma$  by the cytokine GM-CSF is critical for the differentiation of fetal monocytes into alveolar macrophages. *Nature Immunology*. 15 (11), 1026–1037.
- Schön, M.P. (2019) Adaptive and Innate Immunity in Psoriasis and Other Inflammatory Disorders. *Frontiers in Immunology*. 101764.
- Seed, R.I., Taurozzi, A.J., Wilcock, D.J., Nappo, G., Erb, H.H.H., Read, M.L., Gurney, M., Archer, L.K., Ito, S., Rumsby, M.G., Petrie, J.L., Clayton, A., Maitland, N.J. & Collins, A.T. (2019) The putative tumour suppressor protein Latexin is secreted by prostate luminal cells and is downregulated in malignancy. *Scientific Reports*. 9 (1), 5120.
- Segura, E., Valladeau-Guilemond, J., Donnadieu, M.-H., Sastre-Garau, X., Soumelis, V. & Amigorena, S. (2012) Characterization of resident and migratory dendritic cells in human lymph nodes. *The Journal of experimental medicine*. 209 (4), 653–660.
- Sehra, S., Serezani, A.P.M., Ocaña, J.A., Travers, J.B. & Kaplan, M.H. (2016) Mast Cells Regulate Epidermal Barrier Function and the Development of Allergic Skin Inflammation. *The Journal of investigative dermatology*. 136 (7), 1429–1437.
- Shao, T., Song, P., Hua, H., Zhang, H., Sun, X., Kong, Q., Wang, J., Luo, T. & Jiang, Y. (2018) Gamma synuclein is a novel Twist1 target that promotes TGF- $\beta$ -induced cancer cell migration and invasion. *Cell Death & Disease*. 9 (6), 625.



- Sharma, s & Yousef, H. (2017) '*Anatomy, Skin (Integument), Epidermis*', in [Online]. p.
- Shin, J.-S. & Greer, A.M. (2015) The role of FcεRI expressed in dendritic cells and monocytes. *Cellular and molecular life sciences : CMLS*. 72 (12), 2349–2360.
- Singh, S.K., Baker, R., Sikkink, S.K., Nizard, C., Schnebert, S., Kurfurst, R. & Tobin, D.J. (2017) E-cadherin mediates ultraviolet radiation- and calcium-induced melanin transfer in human skin cells. *Experimental Dermatology*. 26 (11), 1125–1133.
- Solé-Boldo, L., Raddatz, G., Schütz, S., Mallm, J.-P., Rippe, K., Lonsdorf, A.S., Rodríguez-Paredes, M. & Lyko, F. (2020) Single-cell transcriptomes of the human skin reveal age-related loss of fibroblast priming. *Communications Biology*. 3 (1), 188.
- Soler, D., Humphreys, T.L., Spinola, S.M. & Campbell, J.J. (2003) CCR4 versus CCR10 in human cutaneous TH lymphocyte trafficking. *Blood*. 101 (5), 1677–1682.
- Sorrell, J.M. & Caplan, A.I. (2004) Fibroblast heterogeneity: more than skin deep. *Journal of Cell Science*. 117 (5), 667.
- Sprangers, S., de Vries, T.J. & Everts, V. (2016) Monocyte Heterogeneity: Consequences for Monocyte-Derived Immune Cells. *Journal of immunology research*. 20161475435–1475435.
- Ståhl, P.L., Salmén, F., Vickovic, S., Lundmark, A., Navarro, J.F., Magnusson, J., Giacomello, S., Asp, M., Westholm, J.O., Huss, M., Mollbrink, A., Linnarsson, S., Codeluppi, S., Borg, Å., Pontén, F., Costea, P.I., Sahlén, P., Mulder, J., Bergmann, O., et al. (2016) Visualization and analysis of gene expression in tissue sections by spatial transcriptomics. *Science*. 353 (6294), 78.
- Stanko, K., Iwert, C., Appelt, C., Vogt, K., Schumann, J., Strunk, F.J., Ahrlich, S., Schlickeiser, S., Romagnani, C., Jürchott, K., Meisel, C., Willimsky, G., Köhl, A.A. & Sawitzki, B. (2018) CD96 expression determines the inflammatory potential of IL-9–producing Th9 cells. *Proceedings of the National Academy of Sciences*. 115 (13), E2940.
- Steinert, P.M. & Marekov, L.N. (1995) The Proteins Elafin, Filaggrin, Keratin Intermediate Filaments, Loricrin, and Small Proline-rich Proteins 1 and 2 Are Isodipeptide Cross-linked Components of the Human Epidermal Cornified Cell Envelope. *Journal of Biological Chemistry*. 270 (30), 17702–17711.
- Stoitzner, P., Tripp, C.H., Douillard, P., Saeland, S. & Romani, N. (2005) Migratory Langerhans Cells in Mouse Lymph Nodes in Steady State and Inflammation. *Journal of Investigative Dermatology*. 125 (1), 116–125.
- Surguchov, A., Palazzo, R.E. & Surgucheva, I. (2001) Gamma synuclein: Subcellular localization in neuronal and non-neuronal cells and effect on signal transduction. *Cell Motility*. 49 (4), 218–228.

- Suscsek, C.V., Mahotka, C., Schnorr, O. & Kolb-Bachofen, V. (2004) UVB Radiation-Mediated Expression of Inducible Nitric Oxide Synthase Activity and the Augmenting Role of Co-Induced TNF- $\alpha$  in Human Skin Endothelial Cells. *Journal of Investigative Dermatology*. 123 (5), 950–957.
- Tabib, T., Morse, C., Wang, T., Chen, W. & Lafyatis, R. (2018a) SFRP2/DPP4 and FMO1/LSP1 Define Major Fibroblast Populations in Human Skin. *Journal of Investigative Dermatology*. 138 (4), 802–810.
- Tabib, T., Morse, C., Wang, T., Chen, W. & Lafyatis, R. (2018b) SFRP2/DPP4 and FMO1/LSP1 Define Major Fibroblast Populations in Human Skin. *Journal of Investigative Dermatology*. 138 (4), 802–810.
- Tamoutounour, S., Guilliams, M., Montanana Sanchis, F., Liu, H., Terhorst, D., Malosse, C., Pollet, E., Ardouin, L., Luche, H., Sanchez, C., Dalod, M., Malissen, B. & Henri, S. (2013) Origins and Functional Specialization of Macrophages and of Conventional and Monocyte-Derived Dendritic Cells in Mouse Skin. *Immunity*. 39 (5), 925–938.
- Tamoutounour, S., Han, S.-J., Deckers, J., Constantinides, M.G., Hurabielle, C., Harrison, O.J., Bouladoux, N., Linehan, J.L., Link, V.M., Vujkovic-Cvijin, I., Perez-Chaparro, P.J., Rosshart, S.P., Rehmann, B., Lazarevic, V. & Belkaid, Y. (2019) Keratinocyte-intrinsic MHCII expression controls microbiota-induced Th1 cell responses. *Proceedings of the National Academy of Sciences*. 116 (47), 23643.
- Tang, F., Barbacioru, C., Wang, Y., Nordman, E., Lee, C., Xu, N., Wang, X., Bodeau, J., Tuch, B.B., Siddiqui, A., Lao, K. & Surani, M.A. (2009) mRNA-Seq whole-transcriptome analysis of a single cell. *Nature Methods*. 6 (5), 377–382.
- Tani, T., Karttunen, T., Kiviluoto, T., Kivilaakso, E., Burgeson, R.E., Sipponen, P. & Virtanen, I. (1996) Alpha 6 beta 4 integrin and newly deposited laminin-1 and laminin-5 form the adhesion mechanism of gastric carcinoma. Continuous expression of laminins but not that of collagen VII is preserved in invasive parts of the carcinomas: implications for acquisition of the invading phenotype. *The American journal of pathology*. 149 (3), 781–793.
- Tanner, S.D., Baranov, V.I., Ornatsky, O.I., Bandura, D.R. & George, T.C. (2013) An introduction to mass cytometry: fundamentals and applications. *Cancer Immunology, Immunotherapy*. 62 (5), 955–965.
- Thiriot, A., Perdomo, C., Cheng, G., Novitzky-Basso, I., McArdle, S., Kishimoto, J.K., Barreiro, O., Mazo, I., Triboulet, R., Ley, K., Rot, A. & von Andrian, U.H. (2017) Differential DARC/ACKR1 expression distinguishes venular from non-venular endothelial cells in murine tissues. *BMC biology*. 15 (1), 45–45.
- Thomas, A.C., Cullup, T., Norgett, E.E., Hill, T., Barton, S., Dale, B.A., Sprecher, E., Sheridan, E., Taylor, A.E., Wilroy, R.S., DeLozier, C., Burrows, N., Goodyear, H., Fleckman, P., Stephens, K.G., Mehta, L., Watson, R.M., Graham, R., Wolf, R., et al.

- (2006) ABCA12 Is the Major Harlequin Ichthyosis Gene. *Journal of Investigative Dermatology*. 126 (11), 2408–2413.
- Tirosh, I., Izar, B., Prakadan, S.M., Wadsworth, M.H., 2nd, Treacy, D., Trombetta, J.J., Rotem, A., Rodman, C., Lian, C., Murphy, G., Fallahi-Sichani, M., Dutton-Regester, K., Lin, J.-R., Cohen, O., Shah, P., Lu, D., Genshaft, A.S., Hughes, T.K., Ziegler, C.G.K., et al. (2016) Dissecting the multicellular ecosystem of metastatic melanoma by single-cell RNA-seq. *Science (New York, N.Y.)*. 352 (6282), 189–196.
- Tracy, L.E., Minasian, R.A. & Caterson, E.J. (2016) Extracellular Matrix and Dermal Fibroblast Function in the Healing Wound. *Advances in wound care*. 5 (3), 119–136.
- Trebaul, A., Chan, E.K. & Midwood, K.S. (2007) Regulation of fibroblast migration by tenascin-C. *Biochemical Society Transactions*. 35 (4), 695.
- Vaahtomeri, K., Brown, M., Hauschild, R., De Vries, I., Leithner, A.F., Mehling, M., Kaufmann, W.A. & Sixt, M. (2017) Locally Triggered Release of the Chemokine CCL21 Promotes Dendritic Cell Transmigration across Lymphatic Endothelia. *Cell reports*. 19 (5), 902–909.
- Valladeau, J., Ravel, O., Dezutter-Dambuyant, C., Moore, K., Kleijmeer, M., Liu, Y., Duvert-Frances, V., Vincent, C., Schmitt, D., Davoust, J., Caux, C., Lebecque, S. & Saeland, S. (2000) Langerin, a Novel C-Type Lectin Specific to Langerhans Cells, Is an Endocytic Receptor that Induces the Formation of Birbeck Granules. *Immunity*. 12 (1), 71–81.
- Veerman, K., Tardiveau, C., Martins, F., Coudert, J. & Girard, J.-P. (2019) Single-Cell Analysis Reveals Heterogeneity of High Endothelial Venules and Different Regulation of Genes Controlling Lymphocyte Entry to Lymph Nodes. *Cell Reports*. 26 (11), 3116-3131.e5.
- Veljkovic Vujaklija, D., Dominovic, M., Gulic, T., Mahmutefendic, H., Haller, H., Saito, S. & Rukavina, D. (2013) Granulysin expression and the interplay of granulysin and perforin at the maternal–fetal interface. *Journal of Reproductive Immunology*. 97 (2), 186–196.
- Venetz, D., Ponzoni, M., Schiraldi, M., Ferreri, A.J.M., Bertoni, F., Doglioni, C. & Uguccioni, M. (2010) Perivascular expression of CXCL9 and CXCL12 in primary central nervous system lymphoma: T-cell infiltration and positioning of malignant B cells. *International Journal of Cancer*. 127 (10), 2300–2312.
- Vento-Tormo, R., Efremova, M., Botting, R.A., Turco, M.Y., Vento-Tormo, M., Meyer, K.B., Park, J.-E., Stephenson, E., Polański, K., Goncalves, A., Gardner, L., Holmqvist, S., Henriksson, J., Zou, A., Sharkey, A.M., Millar, B., Innes, B., Wood, L., Wilbrey-Clark, A., et al. (2018) Single-cell reconstruction of the early maternal–fetal interface in humans. *Nature*. 563 (7731), 347–353.

- Verkman, A.S. (2002) Aquaporin water channels and endothelial cell function. *Journal of anatomy*. 200 (6), 617–627.
- Villani, A.-C., Satija, R., Reynolds, G., Sarkizova, S., Shekhar, K., Fletcher, J., Griesbeck, M., Butler, A., Zheng, S., Lazo, S., Jardine, L., Dixon, D., Stephenson, E., Nilsson, E., Grundberg, I., McDonald, D., Filby, A., Li, W., De Jager, P.L., et al. (2017) Single-cell RNA-seq reveals new types of human blood dendritic cells, monocytes, and progenitors. *Science*. 356 (6335), .
- Waise, S., Parker, R., Rose-Zerilli, M.J.J., Layfield, D.M., Wood, O., West, J., Ottensmeier, C.H., Thomas, G.J. & Hanley, C.J. (2019) An optimised tissue disaggregation and data processing pipeline for characterising fibroblast phenotypes using single-cell RNA sequencing. *Scientific Reports*. 9 (1), 9580.
- Wang, X.-N., McGovern, N., Gunawan, M., Richardson, C., Windebank, M., Siah, T.-W., Lim, H.-Y., Fink, K., Yao Li, J.L., Ng, L.G., Ginhoux, F., Angeli, V., Collin, M. & Haniffa, M. (2014) A three-dimensional atlas of human dermal leukocytes, lymphatics, and blood vessels. *The Journal of investigative dermatology*. 134 (4), 965–974.
- Wang, Y., Szretter, K.J., Vermi, W., Gilfillan, S., Rossini, C., Cella, M., Barrow, A.D., Diamond, M.S. & Colonna, M. (2012) IL-34 is a tissue-restricted ligand of CSF1R required for the development of Langerhans cells and microglia. *Nature immunology*. 13 (8), 753–760.
- Watanabe, M., Natsuga, K., Shinkuma, S. & Shimizu, H. (2018) Epidermal aspects of type VII collagen: Implications for dystrophic epidermolysis bullosa and epidermolysis bullosa acquisita. *The Journal of Dermatology*. 45 (5), 515–521.
- Watanabe, R., Gehad, A., Yang, C., Scott, L.L., Teague, J.E., Schlapbach, C., Elco, C.P., Huang, V., Matos, T.R., Kupper, T.S. & Clark, R.A. (2015) Human skin is protected by four functionally and phenotypically discrete populations of resident and recirculating memory T cells. *Science translational medicine*. 7 (279), 279ra39-279ra39.
- Wehrle-Haller, B. (2003) The Role of Kit-Ligand in Melanocyte Development and Epidermal Homeostasis. *Pigment Cell Research*. 16 (3), 287–296.
- Westerhof, W. & Dingemans, K.P. (1986) The morphological details of globular keratohyalin granules. *Journal of Cutaneous Pathology*. 13 (5), 375–382.
- Wikramanayake, T.C., Stojadinovic, O. & Tomic-Canic, M. (2014) Epidermal Differentiation in Barrier Maintenance and Wound Healing. *Advances in wound care*. 3 (3), 272–280.
- Wilhelmsen, K., Farrar, K. & Hellman, J. (2013) Quantitative in vitro assay to measure neutrophil adhesion to activated primary human microvascular endothelial cells under static conditions. *Journal of visualized experiments : JoVE*. (78), e50677–e50677.

- Williams, A.R., Klaver, E.J., Laan, L.C., Ramsay, A., Fryganas, C., Difborg, R., Kringel, H., Reed, J.D., Mueller-Harvey, I., Skov, S., van Die, I. & Thamsborg, S.M. (2017) Co-operative suppression of inflammatory responses in human dendritic cells by plant proanthocyanidins and products from the parasitic nematode *Trichuris suis*. *Immunology*. 150 (3), 312–328.
- Wolf, F.A., Angerer, P. & Theis, F.J. (2018) SCANPY: large-scale single-cell gene expression data analysis. *Genome Biology*. 19 (1), 15.
- Wolf, F.A., Hamey, F.K., Plass, M., Solana, J., Dahlin, J.S., Göttgens, B., Rajewsky, N., Simon, L. & Theis, F.J. (2019) PAGA: graph abstraction reconciles clustering with trajectory inference through a topology preserving map of single cells. *Genome Biology*. 20 (1), 59.
- Wollenberg, A., Kraft, S., Hanau, D. & Bieber, T. (1996) Immunomorphological and ultrastructural characterization of Langerhans cells and a novel, inflammatory dendritic epidermal cell (IDEC) population in lesional skin of atopic eczema. *The Journal of investigative dermatology*. 106 (3), 446–453.
- Wollenberg, A., Oppel, T., Schottdorf, E.-M., Günther, S., Moderer, M. & Mommaas, M. (2002) Expression and Function of the Mannose Receptor CD206 on Epidermal Dendritic Cells in Inflammatory Skin Diseases. *Journal of Investigative Dermatology*. 118 (2), 327–334.
- Wolock, S.L., Lopez, R. & Klein, A.M. (2019) Scrublet: Computational Identification of Cell Doublets in Single-Cell Transcriptomic Data. *Cell Systems*. 8 (4), 281-291.e9.
- Wong, K.L., Yeap, W.H., Tai, J.J.Y., Ong, S.M., Dang, T.M. & Wong, S.C. (2012) The three human monocyte subsets: implications for health and disease. *Immunologic Research*. 53 (1), 41–57.
- Woo, S.-H., Lumpkin, E.A. & Patapoutian, A. (2015) Merkel cells and neurons keep in touch. *Trends in cell biology*. 25 (2), 74–81.
- Woodfin, A., Voisin, M.-B., Beyrau, M., Colom, B., Caille, D., Diapouli, F.-M., Nash, G.B., Chavakis, T., Albelda, S.M., Rainger, G.E., Meda, P., Imhof, B.A. & Nourshargh, S. (2011) The junctional adhesion molecule JAM-C regulates polarized transendothelial migration of neutrophils in vivo. *Nature immunology*. 12 (8), 761–769.
- Wright, M.C., Logan, G.J., Bolock, A.M., Kubicki, A.C., Hemphill, J.A., Sanders, T.A. & Maricich, S.M. (2017) Merkel cells are long-lived cells whose production is stimulated by skin injury. *Developmental biology*. 422 (1), 4–13.
- Xia, P., Gamble, J.R., Rye, K.A., Wang, L., Hii, C.S., Cockerill, P., Khew-Goodall, Y., Bert, A.G., Barter, P.J. & Vadas, M.A. (1998) Tumor necrosis factor-alpha induces adhesion molecule expression through the sphingosine kinase pathway. *Proceedings of the National Academy of Sciences of the United States of America*. 95 (24), 14196–14201.

- Yang, J., Park, Y., Zhang, H., Gao, X., Wilson, E., Zimmer, W., Abbott, L. & Zhang, C. (2009) Role of MCP-1 in tumor necrosis factor-alpha-induced endothelial dysfunction in type 2 diabetic mice. *American journal of physiology. Heart and circulatory physiology*. 297 (4), H1208–H1216.
- Yao, Y., Liu, R., Shin, M.S., Trentalange, M., Allore, H., Nassar, A., Kang, I., Pober, J.S. & Montgomery, R.R. (2014) CyTOF supports efficient detection of immune cell subsets from small samples. *Journal of immunological methods*. 4151–5.
- Yaszay, B., Trindade, M.C.D., Lind, M., Goodman, S.B. & Smith, R.L. (2001) Fibroblast expression of C—C chemokines in response to orthopaedic biomaterial particle challenge in vitro. *Journal of Orthopaedic Research*. 19 (5), 970–976.
- Yoshida, K., Kubo, A., Fujita, H., Yokouchi, M., Ishii, K., Kawasaki, H., Nomura, T., Shimizu, H., Kouyama, K., Ebihara, T., Nagao, K. & Amagai, M. (2014) Distinct behavior of human Langerhans cells and inflammatory dendritic epidermal cells at tight junctions in patients with atopic dermatitis. *Journal of Allergy and Clinical Immunology*. 134 (4), 856–864.
- Yoshino, M., Yamazaki, H., Nakano, H., Kakiuchi, T., Ryoke, K., Kunisada, T. & Hayashi, S. (2003) Distinct antigen trafficking from skin in the steady and active states. *International Immunology*. 15 (6), 773–779.
- Yoshino, M., Yamazaki, H., Shultz, L.D. & Hayashi, S.-I. (2006) Constant rate of steady-state self-antigen trafficking from skin to regional lymph nodes. *International Immunology*. 18 (11), 1541–1548.
- Young, A., Wu, W., Sun, W., Benjamin Larman, H., Wang, N., Li, Y.-S., Shyy, J.Y., Chien, S. & García-Cardeña, G. (2009) Flow activation of AMP-activated protein kinase in vascular endothelium leads to Krüppel-like factor 2 expression. *Arteriosclerosis, thrombosis, and vascular biology*. 29 (11), 1902–1908.
- Zaba, L.C., Krueger, J.G. & Lowes, M.A. (2009) Resident and ‘inflammatory’ dendritic cells in human skin. *The Journal of investigative dermatology*. 129 (2), 302–308.
- Zeitvogel, J., Jokmin, N., Rieker, S., Klug, I., Brandenberger, C. & Werfel, T. (2017) GATA3 regulates FLG and FLG2 expression in human primary keratinocytes. *Scientific Reports*. 7 (1), 11847.
- Zhang, H., Kouadio, A., Cartledge, D. & Godwin, A.K. (2011) Role of gamma-synuclein in microtubule regulation. *Experimental Cell Research*. 317 (10), 1330–1339.
- Zhang, W., Ge, Y., Cheng, Q., Zhang, Q., Fang, L. & Zheng, J. (2018) Decorin is a pivotal effector in the extracellular matrix and tumour microenvironment. *Oncotarget*. 9 (4), 5480–5491.
- Ziegler-Heitbrock, L., Ancuta, P., Crowe, S., Dalod, M., Grau, V., Hart, D.N., Leenen, P.J.M., Liu, Y.-J., MacPherson, G., Randolph, G.J., Scherberich, J., Schmitz, J., Shortman, K., Sozzani, S., Strobl, H., Zembala, M., Austyn, J.M. & Lutz, M.B.

- (2010) Nomenclature of monocytes and dendritic cells in blood. *Blood*. 116 (16), e74–e80.
- Zocco, M. & Blanpain, C. (2017) Identifying the niche controlling melanocyte differentiation. *Genes & development*. 31 (8), 721–723.
- Zomer, H.D. & Trentin, A.G. (2018) Skin wound healing in humans and mice: Challenges in translational research. *Journal of Dermatological Science*. 90 (1), 3–12.
- Zonneville, J., Safina, A., Truskinovsky, A.M., Arteaga, C.L. & Bakin, A.V. (2018) TGF- $\beta$  signaling promotes tumor vasculature by enhancing the pericyte-endothelium association. *BMC cancer*. 18 (1), 670–670.

## 9 Publications and Presentations

### 9.1 Publications

\*Authors provided equal contribution to the publication

**2017. *Single-cell RNA-seq reveals new types of human blood dendritic cells, monocytes, and progenitors.* Science, 356.** Alexandra-Chloé Villani\*, Rahul Satija\*, Gary Reynolds, Siranush Sarkizova, Karthik Shekhar, **James Fletcher**, Morgane Griesbeck, Andrew Butler, Shiwei Zheng, Suzan Lazo, Laura Jardine, David Dixon, Emily Stephenson, Emil Nilsson, Ida Grundberg, David McDonald, Andrew Filby, Weibo Li, Philip L. De Jager, Orit Rozenblatt-Rosen, Andrew A. Lane, Muzlifah Haniffa, Aviv Regev, Nir Hacohen

**2017. *Phenotypic and functional consequences of different isolation protocols on skin mononuclear phagocytes.* J Leukoc Biol, 101, 1393-1403.** Rachel A Botting\*, Kirstie M Bertram\*, Heeva Baharlou, Kerrie J Sandgren, **James Fletcher**, Jake W Rhodes, Hafsa Rana, Tobi M Plasto, Xin M Wang, Jake JK Lim, Laith Barnouti, Mark Kohout, Tim Papadopoulos, Steve Merten, Norman Olbourne, Anthony L Cunningham, Muzlifah Haniffa, Andrew N Harman

**2017. *Mononuclear Phagocyte System.* eLS Wiley Online Library. Accessible at: <https://doi.org/10.1002/9780470015902.a0001217.pub2>** Peter Vegh, **James Fletcher**, David Dixon, Muzlifah Haniffa

**2017. *Mechanisms of immune evasion in extramammary Paget disease.* Br J Dermatol, 176, 293-294.** **J. Fletcher**, M. Haniffa

**2017. *The Human Cell Atlas: from vision to reality.* Nature, 550, 451-453.** Orit Rozenblatt-Rosen, Michael J Stubbington, Aviv Regev, Sarah A Teichmann (**3D cell figure, Image: Kathryn White, Reconstruction: James Fletcher**)

**2018. *Gene expression variability across cells and species shapes innate immunity.* Nature, 563, 197-202.** Tzachi Hagai, Xi Chen, Ricardo J. Miragaia, Raghd Rostom, Tomás



Gomes, Natalia Kunowska, Johan Henriksson, Jong-Eun Park, Valentina Proserpio, Giacomo Donati, Lara Bossini-Castillo, Felipe A. Vieira Braga, Guy Naamati, **James Fletcher**, Emily Stephenson, Peter Vegh, Gosia Trynka, Ivanela Kondova, Mike Dennis, Muzlifah Haniffa, Armita Nourmohammad, Michael Lässig & Sarah A. Teichmann

**2019. *Identification of HIV Transmitting CD11c+ Human Epidermal Dendritic Cells.***

**Nature Communications, 10, 2759.** Kirstie M Bertram\*, Rachel A Botting\*, Heeva Baharlou\*, Jake W Rhodes, Hafsa Rana, J Dinny Graham, Ellis Patrick, **James Fletcher**, Toby M Plasto, Naomi R Truong, Caroline Royle, Chloe M Doyle, Orion Tong, Najla Nasr, Laith Barnouti, Mark Kohout, Andrew J Brooks, Michael P Wines, Peter Haertsch, Jake Lim, Martijn P Gosselink, Grahame Ctercteko, Jacob D Estes, Melissa J Churchill, Paul U Cameron, Eric Hunter, Muzlifah A Haniffa, Anthony L Cunningham, Andrew N Harman

**2019. *Decoding human fetal liver haematopoiesis.* Nature, 574, 365-371.**

Dorin-Mirel Popescu\*, Rachel A. Botting\*, Emily Stephenson\*, Kile Green, Simone Webb, Laura Jardine, Emily F. Calderbank, Krzysztof Polanski, Issac Goh, Mirjana Efremova, Meghan Acres, Daniel Maunder, Peter Vegh, Yorick Gitton, Jong-Eun Park, Roser Vento-Tormo, Zhichao Miao, David Dixon, Rachel Rowell, David McDonald, **James Fletcher**, Elizabeth Poyner, Gary Reynolds, Michael Mather, Corina Moldovan, Lira Mamanova, Frankie Greig, Matthew D. Young, Kerstin B. Meyer, Steven Lisgo, Jaume Bacardit, Andrew Fuller, Ben Millar, Barbara Innes, Susan Lindsay, Michael J. T. Stubbington, Monika S. Kowalczyk, Bo Li, Orr Ashenberg, Marcin Tabaka, Danielle Dionne, Timothy L. Tickle, Michal Slyper, Orit Rozenblatt-Rosen, Andrew Filby, Peter Carey, Alexandra-Chloé Villani, Anindita Roy, Aviv Regev, Alain Chédotal, Irene Roberts, Berthold Göttgens, Sam Behjati, Elisa Laurenti, Sarah A. Teichmann, Muzlifah Haniffa

**(Under review 2020). *Identification of HIV-Transmitting Sub-Epithelial Mononuclear Phagocytes in Human Anogenital and Colorectal Tissues.* Nature Communications.**

Jake W Rhodes\*, Rachel A Botting\*, Kirstie M Bertram, Hafsa Rana, Heeva Baharlou, Erica E Longmuir-Vine, Peter Vegh, **James Fletcher**, Thomas R O'Neill, Grant P Parnell, J Dinny Graham, Najla Nasr, Jake J K Lim, Laith Barnouti, Peter Haertsch, Martijn P Gosselink, Angelina Di Re, Grahame Ctercteko, Gregory J Jenkins, Andrew J Brooks, Michael Wines,

Ellis Patrick, Scott N Byrne, Muzlifah A Haniffa, Anthony L Cunningham and Andrew N Harman

**(Under review 2020). *Developmental programs are co-opted in inflammatory skin disease. Science.*** Gary Reynolds\*, Peter Vegh\*, **James Fletcher\***, Elizabeth F.M. Poyner\*, Emily Stephenson, Issac Goh, Rachel A. Botting, Ni Huang, David Dixon, Kile Green, Daniel Maunder, Justin Engelbert, Anna Dubois, Mirjana Efremova, Krzysztof Polański, Laura Jardine, Claire Jones, Christopher Carey, Dorin-Mirel Popescu, Simone Webb, Xiao-nong Wang, Ben Sayer, Jong-Eun Park, Bayanne Olabi, Victor A. Negri, Daria Belokhvostova, Magnus Lynch, David McDonald, Andrew Filby, Tzachi Hagai, Kerstin B. Meyer, Akhtar Husain, Jonathan Coxhead, Roser Vento-Tormo, Sam Behjati, Steven Lisgo, Alexandra-Chloé Villani, Jaume Bacardit, Phil Jones, Neil Rajan, Edel A. O’Toole, Graham S. Ogg, Nick J. Reynolds, Sarah A. Teichmann\*, Fiona Watt\*, Muzlifah Haniffa\*

## 9.2 Presentations

**Poster Presentation: September 2017, INSERM 247 Mass Cytometry Conference.**

***Defining the landscape of human tissue mononuclear phagocytes using single cell RNA sequencing.*** James Fletcher, Emily Stephenson, Peter Vegh, Rachel A. Botting, Roser Vento, David Dixon, Kathryn White, Ross Laws, Andrew Filby, Fiona Watt, Nir Hacohen, Alexandra-Chloé Villani, Sarah Teichmann, Muzlifah Haniffa

**Oral Presentation: November 2017, ICM Research Seminar.** ***Defining the landscape of human tissue mononuclear phagocytes using single cell RNA sequencing and mass cytometry.*** James Fletcher, Prof. M. Haniffa, Prof. N. Reynolds

**Poster Presentation: March 2018, Wellcome Single Cell Sanger Conference.** ***Defining the cellular landscape of human skin using single cell RNA sequencing.*** James Fletcher, Emily Stephenson, Peter Vegh, Rachel A. Botting, Roser Vento, David Dixon, Andrew Filby, Nick Reynolds, Fiona Watt, Nir Hacohen, Alexandra-Chloé Villani, Sarah Teichmann, Muzlifah Haniffa

**Oral Presentation: March 2018, British Society for Investigative Dermatology.** ***Defining the cellular landscape of human skin using single cell RNA sequencing.*** James Fletcher, Muzlifah Haniffa, Nick Reynolds

**Oral Presentation: November 2018, Genomics in Dermatology Wellcome Conference.** ***Lessons from single cell profiling of human skin.*** James Fletcher, Muzlifah Haniffa.

**Oral Presentation: January 2019, ICM Research Seminar.** ***Single cell profiling of human skin.*** James Fletcher, Muzlifah Haniffa, Nick Reynolds

**Oral Presentation: July 2019, III Theme Meeting.** ***Human Skin Cell Atlas.*** James Fletcher, Peter Vegh, Gary Reynolds, Muzlifah Haniffa